CHEMICAL REVIEWS

Review

Cite This: *Chem. Rev.* 2018, 118, 4731−4816

pubs.acs.org/CR

Conducting Polymers in the Fields of Energy, Environmental Remediation, and Chemical−Chiral Sensors

Jorge G. Ibanez,[†] Marina. E. Rincón,[‡] Silvia Gutierrez-Granados,[§] M'hamed Chahma,[∥] Oscar A. Jaramillo-Quintero,[⊥] and Bernardo A. Frontana-Uribe*[,#,∇]

[†]Departamento de Ingeniería y Ciencias Químicas, Universidad Iberoamericana, Prolongación Paseo de la Reforma 880, 01219 Ciudad de México, Mexico

[‡]Instituto de Energías Renovables, Universidad Nacional Autónoma de México, Apartado Postal 34, 62580, Temixco, MOR, Mexico

[§]Departamento de Química, DCNyE, Campus Guanajuato, Universidad de Guanajuato, Cerro de la Venada S/N, Pueblito de Rocha, 36080 Guanajuato, GTO Mexico

[∥]Laurentian University, Department of Chemistry & Biochemistry, Sudbury, ON P3E2C6, Canada

[⊥]CONACYT-Instituto de Energías Renovables, Universidad Nacional Autónoma de México, Apartado Postal 34, 62580 Temixco, MOR, Mexico

[#]Centro Conjunto de Investigación en Química Sustentable, UAEM-UNAM, Km 14.5 Carretera Toluca-Ixtlahuaca, Toluca 50200, Estado de México Mexico

[∇]Instituto de Química, Universidad Nacional Autónoma de México, Circuito exterior Ciudad Universitaria, 04510 Ciudad de México, Mexico

ABSTRACT: Conducting polymers (CPs), thanks to their unique properties, structures made on-demand, new composite mixtures, and possibility of deposit on a surface by chemical, physical, or electrochemical methodologies, have shown in the last years a renaissance and have been widely used in important fields of chemistry and materials science. Due to the extent of the literature on CPs, this review, after a concise introduction about the interrelationship between electrochemistry and conducting polymers, is focused exclusively on the following applications: energy (energy storage devices and solar cells), use in environmental remediation (anion and cation trapping, electrocatalytic reduction/oxidation of pollutants on CP based electrodes, and adsorption of pollutants) and finally electroanalysis as chemical sensors in solution, gas phase, and chiral molecules. This review is expected to be comprehensive, authoritative, and useful to the chemical community interested in CPs and their applications.

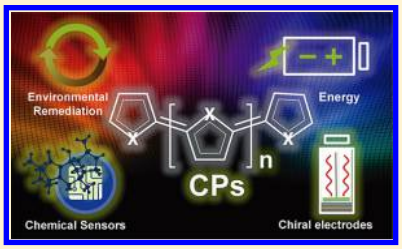

CONTENTS

1. Introduction 4732
2. Interrelationship between Electrochemistry and Conducting Polymers 4732
 2.1. Electrochemical Syntheses and Electropolymerization Mechanisms 4732
 2.2. Electrochemical Control of Polymeric Redox Reactions (Doping/Dedoping or Undoping) 4734
 2.3. Rationalizing CP Properties. Proposed Models 4736
 2.4. Other Technological Applications 4739
  2.4.1. Applications in the Medical and Biological Fields 4739
  2.4.2. Actuators 4739
  2.4.3. Antistatic Foils 4740
  2.4.4. Corrosion Protection 4741
  2.4.5. Electrochromic Devices 4741
  2.4.6. Electrocatalysis 4741
  2.4.7. Organic Electronics 4743
  2.4.8. Future Applications 4743
3. Part 1. Applications That Take Advantage of the Tridimensional Structure of the Conducting Polymer. 4744
 3.1. Applications of Conducting Polymers in Energy 4744
  3.1.1. Introduction to Energy Storage Devices 4744
  3.1.2. CPs in Energy Storage Devices 4746
  3.1.3. Applications of CPs in Solar Cells 4748
  3.1.4. The Future of CPs in Energy Storage and Photovoltaic Conversion 4753
 3.2. Applications of Conducting Polymers to Environmental Remediation 4754
  3.2.1. Introduction 4754
  3.2.2. Incorporation and Release of Pollutants in CPs 4754

Special Issue: Electrochemistry: Technology, Synthesis, Energy, and Materials

Received: August 18, 2017
Published: April 9, 2018

DOI: 10.1021/acs.chemrev.7b00482
Chem. Rev. 2018, 118, 4731−4816

3.2.3. Electrocatalytic Reduction/Oxidation 4756
3.2.4. Other Various Applications in Environmental Remediation 4757
3.2.5. The Future of CPs in Environmental Sciences 4762
4. Part 2. Applications That Take Advantage of Modifications at the Polymer−Electrolyte Interface 4762
4.1. Application of Conducting Polymers in Electroanalysis 4762
4.1.1. Introduction to Application of Conducting Polymers in Electroanalysis 4762
4.1.2. CP Based Chemical Sensors for Analytes in Solution 4763
4.1.3. CP Based Chemical Sensors for Analyses in Gas Phase 4774
4.1.4. Chiral Conducting Polymer in Sensor and Chiral Applications 4780
4.1.5. The Future of CPs in Electroanalysis 4791
5. Final Remarks about Conducting Polymers in the Reviewed Applications 4792
Author Information 4793
Corresponding Author 4793
ORCID 4793
Notes 4793
Biographies 4793
Acknowledgments 4793
References 4793

1. INTRODUCTION

Conducting polymers (CPs) have become a fascinating area of research due to their very unique characteristic of being organic materials with electrical conductivity. Since their discovery, they have attracted the attention of a large group of researchers working in edge technological applications. The historical development of these materials[1,2] started with poly(sulfur nitride) or $(SN)_x$, followed by polyacetylene and N- or S-polyheterocycles and polyaniline (PANi).[3] CP progress continues nowadays, and classification of CPs in nine families was recently proposed by Otero:[4] (a) salts of pure conducting polymer (e.g., polythiophene/ClO_4 doped), (b) substituted conducting polymers (e.g., poly(3,4-ethylene dioxythiophene), PEDOT), (c) self-ionized conjugated polymers (e.g., PEDOT−3-butanesulfonic acid, sodium salt, PEDOT-S), (d) copolymers (e.g., poly(EDOT−pyrrole−EDOT), (e) CP−organic compound blends (e.g., PEDOT:PSS), (f) CP−inorganic compound blends (e.g., polypyrrole (PPy)−polyoxometalates), (g) organic and carbon based electroactive composites (e.g., fullerene charged poly(3-hexylthiophene)), and (h) other composites using conducting polymers (e.g., Au nanoparticles charged poly(3-hexylthiophene)). The donor−acceptor conducting polymers,[5,6] which are in fact copolymers in the previous classification, the magneto-optical π-conjugated polymers,[2,7−9] which are organic or inorganic blends, and the composite materials have particularly enriched the field. Thus, classical CPs[10,11] are copolymerized,[6] mixed with graphene,[12] or charged with nanotubes,[13,14] clays,[15] zeolites,[16] montmorillonites,[17] and other constituents yielding materials that combine the advantages of each component and exhibit special properties. In these composites, interfacial interactions and synergistic or complementary effects are present, and therefore special models have been developed to explain their conductivity.[18] Self-ionized conjugated polymers[19] (also called *self-doped* or *self-compensated* CPs) combine electronic charge transport through the conjugated polymer backbones with polyelectrolyte properties arising from structurally incorporated ionic moieties.[20−22] Even though this class of CPs has been known for a long time,[20,23,24] recent work has demonstrated the great potential of self-compensated polymers in technological challenges like tuning of electrode work functions to produce ohmic contacts,[25] preparation of air-stable, water-soluble conductive materials for organic electronics,[26] increasing stability or efficiency in organic[27−29] and perovskite[30] solar cells, and enhancing the performance of supercapacitors,[31] and other organic electronic devices.[32]

Synthesis of these polymers can be achieved by electrochemical (see section 2.1) or chemical methods like cross-coupling or metathesis reactions,[33,34] oxidative polymerization,[35,36] and vapor phase polymerization.[37,38] These methods also allow one to obtain fine control of polymeric structures and are suitable for other specific applications.[39−41] Chemical preparation of CPs will not be further discussed in this review since excellent reviews[42] and books[43,44] are available.

In view of the copious information existing in the CP field, after a concise description of the interrelationship between electrochemistry and CPs, this review will mainly focus on electrochemical applications of CPs dealing with areas of great potential for technological applications such as energy, environmental remediation, and chemical sensors in analytical chemistry (including chiral recognition). The applications are grouped according to the manner in which conducting polymers are used. Therefore, those applications where the entire three-dimensional structure of the CP is used are discussed first (i.e., energy and environmental remediation), and we end with the chemical sensors section, where the important recognition phenomena essentially occur at the CP−solution interface.

2. INTERRELATIONSHIP BETWEEN ELECTROCHEMISTRY AND CONDUCTING POLYMERS

For electrochemists interested in CPs, the first choice for their preparation involves electrooxidation[19,45−51] of suitable monomeric species, such as the classical examples of five-membered aromatic heterocycles (e.g., thiophene or pyrrole) or aromatic amines. This approach allows one to make CP deposits on electrode surfaces with specific and controlled properties that depend on the electropolymerization conditions, making it possible to fine-tune the performance and quality of a wide variety of materials. This section intends to give enough and concise information about the most important aspects in the electrochemical preparation of CPs and their electrochemical behavior. This will facilitate understanding of the applications that represent the core of this contribution.

2.1. Electrochemical Syntheses and Electropolymerization Mechanisms

Anodic electrochemical polymerization follows a series of steps, namely, radical-cation production, oligomer formation, nucleation, and polymer growth. Once formed, the conducting polymer can undergo solid-state redox reactions (i.e., doping), which will be discussed in section 2.2. The complete reaction equation for the polymerization of a suitable monomeric species HMH is eq 1:

DOI: 10.1021/acs.chemrev.7b00482
Chem. Rev. 2018, 118, 4731−4816

Scheme 1. Accepted Mechanism for the Anodic Electropolymerization of a Monomeric Heterocycle

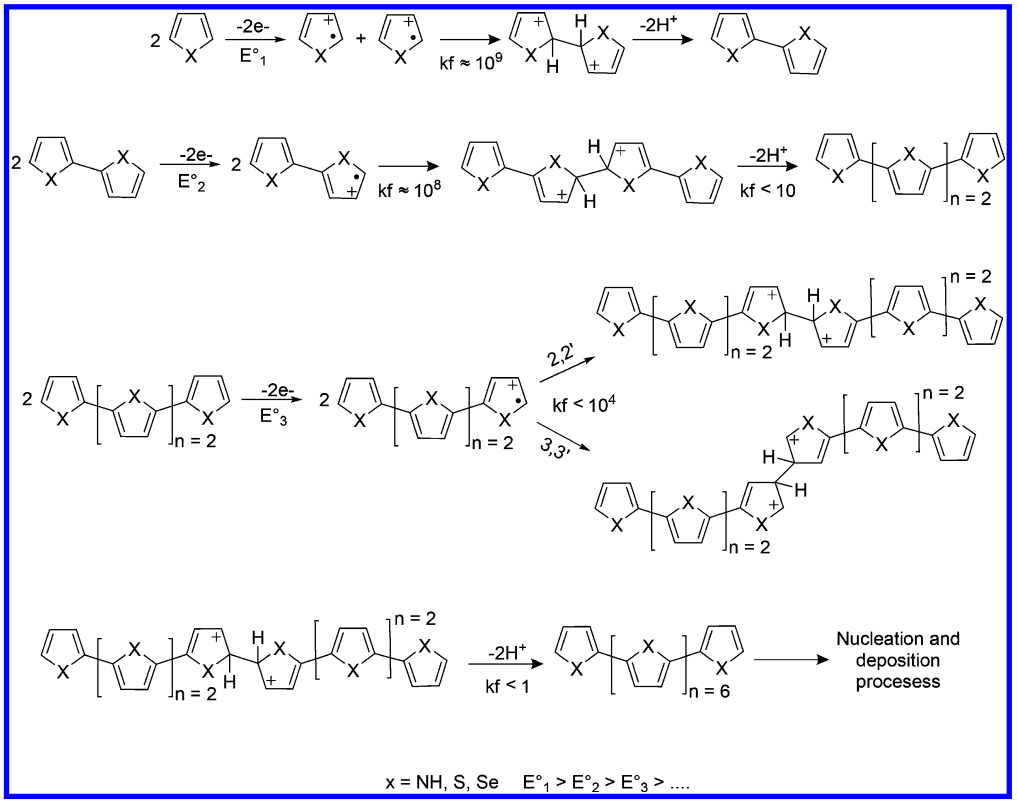

Reproduced from ref 19. Copyright 2010 American Chemical Society.

$$(n + 2)\mathrm{HMH} \rightarrow \mathrm{HM(M)}_n\mathrm{MH}^{nx+} + (2n + 2)\mathrm{H}^+ + (2n + 2 + nx)\mathrm{e}^- \quad (1)$$

The anodic process requires $(2n + 2 + nx)$ F·mol^{-1} to form the conducting polymer film. Once formed, the highly conjugated chain immediately undergoes oxidation and gives rise to the charge of the polymer matrix with an additional charge consumption. (Here, *nx* indicates the polymer's doping level, see section 2.2).[52] In general, the total electropolymerization process has a final electrochemical stoichiometry between 2.1 and 2.5 F·mol^{-1}.

The most widely accepted electropolymerization mechanism is a modification of that initially postulated by Diaz[52] in 1983 (Scheme 1), where a kind of chain propagation reaction involves a cascade of E(CCE)$_n$ steps. In these reactions, the monomers dimerize at the α-position of the radical-cation species generated after oxidation at the electrode,[53,54] producing the doubly charged σ-dimer from which proton elimination occurs and yields a neutral dimer. Because of the greater conjugation in this dimeric species, its redox potential is lower than that of the monomer and it is therefore more easily oxidized. This process immediately produces the corresponding radical cation, which undergoes an equivalent series of coupling steps. In this way, a high order oligomeric species is generated at the electrode interface.

The more realistic nucleation process model assumes that the soluble oligomers present in the diffusion layer in front of the electrode saturate this interface and the CP nucleation and growth starts; this proposal is based on rotating ring-disk electrode (RRDE) and spectroscopic observations.[55−57] By means of chronoamperometric experiments[58] instantaneous (2D or 3D) nucleation and 3D growth mechanisms have been elucidated for 5 membered heterocyclic rings,[59−62] whereas a progressive nucleation and 3D growth with layer by layer deposition mechanisms were observed during aniline electropolymerization (Figure 1).[63,64] All of these terms refer to the classical metal electrodeposition models developed by electrochemists long ago.[65]

Because of the limited reactivity of the radical cations, high-order oligomers stabilize charges better as the conjugation increases (see the constant values in Scheme 1),[19,66,67] the size of the resulting conjugated chain will depend on the electropolymerization potential. Therefore, the higher the charge in the oligomer (i.e., a high doping level), the more reactive it will be toward dimerization. A classical example involves pyrrole polymerization, where a conducting polymer mainly formed by 8−16 oligomeric units was obtained using a low electropolymerization potential.[68] When this potential was increased, the polymer's composition changed to 32−64 pyrrole units, whereas a cross-linked network was formed at higher potentials, yielding a highly conjugated polymer.[69] Therefore, the final conductive polymeric structure will consist of a mixture of units with different conjugation degrees (i.e., a *polydisperse* polymer) that may be cross-linked (i.e., *reticulated*), forming an intricate porous matrix with redox responses in a broad potential range.[70] Consequently, the classical capacitive plateau observed in cyclic voltammetry is in fact a superposition of the accessible redox states of polymeric units with different sizes,[71,72] and different faradaic processes occur in those potential values (Figure 2, see section 2.2).

The electropolymerization process can therefore be summarized in three main steps: (a) formation of a high oligomer concentration region in the electrode diffusion layer, via the anodic oxidation of the monomer through a consecutive

DOI: 10.1021/acs.chemrev.7b00482
Chem. Rev. 2018, 118, 4731−4816

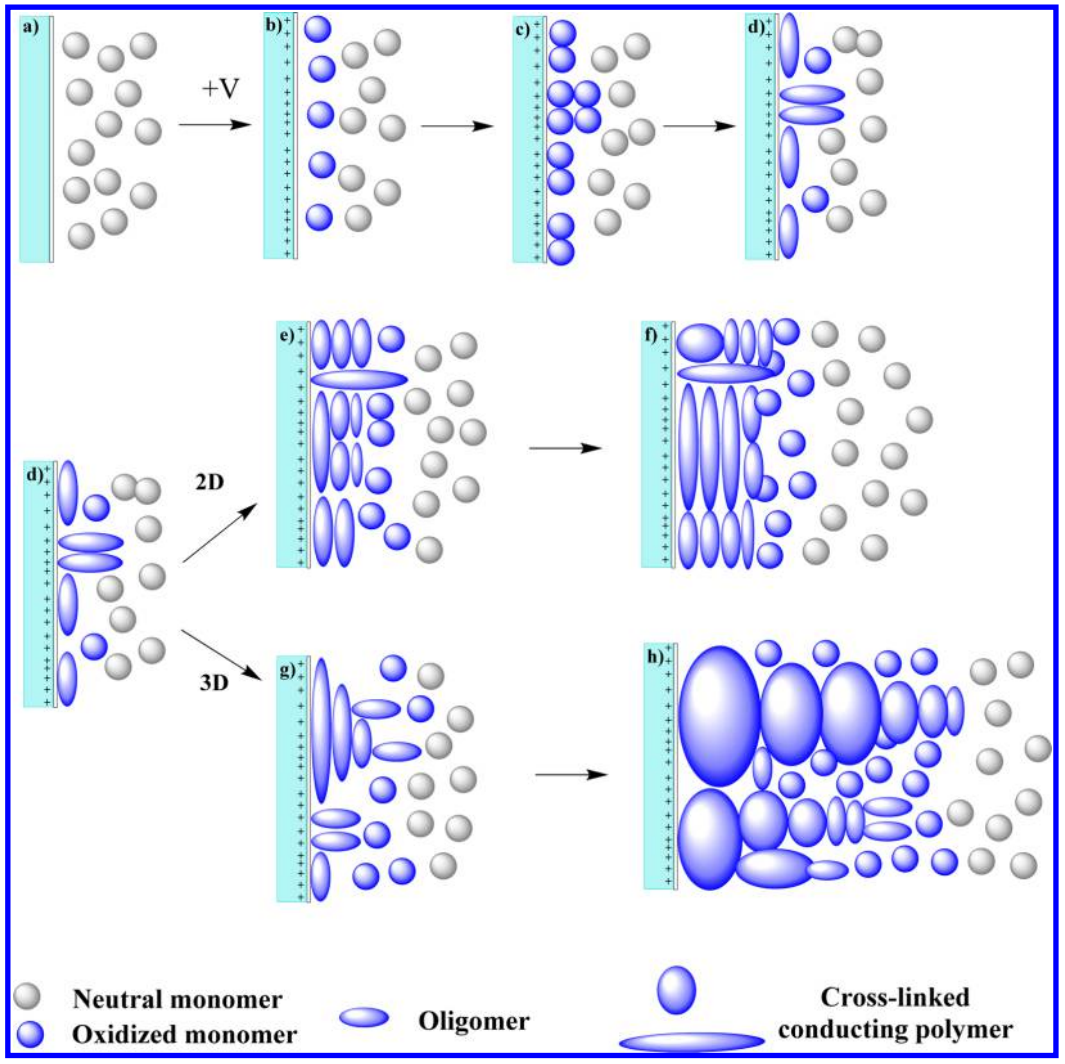

Figure 1. Cartoon representation of the electropolymerization mechanism of conducting polymers. (a) Uncharged interface with monomer, (b) positively charged interface generates radical-anion species, (c) radical-cation coupling to generate σ-dimers, (d) oligomer formation after proton release, (e, f) 2D nucleation−growth pathway, (g, h) 3D nucleation−growth pathway.

sequence of oxidation, dimerization, and proton release reactions, (b) nucleation and growth of short-chain polymeric structures, and (c) solid-state redox reactions that generate longer chains, expanded conjugation, and a reticulated porous matrix.

This expeditious overview has not discussed in detail particular aspects of the electropolymerization process like the dimerization constants (which decrease with oligomer size), the propensity to σ-dimer formation and proton elimination (favored in certain solvents or additives in the electropolymerization solution), nor experimental parameters (e.g., potentiostatic or galvanostatic modes) that are critical for the production of good quality and self-standing CPs. This review is not focused on detailed discussions of electrochemical aspects of CPs but on the review of selected key applications. For more specific information about the electropolymerization process, the reader is encouraged to consult the references cited at the beginning of this section. Particularly useful are the excellent publications by Heinze,[19] Otero,[45,73] Audebert,[74] and Cosnier.[49]

2.2. Electrochemical Control of Polymeric Redox Reactions (Doping/Dedoping or Undoping)

The main peculiarity of a CP is its capacity to change redox state from neutral to a charged or doped state. The most common case is the p-doping, equivalent to a polymer oxidation (eq 2, Figure 3). Here, the conjugated system stabilizes the positive charge carriers by delocalization. The n-doping case, corresponding to the polymer's reduction, is rare and requires ultradry solvents or specially designed monomers to stabilize the injected negative charges.[72,75,76] Many of the interesting properties of these materials are direct consequences of this simple redox reaction.

Suitable oxidizing reagents like Fe^{3+}, Cu^{2+}, $S_2O_8^{2-}$ salts,[77] and iodine can induce polymerization and redox changes. In the case of electrochemistry, an external potential applied in an electrochemical cell promotes such redox reactions. To maintain electroneutrality, *counterions* (i.e., A^- in eq 2, also named *dopants*) are simultaneously incorporated into the polymeric matrix, provoking an enormous structural change due to the solvation molecules that surround the charged species.[4,78] During the reduction process, counteranions and solvent molecules diffuse out in response to the external electrical perturbation, that injects electrons to the positively

DOI: 10.1021/acs.chemrev.7b00482
Chem. Rev. 2018, 118, 4731−4816

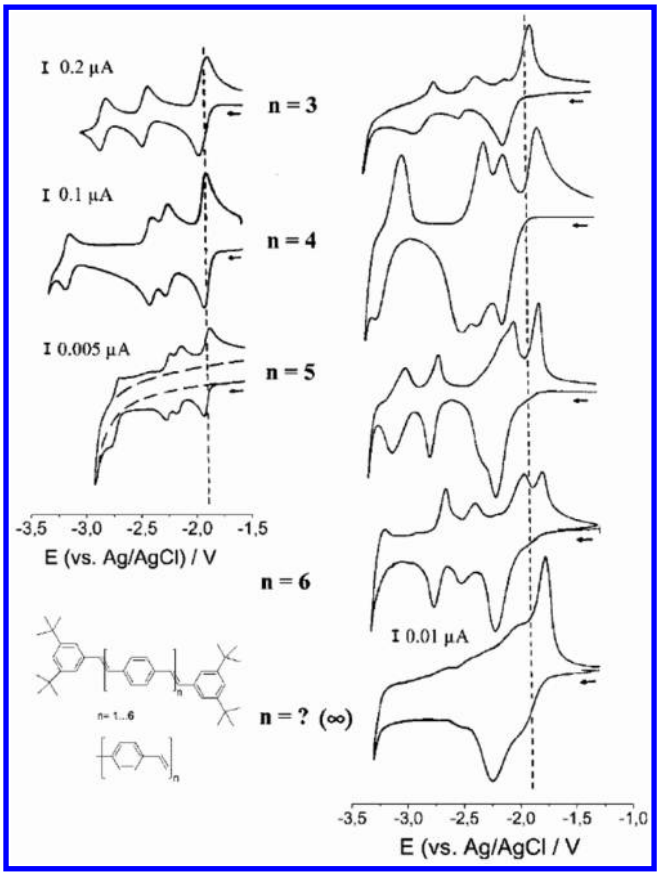

Figure 2. Cyclic voltammograms of the reduction of oligo(*p*-phenylene vinylenes) (left) in solution (T = −65 °C, ν = 100 mV s^{-1}) in THF/$TBAPF_6$, and (right) under solid state conditions (T = −65 °C, ν = 10 mV s^{-1}) in DMA/TBABr. Reprinted with permission from ref 71. Copyright 1998, John Wiley and Sons.

charged matrix; this process generates a compact structure (Figure 3). Such a doping is not equivalent to that described by the terminology utilized for classical semiconductors, where the doping species are always located in the matrix.

As previously mentioned, the anodic charging process is a sequence of discrete overlappings of the polymer's redox states that generate the capacity-like plateau observed in cyclic voltammetry. This is also observed during the reduction process, albeit with an inverse current sign (see the inset in Figure 4). Monolayers of redox deposits should ideally show

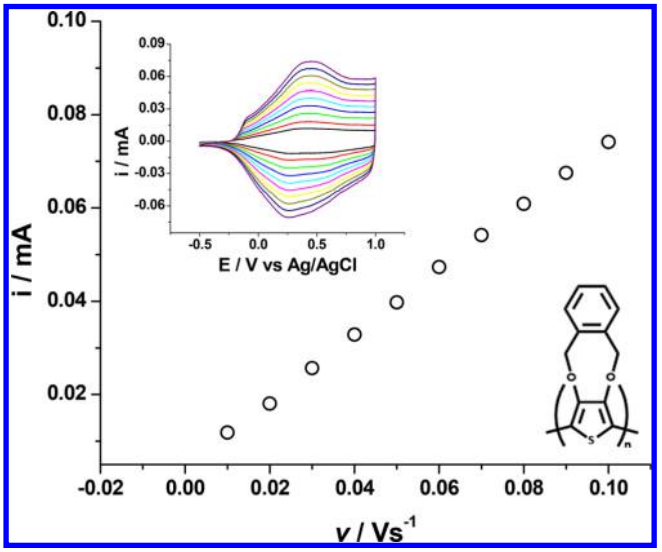

Figure 4. Peak current vs scan rate of poly(*o*-xylene dioxythiophene) (PXDOT). Inset: Cyclic voltammetry of PXDOT in ACN/0.1 M TBAP at different scan rates (50−500 mV s^{-1}).

here the specular image of the oxidation wave, and the peak current (i) should be proportional to the scan rate, ν (Figure 4).[79] As the film thickness increases, counterion diffusion into the polymer matrix becomes more difficult and the mirror image signals change to the generally observed asymmetrical shape. Also, i now is proportional to $\nu^{0.5}$, as in the case of redox species in solution, where the faradaic reaction is diffusion controlled.

During the oxidation or doping process, a fraction of the polymer will stabilize a certain number of positive charges depending on the polymeric structure and charge potential; the mole fraction of the corresponding charged monomers is the *doping level*. Typical values of doping levels are between 0.1 (i.e., one charge per every ten monomeric units, which represents a low doping level) and 0.5 (i.e., one charge per every two monomeric units, which represents a high doping level). Most of the properties summarized in Table 1 depend directly on this value, and therefore several methods for doping

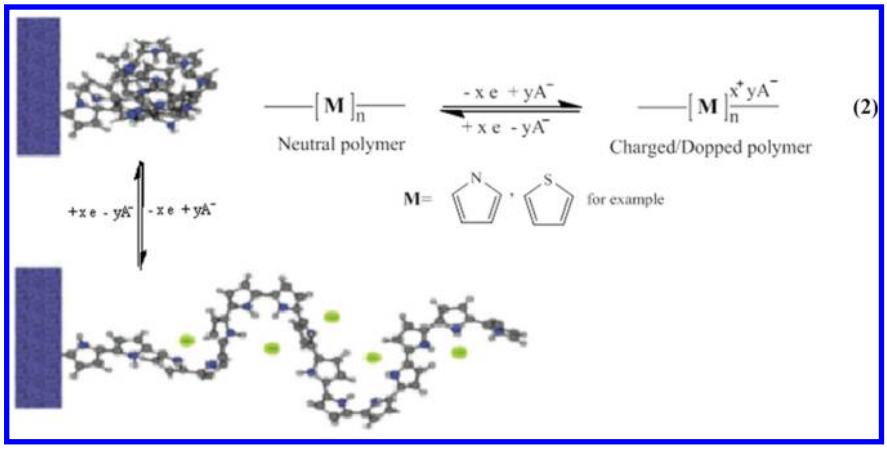

Figure 3. Structural change during the doping/dedoping process of a conducting polymer. Adapted with permission from ref 4. Copyright 2016 Royal Society of Chemistry.

DOI: 10.1021/acs.chemrev.7b00482
Chem. Rev. 2018, 118, 4731−4816

Table 1. CP Applications and Related Properties

Application	Property modified by the doping process
batteries or capacitor materials	charge
electrochromic displays	optical absorption
organic light emitting diodes	reactivity of the e^-/h^+ pairs
antistatic foils	conductivity
electronic devices	conductivity
actuators	structural change and volume
sensors	chemical or physical properties
coatings	surface tension
materials for drug release	charge and structural change
membranes	ionic conductivity
tissue engineering applications	biocompatibility, hydrophobicity
corrosion protection	equilibrium potential
compound release	diffusion and adsorption
components of organic solar cells	work function, conductivity, tunable band gap
electrocatalysis	electrochemical properties

level determination have been developed.[80−85] Beyond these values, the Coulombic repulsion dramatically increases and chemical changes (generically known as *overoxidation*) occur, thus altering the CP's normal behavior.[86,87]

In situ electron spin resonance (ESR) studies of charge and discharge processes have demonstrated that radical cations are indeed responsible for the charges in the polymer in the case of p-doping, whereas radical anion species cause n-doping. Both radical ions develop ESR signals due to their $S = 1/2$ value (Figure 5).[88,89] In the classical CP literature (and adhering to the terminology previously developed for conductive species in crystalline semiconductors),[90] these reactive species are known as *polarons* and have been proposed as intermediates for the generation of the more stable *bipolaron* species (i.e., diionic species with $S = 0$, see section 2.3). This nomenclature is still currently used despite the development of new models that explain the discrepancies of the initial band model.

2.3. Rationalizing CP Properties. Proposed Models

The conductivity in a CP is a consequence of its doped state, where positive or negative charges can move along the polymeric chain in the presence of an external potential via electron delocalization of the π-conjugated network. Different theories and their validation by experimental results have led to various models to explain the conductivity of these organic materials. Band theory is based on Hückel's molecular orbital theory (HMO) and was used at the end of the 1970s by Brédas to understand the CP properties known until then.[91,92] It has been continuously invoked to explain several CP properties.[93,94] Theoretical calculations suggest three absorption bands for the polaron and two for the bipolaron states,[92,95] and they have been experimentally observed in numerous CP absorption spectra (Figure 6).[96−99]

Despite its success for predicting optical behavior, several experiments have demonstrated that this model it is not universally valid. The model was conceived for an ideal conjugated linear polymer (i.e., an infinite number of units without defects), and therefore, as far as electronic properties are concerned, a highest occupied electron band (valence band, VB) and a lowest unoccupied band (conduction band, CB) can be proposed as a consequence. Nevertheless, recent experiments have demonstrated that electropolymerization produces materials with a finite (and low) number of monomers (i.e., less than 100 units) and that cross-linked porous materials are manly obtained (see the section 2.2). Thus, electrical conduction in these materials not only should be linear (as initially considered by the bipolaron model), but also must involve an interchain component. This can be better explained by a hopping process.[100−102] A second point in debate is the explanation of the maximum conductivity of a CP that is experimentally obtained when the charge carriers are spinless (i.e., no ESR signals); at first sight, this is in agreement with the bipolaron model. However, at high charging levels, a questionable argument arises since this model predicts a metallic behavior (i.e., higher conductivity values) due to the enlargement of the bipolaronic VB and CB. Ideally, they should merge at very high charge levels (Figure 6). This behavior has not been experimentally observed, and CPs charged at very high doping levels show a dramatic conductivity decrease (Figure 7),[103,104] which is contrary to the predictions of the bipolaron model. This conductivity drop has sometimes been associated with an overoxidation of the polymeric chain. Nevertheless, the cyclic voltammetric signals remain essentially intact.[105,106]

New models try to overcome the failures of the classical bipolaron model. The σ-dimer model has been proposed by Heinze[68,107,108] to explain the lack of ESR signal in the high-doped state, as well as the conductivity drop mentioned above. This model also explains the obvious hysteresis between the anodic doping wave and that resulting from the cathodic discharging process, which was initially attributed to changes in electron-transfer kinetics.[109,110] The hypothesis here is that the charged interchain structure is engendered during electro-

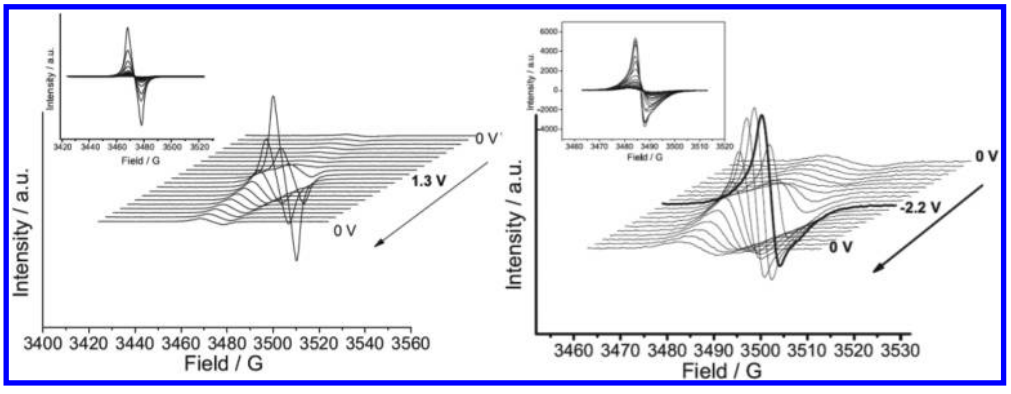

Figure 5. *In situ* ESR spectra of poly(2-methoxynaphthalene) during (left) p-doping and (right) n-doping. Adapted with permission from ref 89. Copyright 2014 Elsevier.

DOI: 10.1021/acs.chemrev.7b00482
Chem. Rev. 2018, 118, 4731−4816

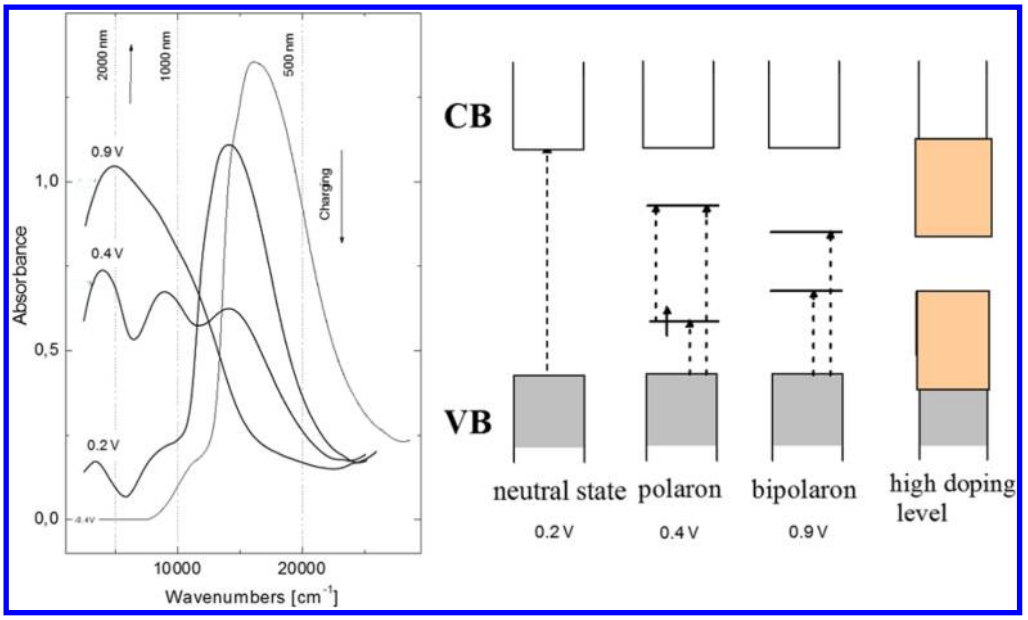

Figure 6. UV−vis−NIR spectra of poly(4,4′-dimethoxy-2,2′-bithiophene) during electrochemical charging and explanation of the observed bands following the bipolaron model. Adapted with permission from ref 99. Copyright 2007 J. Heinze.

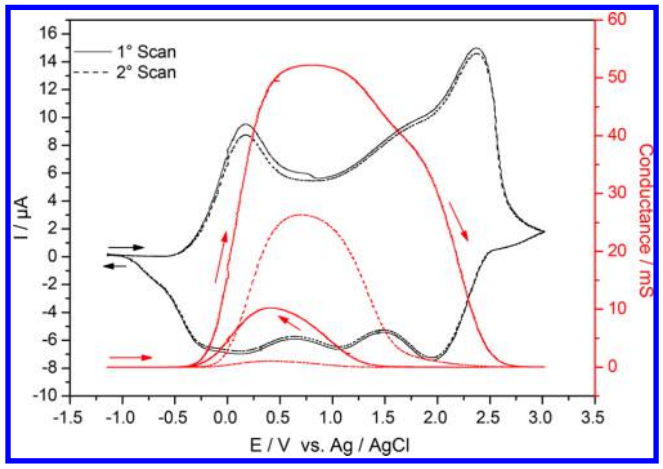

Figure 7. Cyclic voltammetry and *in situ* conductance measurements of poly(4,4′-dimethoxybithiophene) in CH_2Cl_2, 0.1 M $TBAPF_6$, v = 5 mV s^{-1}, T = 273 K. Black line, cyclic voltammogram; red line, conductance as a function of the potential measured during potentiodynamic cycling. Reproduced from ref 19. Copyright 2010 American Chemical Society.

polymerization, and charge−discharge cycles stabilize charged interchain σ-dimers (Scheme 2). These species can be formed at the higher charge level (i.e., very positive potentials) where the reactivity of the system is sufficiently high,[111] affecting the conductivity of the system and rendering the discharge of the conducting polymer difficult.[19,112]

Janssen and Brédas[113,114] made an interesting new proposal several years ago, which includes the presence of two polarons (i.e., diradicals)[115] in a singlet ground state at the oligomeric chain. Under this scheme, DFT molecular system calculations of oligomers[116] can be used instead of the solid crystalline approach (i.e., the bipolaron model) to predict spectroscopic and electronic properties. The diradical character of polyenes has been reported very recently, which is predicted by valence bond self-consistent field (VBSCF) calculations.[117] This novel approach admits that CPs should be theoretically treated as whole molecular systems using quantum chemistry,[118,119] and its expansion to the charge-transfer process has been recently developed by incorporating the structural/solvent reorganization. The predictions thus generated are equivalent to those obtained with the Marcus−Hush theory during the analysis of π-conjugated poly(*p*-phenylene) cation radicals.[120] The use of

Scheme 2. Charging−Discharging of Conducting Polymers with Formation of Interchain σ-Couplings[a]

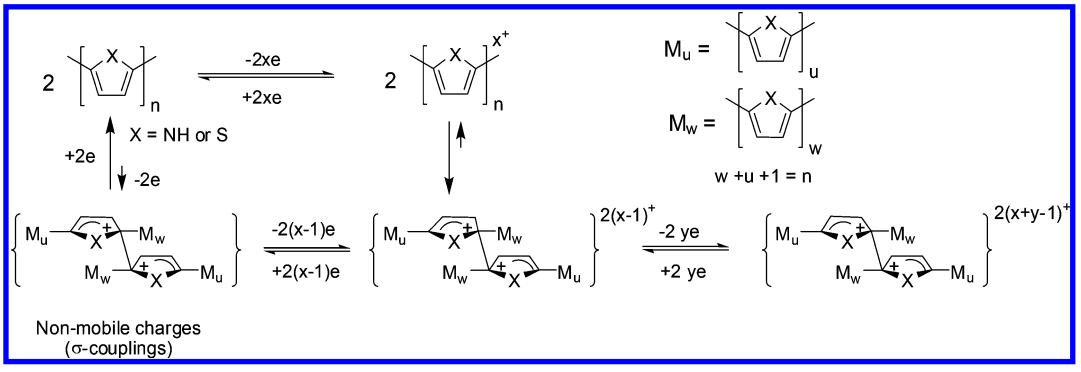

Reproduced from ref 19. Copyright 2010 American Chemical Society. [a]The exact position where the σ-coupling occurs has not been determined.

DOI: 10.1021/acs.chemrev.7b00482
Chem. Rev. 2018, 118, 4731−4816

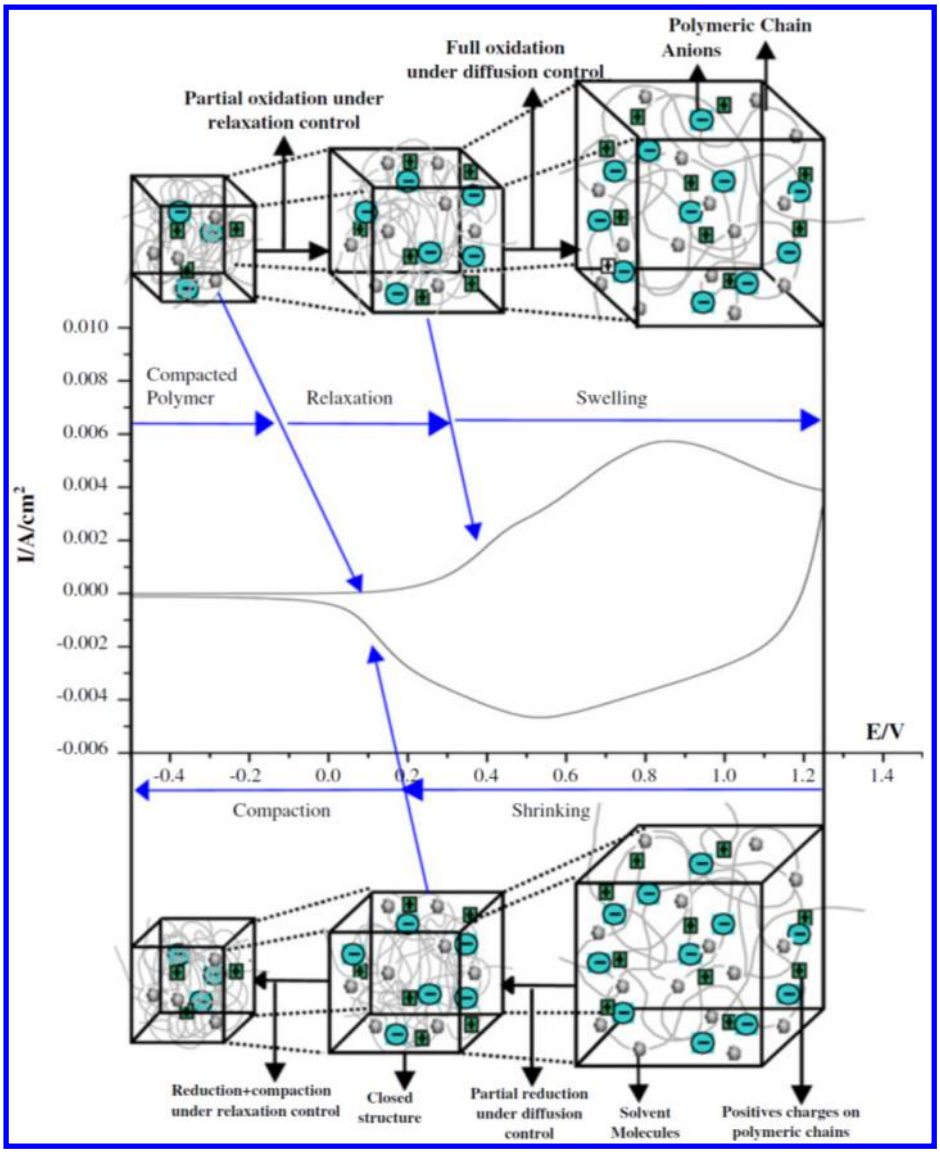

Figure 8. Voltammogram obtained with a p3-MTh film in 0.1 M $LiClO_4$–acetonitrile solutions, between −0.6 and 1.25 V vs Ag/AgCl, at 0.1 V s^{-1} and 25 °C showing the relaxation/swelling and shrinking/packing processes. Reproduced with permission from ref 131. Copyright 2007 Elsevier.

the *multiconfiguration pair-density functional theory* (MC-PDFT) allows performing calculations in conjugated oligomers with orbital-optimized active spaces up to 50 electrons and 50 orbitals, with a dynamic correlation resulting from an on-top density functional.[121] Recently, Kang and Snyder[122] analyzed together the electrical conductivity and Seebeck's coefficient of several CPs, and determined that most polymers (except possibly PEDOT:tosylate) show thermally activated and itinerant conductivities typically found in crystalline semiconductors. As a result, a new model for charge transport in CPs was developed, where the different electrical transport properties in polymers may be a consequence of the percolation of charge carriers through the polymeric materials. These recent findings confirm that the molecular treatment of the conducting polymers using powerful and modern quantum chemistry tools for the prediction of properties is a hot topic in the field of theoretical chemistry.

The conductivity and band gap in CPs have been associated with the possibility of change between the quinoid/aromatic structures along the main chain during the doping–dedoping process (see Figure 3);[143,123] both properties offer unique phenomena and functions that are exploitable in organic electronics (see sections 2.4 and 3.1.3). Associated with this structural change, a conjugated backbone planarity is an essential requisite to have low band gap polymers with high mobility charge carriers.[143] Efforts to understand the complex interplay of atomistic changes and a backbone structure toward modeling the charge transport properties have been recently made using density functional theory in π-conjugated regioregular polymers.[124,125]

In order to rationalize the structural changes of the polymeric matrix and current decay during a CP charging–discharging process, Aoki[126,127] proposed the percolation theory, while Otero developed the electrochemically stimulated conformational relaxation model (ESCR), which is widely used to understand the mechanical properties of CPs.[128,129] Both models predict a slow current logarithmic decay in chronoamperometric experiments, as is indeed experimentally observed. The slow relaxation in the percolation theory is either provoked by a slow reorganization of the polymeric matrix after the redox reaction, or by a sluggish electron transfer in the conducting polymer due to anion percolation through the

DOI: 10.1021/acs.chemrev.7b00482
Chem. Rev. 2018, 118, 4731–4816

polymer (which is required to stabilize the created charges).[130] On the other hand, the ESCR model considers that the processes that determine the redox switching kinetics in conducting polymers are (a) electronic and ionic charge transport and (b) conformational changes and swelling of the polymer induced by electrostatic repulsions among the chains, as well as the presence of counterions that stabilize the charges thus generated (Figure 8). In this model, the last process is known as *relaxation* and affects the rate of the electrochemical transformation. For this reason, relaxation may last much longer than the faradaic processes.[131] Thus, the first phenomenon proposed after the anodic perturbation into a neutral polymer is the expansion of the closed polymeric structure. Partial oxidation takes place at the very end of the polymeric electrolyte structure, where counterions can access rapidly (influenced by the electrical field and the positive charges generated in the polymer's backbone). Next, full oxidation continues toward the inner part of the open polymeric matrix, reaching the electrode−polymer interface under diffusion control. During reduction, the inverse processes take place until a full compact polymeric structure is formed. Thermodynamic and kinetic information about the charging/discharging processes is obtained using the mathematical expressions derived from the theoretical treatment of the processes involved. Thus, the ESCR model has been applied to important CP fields like organic actuators[132] and organic semiconductors.[133] Recent reviews on this subject are available.[134,135]

2.4. Other Technological Applications

Many of the interesting properties of CPs like optical response,[136−139] ionic and electronic conductivity,[140−142] surface tension, volume change, and tunable band-gaps[143,144] are direct consequences of the solid state redox reactions known as polymer charging/discharging (see section 2.1, Figure 3), and have been exploited for technological applications (Table 1). These properties can be controlled with the doping level of the material, and new possibilities for a wide range of industrial applications[145,146] are being developed. Moreover, because of their capability to be solution-processed with a large area uniformity and improved mechanical and electronic properties, their use has been extensively explored in recent years.[147−150] It is important to note that the basic charge/discharge redox reaction is possible in the different families of CPs mentioned in the introduction, but depending on the application or technological device where the CP is used, a particular oxidation state or switching between both may be required.[73,145,146]

Because of the vast quantity of information available, next we will concisely discuss the various applications, whereas those on which this review is focused (i.e., energy, environmental remediation, and sensors) are more deeply discussed in the following sections.

2.4.1. Applications in the Medical and Biological Fields. The facile modification of CPs' chemical, electrical, structural, and physical properties is a major advantage for the development of new applications. Moreover, some CPs and their composite derivatives have shown biocompatibility.[151−153] Since the seminal work of Wong et al. in 1994,[154] who demonstrated the cell growth dependence on the oxidation state of PPy, the possibility of using CPs as supports for growing cells has been explored.[151,155−159] In this direction, for example, human glioblastoma multiform cells (T98G), primary human dermal fibroblasts (hDF),[160] and Madin−Darby canine kidney (MDCK II) epithelial cells[161] were recently cultured on PEDOT:PSS films. These biointerfaces have attracted attention in the neurosciences because CPs may serve as nerve conduits, drug carriers, and neurite guidance platforms in neuroregeneration, where neuronal cells have been grown for their study on these polymers.[162,163] PPy-coated electrodes were implanted in brain tissue of mice for 3 weeks.[164] Despite the relevance of these reports, more *in vivo* studies about possible inconveniences like inflammation, cytotoxicity, and biodegradability are required before their application in humans. CPs' rigidity and fragility as well as poor solubility also limit their use, and therefore composites and blends are promising materials to overcome these problems.[151] CPs possess properties that are exploitable in biomedicine such as in biosensors (i.e., chemical and physicochemical properties), biocompatible coatings,[165−167] and tissue-engineering (i.e., ionic transport, biocompatibility, and hydrophilicity),[157,159] selective membranes (i.e., ionic and electronic conductivity),[168] neural interfaces and neural probes (i.e., ionic and electronic conductivity),[169−172] drug-delivery devices (i.e., reversible doping, see below), and bioactuators (i.e., structural changes, see below), which have been reviewed, and they highlight the potential of polythiophenes[173] and polyanilines[174] in this field.

In relation to delivery and actuator applications,[175−177] they are based on the CPs' structural changes occurring during the charging/discharging processes[132,190] (see Figure 8), which trigger the reversible movement of ions in the polymeric structure. In this way, charged drugs can be incorporated into a CP and, with electrical stimulation, a controlled dosing is achieved.[178,179] For example, risperidone,[180] nerve growth factor,[181] neurotrophin-3,[182] safranin,[183] and dexamethasone[184] have been demonstrated controlled release from PPy using this concept. Recently, CP nanostructures have also been proposed as sponge-like materials for this application,[185−188] whereby a higher electroactive surface increases the loading of bioactive molecules (Figure 9).

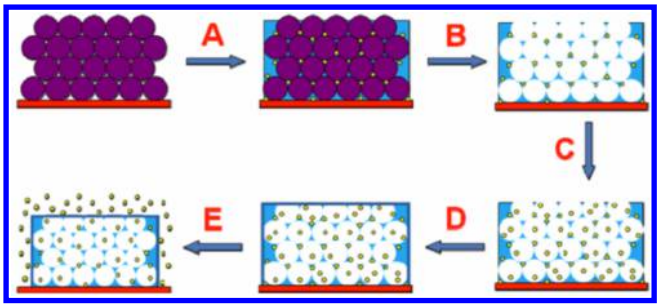

Figure 9. Schematic process of the synthesis and drug release of a nanostructured PPy film. (A) Immersion of the template-modified electrode into the pyrrole solution containing drugs and electropolymerization. (B) Dissolution of the polystyrene nanobeads. (C) Addition of an extra drug. (D) Electrodeposition of a thin PPy layer. (E) Application of a potential to release the loaded drugs. Reproduced with permission from ref 185. Copyright 2009 Elsevier.

2.4.2. Actuators. Actuators are defined as "macroscopic or microscopic devices, or polymer chains transducing energy from different sources (electric fields, electrical currents, light, temperature, pressure, and so on) into macroscopic mechanical energy by interaction with polymer films".[175] Polymeric actuators are also known in the literature as artificial muscles. They are divided into two families:[189] (a) electromechanical

DOI: 10.1021/acs.chemrev.7b00482
Chem. Rev. 2018, 118, 4731−4816

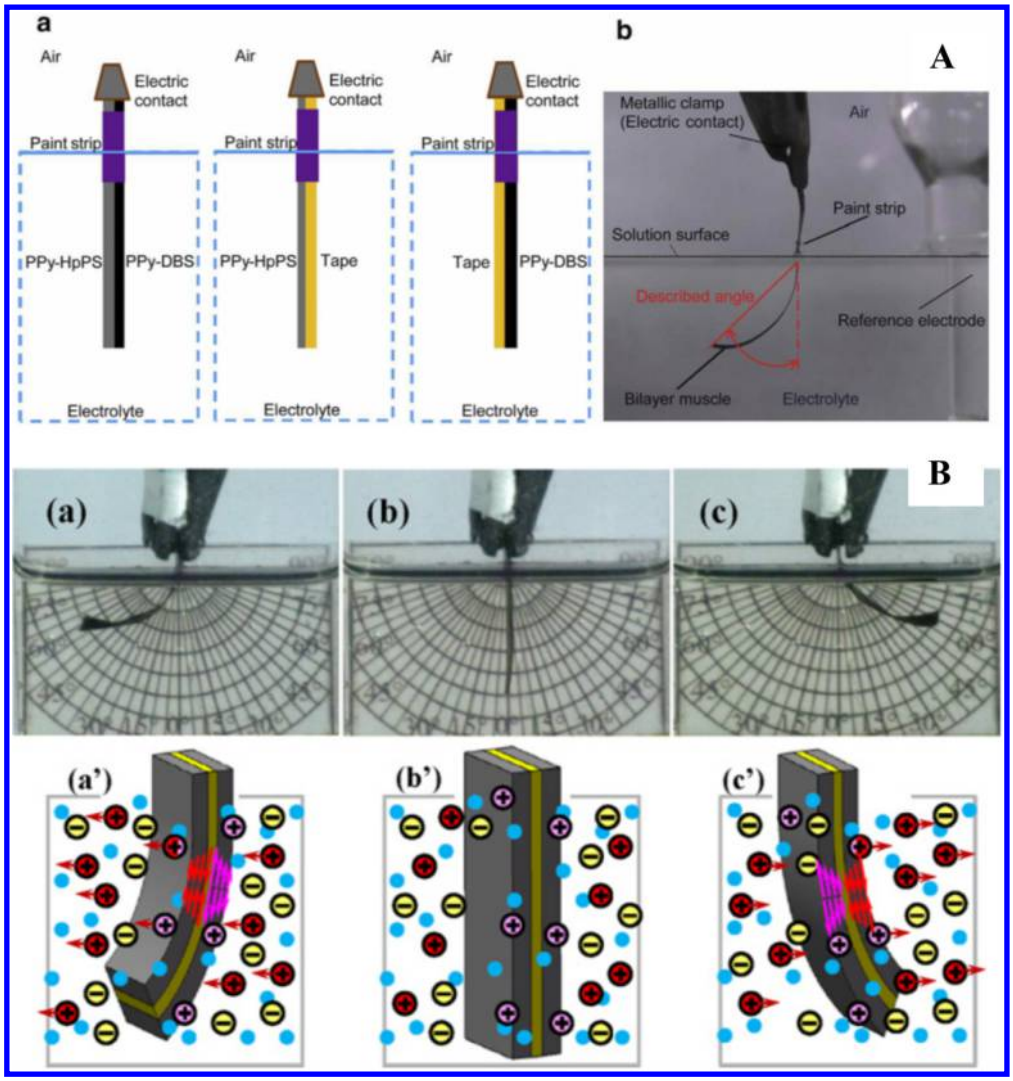

Figure 10. (A) Bilayer and (B) trilayer polymeric actuators. Adapted with permission from refs 194 and 195. Copyright 2016 and 2011 Elsevier and The Royal Society of Chemistry.

actuators and (b) electrochemomechanical actuators, where their main difference is the presence of reactive or nonreactive electrodes. As far as the electrochemical applications, the electrochemomechanical actuators are of our interest since their responses are based on the faradaic reactions and on the changes in the polymeric structures described above in the CP charging/discharging description.[132,190,191] These electrochemical actuators are typically laminated electrodes containing a simple bilayer (CP/plastic),[192] an asymmetrical bilayer (CP1/CP2),[193,194] or a triple layer (CP/plastic/CP),[195,196] where the electrical stimulus generates their bending due to the doping/dedoping process (see Figure 10A,B). CPs are used as pure or composite materials. Examples of the latter case include the silk−PPy,[197] and the silk−PANi[198] actuators, which are reported as biocompatible. Recent reviews[4,45,132,135,175,190,199,200] cover the abundant literature in this field.

2.4.3. Antistatic Foils. Antistatic materials inhibit triboelectric charging that consists of the buildup of electric charge (i.e., static electricity) by friction or contact between different materials. Static charges represent an important issue in some industries because of the possibility of flammable vapor ignition, dust attraction, or damage to electronic devices, whereby charge dissipation with suitable conducting materials may be crucial. The possibility of preparing water dispersions of conducting polymers using polyanions to balance the positive charges present in the charged structure has prompted the development of antistatic foils, widely used for packing and protection.[201] CPs are used in their doped state to take advantage of their conductivities and the relative flexibility of films obtained from water-soluble dispersions. The transparent conducting 3,4-ethylenedioxithiophene polymer with poly(styrene sulfonate) polyanions (PEDOT:PSS) is the most commonly used water-soluble polymer for this application. The Bayer and AFGA companies patented it in the 1980s as an antistatic protection for photographic films,[202] still used in our days.[203] PEDOT:PSS has a high conductivity (i.e., 300−500 S cm^{-1}), is stable under ambient conditions, and can resist up to 1000 h at 100 °C without loss of conductivity.[204,205] This principle has evolved, and now it is the basis of the buffer layer in organic and perovskite solar cells (see Organic Electronics, section 2.4.7, and also section 3.1.3). Other CP families have been studied for this application (e.g., polyanilines (PANi), polypyrroles (PPy), and polythiophenes (PTh)).[206] In addition to films, other packing materials and textiles have been proposed to fulfill market requirements.[207]

DOI: 10.1021/acs.chemrev.7b00482
Chem. Rev. 2018, 118, 4731−4816

2.4.4. Corrosion Protection. PANi,[208,209] PPy,[210] and polycarbazole[211] are the most studied CPs for the protection of ferrous materials, where diverse mechanisms like galvanic protection, ennobling, passivation, and inhibition have been enabled.[212] The most studied mechanism, galvanic protection, is based on the positive equilibrium of the p-doped CP (PPy, 0.1 to +0.3 V; PANi, +0.4 to +1.0 V; PTh, +0.8 to +1.2 V vs SHE) with respect to those corresponding to iron or aluminum (i.e., Fe^0/Fe^{2+}, −0.44; Al^0/Al_2O_3, −1.96 V vs SHE).[213] Under such conditions, a CP film should provide anodic protection similar to that obtained with Cr deposits, generally obtained from toxic Cr(VI) salts,[206] but using a nontoxic material. Nonferrous materials like zinc[214] and its alloys can also be protected against corrosion using these polymeric coatings. The most popular electrochemical techniques for the study of this protection effect include Tafel plots (i.e., potential versus log of current) obtained from linear scan voltammetry experiments (Figure 11), electrochemical impedance spectroscopy (EIS), and polarization resistance measurements.[215]

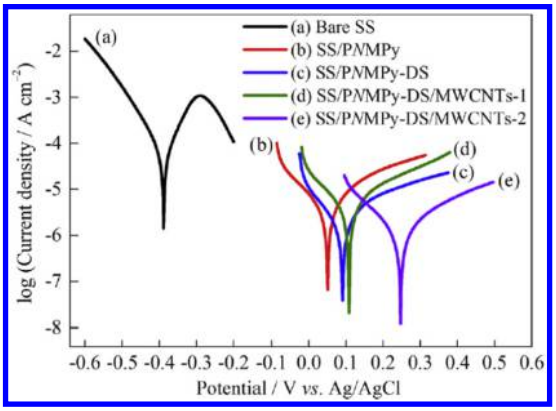

Figure 11. Tafel plots of (a) the bare SS, (b) PNMPy coating, (c) PNMPy−dodecylsulfonate (DS) coating, (d) PNMPy-DS/MWCNTs-1, and (e) PNMPy-DS/MWCNTs-2 coated SS electrodes in 0.5 M H_2SO_4. Displacements toward more anodic potentials and lower corrosion currents are evident in the CP-covered SS samples. Reproduced with permission from ref 217. Copyright 2015, Elsevier.

Not only CPs but also their composites with other conducting materials like graphite,[206,216] nanotubes,[217] and other polymeric materials are also useful to prevent metallic corrosion. Recent publications extensively describe different materials used as well as proposed mechanisms and techniques for the analysis of corrosion protection phenomena in metals.[211−213,218−222]

2.4.5. Electrochromic Devices. The delocalized π-electron band of a CP structure gives rise to its VB and CB (Figure 6). These bands define the intrinsic optical properties of such materials.[223] The bipolaron model predicts an important change in optical properties (i.e., band gap)[224] when the CP is electrochemically switched from its neutral to a charged state. This is provoked by the presence of absorption bands in different regions for each redox state and the shift between the benzenoid and quinoid structures (Figure 12). Those materials that behave in this manner are called *electrochromic*.[225,226] The basic principles of electrochromism in CPs were enunciated several years ago,[227−230] and recent revisions on the field confirm the high level of color control that some devices have reached by using mixtures of donor−acceptor (D-A) heterocyclic units in the polymer skeleton and fast switch response times (i.e., lower than ∼1 s).[231−238] Absorption wavelengths typically shift toward higher values upon doping. For example, PPy shifts from λ = 420 nm to λ = 670 nm; PANi, from $\lambda \leq$ 330 to ∼440 nm; PTh, from λ = 470 nm to λ = 730 nm; MEH−PPPV, from 510 to ∼750 nm; and PEDOT, from 590 to 900 nm (Figure 12).[130,231] Fine tuning of these changes can be obtained when using the D−A approach.[237] With these intense changes in both redox states of CPs, electrochromic windows (also called *smart windows*),[239,240] displays,[241,242] and other electrochromic devices[243,238] have been fabricated.

Their construction involves a sandwiched structure with the CP located between two sheets of conducting glass or plastic covered with a transparent inorganic conducting layer (e.g., fluorine-doped tin oxide, FTO, or indium tin oxide, ITO).[231,234] Practical applications require low cost, all-polymer electrochromic devices, and therefore plastic/PEDOT:PSS,[242,244−248] highly stable plastic/Ag-nanowires/PEDOT,[249] transparent conducting electrodes, and flexible carbon nanotube transparent conductive films[250] have been recently developed. Not only the selected polymer determines the performance of a device, but also the electrode material plays a key role.[251] Electrochromic textiles are currently under intense study, and promising results have been obtained with viscose, polyester, and Spandex fibers charged with CPs.[252]

2.4.6. Electrocatalysis. Electrocatalysis facilitates electrochemical reactions that occur at electrode surfaces by increasing electron transfer rates and enables the development of technological applications because the overall reactions require less energy (Figure 13).[253] An electrocatalyst can also be regenerated on the electrode surface and used for homogeneous electron transfer (Figure 14). These species are known as redox mediators[254] and are very useful, for example, in sensor design, CO_2 reduction,[255] and electrosynthesis. Electrocatalysis in organic synthesis allows a reduction in energy cost, avoids the use of stoichiometric quantities of redox reagents, and increases safety. Both concepts agree well with the green chemistry focus of modern synthetic organic electrochemistry.[256,257]

Most electrocatalytic materials are based on noble or precious metals or transition metal elements, either as pure electronic conducting metals or as alloys, as well as electronic semiconductors.[253] Therefore, interest in substituting expensive precious metals with cheaper organic compounds has been the subject of very active research. For example, well-defined 2D covalent organic polymers[258,259] and carbon organic frameworks[260,261] act like CPs, since they also involve π-conjugated polymeric layers containing heterocycles and aromatic moieties with precisely controlled molecular structures and empty spaces.

CPs by themselves can have intrinsic electrocatalytic properties toward certain redox reactions. It is also possible to use the interchain cavities in these materials to incorporate metals so that electrocatalysts can be generated.[262] CPs have also been used to immobilize redox mediators, thus boosting the homogeneous electron transfer in the catalytic cycle.[263−265] This approach is based on the efficient immobilization of biomolecules like proteins, enzymes, or oligonucleotides[266] through the very strong interaction with avidin via an affinity coupling with biotin.[267] For this purpose, pyrrole,[268,269] terthiophene,[270] and EDOT[271] derivatives have been explored. Heterogeneous catalysts such as metal oxides[272,273] and catalytic metal nanoparticles[274] have been incorporated to a conducting polymer matrix in order to generate a catalytic

DOI: 10.1021/acs.chemrev.7b00482
Chem. Rev. 2018, 118, 4731−4816

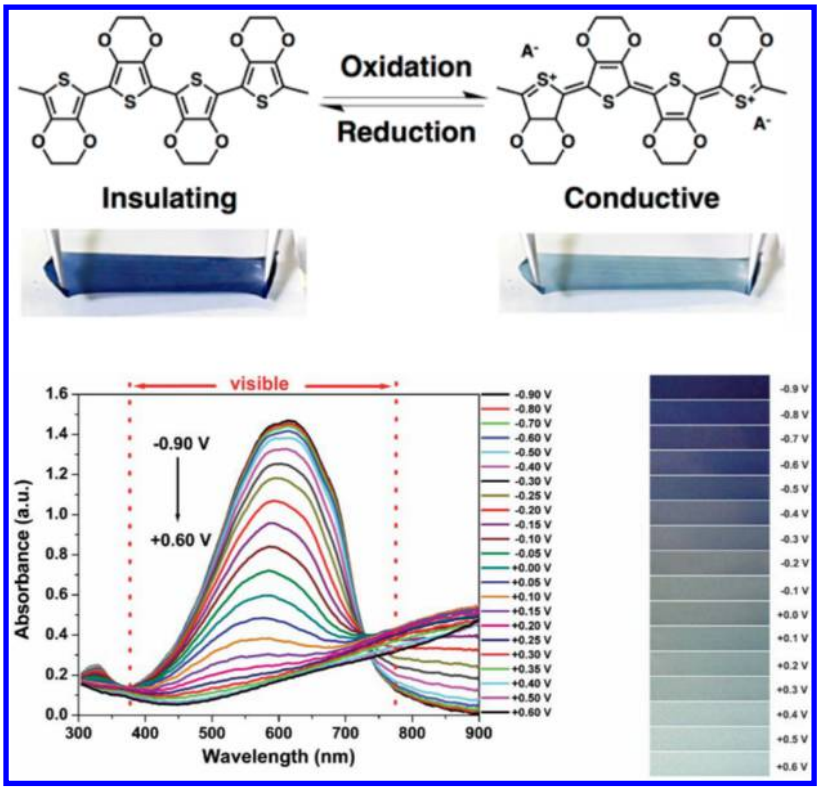

Figure 12. Electrochemical doping and dedoping processes in PEDOT. Top: Electronic structure change between neutral and oxidized states, and electrochromic color display in the stretchable support of a composite film of poly(3,4-ethylene dioxythiophene) and polyurethane. Bottom: (Left) Spectroelectrochemistry of a PEDOT film showing the optical variation in the visible region as a function of applied potential. (Right) Applied potential dependence of the blue color produced by PEDOT films. Adapted with permission from references234 and 242. Copyright 2005 and 2017, The Royal Society of Chemistry and American Chemical Society.

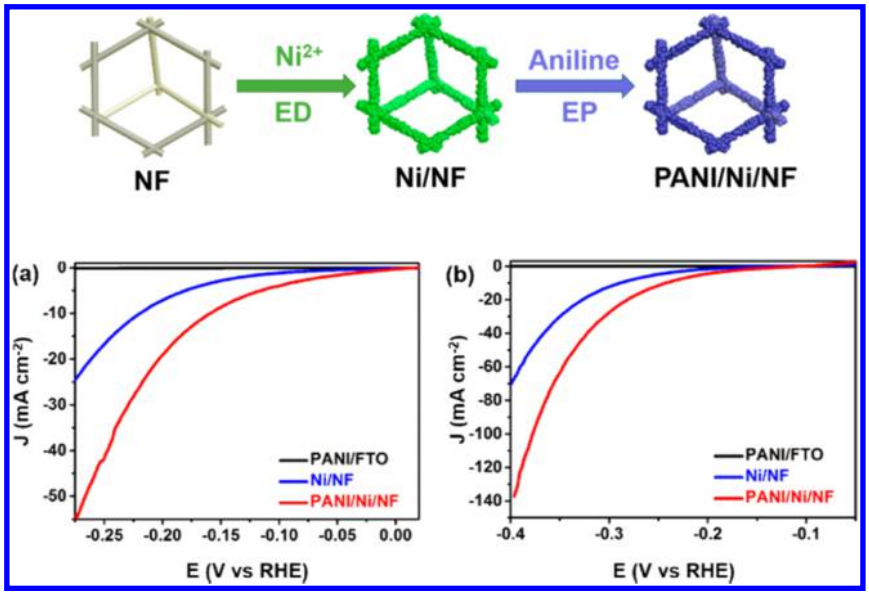

Figure 13. (top) Schematic preparation of PANi/Ni/NF (ED, electrodeposition of Ni nanoparticles; EP, electropolymerization of PANi) for catalytic H2 production. (bottom) Linear sweep voltammograms of PANi/FTO, Ni/NF, and PANi/Ni/NF collected at a scan rate of 5 mV s^{-1} in (a) 1.0 M phosphate buffer at pH = 7 and (b) 0.5 M H_2SO_4 at pH = 0. Adapted with permission from ref 281. Copyright 2018 American Chemical Society.

electrode. This is a very convenient way to decrease the particle size and maximize the surface (and therefore the noble metal loading), resulting in an enhancement of the electrocatalytic activity.[275] CPs also have potential usefulness in electrocatalytic reactions like the oxygen evolution reaction (OER),[276−278] O_2 reduction,[279,280] and hydrogen evolution reaction (HER),[276,281−283] the I_3/I^- system in dye sensitized organic solar cells (see section 3.1.3), chemosensors[284−286] (see section 4.1), and biosensors.[287−290] These reactions are typically catalyzed by precious metals,[291−293] and the use of CPs can

DOI: 10.1021/acs.chemrev.7b00482
Chem. Rev. 2018, 118, 4731−4816

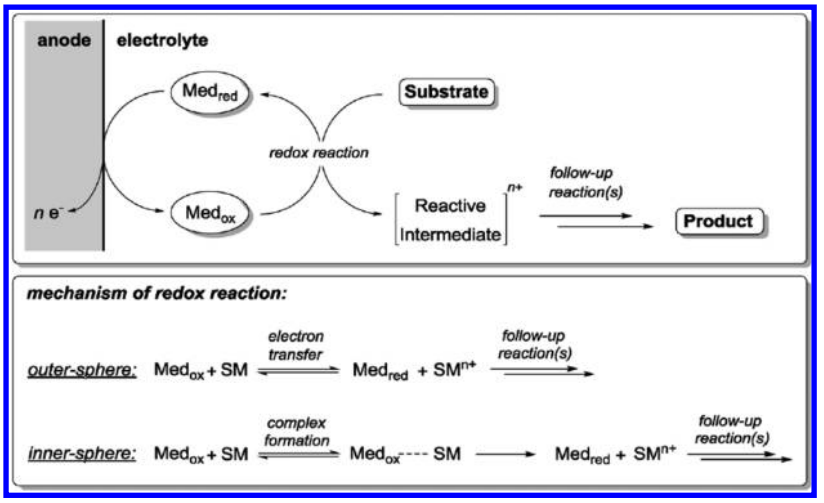

Figure 14. General principle of redox mediation (top) and possible mechanisms for the homogeneous electron transfer (bottom). Reproduced with permission from ref 254. Copyright 2014 The Royal Society of Chemistry.

trigger future industrial applications. Therefore, their high conductivity and other properties discussed earlier make them suitable as catalysts for diverse redox reactions.[279,294] Modern density functional theory methods have been employed to understand electrocatalytic reactions like OER on PEDOT.[295]

2.4.7. Organic Electronics. Organic light-emitting diodes (OLEDs), organic thin-film transistors (OTFTs), organic field-effect transistors (OFETs), and organic photovoltaic cells (OPVCs, discussed in section 3.1.3) belong to the group of devices generally named *organic electronics*.[296−298] Other interesting organic electronics like organic photodetectors,[299] flexible electronic papers,[317] and OTFT sensors[300−302] are under development for chemical and biological applications. The basic configuration of an OLED-organic solar cell (OSC) is depicted in Figure 15. Conducting polymers can behave as

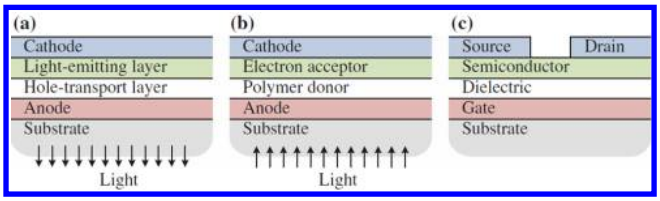

Figure 15. Schematic cross section of simple organic-based devices. (a) Organic light-emitting diode, (b) organic photovoltaic cell, and (c) organic thin-film transistor. Reproduced with permission from ref 297. Copyright 2015, Springer Nature.

semiconductors that are exploitable in these devices. Inorganic thin film devices often require high processing temperatures and energy demanding deposition methods;[303] therefore their cost is higher than that of organic materials. The opportunity to fabricate cost-effective disposable devices is now available with the organic electronics. With some soluble polymers, it is possible to use massive production processes[304] such as flexography or gravure printing;[305,306] other polymers can be electropolymerized on suitable electrode surfaces to fabricate a device.[307−310] For example, an OPVC can be 2D-printed or roll-to-roll processed, thus making its mass production rather attractive.[311,312] 3D-printing techniques have also been explored to design new architectures for these electronic components.[313] CVD also yields excellent polymeric deposits with fine-tuned morphology.[314]

Most of the CPs can be used in their undoped states as organic semiconductors because they intrinsically possess this property.[315,316] Their characteristics and performance are obviously related to the structure and the nature of the molecules used in their fabrication.[317,318] PEDOT:PSS has also been used as a flexible electrode in these devices[242,244−248,317,319] or as an anode buffer in OPVCs[320] and perovskite cells.[320,321]

OLEDs were initially proposed in 1987 by Tang and Van Slyke.[322] Their basic structure includes two organic semiconductor thin films (i.e., hole-transporting and light-emitting layers) sandwiched between the transparent electrodes (Figure 15a). The two organic layers create a pn-junction, while an external voltage generates holes and electrons in the structure; the recombination of these species emits light.[323] Modern preparation methods include solution-processable organic materials, among which ionic organic semiconductors (based on conjugated polymers) have proven to be very efficient.[324] On the other hand, an organic thin film transistor (OTFT) is a transistor that uses an organic compound in the semiconducting channel. Tsumura was the first to show the potential use of organic semiconductors (i.e., polythiophene) for this application.[325] The basic structure of an OTFT (Figure 15c) consists of a three-terminal device (gate, source, and drain) of four thin-film layers deposited on an insulating substrate;[326,327] its behavior is also described by the equations deduced for the metal oxide field effect transistor.[328] Since the first report in 1986, diverse organic materials have been explored as semiconductors for their fabrication and have been extensively reviewed in the literature.[329] These electronics work as voltage controlled-current sources whereby, upon application of a bias voltage between the gate and source, mobile charge carriers accumulate near the semiconductor/insulator interface. This phenomenon provokes a current flow through the layers when a suitable drain-to-source potential is applied.[327,329] OTFTs have been used in radio frequency identification tags (RFID), printed memories, backplanes for mechanically flexible displays, thin flexible tactile sensors, and organic inverter circuits.[297,329]

2.4.8. Future Applications. Conductivity or any of the other key properties of CPs are not enough to place organic electronics or their technological devices in the real market. Other important aspects such as the quality of the electrical

DOI: 10.1021/acs.chemrev.7b00482
Chem. Rev. 2018, 118, 4731−4816

contact between the conducting polymer and the electronic conductor,[330,331] controlled and optimized morphology,[332−336] and enhanced stability[337,338] will surely open the door to commercial organic electronic devices containing conducting polymers and organic semiconductors. Excellent reviews have been published recently for each of the applications described above. New uses for CPs like synthetic mimics for cosmic dust and micrometeorites in space science,[339] organic heaters, and resistances,[340,341] as well as new studies directed to find better performance of known properties are new and rich fields of research in this area. For example, CP conductivity has been manipulated with cosolvents, where the most prominent example studied until now has been the technologically relevant poly(3,4-ethylene dioxythiophene) (PEDOT).[204,417] This CP has an intrinsic conductivity around 300 S cm^{-1}, which can be significantly enhanced to more than 2000 S cm^{-1} by the addition of ionic liquids and surfactants, salts, zwitterions, or acids.[342,343] A surprising increase in conductivity of PEDOT:PSS films to more than 4000 S cm^{-1} (which is comparable to that of ITO electrodes) was reported after post-treatment with H_2SO_4.[344] One can therefore predict that the coming years will see a promising future for conductive polymers with new and interesting results in basic and applied science.

3. PART 1. APPLICATIONS THAT TAKE ADVANTAGE OF THE TRIDIMENSIONAL STRUCTURE OF THE CONDUCTING POLYMER.

3.1. Applications of Conducting Polymers in Energy

This section will provide the basic definitions and fundamentals to understand state of the art of conducting polymers (CPs) in energy-related applications, particularly those related to electrochemical energy storage and photovoltaic conversion.

3.1.1. Introduction to Energy Storage Devices. Energy storage devices can be classified in terms of specific energy (Wh/kg) and specific power (W/kg) using the Ragone plot.[345,346] In this plot (Figure 16), conventional capacitors have the highest specific power and the lowest specific energy, due to the fast electrostatic charging and discharging of the electrodes; charge is stored physically through the reversible adsorption/desorption of ions from the electrolyte onto the electrode surface. Batteries and fuel cells, on the other hand, have the highest specific energy and lowest specific power due to the reaction kinetics and mass transfer issues brought out by the faradaic oxidation/reduction reactions occurring during storage.

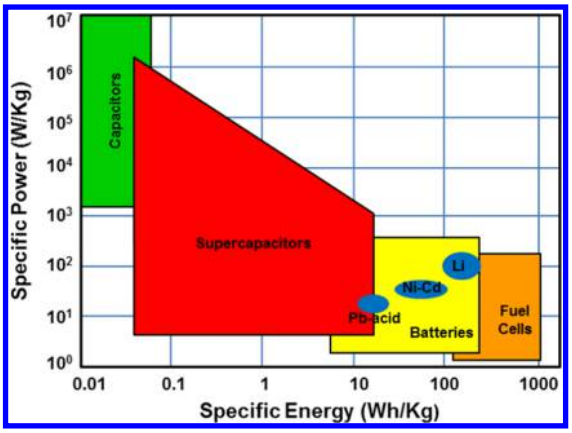

Figure 16. Ragone plot for typical energy storage devices.

Supercapacitors have charge storage mechanisms that give orders of magnitude improvement in capacitance (and energy density) when compared to conventional capacitors. In double-layer supercapacitors, the sources of improvement are large surface areas and minimal magnitude of charge separation. For supercapacitors showing faradic capacitance (i.e., pseudocapacitance), two processes have been proposed:[347] (a) redox reactions where the potential depends on the initial and final redox species and (b) two-dimensional underpotential deposition. The former is the source of enhancement in CPs showing high gravimetric and volumetric pseudocapacitance that usually refer to reversible redox reactions at the electrode/electrolyte interface (i.e., no diffusion-control). It is worth mentioning the similarity to ion diffusion in battery materials, where the injection of electrons in a bulk electroactive phase is balanced by the diffusion of naked ions in vacant lattice sites, including the capacity contribution of unsolvated ions in ultramicropores (pore size <1 nm). The latter has been a major contribution to the field of double-layer supercapacitors and has been discussed thoroughly by Dubal et al.[348]

Hybridization of supercapacitors and batteries has been a subject of increasing importance in the past decade, and the definition and classification of the various combinations of materials, electrodes, devices, and metrics can be found in the published literature.[349,350,348] The subject is too broad for this contribution, although hybrid materials will be discussed in the context of device performance.

3.1.1.1. Metrics. The metrics used to evaluate electrochemical energy storage devices are usually specific capacitance and energy and power densities. For ideal electrochemical double layer capacitors (EDLC), the specific capacitance (F/g) is calculated from the slope of the galvanostatic charge/discharge curves (see Figure 17a). The energy stored in these devices can be expressed as $E = 1/2(CV^2)$, and the maximum power delivered is $P_{max} = V^2/(4R)$, where C is the overall cell capacitance, V is the cell voltage, and R is the equivalent series resistance. For pseudocapacitors, nonlinearity appears in the galvanostatic charge/discharge curves as shown in Figure 17b, and different calculations (i.e., integration) must be adapted to obtain adequate information.[351−355] For EDLC, $C = It/\Delta E$, where I is the applied constant current in amperes and t is the discharge time in seconds, which corresponds to the interval between the initial state of discharge (t_0) and the total discharge state (t_f).

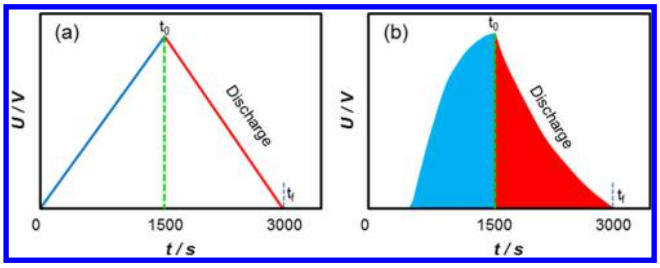

Figure 17. Schematic representation of galvanostatic charge−discharge characteristics in electrochemical double layer (a) capacitors and (b) supercapacitors.

Lithium-ion batteries (LIBs) use different metrics to evaluate performance, namely, the lithium storage or discharge capacity, measured in mAh/g, the discharge rate capability of the cells

DOI: 10.1021/acs.chemrev.7b00482
Chem. Rev. 2018, 118, 4731−4816

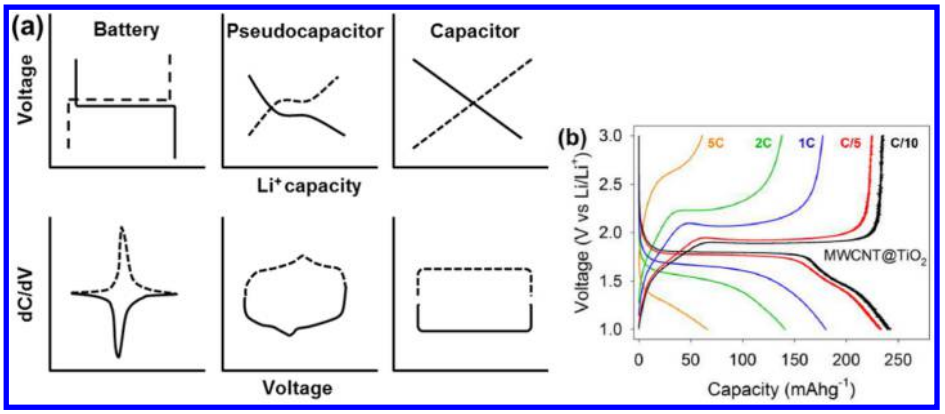

Figure 18. (a) Idealized voltage and differential capacity (dC/dV) profiles for three basic charge-storage mechanisms and (b) charge−discharge curves at different rates for MWCNT@TiO_2 core@shell composites. Reproduced with permission from ref 357. Copyright 2014 Elsevier.

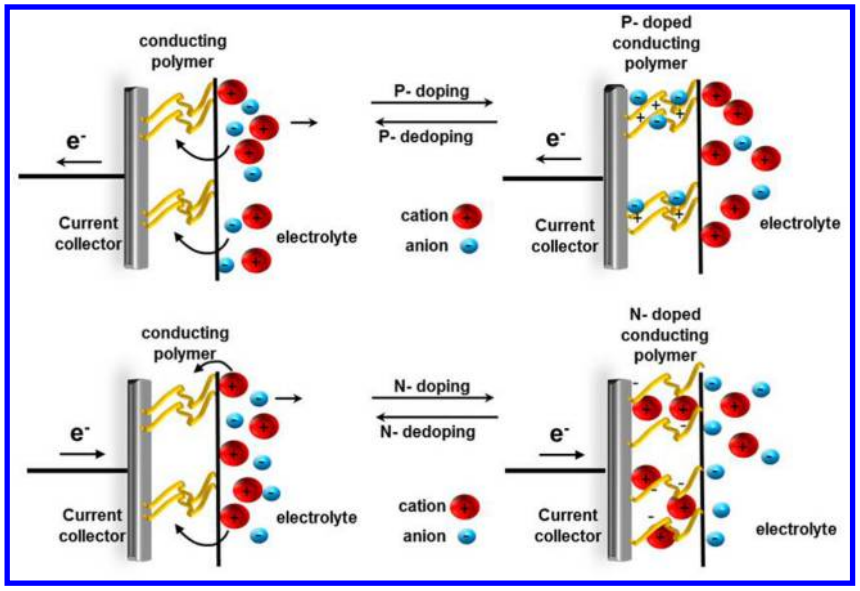

Figure 19. Charge/discharge process in p-doped and n-doped polymeric electrodes, showing the swelling effect. Adapted with permission from ref 386. Copyright 1999, Springer Nature.

measured by the capacity retention at high C-rate discharge, the Coulombic efficiency, and the long-term stability. For electrodes having battery-like behavior, the proper term is *capacity*, since the redox electrolyte interface displays *capacity* instead of *capacitance*.[356] Figure 18 depicts the idealized voltage and differential capacity profiles for three basic charge storage mechanisms, as well as the low rate capability of MWCNT@TiO_2 LIBs anodes.[357] C-rate refers to the full charge or discharge of a cell in a particular period of time: 1C = 1 h, 10C = 0.1 h, 0.1C = 10 h.

3.1.1.2. Nanocomposites and Hybrid Materials Based on CPs. Energy storage devices require electrode materials with good electronic conductivity to deliver maximum power. As a result, CPs are very attractive due to their broad range of conductivities, from that of semiconductors (10^{-11} to 10^{-3} S cm^{-1}) to that of metals (10^{-1} to 10^{6} S cm^{-1}).[3] Charge storage can be enhanced by controlling the synthetic parameters (i.e., doping agent, temperature, pH) or by designing different morphologies,[358] with the aim of improving electronic conductivity, surface area, and redox activity.

Recent reviews[359] emphasize the development of CP-based materials for energy storage applications. The work of various authors[360−364] demonstrating the relationship between CP morphology and capacitance have led to the conclusion that the higher the aspect ratio of the CP nanostructure (they studied PANi nanospheres, nanorods, and nanofibers), the higher the specific capacitance. One example involves the hierarchically nanostructured conductive polymer gels, which have attracted attention in this field.[365] The enhancement is due to the increase in the level of oxidation/protonation of PANi, faster electrode kinetics, and higher surface area as the aspect ratio increases. PANi nanotubes showed a specific capacitance of 896 F/g at 10 A/g[361] and cycling stability over 5000 cycles.[362−364] The dependence of CP pseudocapacitance on the size and packing of the CP nanoparticles has also been reviewed,[366] leading to the conclusion that controlling the size and morphology of the CP does not improve its performance beyond an intrinsic limit. In general, conductive polymers are attractive in energy storage devices due to their high charge/discharge cycling rate, high conductivity, large surface area, high specific capacitance, and good redox reversibility.

Conventional methods for preparing CP materials for electrode fabrication can be electrochemical or chemical in nature. Conducting polymers electrochemically synthesized directly on the current collectors as thin layers can have high electric conductivity and controlled doping level, as well as

DOI: 10.1021/acs.chemrev.7b00482
Chem. Rev. 2018, 118, 4731−4816

different morphologies.[367−373] Chemical routes, on the other hand, give polymers with low solubility and moderate conductivity.[374,375] See sections 2.1 and 2.2 for details about the mechanisms of the electrochemical polymerization.

Swelling and mechanical stress during cycling (Figure 3) constitute the main problems of CPs in electrochemical energy storage. Usually, ions in the electrolyte must go in to and out of the bulk of the polymer many times to participate in faradaic and non-faradaic processes, as schematically shown in Figure 19. As a consequence, intense research on electrode materials based on CPs bets on the synergetic effect of nanocomposites or hybrid materials, as well as on the use of large heteropolyanions as doping agents. For supercapacitors, electrodes based on graphene (GR)/CP nanocomposites are dominated by polypyrrole (PPy) and polyaniline (PANi).[376−380] Graphene/polypyrrole (GR/PPy) composites have values near 300 F/g and good cyclability (i.e., 90% capacity retention after 500 charge−discharge cycles),[376,377] which are lower than the values obtained for nanocomposites based on (GR/PANi),[378−381] where a record of 1126 F/g with 84% retention after 1000 cycles was obtained for a nanostructured GR/PANi hybrid material.[381] Interestingly, the micromorphology of the PANi between the graphene layers was highly dependent on the dispersion medium.[359] Recent works related to PANi and PPy with carbon nanomaterials have addressed the interplay of heterogeneous electron transfer, electric double layers, and mechanical stability, as well as the importance of nanoscale blending and the use of free-standing membranes.[382−385]

To obtain improved properties, a large number of recent works related to CP nanocomposites focused on CP and metal oxides,[387−390] with most of the faradaic storage occurring in the oxide. In these composites, the CPs act as binding agents providing mechanical stability, porosity, and conductivity. In this context, recent trends include (i) triple hybrid nanocomposites of carbon−CP−metal oxide,[391−393] (ii) atomic layer deposition (ALD) coatings,[394,395] and (iii) polyoxometalates (POMs).[396−399]

ALD involves the conformal deposition of nanoscale thin films and surface layers down to atomic layers with high uniformity and well-controllable thickness and interface, leading to the enhancement of device performance.[394] ALD surface modification is most effective in battery-like electrodes, particularly LIB electrodes. It can effectively suppress the side reactions and prevent the decomposition of the solid electrolyte interface (SEI) by acting as an artificial SEI that provides protection toward further degradation. As an example, an ALD RuO_2 layer on PANi nanowire surface, forming a PANi@RuO_2 core@shell nanostructure, shows improvements in capacity, rate capability, and cycling stability.[395]

Polyoxometalates are a large class of metal oxygen clusters of the early transition elements and some of the most promising building blocks for nanocomposites.[396] Regarding composites based on CPs and polyoxometalates (POMs), they are very promising in energy storage applications because the fast reversible redox reactions of POMs can be combined with the intrinsic redox activity of CPs.[397−399] These composites can be used to enhance the discharge capacity of LIBs and increase the energy density of electrochemical capacitors. They can also improve the structural reversibility, as they cannot be expelled to the surrounding solution during doping−dedoping. Charge compensation during the redox process of CPs proceeds mainly with the participation of small solution cations causing minimum induced mechanical tension. Preparation of PANi−POM nanofibers shows remarkable improvements when compared to the bulk material, particularly on cycling stability.[400] Nevertheless, methods are still needed to have more control over the microstructure of the hybrid material. The most common method involves the chemical or electrochemical oxidation of a monomer molecule to form a polymer film in the presence of a POM solution. The strong oxidizing power, high ionic conductivity, and acidic character of heteropolyacids provide the ideal conditions for the polymerizations of monomers like aniline, thiophene, and pyrrole. The result is a hybrid material in which the CP matrix is doped with the trapped POM molecule.[397]

3.1.2. CPs in Energy Storage Devices. *3.1.2.1. CPs in Supercapacitors.* Supercapacitor cells assembled with CPs electrodes can be classified as follows:[401]

- Type I (symmetric): The cell is assembled with electrodes elaborated with the same p-doped polymer in a configuration known as *symmetric assembly*.
- Type II (asymmetric): The cell is assembled with electrodes having different chemical polymeric structure but with the same oxidation state (p-doped).
- Type III (symmetric): The cell is assembled with electrodes made with the same polymer, but one is oxidized (p-doped) and the other one is reduced (n-doped).
- Type IV (asymmetric): The cell is assembled with electrodes having different chemical polymeric structure where one is p-doped and the other one is n-doped.

Each type of supercapacitor offers a different operational voltage window due to the nature of the electrode materials and the electrolytes. Types I and II work with either organic or aqueous electrolytes, reaching up to 2.4 and 1.25 V, respectively.[370−372] Types III and IV require organic electrolytes, since the operational voltage window can reach up to 3 V.[371,402−404] Asymmetric Type IV cells are the most promising supercapacitors in terms of energy and power density, although the main drawback is the difficulty to obtain n-doped polymers in an efficient way. The Ragone plot of different energy storage devices, showing the tendency to retain specific power using asymmetric devices in aqueous electrolyte, is depicted in Figure 1 of ref 348.

Asymmetric cells are usually assembled with one double-layer-type carbon material and a pseudocapacitive material or battery-type electrode, as shown in Figure 16 and Figure 20.

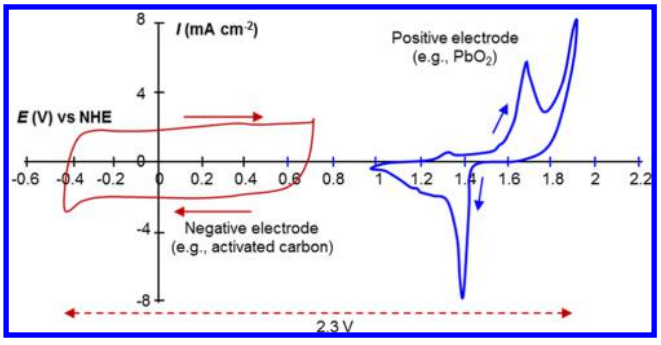

Figure 20. Schematic representation of cyclic voltammograms for asymmetric supercapacitors. The potential window of each electrode is plotted in different color. Adapted with permission from ref 411. Copyright 2010 Cambridge University Press.

DOI: 10.1021/acs.chemrev.7b00482
Chem. Rev. 2018, 118, 4731−4816

One electrode stores charge through a reversible non-faradaic process that is reflected in high specific power values, while the other electrode uses reversible faradaic reactions (i.e., fast redox reactions) to increase the capacity and specific energy of the device.[405,406] This asymmetric assembly concept extends the effective operational voltage window, resulting in a higher specific energy relative to EDLC, and provides a higher specific power relative to conventional battery systems because of the low internal resistance. To improve the cyclability in asymmetric assembly supercapacitors based on CPs, C/CP nanocomposites are preferred.[407−409] Moreover, a longer cycle life is obtained by using a carbon material in the negative electrode and a nanocomposite material in the positive electrode. The information included here can be completed with that in refs 410 and348, which are comprehensive reviews on the various materials used as supercapacitors besides conducting polymers.

3.1.2.2. CPs in Batteries. Taking into account that the desired characteristics in an electrode material are (1) electrochemical stability, (2) high specific capacity, and (3) a cost-effective preparation method, CPs are attractive because they are conductive, low cost, lightweight, and mechanically flexible. CPs improve the performance of electrode materials since they can accommodate large volume variations in large capacity oxides during the charge/discharge process. Usually, the redox process is associated with a phase change where the potential remains constant and follows the Nernst equation. Several strategies to offset the low charge transfer kinetics of the redox process involve decreasing the oxide particle size, controlling its morphology, and introducing highly conductive materials such as CPs. Reducing the size reduces the diffusion path of charge compensated ions in the solid state, but it could also enhance spurious reactions with the electrolyte.[348] Liang et al.[412] prepared a composite with SnO_2 loading on the surface of PANi−rGRO (reduced graphene oxide) by hydrothermal synthesis and used it as an anode for LIBs, obtaining 574 mAh/g after 50 cycles with a current density of 156 mA/g between 0.01 and 3 V. This approach combined an oxide, a CP, and an intercalation compound into a hybrid nanostructured composite material, where the various components are integrated at a molecular level through strong and weak interactions (i.e., covalent, ionic, hydrogen-bonding, or van der Waals interactions). Electroactive hybrid materials provide the opportunity to have faradic and capacitive activities displayed in parallel and merged together for improved performance.[348] Widespread efforts for more cost-effective preparation methods and higher current densities (1000 mA/g) are exemplified by the work of Ye et al.,[392] where mechanochemically synthesized SnO_2/GR, followed by in situ polymerization of PANi, was explored. In these studies, the optimal structure contained PANi nanofibers as conductive bridges and a relatively large surface area, exhibiting stable cycling stability through 100 cycles and excellent charge−discharge rates.[392]

Regarding the use of CPs as cathodes for LIBs, only a few studies are available. Among them, three different morphologies of PPy (i.e., nanotubes, nanofibers, and urchins) obtained from the reactive template route were tested as cathode materials for LIBs. The Li/PPy cell with $LiPF_6$ as the electrolyte showed a capacity of 70.82 mAh/g at a rate of 0.1 C with good cycling stability and rate capability.[413] PPy was reversibly switched between its oxidized and reduced states, releasing and gaining PF_6^- to keep neutrality. Other PPy based cathodes with lower capacities and cycling stability were reported by Park[414] and Qie,[415] respectively. CPs hold more promise as cathode materials in new types of batteries such as Li−S batteries.

3.1.2.3. CPs in Flexible Integrated Energy Systems. The performance of CPs in energy storage devices depends not only on their intrinsic properties but also on the microstructure and composition of the nanostructured or hybrid electrode. As described above, they have been used as a source of pseudocapacitance, as dispersants and binding agents of more electroactive materials, as conductive paths, as electroactive materials, and as bridging contacts in LIB anodes and cathodes. Still, an emergent area of research is that related to flexible fiber-shaped energy storage devices. They meet the demands of modern electronics in terms of flexibility, wearability, and light weight and have recently embraced emerging wire-shaped integrated energy systems, combining energy storage[416,417] and solar cells.[418] One simple design consists of two fiber electrodes based on poly(3,4-ethylene dioxythiophene) (PEDOT) coated carbon nanotube (CNT) yarn, gel electrolyte, and a flexible substrate,[419] as shown in Figure 21.[420] More complex structures

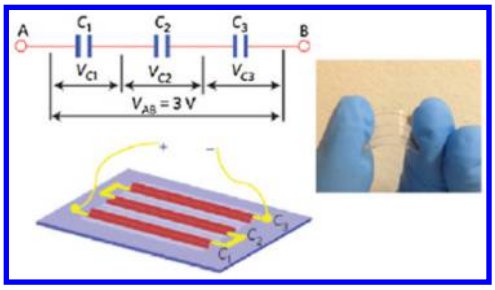

Figure 21. Planar-shaped fiber SC assembly of multiple microfibers in micro-SCs. Reproduced with permission from ref 420. Copyright 2014 Springer Nature.

based on PPy-MnO_2/single-walled carbon nanotubes (SWCNTs) on carbon fibers exhibit excellent mechanical stability but low capacitance,[421] evidencing the need for new architectures that could take advantage of the peculiarities of the active materials. For flexible integrated systems, only a few integrated energy devices realizing both energy conversion and energy storage have been reported;[422,423] still, true integration must contain energy conversion, energy storage, and the powering of some device as depicted in Figure 22.[420] A reasonable 2.1% overall energy conversion efficiency was obtained by integrating an energy wire with PANi/PANi and PANi/TiO_2 coated on a stainless steel wire as a supercapacitor and as a dye-sensitized solar cell, respectively.[422] More recently, a coaxial construction was reported with a polymer solar cell

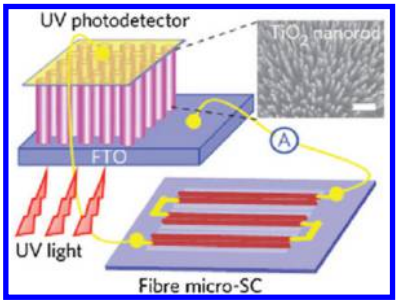

Figure 22. Schematics of a self-powered photodetector (i.e., powered by a fiber micro-supercapacitor). Reproduced with permission from ref 420. Copyright 2014, Springer Nature.

DOI: 10.1021/acs.chemrev.7b00482
Chem. Rev. 2018, 118, 4731−4816

based on poly(3-hexylthiopene) (P3HT):[6,6]-phenyl-C_{60}-butyric acid methyl ester (PCBM) fabricated on one part of a TiO_2 nanotube-modified Ti wire, and a supercapacitor made from CNT sheets attached on another part.[423]

3.1.3. Applications of CPs in Solar Cells. CPs have been identified as promising alternatives in dye-sensitized solar cells (DSSCs), organic solar cells (OSCs), organic–polymer tandem solar cells (TSCs), and more recently in perovskite solar cells (PeSCs) due to their unique optoelectronic properties. Commonly, polythiophene (PT), poly(3,4-ethylene dioxythiophene), poly(3-hexylthiopene), PANi, poly(phenylvinylene) (PPV), and PPy are the most used CPs to fabricate the distinct layers in solar cells. This section reviews the different approaches used in the development of efficient DSSCs and OSCs based on CPs and provides several comprehensive reviews and book chapters as references addressing the subjects of CPs in perovskite solar cells in more detail.

3.1.3.1. Dye-Sensitized Solar Cells (DSSCs). A solar cell is a photovoltaic device that generates electrical energy from light (Figure 23). Particularly, a DSSC consists of a wide band gap

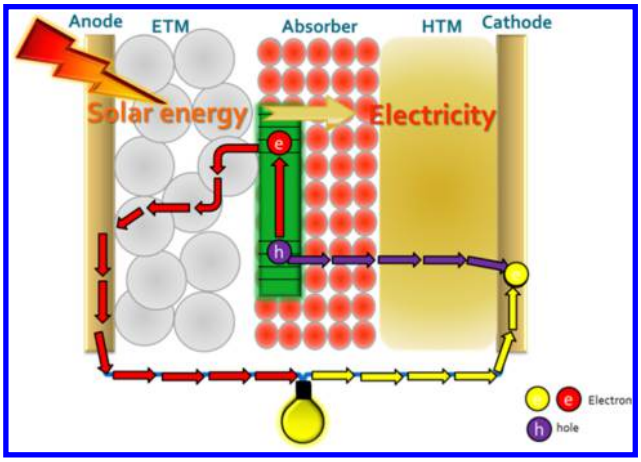

Figure 23. Schematic of a solar cell for photovoltaic conversion in dye-sensitized solar cells.

semiconductor deposited onto a transparent conductive oxide (TCO) glass to form the electron transport material (ETM). Then, a dye molecule monolayer is anchored to the surface of the semiconductor as the photoactive layer, which absorbs light in the visible region and transfers the photoexcited charges to the electron- and hole-conducting materials. The hole transport material (HTM) is a redox-coupled electrolyte, typically iodide/triiodide ions (I^-/I_3^-), in contact with a cathode or counter electrode (CE) where the reduction of the oxidized donor takes place.

The exceptional optical and electrical properties of composites based on CPs allow them to be employed as CE[424] or ETM,[425] as well as HTM and sensitizers in DSSCs.[426,427] Nowadays, the development of CEs for DSSCs plays a crucial role in the final photovoltaic performance of the solar cells. Although Pt is still the most preferred material as CE because of its conductivity and outstanding catalytic properties,[428] it is necessary to find alternative low-cost and noble metal-free materials to replace Pt in DSSCs, and conducting polymers seem to have interesting potential.[429−433] Among the requirements for CP materials to act as CEs in DSSCs are good ohmic contacts, low overvoltage for the reduction of the redox couple, and excellent chemical stability in the presence of ionic electrolytes.[434−436] The electrocatalytic activity is performed by the following electrochemical redox reactions at the CE surface:

$$I_3^- + 2e^- \rightleftharpoons 3I^- \quad (3)$$

$$3I_2 + 2e^- \rightleftharpoons 2I_3^- \quad (4)$$

One suitable candidate for CE is PANi, which presents high conductivity, good chemical and electrical stabilities, and catalytic activity for I_3^-. PANi-nanoparticle CEs with highly porous surface area have been explored in the literature.[437−439] CE films composed of compact and scattered layers of PANi nanoparticles show an increment on the active reaction interface and a decrease in the interfacial charge transfer resistance. The potential peak separation of I_3^-/I^- (I_2/I^-) for a PANi CE was comparable to that for a Pt CE, indicating that the PANi film was electrochemically active for the triiodide redox reaction.[439] In order to improve the electron transfer and porosity, different PANi nanostructured morphologies have been proposed.[440−442] An inexpensive porous PANi nanotube CE was prepared via simple polymerization of aniline with ammonium persulfate in the presence of orthophosphoric acid. DSSCs assembled with PANi nanotubes as the CE obtained a superior photovoltaic performance compared to DSSCs based on Pt, mainly due to the higher electrocatalytic function of the PANi nanotubes.[441] Besides PANi nanostructures, another important approach to enhance the power conversion efficiency in DSSCs using PANi CE is to form composites or complexes with different materials.[443−445] For example, aniline monomers and a reflux process were used to functionalize graphene and form a donor–acceptor complex used as CE. The GR–PANi complex allows the combination of efficient electron transport and transfer from graphene to PANi by covalent bonds between C atoms (graphene) and N atoms (aniline), enhancing the redox performance of PANi.[445]

PPy, PT, and PEDOT are feasible CP alternatives to fabricate efficient CEs for DSSCs.[446−451] PPy CEs synthesized by vapor phase polymerization and regular electropolymerization showed good catalytic behavior. However, the power conversion efficiency of DSSCs with a Pt CE was higher (4.4%), compared to that of vapor and electropolymerized PPy CE (i.e., 3.4% and 3.2%, respectively). This observation was explained by a poor interface between a fluorine-doped tin oxide (FTO) substrate and the PPy CEs rendering lower fill factor (FF) values.[446] Although PT and its derivatives (including PEDOT) present similar electrocatalytic activity to that of PPy CEs, the conductivity of PEDOT is 1−3 times higher than that of PPy.[450,451] PEDOT is generally doped with polystyrene sulfonic acid (PSS) to enhance conductivity and compatibility with protic ionic solvents.[452] A CE fabricated with GR dots or PEDOT:PSS complex sheets exhibited high superficial roughness, which implies a higher electrocatalytic activity for the I^-/I_3^- redox couple and a lower charge transfer resistance at the CE/electrolyte interface than that of PEDOT:PSS CE.[453,454]

On the other hand, in an effort to overcome the leakage problems in liquid electrolyte-based DSSCs, solid state DSSCs (ssDSSCs) provide a suitable solution. Due to the ease of solution-based processing and excellent intrinsic hole transport properties, CPs have been proposed as HTM to replace the standard material used to date, spiro-OMeTAD (2,2′,7,7′-tetrakis(*N*,*N*-di-*p*-methoxyphenylamine)-9,9-spirobifluorene).[455,456] Although spiro-OMeTAD is a small organic molecule that exhibits good infiltration,[455] it is harder to

DOI: 10.1021/acs.chemrev.7b00482
Chem. Rev. 2018, 118, 4731−4816

synthesize, particularly as a film, and has low conductivity[456] (around 2×10^{-8} S cm^{-1}) compared to that of a CP (see Table 2). The ideal features for CP-based materials to act as HTM in ssDSSCs are large hole conductivity, good thermal and chemical stability, excellent pore filling, and no absorption in the visible region.

Table 2. Summary of Conductivity of Common CPs Used As Hole Transport Materials

CP	conductivity (S cm^{-1})	ref
E-PEDOT	ca. 300	204
PEDOT	1.1×10^{-3} to 84	457, 458
PEDOT:PSS[a]	0.4−787.99	459, 460
P3HT	6.77×10^{-5}	461
PPy	50−430	462, 463
PANi	70	464
spiro-OMeTAD	$\sim 2 \times 10^{-8}$	456

[a]PEDOT:PSS with enhanced conductivity reaching 4000 S cm^{-1} can be obtained in special media (see ref 344 for details).

In the context of HTMs based on CPs, P3HT is the CP most widely used as HTM in ssDSSCs. P3HT has been successfully reported as the HTM layer in the regular ssDSSC architecture with different ETMs, such as TiO_2, ZnO, and SnO_2.[465−467] Owing to its excellent film-forming ability, good hole transport, and small band gap, P3HT was used as HTM and assistant sensitizer.[468−470] The main contribution of P3HT to the sensitizing effect is reflected in the enhancement of photocurrent. This result was explained by Föster resonant energy transfer,[471] where light illumination causes the formation of a cascade effect through the dye, and P3HT can transfer charge to the TiO_2. Similarly, PEDOT and PEDOT:PSS layers have been introduced as the HTM layers in conventional and inverted ssDSSC configurations.[472−474] Interestingly, photoinduced absorption spectroscopy measurements confirmed the regeneration of the oxidized dye by hole transfer to PEDOT. Figure 24 shows the mechanism proposed by Park et al.[472] for dye regeneration in ssDSSCs assembled with PEDOT HTM. In this mechanism, the hole transfer from the oxidized dye to PEDOT polarons results in the formation of bipolarons. This is different from what is observed in spiro-OMeTAD-based ssDSSCs.[475] In a recent study, PANi and PPy were incorporated into a poly(acrylic acid)−poly(ethylene glycol) matrix and used as HTM in quasi-ssDSSCs.[476] Both matrices obtained higher power conversion efficiencies than without CPs. These observations were ascribed to the faster migration within matrices fabricated with PANi or PPy, which accelerate the redox reaction kinetics, enhancing the photovoltaic performance of quasi-ssDSSCs.

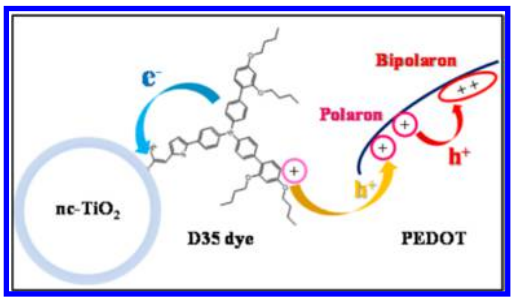

Figure 24. Proposed mechanism for hole transfer from D35$^+$ to PEDOT. Reproduced with permission from ref 472. Copyright 2013 American Chemical Society.

Although using CPs as HTM in ssDSSCs is feasible, the pore filling of the HTM in the nanostructured ETM still remains to be resolved. This problem is mainly due to the high molecular weight of CP HTMs, causing poor chain diffusion into the pores.[472,477] To achieve a higher degree of pore filling, *in situ* photoelectrochemical polymerization of different monomers has been presented.[473,478−482] In this method, upon photoexcitation of the dye, the photoinduced holes cause the monomer's oxidation followed by electron injection into the ETM layer. Then, the CP is synthesized when the newly formed monomers link together. Recently, different organic and inorganic dyes were investigated as donor group structures in PEDOT HTM.[481] It is well-known that during polymerization, the kinetics of PEDOT formation is determined by the light absorbance and redox potentials of the donor−π−acceptor dye molecules. Consequently, different pore filling fractions of the formed PEDOT were observed due to the differences in polymer chain length. Moreover, a high hole conductivity (i.e., 2.0 S cm^{-1}) of PEDOT HTM was reported, which is 7 orders of magnitude higher than that of spiro-OMeTAD HTM in ssDSSCs.[456]

3.1.3.2. Organic Solar Cells. OSCs are devices that employ organic molecules as absorbers, which in general can be CPs or small molecules. In an OSC, incident photon absorption by the donor molecule (D) leads to the creation of an exciton. Excitons diffuse to the donor/acceptor (D/A) interface, where they become separated into electrons and holes followed by free charge transport to different contact electrodes (Figure 25). Two device architectures have been exploited to assemble OSCs, (a) bilayer and (b) bulk heterojunction (BHJ) devices. The difference between these architectures is that the D and A layers are separated in the bilayer heterojunction, whereas in the BHJ, they are mixed.[483]

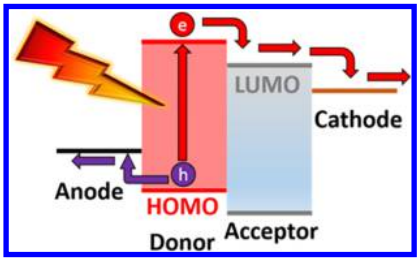

Figure 25. Energy band diagram of an organic solar cell.

Among the CP requirements to achieve efficient OSC devices are high charge conductivity, good processability and stability, low band gap, and optimal HOMO/LUMO levels.[484−486] Despite the good conductivity and solubility of CPs, typical limitations are their band gaps, hygroscopicity, and inappropriate HOMO/LUMO energy levels.[487−489] Nevertheless, diverse strategies have been pursued to surmount these limitations and improve the photovoltaic performance of OSC based on CPs.

P3HT has been extensively investigated as an electron donor (i.e., D layer) in OSCs, due to its relatively low band gap (2 eV) when compared to other CPs.[490] In particular, the BHJ system formed by P3HT blended with PCBM offers a highly reproducible conversion efficiency in the range of 4.7−6.8%[491,492] and a certified efficiency of 3.6%.[490] It has been demonstrated that the efficiency of BHJ OSCs fabricated with

DOI: 10.1021/acs.chemrev.7b00482
Chem. Rev. 2018, 118, 4731−4816

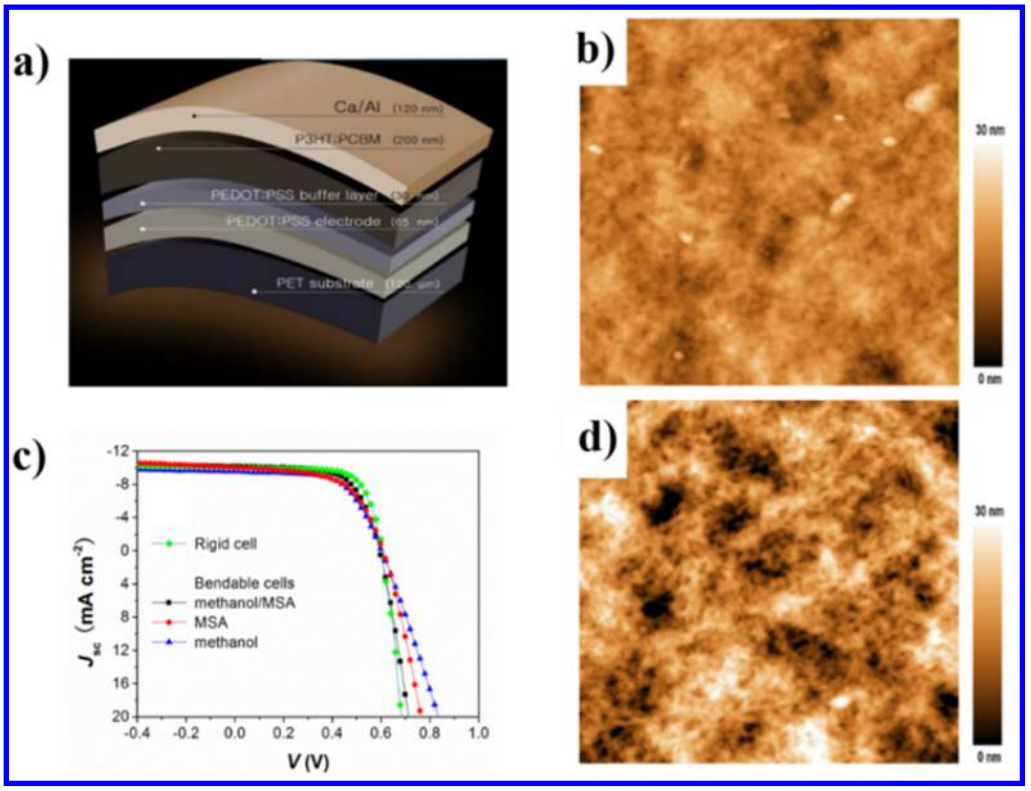

Figure 26. (a) Device configuration, (b) AFM image of a pristine PEDOT:PSS film on a flexible substrate, (c) *J*−*V* curves of the OSCs based on PEDOT:PSS, and (d) AFM image of a methanol/methanesulfonic acid-treated PEDOT:PSS film on a flexible substrate. Reproduced with permission from ref 540. Copyright 2015 American Chemical Society.

P3HT:PCBM is strongly influenced by the deposition technique, blend composition, and post-treatment parameters.[493−498] Many studies have been performed to understand and control the undesired morphology and phase separation of the D and A domains, by incorporating additives to the BHJ blend precursor solution. Upon introduction of different processing additives to the cast P3HT:PCBM solution (i.e., trihydrazone-functionalized cyanopyridine (CPTH-D16),[499] 1,8-diiodooctane,[500] and 1,2,4-trichlorobenzene[501]), a significant enhancement in photovoltaic performance has been observed.

Another intensive area of research incorporates the different post-thermal treatments to manipulate the morphology and optoelectronic properties of P3HT:PCBM films.[497,498,502−510] Different effects on the meso- and nanoscale morphologies of the P3HT:PCBM blend have been reported.[497,502−505] Thermal annealing increases the crystallinity of the P3HT and PCBM domains, improving the diffusion of the exciton to the blend interface,[504] but it can also induce CP degradation.[506] On the other hand, solvent vapor annealing offers the advantage of suppressing the rapid solvent evaporation, promoting phase segregation with domain sizes smaller than those obtained from thermal annealing.[498]

Research on deposition techniques is also important because they determine the potential mass production of OSCs based on P3HT:PCBM. Although solution-processed spin-coating is a standard method extensively used for depositing P3HT:PCBM films,[491,496,507−509] this technique needs the referenced post-treatment methods to improve device performance and can only be adapted to small area deposits. As a result, spray-coating,[510] roll-to-roll coating,[511] and electrohydrodynamic atomization[512] have been implemented as alternative techniques to assemble BHJ OSCs.

The development of third-generation donor−acceptor (D-A) polymers has broadened the design of new building blocks in organic solar cells.[513,514] Electron-deficient fused aromatic units such as diketopyrrolopyrrole (DPP), naphthalene diimide (NDI), and benzobisthiadiazole (BBT) have been extensively used as acceptor molecules.[515−517] Fused heterocycles can achieve either low band gaps or high carrier mobilities depending on the orientation of the fused ring to the polymer main chain.[518]

Just recently, isoindigo, a less known dye that can be isolated as a byproduct from certain biological processes, has shown interesting properties as an acceptor. Due to its two lactam rings, isoindigo exhibits a strong electron-withdrawing character and has been reported to broaden the absorption and increase the open circuit voltage in OSCs, reaching power-conversion efficiencies over 8%.[519−521] Among the key issues to improve device performance are film morphologies and interchain polymer packings. Polymers with centrosymmetric donors such as isoindigo-based polymers exhibit better crystallinity and lamellar packing due to the good interchain $\pi-\pi$ stacking;[513] nevertheless, a synergy of the isoindigo core, donor units, and side chains must exist to improve device performance.[521] Very recent reviews have extensively covered the use of CPs as part of the active layer in bulk heterojunction organic solar cells.[522−526]

Regarding the use of CPs as HTM in OSC, PEDOT:PSS continues to be the preferred hole extraction layer in bilayer and BHJ devices, because it is highly transparent and conductive, has good film forming ability, and is perfectly aligned with the work function of the indium tin oxide substrate

DOI: 10.1021/acs.chemrev.7b00482
Chem. Rev. 2018, 118, 4731−4816

Table 3. Solar Cells That Use CPs as Part of Their Architecture[a]

solar cell architecture	active layer	CP function	remarks	PCE %	ref
			DSSC		
FTO/TiO_2/CYC-B11 dye/I^-/I_3^-/PANi (HFIP) or PEDOT (HFIP)/FTO	CYC-B11 dye	counter electrode	PANi and PEDOT/hexafluoro-isopropanol (HFIP) colloid solutions were prepared by dissolving the doped polymer powders in HFIP. PANi and PEDOT films were deposited by spin-coating or drop casting methods.	8.8−9	561
FTO/TiO_2/N719 dye/I^-/I_3^-/HCl-doped PPy nanoparticles/FTO	N719 dye	counter electrode	spherical PPy were prepared by chemical oxidative polymerization within micelles composed of myristyl trimethyl ammonium bromide and decyl alcohol as the nanoreactors. Films were deposited by drop-casting using a methanol-based colloidal dispersion containing 5 wt % PPy	7.73	562
FTO/TiO_2/N719 dye/I^-/I_3^-/Gr dots−PEDOT:PSS/FTO	N719 dye	counter electrode	Solution containing 50 vol % PEDOT:PSS aqueous solution, 30 vol % graphene (Gr) dots solution, and 20 vol % ethanol was used for preparing the Gr dots−PEDOT:PSS composite film. These films were fabricated on FTO substrates via drop-coating method.	7.36	453
FTO/TiO_2/N719 dye/I^-/I_3^-/rGO/PEDOT:PPS/FTO	N719 dye	counter electrode	rGO/PEDOT:PPS was prepared by mixing water-soluble reduced graphene oxide (rGO) (1 wt %) with PEDOT:PSS solution. The rGO/PEDOT:PSS films were spin coated on FTO substrates	5.10	454
FTO/TiO_2/N719 dye/I^-/I_3^-/PANi (NR)/rGO/FTO	N719 dye	counter electrode	PANi nanorod arrays on FTO substrates modified with reduced graphene oxide (rGO) were prepared by potentiostatic polymerization at low potential to achieve uniform growth of the array in the emeraldine base form.	7.30	442
FTO/TiO_2/N719 dye/I^-/I_3^-/Ag-PPy-FMWCNT/SS	N719 dye	counter electrode	silver−polypyrrole-functionalized multiwall carbon nanotube (Ag-PPy-FMWCNT) nanocomposites were prepared via electrodeposition method on stainless steel (SS) substrates.	7.60	447
FTO/TiO_2/N719 dye/I^-/I_3^-/PEDOT:PSS−TiO_2 NP/FTO	N719 dye	counter electrode	5 wt % dimethyl sulfoxide was mixed with PEDOT:PSS and TiO_2 nanoparticles (NP) and deposited on FTO substrate by spin-coating.	8.27	451
FTO/TiO_2/D149/P3HT/PEDOT:PSS/Au	metal-free organic dye D149	hole transport and electron-blocking layers	P3HT was incorporated by spin coating and PEDOT:PSS was deposited via spray coating	2.70	465
FTO/TiO_2/LEG4/PEDOT/Ag	metal-free organic dye LEG4	hole transport layer	PEDOT was in situ photoelectrochemically polymerized on FTO/TiO_2/dye electrodes using 10 mM bis-EDOT and 0.1 M LITFSI in acetonitrile and a constant potential of 0.4 V/NHE. The white light was provided by a LED lamp.	7.11	473
FTO/TiO_2/DPP07/PEDOT/Ag	Diketo-pyrrolopyrrole-based dye DPP07	Counter electrode	PEDOT was in situ photoelectrochemically polymerized onto FTO/TiO_2/dye electrodes.	5.50	481
			OSC		
ITO/ZnO/P3HT:PCBM/Ag	P3HT:PCBM	active layer	Blend of P3HT/$PC_{60}BM$ (1:0.8 wt %) contained 36 mg mL^{-1} in chlorobenzene. It was doctor-bladed in air, with a resulting thickness of ∼180 nm.	3.50	489
ITO/LiCl modified PEDOT:PSS/P3HT:PCBM/Al	P3HT:PCBM	buffer and active layers	PEDOT:PSS was mixed with LiCl and used as powders and as aqueous solutions (1 mg of the metal salt to 1 mL of PEDOT:PSS solution) and spin-coated on ITO substrates. P3HT:PCBM (in 1:1 ratio, 14 mg mL^{-1}) was dissolved in cosolvents of chloroform and chlorobenzene at a 1:1 ratio and spin coated inside a nitrogen-filled glovebox, followed by annealing.	6.82	492
ITO/methanol treated-ZnO/P3HT:PCBM/MoO_3/Au	P3HT:PCBM	active layer	100 nm thin active layers were deposited by spin coating a P3HT:PCBM (1:1 w/w) blend solution, dissolved in chlorobenzene, followed by annealing on a hot plate at 150 °C in a nitrogen-filled glovebox.	4.14	509
ITO/PEDOT:PSS modified with PEI/P3HT:$PC_{61}BM$/MoO_3/Ag	P3HT:$PC_{61}BM$	electron transport and active layers	Polyethylenimine (PEI) films at different pH values were spin-coated on PEDOT:PSS/ITO substrates. A 1,2-dichlorobenzene solution of P3HT and $PC_{61}BM$ (1:1 w/w, polymer concentration of 10 mg mL^{-1}) was also spin coated on top of the dry PEDOT:PSS film.	7.94	532
PET/modified-PEDOT:PSS/P3HT:PCBM/Ca/Al	P3HT:PCBM	buffer and active layers	PEDOT:PSS films were prepared with the combined treatments of methanol/MSA. PEDOT:PSS aqueous solutions were spin-coated on the PET substrates. The blend solution of P3HT and PCBM in *o*-dichlorobenzene (DCB; 1:1 w/w, 34 mg mL^{-1}) was spin-coated on top of the PEDOT:PSS buffer layer in a nitrogen filled glovebox.	3.92	540
ITO/PEDOT:PSS/P3HT:F8-DPPTCN/PFN/Al	P3HT:F8-DPPTCN	buffer and active layers	PEDOT:PSS spin-coated on ITO substrates. The active layer was spin-cast from a solution of P3HT and F8-DPPTCN in chloroform at a total solid concentration of 20 mg mL^{-1}. F8-DPPTCN is a non-fullerene electron acceptor developed using fluorene as the core, with arms of diketopyrrolopyrrole (DPP) having thiophene-2-carbonitrile as the terminal units.	2.37	484
steel/insulator/Al/ZnO/P3HT:PCBM/MoO_3/Al	P3HT:PCBM	active layer	P3HT:PCBM blend solution was prepared by mixing regioregular poly(3-hexylthiophene) (30 mg mL^{-1}) and phenyl-C_{61}-butyric acid methyl ester (PCBM) (30 mg mL^{-1}), in chlorobenzene. The solution was then spin coated on cleaned ZnO coated substrates followed by annealing at 130 °C for 20 min under a nitrogen atmosphere.	1.35	507

DOI: 10.1021/acs.chemrev.7b00482
Chem. Rev. 2018, 118, 4731−4816

Table 3. continued

solar cell architecture	active layer	CP function	remarks	PCE %	ref
			PeSC		
ITO/PPP/$MAPbI_3$/C_{60}/BCP/Ag	$MAPbI_3$	hole transport layer	poly(*p*-phenylene) (PPP) was grown via electrochemical polymerization on ITO substrates at +1.70 V. The electrolyte solution was freshly distilled BFEE/CH_2Cl_2 (vol. ratio 7:1) containing 30 mM biphenyl monomer. BCP = bathocuproine	15.80	547
ITO/TiO_2/$MAPbI_3$:BHJ/MoO_3/Ag	$MAPbI_3$:BHJ, BHJ = DOR3T-TBDT/$PC_{71}BM$	active layer	Concentration of DOR3T-TBDT was 18 mg mL^{-1}. Solution of DOR3T-TBDT/$PC_{71}BM$ (1:0.8 w:w) in chloroform was used to fabricated the tandem device by spin coating.	14.30	555
ITO/PSS-*g*-PANi:PFI/$MAPbI_3$/PCBM/Al	$MAPbI_3$	hole transport layer	Solution of PSS-*g*-PANi was mixed with 5 wt % tetrafluoroethylene-perfluoro-3,6-dioxa-4-methyl-7-octene-sulfonic acid copolymer (PFI) for PSS-*g*-PANi:PFI and then spin-coated on top of ITO substrates. PSS:poly(4-styrenesulfonate).	12.40	30
PET/Ag-mesh/PH1000/PEDOT:PSS/$MAPbI_3$/PCBM/Al	$MAPbI_3$	hole transport layer and transparent contact	The highly conductive polymer PH1000 (Heraeus, Clevios PH1000, Germany) was spin-coated on the PET/Ag-mesh. A thick buffer layer of PEDOT:PSS was subsequently spin-coated and baked in ambient air.	13.70	545
FTO/SnO_2/$MAPbI_3$/RCP/Au	$MAPbI_3$	hole transport layer	RCP = random copolymer based on benzo[1,2-*b*:4,5:*b*′]dithiophene and 2,1,3-benzothiadiazole.	17.30	546
ITO/PEDOT:GSL/$MAPbI_3$/PCBM/Al	$MAPbI_3$	hole transport layer	Sulfonated-acetone−formaldehyde was grafted with alkali lignin to prepare grafted sulfonated-acetone−formaldehyde lignin (GSL). GSL was applied as p-type semiconductive dopant for PEDOT to prepare water-dispersed PEDOT:GSL which was spin coated on ITO substrates.	14.94	550
ITO/PEDOT:PSS/$MAPbI_3$/PNDI-2T doped with N-DMBI/PEI/Au	$MAPbI_3$	buffer and electron transport layers	PEI (interface-modifying layer), PNDI-2T (semiconductor polymer, poly{[*N*,*N*′-bis(2-octyldodecyl)-1,4,5,8-naphthalene diimide-2,6-diyl]-*alt*-5,5′-(2,2′-bithiophene)}; *N*-DMBI (n-type dopant, ((4-(1,3-dimethyl-2,3-dihydro-1*H*-benzoimidazol-2-yl) phenyl)dimethylamine). PNDI-2T, *N*-DMBI, and PEI were spin coated successively.	13.93	551
FTO/TiO_2/$MAPbI_3$/MEH-PPV/Au	$MAPbI_3$	hole transport layer	Hole-transport layer was obtained by a spin-coating in nitrogen atmosphere (glovebox), 5-(2′-ethyl-hexyloxy)-*p*-phenylene vinylene (MEH-PPV, 5−15 mg mL^{-1}) solution in chlorobenzene.	9.65	574
ITO/PEDOT:PSS/PTB7:$MAPbI_3$/PCBM/BCP/Au	PTB7:$MAPbI_3$	hole transport and active layer	Poly[[4,8-bis[(2-ethylhexyl)oxy]benzo[1,2-*b*:4,5-*b*′]dithiophene-2,6-diyl][3-fluoro-2-[(2-ethylhexyl)carbonyl]thieno[3,4-*b*]thiophenediyl]] (PTB7) was prepared by dissolving 4 mg in 1 mL of chlorobenzene. PEDOT:PSS and PTB7 films were spin-coated. The weight ratio of PTB7 to $CH_3NH_3PbI_3$ in the fabricated composite layer was estimated as ∼1:80.	14.40	560
ITO/PEDOT:PSS/$MAPbI_3$−PCBM/PCBM/Al	$MAPbI_3$−PCBM	hole transport layer	PEDOT:PSS was spin-coated on ITO substrates.	16.0	556
ITO/s-PANi:PSS/$MAPbI_3$/PCBM/Au	MAPbI3/PCBM	hole transport layer	An s-PANi:PSS layer was deposited on ITO substrates by spin coating a prepared PANi:PSS solution obtained via oxidative chemical polymerization of aniline in the presence of commercial PSS, and further modified with the surfactant Triton X-100.	11.67	557
FTO/TiO_2/$MAPbI_3$/PVK/spiro-OMeTAD/Au	$MAPbI_3$/PVK	hole transport and protective layer	Protective multifunctional PVK layer sandwiched between perovskite and spiro-OMeTAD. Both polymeric films were spin-coated.	16.90	559

[a]From 2015 to date.

DOI: 10.1021/acs.chemrev.7b00482
Chem. Rev. 2018, 118, 4731−4816

(ITO).[527−529] Despite these excellent properties, corrosion of ITO by PEDOT:PSS at elevated temperatures and upon exposure to air must be addressed.[530,531] The water solubility and strongly acidic nature of PSS due to the presence of the sulfonic acid group ($-SO_3$) causes moisture absorption from the surroundings and the diffusion of In ions to other layers. The proposed reaction mechanism for ITO corrosion is as follows:[530]

$$H_2O + PSS(HSO_3) \rightarrow H_3O^+ + PSS(SO_3)^- \quad (5)$$

ITO corrosion and transport of the etch products toward the active layer of OSCs can be reduced by the introduction of a polyethylenimine[532] or graphene oxide (GRO) interlayer film.[533] Among the key factors contributing to minimize ITO corrosion are the reduced hygroscopicity and acidity of the modified PEDOT:PSS HTM, causing important improvements on photovoltaic performance and stability when compared to those OSCs without interlayers. Electrochemically deposited PEDOT (E-PEDOT) has also been used as an alternative to PEDOT:PSS, showing promising results, which suggest that electropolymerization may be an excellent way to deposit PEDOT layers on ITO electrodes.[534−539] Another approach is ITO-free electrodes,[540−542] as depicted in Figure 26, where the rigid glass/ITO electrode is replaced by the flexible poly(ethylene terephthalate) (PET)/PEDOT:PSS (Figure 26a,b). Further improvement was obtained by treating PEDOT:PSS with methanol and methanesulfonic acid (Figure 26c,d).[541] After the methanol/methanesulfonic acid treatment, the films showed better phase separation between PEDOT and PSS, as well as more interconnected conductive PEDOT chains, resulting in a higher photovoltaic performance (compare Figure 26 b.,d).

3.1.3.3. Perovskite Solar Cells. In perovskite solar cells (PeSCs) the incident light is absorbed by the perovskite semiconductor material, inducing the formation of electron−hole pairs. Electrons and holes are separated by the ETM and HTM, respectively, followed by their transport to the ohmic contact electrodes. Organic/inorganic halide perovskites, including the most widely used methylammonium lead triiodide ($MAPbI_3$), are characterized by the general formula ABX_3, where A is an organic molecule, B is a metal cation, and X is a halide anion. There are two types of device architectures: mesoporous (nearly identical to conventional DSSCs) and planar (thin film solar cells).[543] CPs have been used in rigid and flexible PeSCs as HTMs,[544−550] as ETMs,[551] and also as protection from moisture.[551−554] Moreover, a new kind of solar cell has been implemented by the interaction between a perovskite and a BHJ photovoltaic device.[555,556]

Since the majority of perovskite materials are solution-processable as CPs,[166] both are perfect candidates to assemble a fully solution-processed PeSCs. In addition to the requirements for CPs discussed above, it is important to investigate alternative doping agents to improve the CP conductivity without inducing undesirable chemical damage. As known, the main factor affecting the performance and degradation of hybrid solar cell devices stem from the interface instability of doped CP. For instance, the hygroscopic and acidic nature of PSS in PEDOT:PSS causes ion diffusion and moisture absorption.[530,531] In this regard, a simple solution-processable CP including a PANi:PSS blend was employed as HTM in an inverted PeSC device configuration.[557,558] Here, a nonionic surfactant (Triton X-100) added to a PANi:PSS aqueous solution improved the hole extraction capability that enhanced the device efficiency from 7.46% to 11.67%. This enhancement was related to the surface tension reduction of the aqueous solution induced by the surfactant, which improved both the wetting properties of PANi:PSS onto the ITO substrate as well as the morphology and composition of the PANi:PSS film. Another strategy was explored by Su et al.[559] by introducing a thin organic CP interlayer, poly(*N*-vinylcarbazole) (PVK), at the perovskite/HTM interface. They demonstrated that this PVK interlayer suppressed the moisture and reduced charge recombination, which is attributed to the good hydrophobicity and conductivity properties of the PVK thin layer. After aging-control experiments performed to investigate the device stability for 700 h, it was found that when comparing PeSCs fabricated with and without PVK interlayer, the former lose their efficiency much more slowly than devices without PVK, exhibiting a retention of 90% and 73% of the initial efficiency, respectively.

A CP was used very recently as an active material combined with $MAPbI_3$. In this study, a composite active layer was fabricated by depositing a photoactive conducting polymer, poly[[4,8-bis[(2-ethylhexyl)oxy]benzo[1,2-*b*:4,5-*b*′]-dithiophene-2,6-diyl][3-fluoro-2-[(2-ethylhexyl)carbonyl]-thieno[3,4-*b*]thiophenediyl]] (PTB7), onto a previously deposited PbI_2 thin film, followed by the addition of a methylammonium iodide (MAI) solution to complete the chemical reaction.[560] The devices assembled with the formed PTB7/$MAPbI_3$ composite show a superior photovoltaic performance compared to that of $MAPbI_3$, mainly due to the enhancement in light absorbance in the wavelength range from 650 to 750 nm. Simultaneously, the CP also creates a barrier layer at the interfaces providing moisture protection to the $MAPbI_3$ perovskite without sacrificing the optoelectronic properties.

Table 3 gives more detail about the solar cell architecture and the function of the CPs in DSSCs, OSCs, and PeSCs. It focuses only on the most recent works (since 2015) and presents the information chronologically. It is notorious that in any type of cell, the record numbers in power conversion efficiency have been compromised due to the need for scaling up and increasing the stability of these systems. Liquid electrolytes have been substituted for semiconductor CPs in DSSCs, and ITO and FTO for more economic and flexible substrates in OSC. It is also interesting the changes in cell architecture and substitution of the expensive spiro-OMeTAD in PeSC, where the major problem continues to be the stability of the absorbing material.

3.1.4. The Future of CPs in Energy Storage and Photovoltaic Conversion. Today, state-of-the-art LIBs offer volumetric and gravimetric energy densities up to 770 Wh/L and 260 Wh/kg, respectively, which was not expected a few years ago.[563] Unfortunately, the energy density of conventional LIBs will soon reach its physicochemical limit near 800 Wh/L,[564] in contrast to the demand of higher energy density as well as high power density batteries. New types of batteries have undergone intensive research, and some of them use CPs. Li−S batteries couple high-capacity sulfur positive electrodes with lithium negative electrodes. The redox chemistry proceeds through lithium polysulfide (LiPS) intermediates consisting of Li_2S_x chains, with $x > 1$, and it is now widely recognized that high sulfur loading electrodes are essential for advancing this technology.[565] A variety of chemical interactions can be recognized in different sulfur host materials: surface functionality, intrinsic polarity, electro- or nucleophilicity, and redox

DOI: 10.1021/acs.chemrev.7b00482
Chem. Rev. 2018, 118, 4731−4816

potential play an important role in determining the strength of the interaction between sulfur and the host. Coating sulfur nanoparticles with conductive poly(3,4-ethylene dioxythiophene) can enhance conductivity and LiPS binding capability. A minimum thickness of this layer (ca. 20 nm) is required to sustain the LiPS binding and entrapment over prolonged cycling.[566] Li_2S−PPy composite structures have also been explored for high performance Li_2S cathodes.[567] Computational chemistry can guide the way in the near feature to design smart cathode architectures that are elastic and conductive, and CPs are potential candidates. Likewise, hybrid energy storage, the merging of battery and supercapacitor chemistries, will continue showing advances on the design of hybrid materials, electrodes, and devices, aiming to high power and high energy density, and CPs are good candidates for hybridization with other components.

Regarding the future of CPs in solar cells, flexible and low cost substrates will continue being explored as substitutes of ITO,[568,382,569] particularly those based on PEDOT:PSS films on plastic substrates.[569] Solution-processed methods and environmentally sound printing of organic tandem solar cells,[570−572] aiming at a 20% power conversion efficiency, will make important progress in the near future. Doping agents such as POMs, reported recently to improve the conductivity of CPs without inducing undesirable chemical damage that weakens their photooxidation stability in air,[573] will continue being explored. For perovskite solar cells (PeSCs), research on HTMs based on CPs will intensify.[574] Most perovskite materials are solution-processable as well as the CPs, and therefore both are perfect candidates to assemble a fully solution-processed PeSCs.

3.2. Applications of Conducting Polymers to Environmental Remediation

3.2.1. Introduction. Conducting polymers (CPs) can aid pollutant detection, quantitation, and removal in multiple ways. Regarding pollutant removal, polymers can act as sorbents, membranes, ion exchangers, filters, or chemical reactors involving complexation or redox processes.[575−579] The main mechanisms assisted by conducting polymers (or their composites) under an applied potential include pollutant incorporation (or uptake) and release,[576] doping/dedoping,[580] and electrocatalytic reduction/oxidation. This is the target scope of the present section.

3.2.2. Incorporation and Release of Pollutants in CPs. The removal of charged pollutants from aqueous solutions or liquid wastes can be promoted by their incorporation into charged or uncharged CP thin films deposited on conductive substrates (e.g., Au, Pt, Ti, vitreous C, graphite felts, etc.).[575,581−584] In the case of uncharged CPs, metal ion complexation (e.g., of Hg^{2+}) by nitrogen-containing functional groups (e.g., imine, protonated imine, amine) in a PANi matrix[577] or by the nitrogen in the PPy ring of selected composites and nanofibers (for Hg^{2+}, Pb^{2+}, Ni^{2+}, Zn^{2+}, Cd^{2+}, and Cr^{6+})[585] can play a key role. In the case of charged CPs, load/unload cycles are based on the necessity for charge compensation. Uptake of charged pollutants by a conducting polymer is stimulated by the application of an electric field of the opposite sign to that of the pollutant species, as shown below. This *electrochemically assisted removal of charged pollutants* is a form of electrochemical ion exchange.[576] It is also called *electrically switched ion exchange*[586] and is based either on cation or anion dynamics schemes that can be evidenced, for example, with an electrochemical quartz crystal microbalance (EQCM),[581,576,587] cyclic voltammetry (CV),[586,588] Fourier transform infrared spectroscopy (FTIR),[580] scanning probe microscopy (SPM),[580] X-ray photoelectron spectroscopy (XPS),[586] and electrochemical surface plasmon resonance (ESPR).[580] Ion transport here is slower than electron transport, and therefore ion dynamics govern the CP redox properties.[588]

3.2.2.1. Cationic Pollutant Dynamics. Let CP be the conducting polymer matrix, M^{m+} the mobile pollutant metal cation (or a complex metal cation, ML_a^{m+}), and A^- the initial charge compensation anion (e.g., Cl^-), acquired during the polymer's synthesis process and incorporated in the CP bulk (see Figure 27). The general uptake equation (in the case of a positively charged polymer like polypyrrole, PPy) is then:

$$CP^{n+}\cdot nA^-(s) + (n/m)M^{m+}(aq) + ne^- \rightarrow CP^0\cdot nA^-\cdot(n/m)M^{m+}(s) \quad (6)$$

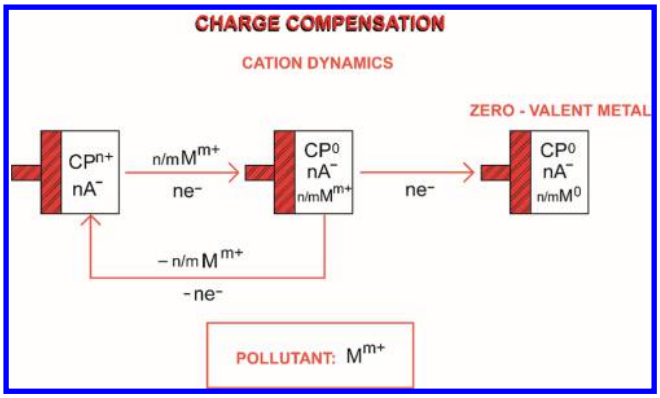

Figure 27. Charge separation with cation dynamics.

Dopant anions[589] can be classified according to their mobility inside a polymer matrix as *easily mobile*, *mobile with restriction*, or *essentially immobile* (see also section 2.2).[583] In the present scheme, the anion A^- must be bulky to remain entrapped in the solid matrix and yield an anion-functionalized polymer;[581,588] this provides a pure cation exchange pathway.[587] Evidently, dopants must be electroinactive in the entire working potential range.[590] Examples of A^- include poly(styrene sulfonate) (PSS),[591] dodecyl benzenesulfonate (DBS),[588] poly(vinyl sulfonate) (PVS), melanin, and catechol anions.[581,582] The amount of incorporated cations reflects the cation-exchange properties of the system[581] and is related to the electrolyte composition by an osmotic balance in such a way that in diluted electrolytes the CP tends to take water whereas in concentrated electrolytes it tends to take up the salt.[588] Upon potential inversion, the general dopant ion release equation (for the case of a metal ion) is

$$CP^0\cdot nA^-\cdot(n/m)M^{m+}(s) \rightarrow CP^{n+}\cdot nA^-(s) + (n/m)M^{m+}(aq) + ne^- \quad (7)$$

The controlled uptake of alkali metal ions,[587,592] alkaline earth metal ions,[587,592,593] and Cd(II), Pb(II), Ni(II), Cu(II), and Co(II) ions[576,581,582,594,595] has been studied. This can impact, for example, the softening of water and the removal of noxious and toxic ions.[586,587] A nuclear waste-related potential application is the uptake of radioactive Cs(I),[592] often removed

DOI: 10.1021/acs.chemrev.7b00482
Chem. Rev. 2018, 118, 4731−4816

by simple adsorption. In a related way, radioactive ^{57}Co can be rapidly removed by a PPy−waste biomass (e.g., sawdust) composite.[596]

Ion selectivity can be achieved in specific cases based on size, charge, acid/base, complexation, mobility, or electroactivity characteristics.[581,582,592] For example, PPy with a monovalent counteranion exclusively exchanges monovalent cations.[587] In another example, Ni(II) uptake is drastically favored over that of Na(I) in a mixture of both ions due to its larger size.[581,582] Likewise, metal chelation by crown-ether functionalized conducting bithiophene−PPy films serves to complex Ba(II) ions.[593] To prevent the metal ion from leaching, a clever approach involving an organic−inorganic composite cation exchanger based on poly(3,4-ethylene dioxythiophene):poly-(styrenesulfonate)−zirconium, PEDOT:PSS-Zr(IV), phosphate has been used for the selective removal of Cd(II). Here, the organic polymer binds with the inorganic counterpart and prevents the leaching of the Cd(II) ions.[597] Polythiophene nanocomposites are efficient for the removal of Cd(II).[598] Another novel approach uses PANi hollow nanospheres for the removal of Pb(II) ions from water.[594]

Interestingly, in these approaches the metal ions retain their original oxidation states, and the overall process can be viewed as a preconcentration stage.[576] Compared to processes like coagulation−precipitation for the removal of polluting metal ions, advantages when using this charge dynamics scheme with an electrochemical regeneration step include (a) avoidance of the addition of further chemicals, (b) no generation of further wastes, (c) prevention of drastic pH changes, (d) autonomy from solubility equilibria parameters, and (e) independence of the presence of ligands.[582] Compared to classical ion-exchange processes, the present scheme can regulate the rate of chemical uptake by adjusting the applied potential[576] and has the advantage of not facing the brine disposal problem derived from the use of regeneration agents.[599] Challenges to be faced involve possible conformational changes in the CP structure caused by the intercalation of bulky counterions, which may be responsible for changes in ion uptake/release kinetics,[576] changes in volume (e.g., PPy swells on reduction and shrinks upon oxidation),[580,589] and changes in the CP electronic band structure.[576] Conversely to the process just described, in some cases it is more convenient to retain a metal in the matrix as a *zerovalent* metal (typically for catalytic purposes)[582,600] as shown in Figure 27, whereby the general equation is

$$CP^0{\cdot}nA^-{\cdot}(n/m)M^{m+}(s) + ne^- \rightarrow CP^0{\cdot}nA^-{\cdot}(n/m)M^0(s)$$
$$\text{or} \quad [CP{\cdot}nA{\cdot}(n/m)M(s)]^{n-} \qquad (8)$$

For example, nanocrystalline Pt particles in PPy act as catalytic sites for multielectron transfer reactions.[600] Purely chemical routes can also be used to prepare zerovalent metals inside polymers. Examples include (a) Pd nanoparticles prepared and immobilized in electrospun polyethylenimine (PEI)/poly(vinyl alcohol) (PVA) nanofibers by reduction of a Pd(II) solution with $NaBH_4$,[601] and (b) positively charged PPy films electrosynthesized in a ClO_4^- electrolyte, where these ions become assimilated into the film to compensate charges in which $PdCl_4^{2-}$ ions are then exchanged with the ClO_4^- and become reduced, forming Pd^0 nanoparticles.[602] The zerovalent metal can be released through the regeneration step described above, aided by the presence of strong complexing agents like EDTA in the receiving aqueous solution that afford more favorable system thermodynamics.[582]

3.2.2.2. Anionic Pollutant Dynamics. The general equations for the removal of undesirable anions, B^-, by a conducting polymer are

$$CP^{n+}{\cdot}nA^-(s) + nB^-(aq) \rightarrow CP^{n+}{\cdot}nB^-(s) + nA^-(aq) \qquad (9)$$

$$CP^{n+}{\cdot}nB^-(s) + ne^- \rightarrow CP^0(s) + nB^-(aq) \qquad (10)$$

where B^- is, for example, $1/2CrO_4^{2-}$ or $1/m\ ML_b^{m-}$ (see Figure 28). The CP regeneration step is then:

$$CP^0(s) + nA^-(aq) \rightarrow CP^{n+}{\cdot}nA^-(s) + ne^- \qquad (11)$$

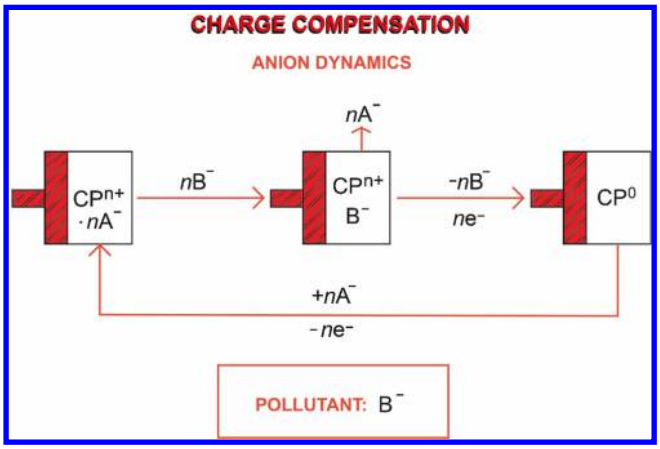

Figure 28. Charge separation with anion dynamics.

When CP^{n+} is reduced to its neutral state as shown in eq 10, electroneutrality can be achieved either by the expulsion of B^- or by the incorporation of cations (e.g., M^{m+}) shown in eq 6.[587,592] The rate of release of anions (e.g., Br^-, $[Fe(CN)_6]^{3-}$) during this reduction step depends on surface morphology, as evidenced by atomic force microscopy (AFM) and also on the reduction potential, as evidenced by scanning electrochemical microscopy (SECM).[590] The nature and size of dopants inside a CP matrix may influence several of its physicochemical properties like porosity, electrical conductivity, hydrophobicity/hydrophilicity, density, cross-linking degree, isotropy/anisotropy, permeability, and mechanical properties.[591] For example, small inorganic anion dopants yield larger pore diameters than bulky amphiphilic anions in PPy (Figure 29).[591]

The removal of charged pollutants with CP-based systems has been tested successfully, for example, in (a) the removal of NO_3^- using a phenothiazine polymer (PAA), where the electrochemical anion recognition selectivity over, for example, Cl^- anions can be evaluated by AC-electrogravimetry (i.e., the combination of electrochemical and mass impedance spectroscopy),[603] (b) the removal of ClO_4^- using a PPy−carbon nanotube composite (PPyCNT)[586] or a nanostructured poly(aniline-*co*-*o*-aminophenol) (PANOA) conducting copolymer,[599] and (c) the removal of F^- from water (i.e., defluoridation) using large surface area CP/inorganic hybrid composites, like PANi/montmorillonite (PANi−MMT) and PPy−MMT,[604] or using ecofriendly conducting polymer/biopolymer composites, like PANi/chitosan (PANi/Ch) and PPy/Ch. FTIR, X-ray, scanning electron microscopy, SEM, and energy-dispersive X-ray analysis (EDAX) patterns suggest that defluoridation occurs via a dopant-exchange mechanism on the N atoms present in the CP.[605] Although the charge dynamics approaches just discussed are not amenable for the removal of

DOI: 10.1021/acs.chemrev.7b00482
Chem. Rev. 2018, 118, 4731−4816

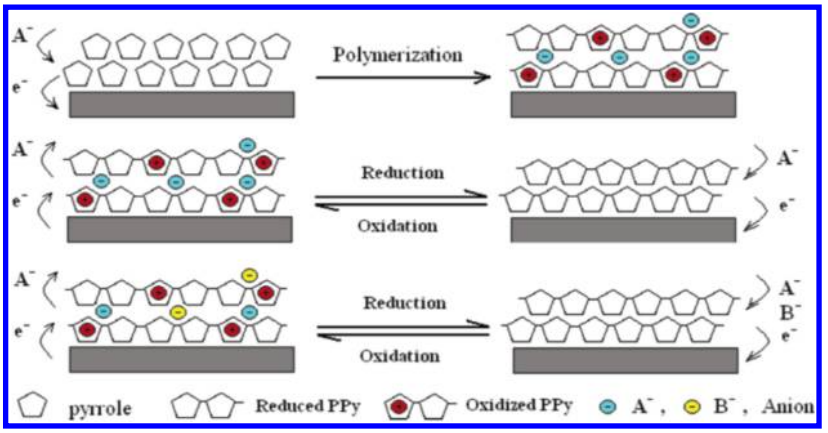

Figure 29. Anion intake and elution accompanied by the oxidation/reduction of PPy. Note that there are three or four Py units per positive charge in the oxidized PPy. Reproduced with permission from ref 586. Copyright 2006 American Chemical Society.

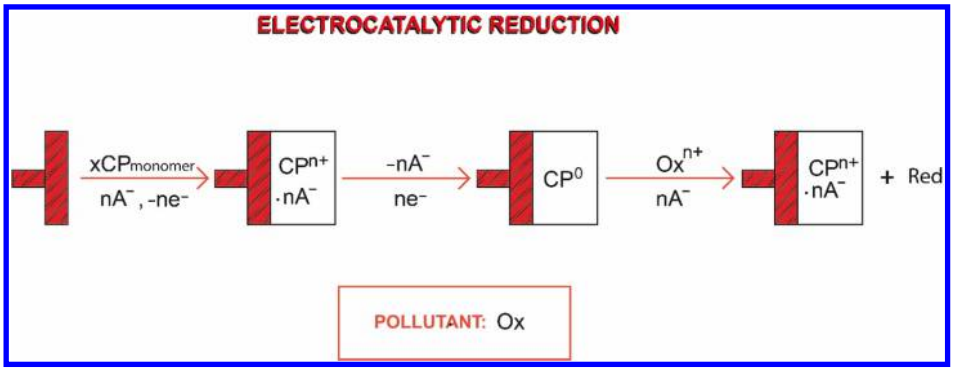

Figure 30. Pollutant removal or transformation through electrocatalytic reduction.

soluble neutral metal complexes, the addition of specific species (e.g., charged ligands, H^+, or OH^- ions) to form the corresponding positively or negatively charged complexes may render them apt for removal.[582]

3.2.3. Electrocatalytic Reduction/Oxidation. CPs are often suitable for electron transfer that can be used advantageously for pollutant remediation. They display higher stability and hydrophobicity than monolayers of adsorbed or covalently bound catalysts and require less energy expenditure than adsorption, demineralization, or photolytic approaches for the removal of sample pollutants.[606]

3.2.3.1. Electrocatalytic Reduction. Probably the most studied system is the reduction of harmful and highly mobile $Cr_2O_7^{2-}/CrO_4^{2-}$ ions with (a) PPy,[575,607−609] (b) PPy composites with Fe_3O_4,[610] carbon nanotubes,[611] cellulose fiber,[612] or 2,5-diaminobenzenesulfonic acid,[613] (c) PANi,[584,608] (d) PPy−PANi composite nanofibers,[578] (e) PANi−titanotungstate composites,[614] and (f) Pd-decorated PANi,[608] among others. This reduction is mainly based on two phenomena: (i) a spontaneous chemical reaction between PPy and CrO_4^{2-} driven by their different reduction potentials,[578] and (ii) an anion exchange process prompted by the electroneutrality requirement resulting from the polymer oxidation step,[575] as shown in Figure 30.

The generalized reaction sequence is as follows:

$$x\mathrm{CP}_{\mathrm{monomer}}(\mathrm{aq}) + n\mathrm{A}^-(\mathrm{aq}) \rightarrow \mathrm{CP}^{n+}\cdot n\mathrm{A}^-(\mathrm{s}) + n\mathrm{e}^- \quad (12)$$

$$\mathrm{CP}^{n+}\cdot n\mathrm{A}^-(\mathrm{s}) + n\mathrm{e}^- \rightarrow \mathrm{CP}^0(\mathrm{s}) + n\mathrm{A}^-(\mathrm{aq}) \quad (13)$$

$$\mathrm{CP}^0(\mathrm{s}) + \mathrm{Ox}^{n+}(\mathrm{aq}) + n\mathrm{A}^-(\mathrm{aq}) \rightarrow \mathrm{CP}^{n+}\cdot n\mathrm{A}^-(\mathrm{s}) + \mathrm{Red}(\mathrm{aq}) \quad (14)$$

where $CP_{monomer}$ is the monomer of the conducting polymer, Ox is a pollutant in its oxidized form (e.g., CrO_4^{2-}), Red is its reduced form (e.g., Cr(III)), and all the other symbols are the same as in the previous equations. Note that in this system there is no need for a regeneration step since the pollutant itself regenerates the conductive polymer's active form (eq 14).

However, the conversion decrease upon repetitive cycling presents a challenge.[607,615] Adsorption of the pollutant onto the polymer is an additional removal pathway, and it can make the process even more useful.[608,616,617] X-ray photoelectron spectroscopy (XPS) has shown that the product, Cr(III), can also be adsorbed. In addition, the electrode material itself may contribute to the reduction of Cr(VI) like in the case of reticulated vitreous carbon (RVC).[609] The direct reduction route on a PANi/vitreous carbon electrode was modeled considering both a plug-flow reactor (PFR) and a continuously stirred tank reactor (CSTR) to determine the mass transfer coefficients from concentration−time profiles. The respectable overall current efficiency and energy consumption values thus obtained encourage further study of this approach.[618]

The use of zerovalent nanoparticle Pd in nanofibrous polymeric materials in the presence of a reducing agent provides excellent catalytic activity and reusability for the reduction of Cr(VI) to Cr(III).[601] Electrocatalytic dehalogenation of organics using zerovalent Pd in a conducting polymer matrix (e.g., PPy) presents an alternative remediation strategy

DOI: 10.1021/acs.chemrev.7b00482
Chem. Rev. 2018, 118, 4731−4816

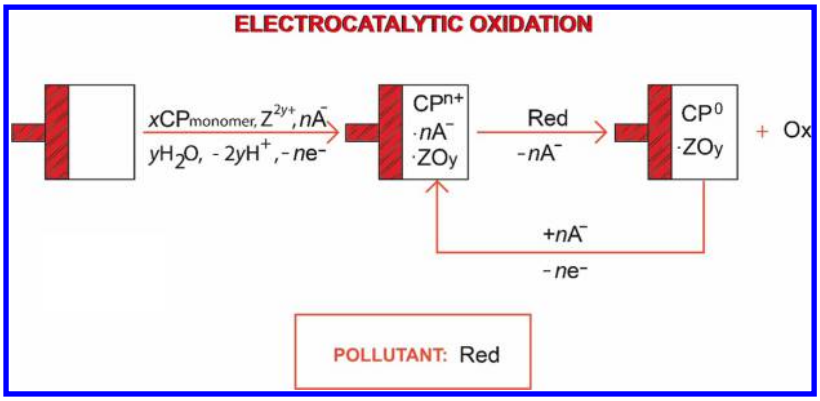

Figure 31. Pollutant removal or transformation through electrocatalytic oxidation.

for harmful halogenated compounds, and it will be discussed later.[602]

Interest in the electroreduction of NO_3^- ions derives from its synthetic and environmental applications. On the one hand, indirect NO_3^- toxicity has been widely documented (e.g., the blue-baby syndrome).[619] On the other hand, useful NH_3, NH_2OH, and N_2H_4 are obtained at metal electrodes from NO_3^- reduction; for example, NH_3 is the main product when using PPy−Cu electrodes.[620] NO_3^- reduction occurs through electron transfer from PPy through the N-sites located in its ring, whereas NO_3^- removal from water occurs at PANi through the ion exchange mechanism described earlier, between Cl^- and SO_4^{2-} counterions, as assessed by FTIR and XPS.[621]

CO_2 reduction/fixation is also of major interest from the synthetic and environmental perspectives. Perhaps, the most obvious approach is the one involving its heterogeneous methanation at high temperatures. Unfortunately, the practicality of this process is rather small.[622] Electrochemical routes do not require such high temperatures and are worth exploring. For example, the production of acetic, formic, and lactic acids, as well as methanol and ethanol, from CO_2 reduction has been achieved by an ingenious chemical activation of CO_2, stemming from the combination of the electrophilicity of the carbon atom and the amino groups in Fe(II)-immobilized PANi/Prussian blue (PB) laminated electrodes.[622] This, together with the interaction between the basic oxygen atom of CO_2 and the Fe(II) in the complex, as well as the catalytic generation of $H_{(ads)}$ atoms at the zeolitic structure of PB, promotes the hydrogenation of CO_2 to form the organic acids and alcohols mentioned above.

3.2.3.2. Electrocatalytic Oxidation. Here, a material possessing electrocatalytic properties for the oxidation of target pollutants is incorporated into the polymeric matrix, whereby the polymer changes its oxidation state during the process *but not the oxidizer*. A simplified scheme is as follows:

$$x\mathrm{CP}_{\mathrm{monomer}}(\mathrm{aq}) + n\mathrm{A}^-(\mathrm{aq}) + \mathrm{Z}^{2y+}(\mathrm{aq}) + y\mathrm{H_2O(l)} \rightarrow \mathrm{CP}^{n+}\cdot n\mathrm{A}^-\cdot \mathrm{ZO}_y(\mathrm{s}) + 2y\mathrm{H}^+(\mathrm{aq}) + n\mathrm{e}^- \quad (15)$$

$$\mathrm{CP}^{n+}\cdot n\mathrm{A}^-\cdot \mathrm{ZO}_y(\mathrm{s}) + \mathrm{Red(aq)} \rightarrow \mathrm{CP}^0\cdot \mathrm{ZO}_y(\mathrm{s}) + \mathrm{Ox}^{n+}(\mathrm{aq}) + n\mathrm{A}^-(\mathrm{aq}) \quad (16)$$

where ZO_y is the electrocatalytic metal oxide (e.g., PbO_2 forming a hydrophobic composite with PPy on the surface of a SnO_2/Ti substrate), Z^{2y+} is its metal precursor (e.g., Pb(II)), Red is a pollutant in its reduced form (e.g., 2-chlorophenol), and Ox is its corresponding less hazardous oxidized form (e.g., C_2 and C_4 carboxylic acids plus CO_2).[606] The other symbols have the same meaning as in the previous eqs. (Figure 31).

The corresponding electrode regeneration step is then:

$$\mathrm{CP}^0\cdot \mathrm{ZO}_y(\mathrm{s}) + n\mathrm{A}^-(\mathrm{aq}) \rightarrow \mathrm{CP}^{n+}\cdot n\mathrm{A}^-\cdot \mathrm{ZO}_y(\mathrm{s}) + n\mathrm{e}^- \quad (17)$$

In fact, catalysts composed of metal or metal oxide nanoparticles supported on CPs represent an effective approach in energy production and storage due to the enhancement of thermodynamic and kinetic aspects of desired oxidation reactions.[623] PbO_2 is preferred in several processes (like in 2-chlorophenol oxidation) due to its high electrical conductivity, large dioxygen overpotential, low cost, and relative chemical inertness.[606] In a different example, NiO_x films on PPy (grown on graphite) are effective in oxidizing ethanol, probably as a result of the generation of oxidizing Ni(III) active sites in the polymer matrix.[624] Another application focuses on harmful As(III) species, of both natural and anthropogenic origin. A typical treatment involves their oxidation to As(V), which is much less toxic and easily solubilized. Nanocomposites synthesized by incorporation of metal nanoparticles dispersed in a CP matrix show effective electrocatalytic properties toward the oxidation of As(III) to As(V).[625]

3.2.4. Other Various Applications in Environmental Remediation. A variety of additional applications of conducting polymers to environmental remediation are considered next.

3.2.4.1. Pollutant Adsorption. Conducting polymers can function as pollutant adsorbers. For example, an ecofriendly polymer/biopolymer composite (PANi/chitosan) adsorbs large amounts of dyes from aqueous solutions.[626] FTIR helped to confirm the involvement of amino and hydroxyl groups in such adsorption. Polymer roughness, as evidenced by SEM, enhances the possibilities for dye adsorption.[626] For instance, methyl orange is adsorbed at a PANi/clinoptilolite composite.[627] Polythiophene is a useful adsorbent material for the removal of toxic As(III), because these ions become attached to the π-electrons at the backbone of the polymer, resulting in a strong interaction between the S and As atoms.[628] Lastly, the combined sorptional−photocatalytic remediation of dyes can be achieved by PANi−Zr(IV) nanocomposites.[629] The participation of CPs in photocatalysis is further discussed below.

3.2.4.2. Use of 3D Materials. Some of the applications discussed in the present section can be considerably assisted by

DOI: 10.1021/acs.chemrev.7b00482
Chem. Rev. 2018, 118, 4731−4816

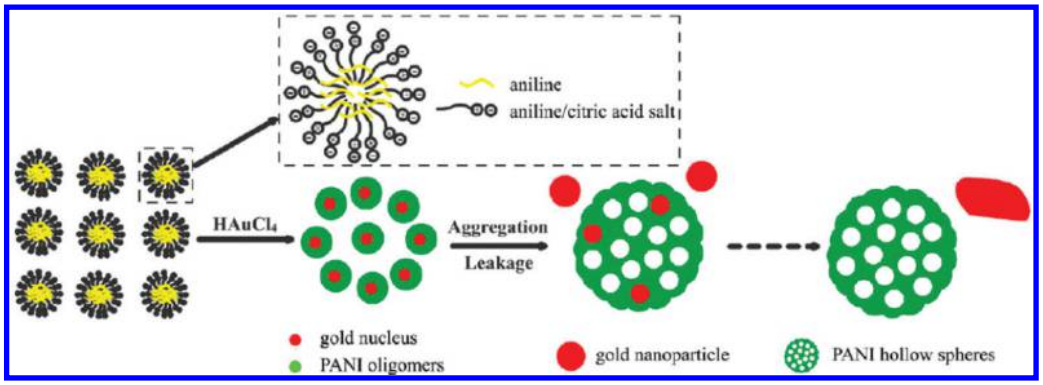

Figure 32. Formation mechanism of PANi hollow nanospheres. Reproduced with permission from ref 594. Copyright 2012 American Chemical Society.

the use of CPs deposited on three-dimensional materials (e.g., porous glassy carbon or graphite felts) since pollutants are frequently present at low concentration levels and, therefore, their mass transfer rates toward the electrodes are severely limited. In addition, the high electroactive areas thus obtained normally increase the target reaction rates.[575] A promising structure is that of PANi hollow nanospheres with controllable discontinuous nanocavities due to their low effective density and high specific surface area (see Figure 32).[594]

3.2.4.3. Use of Conducting Polymer Dendrimers. Exciting properties of these highly branched macromolecules can be exploited for environmental applications such as water purification and pollutant sensing and removal.[630] With regard to the present review, some new-generation dendrimers may be modified to be electronically conductive (see Figure 33). For example, a high density of aromatic anion radicals attached to the outside edges of a dendrimer may lead to intramolecular delocalization, therefore increasing its conductivity.[631] Dendrimers can selectively remove a variety of cationic, anionic, aromatic, and complex water-soluble (e.g., Cu^{2+}, NO_3^-) or insoluble (e.g., polyaromatic hydrocarbons, humic acids) pollutants. They can also contribute to oil dispersion and to the removal of target nanopollutants.[630] High selectivity is often governed by the dendrimer's structure as well as the geometry, size, and charge of the pollutant species to be removed (e.g., the trigonal geometry of monovalent NO_3^- ions versus the tetrahedral monovalent nature of TcO_4^- or the polyvalent nature of SO_4^{2-}, CrO_4^{2-}, AsO_4^{3-}, or PO_4^{3-} species).[630] The pH can also play a role here as some groups within the dendrimers may have their chemistries governed or modified by proton inclusion or removal or by Lewis acid−base/complex-forming interactions.[630]

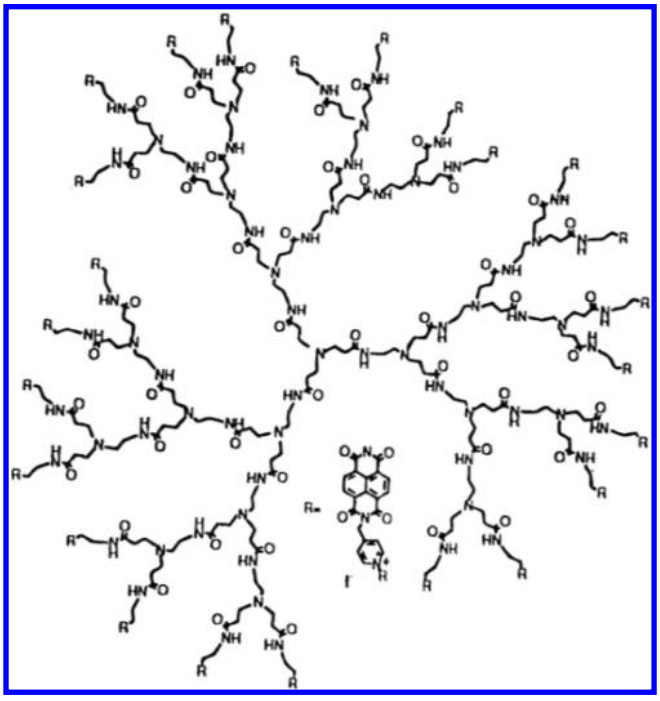

Figure 33. A poly(amidoamine) conducting dendrimer. Reproduced with permission from ref 631. Copyright 1997 American Chemical Society.

3.2.4.4. Gas Removal. Physical adsorption is typically the method of choice for the removal of small-molecule undesired gases like NO_x, NH_3, H_2S, SO_2, CO_2, and CO.[632] However, when these gases are to be removed in the presence of moisture, the strength of the adsorption forces toward the receiving substrates weakens considerably. In such cases, reactive adsorption is preferred.[632] This is the situation of the highly efficient reduction of NO_2 to NO at graphite oxide−PANi composites (see Figure 34), whose importance stems from the much reduced toxicity of NO as compared to NO_2.[632] In addition to the CO_2 reduction described above, highly selective CO_2 removal from a mixture of CO_2, N_2, CH_4, and H_2 can be achieved by S-doped microporous carbon materials synthesized by the chemical activation of a reduced graphene oxide/polythiophene substrate. A stable recycling adsorption capacity combined with a large specific surface area makes this a promising approach (Figure 35).[633]

In principle, most analytes detected by CP sensors could be captured or transformed using this scheme. Other species include[634] hexane, benzene, toluene, xylene, ethylbenzene, methanol, ethanol, acetone, butanone, pentanone, ammonia, triethylamine, acetonitrile, and dioxygen. The photocatalytic approach described below serves well for certain gases, like ammonia, using, for example, a PANi−TiO_2 composite.[635]

3.2.4.5. Dechlorination. Reductive dechlorination has long been proposed as an alternative for the remediation of harmful halogenated organics. It is well-known that the more halogens in an aromatic structure, the more toxic it is.[602,619] Therefore, the removal of halogen atoms is a viable strategy. Interestingly, electrochemical halogen removal can be performed stepwise.[636−639] A dechlorination example using a conducting polymer involves Pd^0 nanoparticles immobilized in a PPy matrix as described above for the reductive dechlorination of

DOI: 10.1021/acs.chemrev.7b00482
Chem. Rev. 2018, 118, 4731−4816

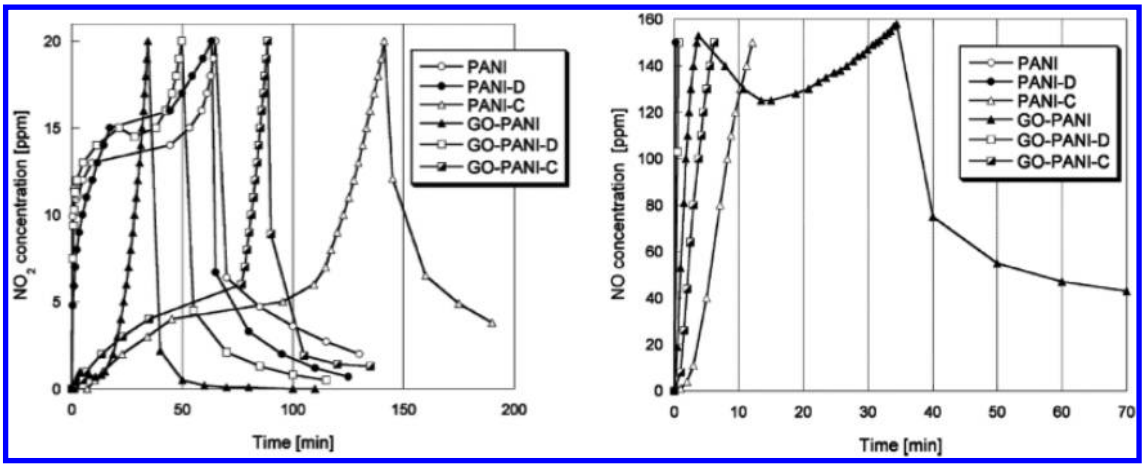

Figure 34. NO_2 reduction to NO at different PANi composites. (left) NO_2 breakthrough curves. (right) NO concentration curves. Note specially the curves for graphite oxide–PANi composite (full triangles). Reproduced with permission from ref 632. Copyright 2007 American Chemical Society.

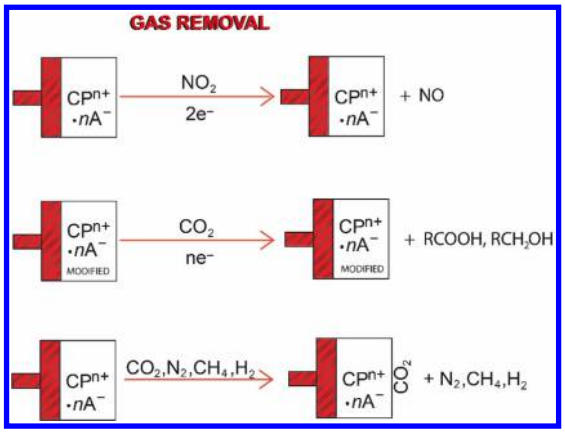

Figure 35. Gas removal using conducting polymers.

harmful 3,3′,4,4′-tetrachlorobiphenyl in the presence of hydrogen. The removal of chlorine atoms leads ultimately to biphenyl, therefore reducing toxicity.[602]

3.2.4.6. Photocatalysis. Photocatalysts are well-known for their ability to degrade harmful pollutants mainly through oxidation mechanisms prompted by the formation of holes in their valence bands.[640] Reduction mechanisms effected by electrons photogenerated in the conduction bands are suitable as well (Figure 36).[640]

The addition of inorganic spherical particles (e.g., TiO_2) to a polymer (e.g., PANi) during polymerization may lead to the tuning of selected physical properties at will (e.g., conductivity).[641] This also provides the salutary effect of avoiding the release of harmful TiO_2 nanoparticles into the environment.[642] Such a CP modification provides alternative pathways for pollutant degradation as shown in Figure 37.

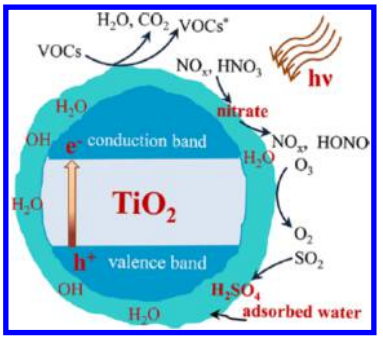

Figure 36. Photooxidations and photoreductions at a TiO_2 particle. Reproduced with permission from ref 640. Copyright 2012 American Chemical Society.

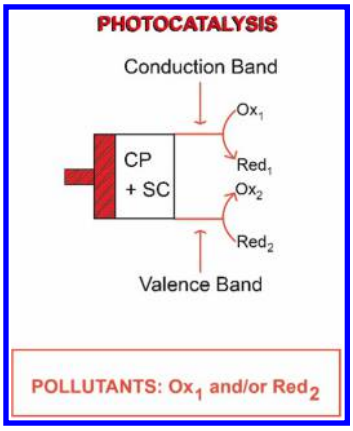

Figure 37. Photocatalysis by semiconductors (SC) inside CP matrices.

For example, PANi is used as a sensitizer and support in a TiO_2 photocatalyst structure prepared by a simple impregnation–hydrothermal process for the degradation of selected dyes (e.g., anthraquinone and reactive brilliant blue, KN-R) under visible light irradiation.[643,644] In addition, conductive poly(3-hexylthiophene) (P3HT) has been coupled to TiO_2 for the efficient photocatalytic degradation of methylene blue also using visible light.[645] The process is aided by the effective charge separation prompted by the heterojunction formed between the semiconductor and the CP. Microwave irradiation can increase the efficiency of a photocatalytic process, like in the degradation of the Orange G dye with a poly(1-naphthylamine), PNA/bentonite clay nanohybrid.[642] An efficient degradation is also achieved using carbonaceous WO_3/TiO_2 composites with PANi and PPy due to their higher porosity, better charge separation, and photoresponse range extension induced by a synergistic effect of PANi/PPy, WO_3, and TiO_2.[646] In addition to the use of TiO_2 as a photocatalyst, other inorganic oxides are used as well. For example, a ZnO composite with the poly(aniline-*co*-*o*-aminophenol) [poly(ANI-*co*-*o*AP)] conducting copolymer is an efficient photocatalyst for

DOI: 10.1021/acs.chemrev.7b00482
Chem. Rev. 2018, 118, 4731–4816

Table 4. Use of Conducting Polymers for Elimination of Undesirable Chemical Species

CP or matrix containing a CP	type of interaction for pollutant removal				ref
	uptake/release	CP oxidation/reduction	CP reduction/oxidation	electrocatalytic reduction/oxidation	
PANi	Hg(II) by complexation with N-functional groups				577
PPy			Pb(II), Cd(II), Ni(II) removal		576
PPy		Na^+, Ca^{2+}, Cl^-, SO_4^{2-} exchange			587
PPy		$Cr_2O_7^{2-}$, CrO_4^{2-} exchange with Cl^-			575
PPy/PANi		$Cr_2O_7^{2-}$, CrO_4^{2-} ion exchange + reduction			578
PANi				$Cr_2O_7^{2-}$, CrO_4^{2-} reduction to Cr^{3+}	584
PANi	adsorption/desorption of $Cr_2O_7^{2-}$ and reduction to Cr^{3+}		adsorption/desorption of $Cr_2O_7^{2-}$ and reduction to Cr^{3+}		579
PANi/MMT	F^- removal by adsorption				604
PPy		large anions (catechol) and cation exchange of Pb^{2+}, Ni^{2+}, Cd^{2+}, Co^{2+}, and Zn^{2+}			581
PPy				Ni^{2+} reduction to Ni^0	582
PPy/CNT	ClO_4^- uptake/release by oxidized/reduced PPy				586
PPy		Na^+, K^+, Cs^+, Mg^{2+}, Cl^-, SO_4^{2-} exchange			592
PPy-bithiophene	Ba^{2+} complexation				593
PANi	Pb^{2+} removal by adsorption				594
PPy	Cu^{2+} removal by adsorption				595
PPy	^{57}Co removal				596
PEDOT	Cd^{2+} removal by cation exchange				597
PPy				PtX_y^{z-} reduced to Pt^0	600
PEI/PVA				Pd^{2+} chemically reduced to Pd^0	601
PPy/PdNP				Pd^{2+} is reduced to Pd^0 to perform reductive dechlorination of PCBs	602
PAA		NO_3^- anion recognition			603
poly(aniline-*co*-*o*-aminophenol)		ClO_4^- uptake/release			599
PANi or PPy/Ch	F-removal by dopant exchange				605
PPy				$Cr_2O_7^{2-}$, CrO_4^{2-} reduction to Cr^{3+}	607
PPy/PANi/Pd				$Cr_2O_7^{2-}$, CrO_4^{2-} reduction to Cr^{3+} and subsequent adsorption	608
PPy				$Cr_2O_7^{2-}$, CrO_4^{2-} reduction to Cr^{3+}	609
PPy/Fe_2O_3	partial Cr(VI) removal by adsorption		$Cr_2O_7^{2-}$, CrO_4^{2-} reduction to Cr^{3+}		610
PPy/OMCNT	partial Cr(VI) removal by adsorption		$Cr_2O_7^{2-}$, CrO_4^{2-} reduction to Cr^{3+}		611
PPy/cellulose	Cr(III) adsorption		initial $Cr_2O_7^{2-}$, CrO_4^{2-} reduction to Cr^{3+}		612
PPy/2,5 diaminobenzenesulfonic acid	$Cr_2O_7^{2-}$, CrO_4^{2-} chemisorption		final $Cr_2O_7^{2-}$, CrO_4^{2-} reduction to Cr^{3+}		613
PANi/TiW	^{134}Cs adsorption and ion exchange				614

DOI: 10.1021/acs.chemrev.7b00482
Chem. Rev. 2018, 118, 4731−4816

Table 4. continued

CP or matrix containing a CP	type of interaction for pollutant removal: uptake/release	CP oxidation/reduction	CP reduction/oxidation	electrocatalytic reduction/oxidation	ref
PPy			$Cr_2O_7^{2-}$, CrO_4^{2-} reduction to Cr^{3+}		615
PPy/threonine	Cr(VI) removal by adsorption				616
PPy/graphene oxide	Cr(VI) removal by adsorption				617
PANi				potentiostatic $Cr_2O_7^{2-}$, CrO_4^{2-} reduction to Cr^{3+}	618
PPy				direct reduction of NO_3^- to NH_3	620
PANi/PB				CO_2 reduction to alcohols and organic acids	622
PPy/PbO_2				oxidation of 2-chlorophenol to C2 and C4 organic acids + CO_2	606
PPy/NiO_x				oxidation of ethanol by Ni(III)	624
PANi/Ch	dye removal by adsorption				626
PANi/Zr(IV)				sorptional and photocatalytic remediation of dyes	629
dendrimers	applications in humic acid antifouling, oil dispersion, copper sensing, and fullerenol remediation				630
PANi/graphite oxide			reactive adsorption of NO_2 for its reduction		632
polythiophene/reduced graphene oxide	CO_2 capture by selective adsorption				633
PANi/TiO_2				photocatalytic degradation of dyes (e.g., methylene blue, anthraquinone, and reactive brilliant blue KN-R)	643
PANi/TiO_2				photocatalytic degradation of dyes	644
P3HT/TiO_2				photocatalytic degradation of methylene blue with visible light	645
PNA/bentonite				photocatalytic degradation of orange G dye	642
PPy/PANi/WO_3/TiO_2				photocatalytic degradation of methylene blue	646
Poly(ANi-*co*-*o*AP)/ZnO				photocatalytic degradation of methylene blue	647
PPy/Bi_2WO_6				photocatalytic degradation of phenol with solar light	648

DOI: 10.1021/acs.chemrev.7b00482
Chem. Rev. 2018, 118, 4731−4816

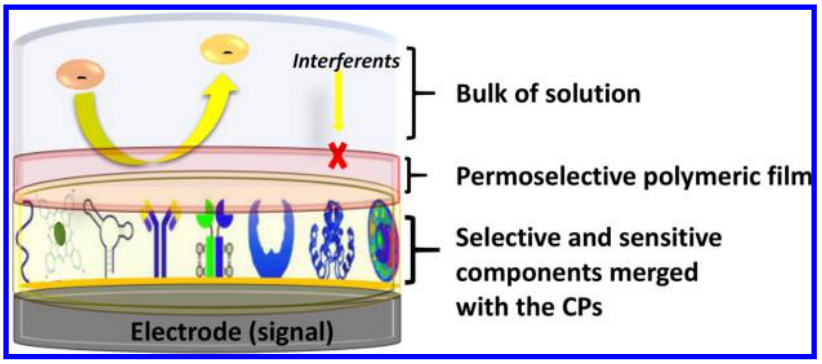

Figure 38. Interaction between a CP matrix and the target analyte to be detected by the transduction system.

MB degradation.[647] A rational design of an efficient system involves recognition of the need for rapid electron transfer kinetics to prevent recombination of photogenerated electrons and holes. Since conducting polymers possess high charge carrier mobility, a PPy/Bi_2WO_6 composite was designed to promote efficient charge separation during the photodegradation of phenol, as a model pollutant, under simulated sunlight irradiation. In this way, the photogenerated holes in the valence band of Bi_2WO_6 were transferred to the highest occupied molecular orbital (HOMO) of PPy, leading to rapid photoinduced charge separation.[648] Lastly, bacterial deactivation and organic pollutant degradation can be achieved with CP-sensitized, highly ordered TiO_2 nanotube arrays.[649]

3.2.4.7. Dioxygen Removal. A further environmentally related application of CPs involves the removal of dioxygen from aqueous solutions to prevent the corrosion of metallic pieces and assemblies. For example, a Ni electrode covered with conducting PPy is capable of reducing dioxygen in neutral solutions to yield hydroxyl ions through a $4e^-$ path.[650]

In order to give to the reader easy access to the information so far discussed, Table 4 shows a summary of the use of CPs for the uptake/release or oxidation/reduction of undesirable chemical species.

3.2.5. The Future of CPs in Environmental Sciences. The applications of CPs to the solution of environmental problems are around the corner, and many of the concepts explored in this review merit further investigation to achieve their full development. Doping and dedoping processes involving anion or cation dynamics are exploited in this field and may be a source of inspiration for new CP-based remediation methodologies, particularly for metallic ions that are difficult to remove. Redox reactions can also be used to advantage for the transformation of multiple contaminants where oxidation states play a key role in their toxicity (e.g., Cr(VI) versus Cr(III), or As(III) versus As(V)). The ability of CPs to incorporate catalysts into their structures can also be exploited to transform pollutants with higher energy efficiency in electrocatalytic schemes. Visible light can be harnessed in photoelectrocatalytic processes to produce pollutant oxidations or reductions. Modern materials (e.g., dendrimers, 3D materials) favor mass transfer and selectivity. All of these concepts are well in accord with modern green chemistry trends where more efficient reactions and new environmentally friendly chemical treatments for pollutants are needed for a sustainable future. This research field is very active and can be a source of innovations for solving real problems and industry applications in the environmental arena.

4. PART 2. APPLICATIONS THAT TAKE ADVANTAGE OF MODIFICATIONS AT THE POLYMER–ELECTROLYTE INTERFACE

4.1. Application of Conducting Polymers in Electroanalysis

4.1.1. Introduction to Application of Conducting Polymers in Electroanalysis. Conductive polymers (CPs) have unique characteristics that enable their customization for specific needs. Properties like color, weight, flexibility, scalability, and resistance to corrosion make CPs a promising option for the fabrication of sensors.[651,652] Recent advances in nanotechnology have prompted the development of electrochemical sensors as an inexpensive method to detect a variety of species with high sensitivity and better performance; for example, Brett has excellently reviewed the preparation, characterization, and application of redox polymers doped with nanotubes for electroanalysis of some important molecules.[653] Such sensors are used in the measurement and amplification of signals in various fields, including medical diagnosis, environmental monitoring of trace metals, and routine analysis in food or pharmaceutical industries. The most important procedures to customize CPs for analytical purposes are described next.

The controlled synthesis of CPs can be done electrochemically by simply adjusting relevant parameters in the electropolymerization protocol (e.g., scan rate and applied potential, electropolymerization media); thus selective modification of metallic electrodes with desired polymer backbone is commonly applied in sensing.[653] An adequate selection of experimental conditions like pH, the nature of the solvent and supporting electrolyte, the amount of charge passed, and the doping agent allows adjustment of the thickness, porosity, viscoelastic properties, morphology, and binding properties for the final CP films.[654] In this section, various strategies reported in the literature to improve the sensitivity of the electrodes in electroanalysis, are illustrated, as well as the most important applications of the sensors and their advantages and disadvantages.

Nanoscale hybridization of CPs[652,655] with carbon nanotubes, graphene, metal nanoparticles, or metal oxide nanoparticles can improve the sensor sorption–adsorption (molecular interaction), electrocatalytic reactivity (electron transfer), or transport behavior (mass transfer). More complex nanohybrids containing CP blends, multiple nanoparticle materials, or gradients thereof can also be envisioned for sensor arrays to analyze gas mixtures (H_2S, NO_x, CO_x) due to the improved sensitivity toward a specific analyte. Recent developments in sensors literature using nanoscale hybridization as a new way to

DOI: 10.1021/acs.chemrev.7b00482
Chem. Rev. 2018, 118, 4731–4816

construct the sensing element of electroanalytical determinations will be reviewed in this section.

Common methods to immobilize recognition elements within the CP sensing film include electrochemical entrapment (i.e., doping), covalent attachment, physical adsorption, and affinity interactions.[656] Molecular imprinting,[657,658] a technique developed more than 30 years ago, is used for designing 3D cavities in the CP matrix, which are useful as sensor electrodes. When the doping process that occurs during the electropolymerization is used to immobilize a recognition element, the polymer is electrochemically oxidized and reduced changing its morphology, charge, and volume. Such a change allows the formation of films that contains a recognition element, which have shown good reproducibility in the detection of various analytes (Figure 38), and it is one of the most used approaches in electroanalysis.

Nanomaterial-modified systems represent a useful tool for the improvement of electrochemical methods since nanomaterials enable functional ability and novel electrical, optical, and catalytic properties, besides surface increment, which results in tremendous gain in terms of sensitivity, selectivity, and versatility.[659,660]

Among the different types of sensors, the electrochemical sensors are the most often employed because of the ease and low cost of manufacturing and the possibility of obtaining results that can be easily analyzed, for which the generated electrical current can be readily related to the analyte concentration in solution or in gas. Thus, electrochemical sensors have been of great interest for the scientific community mainly due to their inexpensive, accurate, and sensitive platform for analysis.[661] These characteristics are obtained by combining specific recognition and signal transduction processes.

It is possible to develop wearable electrochemical sensors that are small and light for seamless integration with the human body for daily life.[662]

Biorecognition has been demonstrated incorporating oligonucleotides, enzymes, aptamer, or antigen/antibodies into specific polymers.[663] Undoubtedly, the main advantage presented by the biosensors is the specificity and very low detection limit, but there are many problems, such as durability, reproducibility, and the high costs of pure biomolecules employed in their construction, which makes it unusual to find the biosensors in the common market, and they are only available for very specific, but expensive, biochemical analysis. One exception is glucose biosensors, which are nowadays a commercially available product.[664] The subject of bioelectrochemical sensors is very broad and has been comprehensively reviewed elsewhere in recent years.[651,653,654,656,665,666] Therefore, this review will be focused on electrochemical sensors for chemical species based on conducting polymers, giving an updated review on this important topic that looks underestimated in analytical chemistry. The development of electrochemical sensors faces multiple challenges on various fronts related to materials, power, analytical procedure, communication, data acquisition, processing, and security. Size, rigidity, stability, and operational requirements of electrochemical sensors must be compatible with the technology, and they are the key analytical challenges.

Applications of CPs for the detection of chemical species by means of sensing electrochemical changes at electrode interfaces include amperometric, potentiometric, impedimetric, electrochemical luminescent, and photoelectrochemical sensors. This review presents a selection of procedures that combine different materials and electrochemical techniques using CP modified electrodes as electrochemical sensors for chemical analytes in liquid and gas phase.

4.1.2. CP Based Chemical Sensors for Analytes in Solution. The preparation of the sensitive polymeric matrix that contains the recognition element is a crucial part of the analytical process. Once the interaction has occurred between a CP and the target analyte, a signal must be detected by the transduction system (Figure 38). Signals are typically electronic in nature (e.g., current, voltage, impedance, and conductance) and are caused by electron exchange, which can be recorded by potentiometric, voltammetric, amperometric, or impedimetric techniques.

4.1.2.1. Neurotransmitters. 4.1.2.1.1. Dopamine. Dopamine (DA) is an important neurotransmitter associated with neurological disorders such as Parkinson's disease and schizophrenia. DA can be detected electrochemically when the molecule is oxidized. A considerable variety of electrode materials have been developed to monitor DA.[667] PEDOT:PSS modified glassy carbon electrodes (GCE) have been used to detect DA and ascorbic acid (AscA).[668] In addition, a composite based on graphene (Gr) and PPy was synthesized via microwave irradiation. The PPy was embedded into Gr flakes to form a 3D structure with higher electrocatalytic activity. This DA sensor showed a detection limit of 2.3×10^{-6} M.[669] Other DA sensors (limit of detection = 5 nM), composed of organic electrochemical transistors (OECTs) based on PEDOT:PSS on various electrodes (e.g., graphite, Ag, and Pt electrode, etc.), displayed substantial reactivity and high sensitivity in the oxidation of DA and AscA. This represents a significant, straightforward approach for a simultaneous and selective measurement of DA and AscA.[670] Very well resolved symmetry and peak separation during DA and AscA simultaneous determination were obtained with a thin film of polytyramine on a carbon electrode (surface roughness = 0.7 nm, limit of detection = 142 nM and 331 nM, respectively).[671] Sensors made of electrochemically deposited polycarbazole (PCz) and poly(carbazole-*co*-*p*-tolylsulfonyl pyrrole) (PCz-*co*-*p*-Tsp) films on single carbon fiber microelectrodes showed an amperometric response to DA concentrations with a limit of detection = 0.27 μM for PCz and 0.5 μM for P(Cz-*co*-*p*-Tsp).[672] Enhanced electrocatalytic performance toward the oxidation of DA can be obtained by improving the electron transfer within the CP. This was achieved with a novel poly(ionic liquid)-functionalized PPy−graphene oxide nanosheet composite (PIL−PPy−GrO) obtained by the polymerization of 1-vinyl-3-ethylimidazolium bromide on the surface of *N*-vinyl imidazolium-modified PPy−GrO nanosheets.[673] In a separate effort to monitor DA, a nanocomposite of poly(3,4-ethylene dioxythiophene)−graphene oxide (PEDOT−GrO) was electrodeposited on a glassy carbon electrode (GCE), followed by electrochemical reduction to obtain the reduced nanocomposite (PEDOT−rGrO).[674] Using the same protocol of preparation, an unreduced form of GrO was incorporated.[675] The detection limit of the PEDOT−rGrO modified sensor was superior (i.e., 39.0 nM versus 83.0 nM with the PEDOT−GrO). This can be understood as GrO is less conducting than rGrO, given that the electrical conductivity can be tuned with the degree of oxidation/reduction.[676] Nevertheless, the PEDOT−GrO modified sensor was successful in eliminating AscA interference because of the significant shift of AscA oxidation potential caused by the electrocatalytic effect of the nanocomposite material.

DOI: 10.1021/acs.chemrev.7b00482
Chem. Rev. 2018, 118, 4731−4816

The preparation of large surface area carbon paste electrode (CPE) modified with a PEDOT−CNT nanocomposite resulted in good detection limits (0.3 μM) for hydroquinone in real cosmetics samples. They show satisfying accuracy for AscA,[677] DA (limit of detection = 20 nM),[678] and nitrobenzene,[679] without interference, with good conductivity, and with excellent catalytic activity. A significant increase in electrocatalytic activity toward the oxidation of DA was demonstrated in a nanocomposite of oligo(phenylene ethynylene) with chemically reduced graphene oxide, resulting in a detection limit of 5 nM.[680]

Poly(brilliant green) (PBG) films for DA sensing were electropolymerized on carbon film electrodes (CFE) from brilliant green monomer, which belongs to the triphenylmethane family, using potential cycling or at fixed potential from different pH solutions. With the aim of improving this response, multiwalled carbon nanotubes (MWCNTs) were deposited on CFE, and then PBG was formed on top of the resulting surface (PBG/CNT/CFE).[681] The determination of DA was successfully achieved without interference by AscA and at a detection limit of 2.4 mM. Other interferents like aspirin, acetaminophen, salicylic acid, and uric acid exhibited no response on the PBG/CNT/CFE modified electrode. A sensor based on Au/PANi hollow nanosphere hybrids, using polystyrene−sulfonated polystyrene core−shell gel particle templates, was built by controlling the shell thickness and the amount of gold nanoparticles decorating the surface of the PANi shell, which led to an advanced transistor in the range of sensor applications (Figure 39).[682] The relative standard

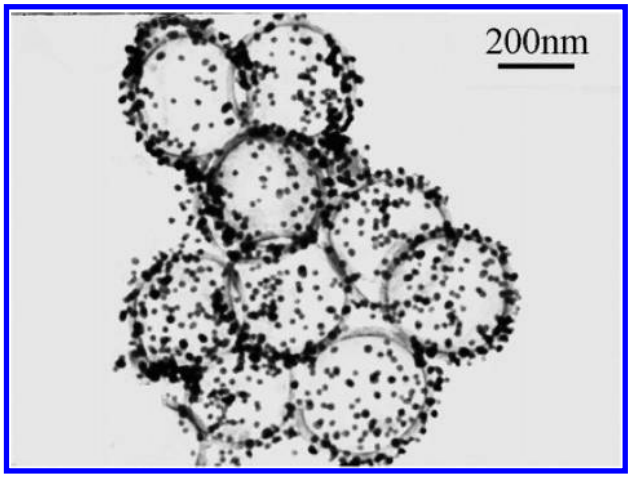

Figure 39. TEM images of PANi/Au hollow spheres. Synthetic conditions: aniline, 1 mmol; APS, 1 mmol; PANi concentration in the Au colloid, 0.5 mg mL^{-1}. Reproduced with permission from ref 682. Copyright 2006 American Chemical Society.

deviations of the catalytic peak current in successive determinations at a DA concentration of 2 mM were 0.4% and 0.5%, respectively, for PANi/Au and PANi- modified GCE.

Simultaneous detection of DA, AscA, and uric acid (UA) was well resolved by using PEDOT modified electrodes with cold plasma treatment. This forms a large variety of reactive species adsorbed on the electrode surface that catalyze the analyte oxidation.[683] For example, the detection limit for dopamine was 140 nM. Another example is the use of flower-like gold nanoparticle-decorated PPy/GrO nanohybrids produced by in situ chemical oxidative polymerization. This ultrasensitive DA detector has a very low detection limit of 18.29 pM and a linear range of 1−5000 nM.[684] As we can see, the electrochemical detection of DA has been extensively investigated. This is due to its importance in the health field and also to its electroactive character that allows its selective detection in complex media. However, it is important to see how the detection limits of DA improve considerably when electrodes modified with CPs are used in combination with materials that facilitate the catalytic oxidation of DA like GO, metallic nanoparticles, etc. These procedures are successful because the judicious combination of materials facilitate electronic transfer and also improve the affinity and orientation of functional groups of the DA with respect to the electrode's components.

4.1.2.1.2. Serotonin. Serotonin (5-hydroxytryptamine, 5-HT) is a biogenic monoamine neurotransmitter and neuromodulator found in the human brain. It plays a fundamental role in the regulation of various physiological functions like eating, sleeping, muscle contraction, sexual activity, and thermoregulation. The role of serotonin is also very important in regulating psychopathological processes such as anxiety disorder, liver regeneration, infantile autism, alcoholism, obsessive-compulsive disorder, and drug dependency.[685] An innovative and sensitive method for the simultaneous determination of dopamine (DA) and 5-HT uses graphene and a poly(4-amino-3-hydroxy-1-naphthalenesulfonic acid) (AHNSA) modified screen printed carbon sensor (SPC).[686] This sensor eased the analysis of DA and 5-HT in the concentration range 0.05−100 μM and 0.05−150 μM with detection limits of 2 nM and 3 nM, respectively. The analytical applicability of the fabricated sensor was established also for the simultaneous detection of DA and 5-HT in pharmacological formulations, human urine, and blood samples (Figure 40).

Another double-layered membrane sensing interface used for the selective detection of 5-HT at high sensitivity is based on rGrO−PANi nanocomposites and molecular imprinted polymers (MIPs) embedded with AuNPs.[687] The conducting membrane was deposited on the modified GCE by electropolymerization at a constant potential, using 5-HT as template molecules, functionalized AuNPs as functional monomers, and *p*-aminothiophenol as cross-linker. An exceptional selectivity for 5-HT against the interference caused by AscA and other interferents was observed, as well as a low detection limit of 11.7 nM. PEDOT−rGrO−silver hybrid nanocomposite modified electrodes were used as a transducer for the detection of 5-HT;[688] several electrochemical techniques such as CV, differential pulse voltammetry (DPV), and CA were used for the detection, with the best detection limit (0.1 nM) provided by DPV. Another low cost and practical sensor constructed with poly(pyrrole-3-carboxylic acid)-modified pencil graphite electrode was used for the determination of 5-HT[689] in blood serum and urine samples and showed a detection limit of 2.5 nM. A Nafion/$Ni(OH)_2$−multiwalled CNT modified GCE (Nafion/$Ni(OH)_2$−MWCNTs/GCE) was also applied to the electrochemical oxidation of DA and 5-HT using CV, DPV, and CA. Detection limits of 0.015 μmol L^{-1} for DA and 0.003 μmol L^{-1} for 5-HT were obtained in human blood serum.[690] Clearly the presence of carbonaceous material in the CP matrix favors the selectivity and performance of the analytical determinations, and it is expected that new carbon-based materials will be used in future developments in the field.

4.1.2.1.3. Epinephrine. Epinephrine (EP) is a catecholamine neurotransmitter that plays an important role in human health. Modified electrochemical sensors are widely used to trace EP, due to the tendency of the oxidation products to adsorb on

DOI: 10.1021/acs.chemrev.7b00482
Chem. Rev. 2018, 118, 4731−4816

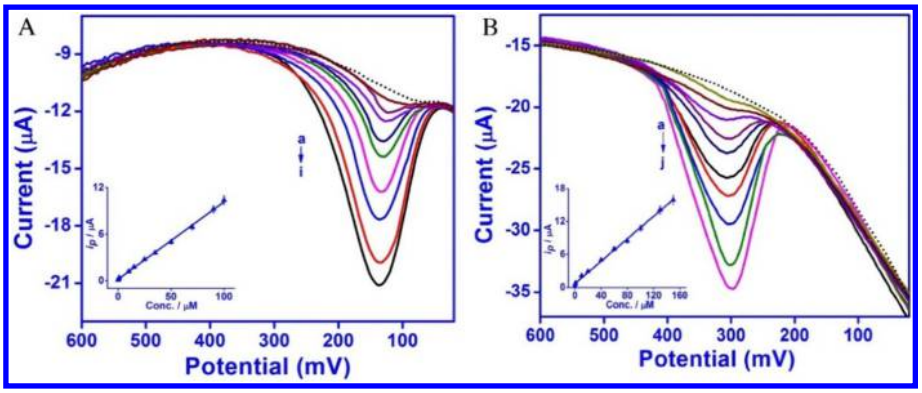

Figure 40. Square wave voltammograms observed for the increasing concentration of DA using Gr/*p*-AHNSA/SPCs in phosphate buffer at pH 7.2. The inset is the calibration plot. (B) Square wave voltammograms for 5-HT using Gr/*p*-AHNSA/SPCs in phosphate buffer at pH 7.20. The inset is the calibration plot. Reproduced with permission from ref 686. Copyright 2017 Elsevier.

bare electrodes.[691] Among those reported, a glassy carbon electrode modified with a polymeric brilliant cresyl blue (BCB) and dihexadecyl phosphate (DHP) dispersed multiwalled CNT (MWCNT) composite film yielded a very good response for EP analysis, with a low detection limit of 1.0×10^{-8} M.[692] A thin film of AuNP/PANi nanocomposite deposited on the surface of a GCE by Langmuir−Blodgett technology displayed a detection limit of 8×10^{-8} M for EP and 2.0×10^{-7} M for UA.[693] Functionalized CNT/PANi doped with metal oxide (TiO_2, RuO_2) and deposited on Au electrode yielded a linear calibration plot for EP in the concentration range of 4.9 to 76.9 μM with detection limits of 0.16 and 0.18 μM for modified TiO_2 and RuO_2 electrodes, respectively.[694] An interference study using DPV showed a clear separation for amino acid and EP oxidation processes, evidencing selective detection of EP without interference from amino acid (AA) signal. The analytical performance of these sensors was evaluated for EP detection in a pharmaceutical sample with satisfactory results. The electrochemical oxidation of EP on a poly(malachite green)/CNT/glassy carbon electrode (PMalG/MWCNT/GCE) at pH 7.0 also showed good separation between the oxidation processes of AA, EP, and uric acid (UA), demonstrating an enhanced electrocatalytic effect with a detection limit of 0.08 μM.[695] All these sensing approaches are based on the electrocatalytic effect of the CP based matrix and are clear examples of the open possibilities when modified electrodes are used.

4.1.2.2. Ascorbate. Ascorbic acid/ascorbate (AscA/Asc) is a vital component of the human diet; it prevents scurvy and is known to take part in many important biological reactions. It is perhaps the primary antioxidant in human blood plasma and is present in the mammalian brain together with various amine neurotransmitters including DP, EP, and norepinephrine (NE). Direct and selective electrochemical detection of Asc at conventional electrodes (metallic/vitreous carbon) is difficult because of its large oxidation overpotential and electrode fouling caused by oxidation products.[696]

Several electrocatalytic strategies have been developed using different types of modified electrodes to reduce such an overpotential, for example, by using carbon nanotube/polyphenazine- and carbon nanotube/poly-(triphenylmethane)-modified electrodes.[653] A sensitive electrode comprising PMalG with CNT on a GCE exhibited the lowest detection limits of 0.23, 0.0820, and 0.12 μM for AscA, EP, and UA, respectively; this modified electrode showed good sensitivity, selectivity, and stability with real samples.[695] Likewise, Pd nanoclusters on polyfuran film electrodeposited onto Pt electrode were reported for the analytical sensing of DA, EP, NE, AscA, and paracetamol (PCM); during DPV analyses, the sensor effectively resolved the overlapping anodic peaks of AscA, DA, and PCM into three well-defined voltammetric peaks, with similar detection limits for DA in the absence and presence of AscA and PCM. This indicates that the oxidation processes of DA, AscA, and PCM are independent and that the simultaneous measurements of the three analytes are possible without interference. The detection limits (S/N = 3) are 7.13×10^{-6}, 4.82×10^{-8}, and 7.64×10^{-8} M for AscA, DA, and PCM, respectively.[697]

Alternatively, a thin film of polytyramine (Pty) deposited on a GCE in a phosphate buffer solution (pH = 4.1) exhibited substantial reactivity and high sensitivity for the simultaneous oxidation of DA and AscA, with a detection limit brought down to 142 nM and 331 nM, respectively,[671] whereas AuNP/PANi/polydopamine hybrids provided a fast stable response in 4 s with low detection limit of 4.0×10^{-7} M for AscA,[698] due to the enhanced the catalytic capability brought out for the AuNPs.

A summary of the detection limits for the amine neurotransmitter sensors described above is presented in Table 5. Significant variations are found for the different sensors depending on their composition and the polymerization method of the monomer. Enhanced electron transfer in the different sensors is attributed to charge hopping through the material, which mediates the effective charge migration through the polymer. The method of polymerization of the CP generates many active sites for charge transfer by making good interfacial contact between the incorporated material and the polymer matrix. The effective electron transport inside the matrix leads to the efficient electrocatalytic oxidation of analytes. The affinity and orientation of the analyte with respect to the material in the modified electrode is an additional factor facilitating electrocatalysis and detection.[699]

4.1.2.3. Uric Acid. Uric acid and other oxypurines are the main final products of purine metabolism in the human body. UA coexists with AscA and DA in biological fluids like blood and urine. Because of the overlapping potentials of these three analytes, electrochemical analysis with unmodified electrodes (e.g., glassy carbon) presents limitations. A voltammetric sensor was proposed for the simultaneous determination of EP and UA. This modified sensor is based on polyaniline−gold nanoparticle (PANi−AuNP) nanocomposites deposited on GCE by Langmuir−Blodgett technology. This combination resulted in a significant electrocatalytic response to EP and UA,

DOI: 10.1021/acs.chemrev.7b00482
Chem. Rev. 2018, 118, 4731−4816

Table 5. Comparison of Detection Limits for Amine Neurotransmitters[a] in several sensors based on conducting polymers

sensor composition	detection limit	ref
Dopamine		
Gr and PPy	2300 nM	669
PEDOT	5 nM	670
polytyramine on glassy carbon	142 nM	671
polycarbazole with *p*-tolylsulfonyl pyrrole	500 nM	672
polycarbazole	270 nM	672
poly(ionic liquid)-functionalized PPy−GrO nanosheet	73.3 nM	673
PEDOT−GrO	83.0 nM	674
PEDOT−rGrO	39.0 nM	675
PEDOT−CNT	20.0 nM	679
oligo(phenylene ethynylene) and chemically rGrO	5 nM	680
poly(brilliant green)/CNT/carbon film electrode	2400 nM	681
PEDOT with cold plasma treatment	140 nM	683
flower-like AuNP/PPy/GrO	0.018 nM	684
AHNSA[b] modified screen printed carbon sensor	2 nM	685
Nafion/$Ni(OH)_2$−multiwalled CNT	15 nM	690
polytyramine (Pty) deposited on GCE	142 nM	671
Serotonin		
AHNSA[b]	3 nM	685
rGrO−PANi nanocomposites and MIPs embedded with AuNPs	11.7 nM	687
PEDOT−rGrO	0.1 nM	688
poly(pyrrole-3-carboxylic acid) modified pencil graphite electrode	2.5 nM	689
Nafion/$Ni(OH)_2$-multiwalled CNT	3 nM	690
Epinephrine		
polymeric brilliant cresyl blue and dihexadecyl phosphate dispersed multiwalled CNT	10 nM	692
Au nanoparticles/PANi nanocomposite thin film on the surface of GCE	80 nM	700
CNT/PANi doped with TiO_2, RuO_2	160 nM	694
CNT/PANi doped with RuO_2	180 nM	694
poly(malachite green)/CNT/GCE	80 nM	695
Ascorbate		
polytyramine on glassy carbon	331 nM	671
poly(malachite) green on glassy carbon	230 nM	695
palladium nanoclusters on polyfuran film modified Pt electrode	7.13 μM	697
AuNP/PANi/polydopamine	400 nM	698

[a]Dopamine, serotonin, epinephrine, and ascorbate. [b]Poly(4-amino-3-hydroxy-1-naphthalenesulfonic acid).

which allowed their stable simultaneous determination with high sensitivity.[700] Although AscA is a major interferent in this electroanalysis, this electrode allows for up to 50-fold excess of AscA in the sample, without interference for EP and UA detection. The relationship between peak currents and concentration for UA was linear in the range 4×10^{-7} to 6×10^{-5} M with detection limit of 2×10^{-7} M. Other modified electrodes have been developed for the detection of UA; for example, layer-by-layer deposited films containing CNT and poly(malachite green) were used with DPV for the determination of EP and UA at pH 4.0 and 7.0. Their linear ranges were up to 0.09 or 0.2 mM, respectively, and for poly(malachite green) electrode, the detection limit was 0.12 μM.[695]

4.1.2.4. Adenine and Guanine. Adenine and guanine are crucial components of DNA that play key roles in the storage of genetic information. Their concentrations are considered an important index for diagnosis of different diseases. The determination of adenine and guanine concentrations is important to bioscience and clinical diagnosis.[701]

It is well-known that PPy films can be further oxidized at higher potentials (overoxidized polypyrrole, OOPPy) in the presence of oxygen to obtain groups such as carbonyl and carboxyl on the surface of the polymeric matrix; thus a film highly permeable to cationic species can be fabricated that selectively repels anions and neutral compounds.[702,703] An innovative electrochemical sensor that uses this concept for the simultaneous detection of adenine and guanine is based on porous-structured films of OOPPy−rGrO. The electrochemical sensor can be applied to the quantification of adenine and guanine with a linear range covering 0.06−100 μM and 0.04−100 μM and a low detection limit of 0.02 μM and 0.01 μM, respectively. Initially the OOPPy−rGrO composite was produced by electrochemical polymerization of pyrrole, with GrO as a dopant, followed by electrochemical reduction of GO in the composite film. The obtained PPy−rGrO modified electrode was then oxidized at a potential of +1.8 V to produce the OOPPy/rGrO-modified GCE.[704]

Another modified electrode based on polythionine/gold nanoparticles/multiwall carbon nanotubes was proposed via a two-step process. The first step consists of ultrasonically synthesized gold nanoparticle/multiwalled carbon nanotube (AuNP/MWCNT) composites, follow by deposition on glassy carbon to prepare the AuNP/MWCNT electrode. The second step consists of electropolymerization of thionine on the surface of AuNP/MWCNTs to prepare the PTH/AuNP/MWCNT modified electrode. This electrode presents good electrocatalytic behavior and stability for the detection of guanine and adenine in 0.1 M PBS (pH 7.0) in synthetic samples and in calf thymus DNA. The detection limit for guanine and adenine was 1×10^{-8} M and 8×10^{-9} M, respectively.[705] In this section some examples reported in the literature for the detection of guanine and adenine with modified electrodes are discussed. They are simple to construct, are made of unsophisticated, nonenzymatic materials, and display very low detection limits.

4.1.2.5. Taurine. The organic compound taurine (2-aminoethanesulfonic acid) participates importantly in a number of physiological and pharmacological processes, such as membrane stabilization and regulation of intracellular Ca^{2+}, a neuromediator and neuromodulator.[706] A potentiometric sensor for this compound was built on the basis of molecularly imprinted conducting polymer films, where film preparation requires the electrochemical polymerization of a 3,4-ethylenedioxy-thiophene/3-acetic acid thiophene (EDOT/AAT) copolymer film doped with flavin mononucleotide (FMN).[707] PEDOT works as a cross-linker, AAT is the monomer that generates the polymeric matrix, FMN is the dopant, and taurine is the template or target molecule (see Figure 41). For taurine concentrations in the range of 10^{-2} to 10^{-4} M, a linear cationic response toward the protonated form of taurine was observed, with a calculated slope of 53.8 ± 2.6 mV/p[taurine]. Moreover, these sensors are not sensitive toward Ca, Mg, Na, and K ions. This is the only reported example of a sensor with this kind of modified electrode for this analyte, but unfortunately the limit of detection was not reported.

4.1.2.6. Glucose. Quantitative determination of glucose is very important, not only to aid in diabetes diagnosis but to fulfill requirements in the food industry, environmental protection, and biotechnology. One approach to such

DOI: 10.1021/acs.chemrev.7b00482
Chem. Rev. 2018, 118, 4731−4816

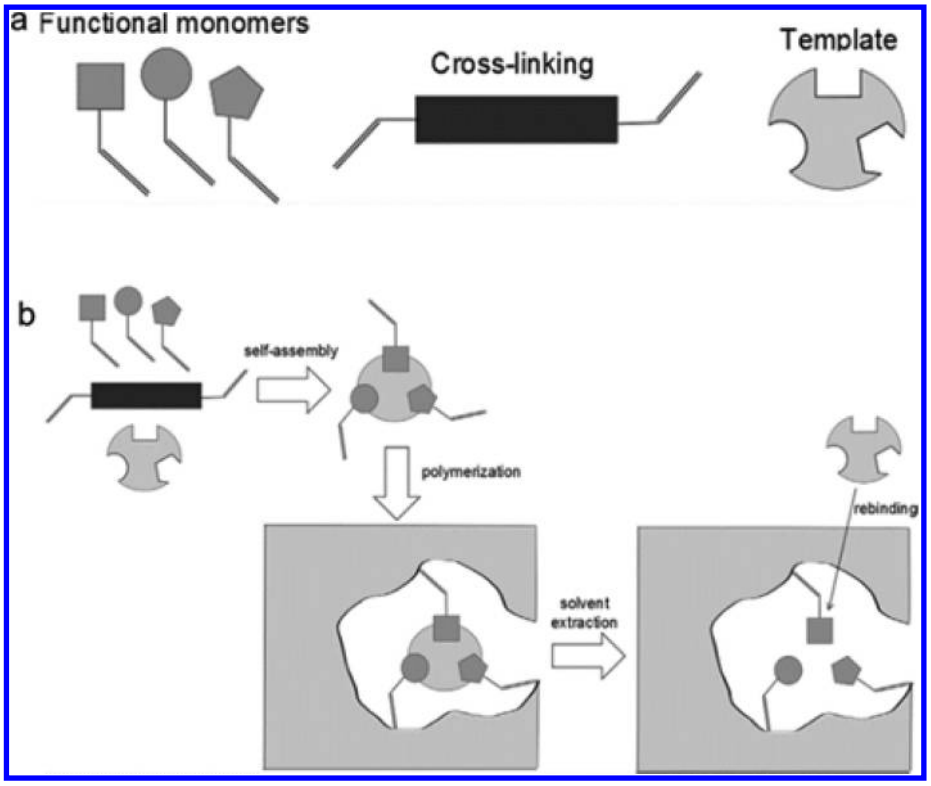

Figure 41. Principles of a molecular imprinting process. Reproduced with permission from ref 707. Copyright 2016 Elsevier.

determination is to develop nonenzymatic electrochemical sensors that are robust and economically accessible, are compatible with biological media, and have low detection limits.[708] A case in point involves a facile two-step electrochemical strategy for enhanced nonenzymatic glucose sensing: the synthesis of reduced graphene oxide (rGrO) and doped conducting poly(3,4-ethylene dioxythiophene) (PEDOT) nanocomposites decorated with Ni nanoparticles (NiNPs) and deposited onto a GCE.[709] The prepared nanocomposite (NiNPs/PEDOT/rGrO) modified electrode revealed exceptional electrocatalytic activity toward the oxidation of glucose in alkaline media (Figure 42), and it was developed into a nonenzymatic glucose sensor. Under optimal conditions, the glucose sensor exhibited a linear range from 1.0 μM to 5.1 mM and a detection limit of 0.8 μM. The sensor showed excellent stability, high reproducibility, and favorable selectivity against common interferents. This nonenzymatic sensor was also successfully applied to the detection of glucose in human serum samples, indicating its potential for clinical applications. A new conductive nanocomposite based on PPy and silver nanoparticles (AgNPs) relies on a reverse microemulsion preparation method and is used as a nonenzymatic electrochemical sensor for glucose detection. This modified PPy−AgNP electrode showed a glucose response in the linear dynamic range of 25 to 2500 μM, with a limit of detection of 3.6 μM. It is applied to human saliva samples.[710]

These are two of the rare examples reported in the literature for the detection of glucose in a nonenzymatic fashion based on CPs. Most of the reported investigations use glucose oxidase (GluOx) enzyme as electrocatalytic element embedded or trapped within the CP matrix and will not be reviewed in this contribution. The main disadvantage of using GluOx is the preparation, which requires much care during the construction and handling of the modified electrode.[711]

4.1.2.7. Hydrogen Peroxide. Hydrogen peroxide sensors are relevant since the use of H_2O_2 is of great importance in clinical and environmental studies as well as in mining, pharmaceutical, textile, and food manufacturing industries.[712] For this reason, much attention has been given to the development of chemical,[713] biochemical,[714] and electrochemical[712,715] sensors for this analyte since they provide high sensitivity, excellent selectivity, a rapid response, and good reliability.

For example, a GCE modified with ultrathin PPy nanosheets decorated with AgNPs was assembled for the detection of hydrogen peroxide (H_2O_2). The device showed high sensitivity toward this analyte, which may be due to the high surface area of the films. These films not only increased the interaction with Ag^+ ions, but also made the Ag surface area available for reaction with H_2O_2 and thus enhanced the reduction current through a catalytic cycle. The limit of detection was 0.57 μM for the linear segment.[716] Likewise, a voltammetric sensor based on a PPy−PtNP nanocomposite was fabricated from PtNPs densely dispersed on PPy nanoparticles (PPyNPs) by a microwave-assisted polyol process (Figure 43).[717] The sensor showed good electrocatalytic activity toward H_2O_2 with a detection limit of 0.6 μM.

A novel amperometric sensor for H_2O_2 determination is based on the incorporation of multiwalled carbon nanotubes (MWCNTs) into a poly(methylene blue) film immobilized on carbon composite electrodes.[718] This shows a detection limit of 20.7 μM. Many of the observations in the above examples can be explained by the larger surface area of the electrode materials, which can increase the interactions between the polymer and the analyte or can produce an electrode surface area suitable for reaction with H_2O_2.

4.1.2.8. Diverse Pharmaceuticals. Electrochemical methods may be applied to the detection of several drugs, and some examples that use CPs as part of the sensing element are

DOI: 10.1021/acs.chemrev.7b00482
Chem. Rev. 2018, 118, 4731−4816

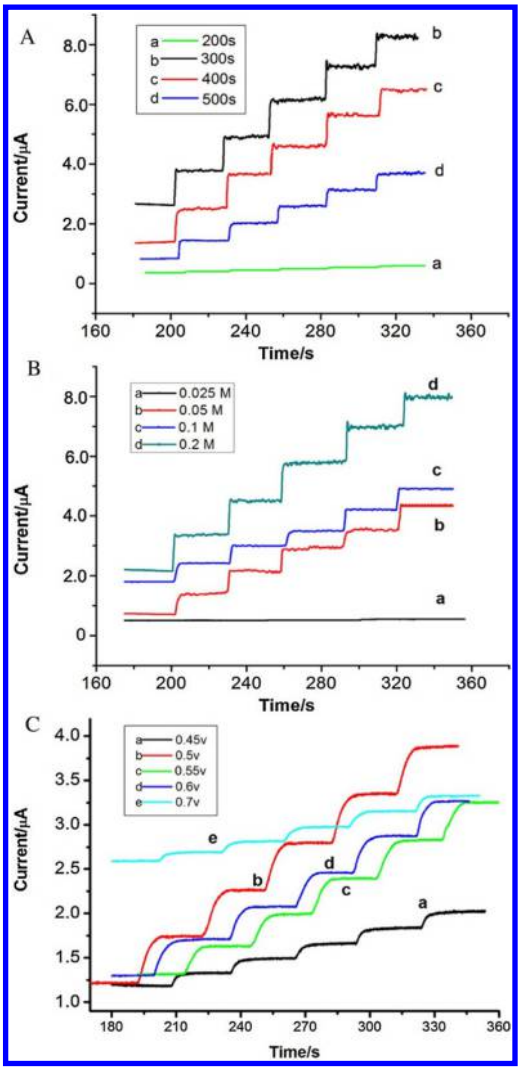

Figure 42. Effects of deposition time of NiNPs (A), NaOH concentration (B), and different applied potential (C), on the amperometric response of the NiNPs/PEDOT/rGO/GCE toward 0.1 mM glucose. Reproduced with permission from ref 709. Copyright 2015 Elsevier.

described in this section. A novel chemosensitive ultrathin film with high selectivity for the detection of naproxen, PCM, and theophylline was developed on the basis of a series of electropolymerizable terthiophene and carbazole monomers for the imprinting of drug molecules into the polymer matrix.[719] Incorporation of ZrO_2 (12 nm) and Bi_2O_3 (90–210 nm) nanoparticles into a PANi matrix by a simple interfacial polymerization technique using ammonium persulfate as an oxidant produced PANi–ZrO_2 and PANi–Bi_2O_3 composites.[720,721] These materials were successfully used to fabricate GCE-modified sensors for the voltammetric analysis of esomeprazole and pramipexole, respectively, giving excellent electrocatalytic activity with a response time of about 9 s and a limit of detection of 97.21 ng mL^{-1} for the first drug and 1.10 mg mL^{-1} for the second. These sensors were successfully used on pharmaceutical formulations. Similarly, an electrochemical sensor for the analysis of betahistine hydrochloride was fabricated with a PANi–ZnO nanocomposite. The method used sodium lauryl sulfate as the dissolving system, which enhanced electrochemical properties and caused a lower detection limit of 19.57 μg mL^{-1}, proving better sensitivity.[722] A sensor imprinted on the surface of a pencil graphite electrode was fabricated via one-step electropolymerization of the imprinted polymer composed of a conductive polymer and sol–gel AuNPs for the determination of lorazepam[723] and caffeine.[724] In the optimized calibration curve for lorazepam with the imprinted sensor, two linear concentration ranges were observed, from 0.2 to 2.0 nM and from 2.0 to 20.0 nM, with a limit of detection of 0.09 nM. For caffeine, the linear ranges of the sensor were from 2.0 to 50.0 and 50.0 to 1000.0 nM, with a limit of detection of 0.9 nM. Furthermore, the proposed method was successfully applied for the determination of lorazepam and caffeine in real samples (i.e., urine, plasma, pharmaceutical tablet, green tea, energy drink, and soda drink). The synergistic effect of combining Gr and a conducting PANi–Bi_2O_3 nanocomposite enhanced the performance of sensors used for the electrocatalytic oxidation of etodolac.[725] The good response developed by the sensor results in a low potential detection of etodolac, good stability, and fast response, with a limit of detection of 10.03 ng mL^{-1}. This sensor was successfully applied to pharmaceutical formulations. Sodium dodecyl sulfate-doped PPyox plus carboxylic acid-functionalized CNT modified GCEs were reported for the detection of the anticancer drug pemetrexed.[726] Under optimum conditions, the method showed an increase in the anodic peak currents of adsorptive stripping differential pulse voltammetry (ASDPV), which was linearly dependent on pemetrexed concentrations (Figure 44). The recorded linear

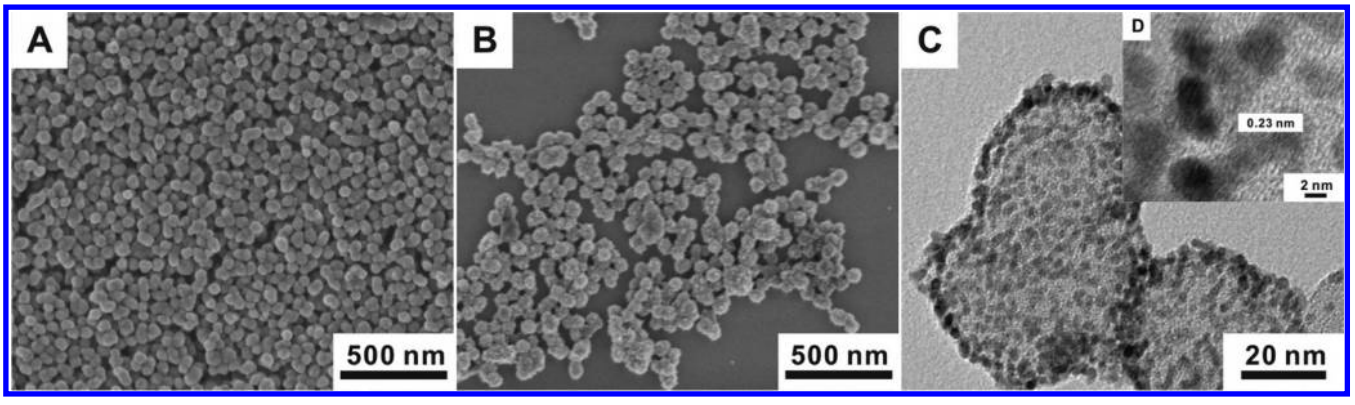

Figure 43. (A) SEM image of the as-synthesized PPyNPs. (B) SEM and (C, D) high resolution TEM images (HRTEM) of the PPy/Pt nanocomposites. Reproduced with permission from ref 717. Copyright 2015 Elsevier.

DOI: 10.1021/acs.chemrev.7b00482
Chem. Rev. 2018, 118, 4731–4816

responses were in the range from 1.00×10^{-8} M to 1.00×10^{-7} M with a detection limit of 3.28×10^{-9} M.

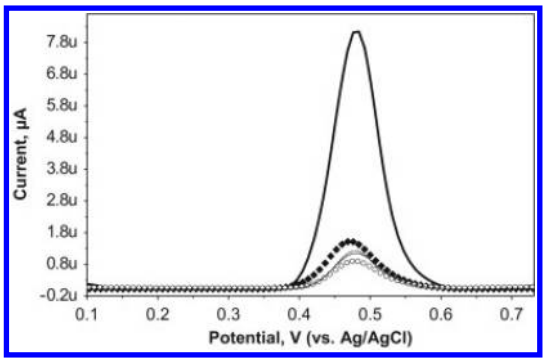

Figure 44. DP voltammograms of the bare GCE (---), MWCNT/GCE (○), MWCNT-COOH/GCE (♦) SWCNT-COOH/GCE (thin line), and PPy/MWCNT-COOH/GCE (thick line) in 0.1 M PBS (pH = 2.0) with 5×10^{-5} M pemetrexed drug. Reproduced with permission from ref 726. Copyright 2014 Elsevier.

MWCNT/tiron-doped 222 PPy nanocomposite was used to modify GCE and fabricate a sensor for the analysis of the antiviral drug acyclovir. It exhibited a response at neutral pH to the electrooxidation of the drug with linear sweep voltammetry.[727] Under optimized conditions, a low detection limit of 10.0 nM for acyclovir was obtained. The sensor provided satisfactory results for the determination of this compound in pharmaceutical and clinical preparations. A PANi and CNT hybrid film-based electrochemical sensor was reported for the determination of omeprazole;[728] here square-wave voltammetry (SWV) was used for detecting its reduction, and a detection limit of 47.2 μg mL^{-1} was found. Another electrochemical CP-based sensor was made with a composite film of Gr and poly(3′-(2-aminopyrimidyl)-2,2′:5′,2″-terthiophene) (pAPT) for the determination of the antiarthritic drug piroxicam.[729] When testing a urine sample, the obtained electrochemical signal displayed a well-shaped individual oxidation peak with high catalytic current for piroxicam; the major interferents were AscA, tyrosine, and UA. The detection limits were 1.86 ± 0.06, 5.29 ± 0.02, 5.97 ± 0.07, and 14.50 ± 0.03 μM, for piroxicam, AA, tyrosine, and UA, respectively. An electrode based on poly(4-vinylpyridine) combined with multiwalled CNTs was prepared, characterized, and used for the electrochemical sensing of PCM by DPV. It resulted in a good linear ratio for the oxidation peak currents and PCM concentrations over the range of 0.02−450 μM, with a limit of detection of 1.69 nM. This electrode was stable for more than 60 days and allowed determination of PCM in tablets and urine samples.[730] A sensor for the anticancer drug irinotecan was reported based on poly(methylene blue) deposited on a GCE.[731] The linear range was between 8.0 and 80 μM, with a detection limit of 0.2 μM. An impedimetric sensor based on CNT−poly(methylene blue) composite was used for the construction of an aptasensor for thrombin using electrochemical impedance spectroscopy.[732] This sensor was able to detect thrombin in the concentration range 1 nM to 1 mM with a limit of detection of 0.7 nM and 0.5 nM monitoring resistance and capacitance changes, respectively. A sensor for ibuprofen as a model anionic drug was based on potential-induced uptake/release of the drug by a smart conducting polymer (molecularly imprinted polymer) as sorbent/recognition element. The sensor was tried in plasma samples using a quartz crystal microbalance (QCM) without any additional treatment. The limit of detection was 0.05 μmol L^{-1}; consequently it was successfully applied for the quantification of trace amounts of ibuprofen in biomedical samples and validated by HPLC.[733] A novel kind of water-dispersible, molecular imprinted sensor with electroactive nanoparticles was prepared by first synthesizing an amphiphilic electroactive copolymer containing a carbazole group through a one-pot free radical copolymerization. The coassembly of the electroactive copolymers with the template molecules (paracetamol) in aqueous solution generated nanoparticles embedded with paracetamol, leading to the formation of molecularly imprinted electroactive nanoparticles (i.e., a MIP sensor). After the extraction of PCM molecules, a sensor for PCM was constructed (Figure 45).[734] Under optimum conditions, two linear ranges from 1 μM to 0.1 mM and 0.1 to 10 mM with a detection limit of 0.3 μM were obtained for PCM detection

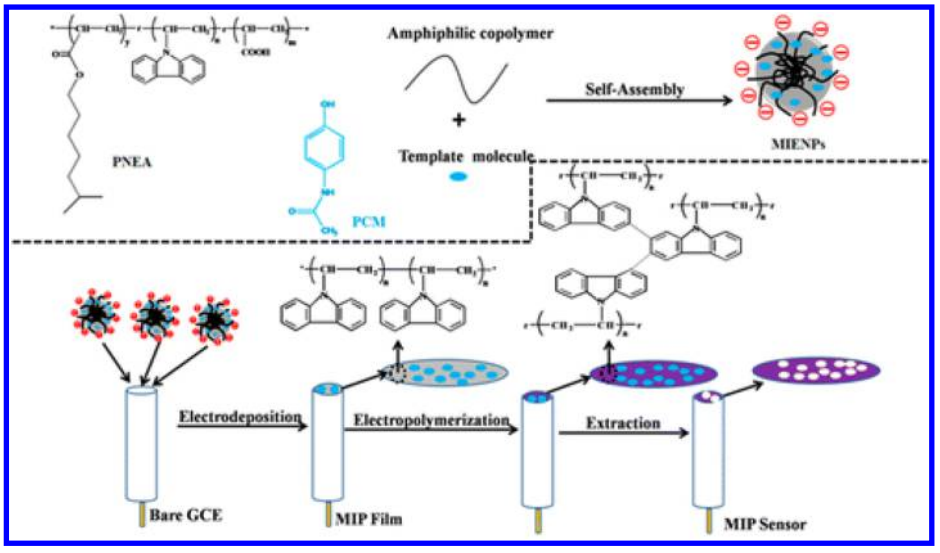

Figure 45. Schematic illustration of the MIP sensor fabrication using the self-assembled molecularly imprinted electroactive nanoparticles and electropolymerization. Reproduced with permission from ref 734. Copyright 2016 American Chemical Society.

DOI: 10.1021/acs.chemrev.7b00482
Chem. Rev. 2018, 118, 4731−4816

Table 6. Limits of Detection for Miscellaneous Pharmaceuticals with C-based electrodes

sensor	drug	limit of detection	reference
PANi and zirconia nanocomposite film	esomeprazole	97.21 ng mL^{-1}	720
PANi and zirconia nanocomposite film	pramipexole	1.10 mg mL^{-1}	721
PANi−ZnO nanocomposite	betahistine, hydrochloride	19.57 μg mL^{-1}	722
imprinted poly(conductive polymer, sol−gel, AuNP)	lorazepam	0.09 nM	723
imprinted polymer (conductive polymer, sol−gel, AuNP)	caffeine	0.9 nM	724
Gr−PANi−Bi_2O_3 hybrid film	etodolac	10.03 ng mL^{-1}	725
PPyox with carboxylic acid-functionalized CNT modified GCE	pemetrexed	3.28 nM	726
MWCNT/tiron-doped 222 PPy	acyclovir	10.0 nM	727
PANi and CNT hybrid film	omeprazole	47.2 μg mL^{-1}	728
poly(3′-(2-aminopyrimidyl)-2,2′:5′,2″-terthiophene) with Gr	piroxicam	1860 nM	729
poly(4-vinylpyridine) and MWCNT	paracetamol	1.69 nM	730
poly(methylene blue) on GCE	irinotecan	200 nM	731
CNT−poly(methylene blue) composite	thrombin	0.7 nM (resistance changes) and 0.5 nM (capacitance changes)	732
nanostructured conducting molecularly imprinted PPy	ibuprofen	50 nM	733
molecularly imprinted with amphiphilic electroactive copolymer, carbazole group, PCM template	paracetamol	300 nM	734

with good selectivity. The sensor also showed good response in real samples like tablets and human urine samples.

Table 6 summarizes the values for the detection limits of the sensors described above that were designed for various pharmaceutical drugs. From this table, it is clear that modified electrodes have excellent detection limits. This is remarkable since the electrodes were modified with numerous materials in a sophisticated way in order to achieve good catalytic properties, as well as offering a large variety of superficial modifications and numerous active sites. These characteristics allowed one to obtain interactions between the modified electrodes and the functional groups of the pharmaceutical drugs, which have complex structures and different functional groups. The most sensitive electrodes, however, are built in simple ways that allow good electronic conduction and therefore a good interaction with the redox target analytes.

4.1.2.9. Phenolic Compounds. Phenolic compounds are used in several industrial processes to manufacture chemicals such as pesticides, explosives, drugs, and dyes, and in the bleaching process during paper manufacturing. They are also used in agriculture as herbicides, insecticides, and fungicides. Phenolic compounds appear naturally, for example, during the decomposition of leaves or wood, and therefore they are found in soils and sediments, possibly leading to wastewater and groundwater contamination. It is important to provide selective and sensitive methods of detection for phenolic compounds, and electroanalytical techniques offer an option. Modified electrodes with CPs, however, can facilitate their detection.[735] The voltammetric determination of 4-aminophenol (4-AP) using a PANi−Gr−GCE-modified sensor was achieved with good analytical performance for the oxidation of the analyte with a detection limit of 6.5×10^{-8} M and a high sensitivity of 604.2 μA mM^{-1}. In addition, a simultaneous detection of 4-AP and PCM was achieved in a large dynamic range without the interference from each other.[736] Poly(malachite green) (PMG) has been used together with MWCNTs for the detection of *p*-nitrophenol, catechol, and quinol with a sensitivity for *p*-nitrophenol of 5 μM, and a linear range up to 1.0 mM.[737] The peak current of *p*-nitrophenol was proportional to its concentration in the range 5.0×10^{-6} to 1.0×10^{-3} M and the detection limit was 5.0×10^{-7} M. An electrochemically active composite film that contains MWCNTs, Nafion, and PMG has been synthesized on GCE, Au, and indium tin oxide (ITO) electrodes for the simultaneous detection of catechol and quinol using DPV in dil. H_2SO_4 (pH 1.5). Detection limits of 5.8 and 1.6 μM were obtained for catechol and quinol, respectively.[738]

4.1.2.10. Nitroaromatic Compounds. Aromatic nitro compounds are toxic substances commonly used in the manufacture of explosives, pesticides, dyes, plasticizers, and pharmaceuticals. These compounds have been detected not only in industrial wastewaters but also in freshwater and marine environments. Accurate measurements and low detection limits for nitroaromatic compounds concentrations are therefore welcomed. Electrochemical sensors can help address these demands as they possess attractive attributes that include high sensitivity and selectivity, speed, wide linear range, compatibility with microfabrication, minimal space and power requirements, and low-cost instrumentation. The redox properties of nitro-based compounds (namely, the presence of easily reducible nitro groups) ideally lend themselves to electrochemical detection. Advances in the development of nanomaterials have a strong potential to create electrochemical sensors for detecting explosives: characteristics such as high surface area-to-volume ratio, convergent rather than linear diffusion, improved selectivity, catalytic activity, and unique electrical and optical properties can be exploited for highly sensitive detection. An example involves a monomer strategy for imprinting of 1,3-dinitrobenzene (DNB) molecules at the surface of PANi. A linear response of DNB concentration between 2.20×10^{-8} and 3.08×10^{-6} M was exhibited with a detection limit of 7.33×10^{-9} M.[739] Co-polypeptide-doped PANi nanofibers detected an ultratrace amount of 2,4,6-trinitrotoluene (TNT). The co-polypeptide, comprising glutamic acid (Glu) and lysine (Lys) units, was *in situ* doped into PANi, resulting in the formation of PANi nanofibers.[740] Adsorptive stripping voltammetry showed that the poly(Glu-Lys)-doped nanofibers confined onto GCEs exhibited a remarkable enriching effect and thus a sensitive electrochemical response to TNT, with a linear dynamic range of 0.5−10 μM and a detection limit of 100 nM.

Thin films of microporous polymer networks (MPNs) have been generated by electrochemical polymerization of a series of multifunctional carbazole-based monomers.[741] Electrochemical

DOI: 10.1021/acs.chemrev.7b00482
Chem. Rev. 2018, 118, 4731−4816

sensing experiments with 1,3,5-trinitrobenzene as a prototype nitroaromatic analyte, show an up to 180 times increased current response on MPN-modified GCEs in relation to the unmodified electrode (Figure 46). The phenomenon probably

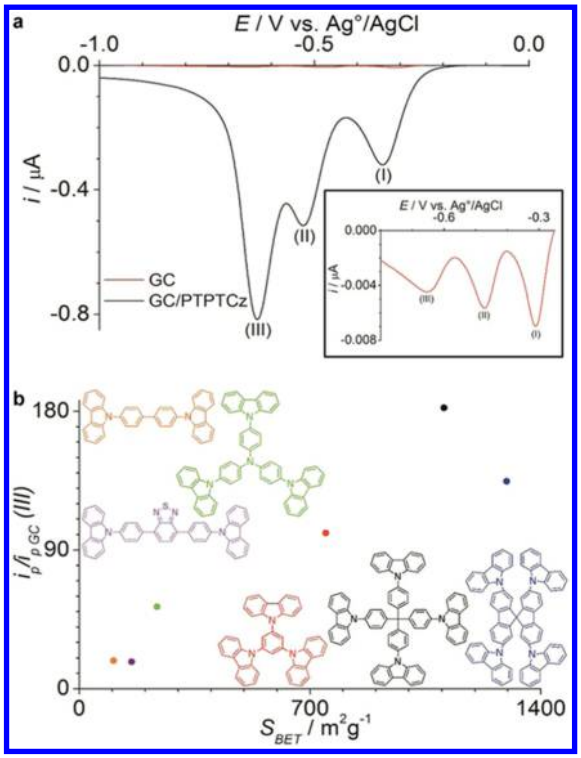

Figure 46. Linear scan voltammograms (after background correction) for unmodified (inset) and PTPTCz-modified GC electrodes for a 0.5 μM TNB concentration, and (b) correlation of the current ratios between modified and unmodified GC electrodes of the third cathodic reduction peak of TNB versus the surface area of the MPN films (scan rate = 0.01 V s^{-1}). Reproduced with permission from ref 741. Copyright 2015 American Chemical Society.

involves intermolecular interactions between the electron-poor nitroaromatic analytes and the electron-rich, high surface area microporous deposits, with the electrochemical reduction at the MPN-modified electrodes being an adsorption-controlled process at low scan rates. An electrochemical sensor based on a molecularly imprinted polymer (MIP), obtained by a noncovalent approach, involves a microporous-metal−organic framework (MMOF) for the sensitive detection of TNT. The MIP is formed *in situ* at the Au electrode surface via electropolymerization of *p*-aminothiophenol-functionalized AuNPs in the presence of TNT as the template molecule. A linear response was obtained with a detection limit of 0.04 fM.[742] This hybrid sensor exhibits sensitive recognition sites toward TNT with good reproducibility and represents a potential application for the detection of TNT in complex matrices such as tap and natural waters.

A sensitive and selective electrochemical sensor for the determination of nitrobenzene (NB) is based on a carbon paste electrode (CPE) modified with poly(3,4-ethylene dioxythiophene) and CNTs. The modified CPE exhibits good conductivity, a large surface area, and excellent catalytic activity toward the electrochemical reduction of NB. Under optimal conditions, the modified CPE is capable of detecting NB in the 0.25 to 43 μM concentration range and with a detection limit at 83 nM. Moreover, the sensor is highly stable and reusable and free of interferences by other commonly present nitro compounds. It was used to determine NB in wastewater samples.[743]

4.1.2.11. Nitrites. Nitrites occur naturally in soil, in water, and in some foods, playing an important role in the environment. They are toxic because an excess of nitrite in blood has proven to promote an irreversible reaction with hemoglobin. In addition, nitrite is recognized as a precursor to form *N*-nitrosamines, the excess of which would generate carcinogens.[744] The electrochemical techniques have proven to be considerably attractive because of their faster, cheaper, and more advantageous real-time analysis for determining compounds, and several nitrite sensors have been developed for its detection during the last years using CPs.

Thionine was electropolymerized on carbon nanotube (CNT)-modified glassy carbon (GC) to fabricate a polythionine (PTH)/CNT/GC electrode since CNTs represent an excellent nanomaterial to improve the electron transfer between the electrode and nitrite with a sensitivity of 5.81 μA mM^{-1} and a detection limit of 1.4 × 10^{-6} M.[745] The modification of a glassy carbon electrode with poly(toluidine Blue O) (GC/poly-TBO) and single-walled carbon nanotubes (SWCNTs) enhanced the electrocatalytic response for nitrite oxidation, as measured by amperometry at +0.92 V and pH = 7.[746] Nitrite response was linear in the 0.001−4 mM range, with a detection limit of 0.37 μM; this sensor was applied to a wastewater sample, and the results were validated spectrophotometrically. Also a GCE was modified electrochemically with GrO-doped PPy and flower-like Co nanostructures.[747] This modified electrode had a synergistic effect between Co nanostructures and GrO/PPy, and showed improved catalytic behavior toward nitrite oxidation. An amperometric oxidation current was found at 0.80 V with a linear range of 1.0−3.2 mM, with a lower detection limit of 15 nM and a response time of 1 s; it was used for the determination of nitrite in pickled radish. A poly(aniline-*co*-*o*-aminophenol)-modified glassy carbon electrode (PAOAP/GCE) was used for aqueous nitrite detection. The film was prepared by cyclic voltammetry by the electrochemical copolymerization of both monomers (*o*-aminophenol and aniline) and presented a higher nitrite response compared to the unmodified electrode. The sensor detected nitrites in the linear range from 5.0 × 10^{-6} to 2.0 × 10^{-3} M with a detection limit of 2 × 10^{-6} M.[748] Four amperometric sensors have been reported for nitrite detection based on polyphenazines with CNT on GCE, PAA, poly(azure A), poly(toluidine blue poly(thionine)), and poly(methylene blue). A synergetic effect of the polymer and CNT led to improved sensor sensitivity, while the bare GCE showed no activity toward nitrite reduction; the highest sensitivity among the four was poly(methylene blue), being 2530 μA cm^{-2} mM^{-1} at +0.77 V vs Ag/AgCl.[653] Ordered PANi nanowire arrays and CNT networks were integrated to create 3D nanostructured PANi/CNT composites with high specific capacitance and excellent cyclability (Figure 47); this material was used as electrochemical sensor for nitrite detection with good sensitivity, a low detection limit of 6.1 mM, and a fast response time of less than 5 s.[749] To improve the selectivity and sensitivity for nitrite, many attempts have been made to develop electrodes modified with conducting polymers, but it is necessary to add some materials like CNT or GrO to reach low detection limits.

DOI: 10.1021/acs.chemrev.7b00482
Chem. Rev. 2018, 118, 4731−4816

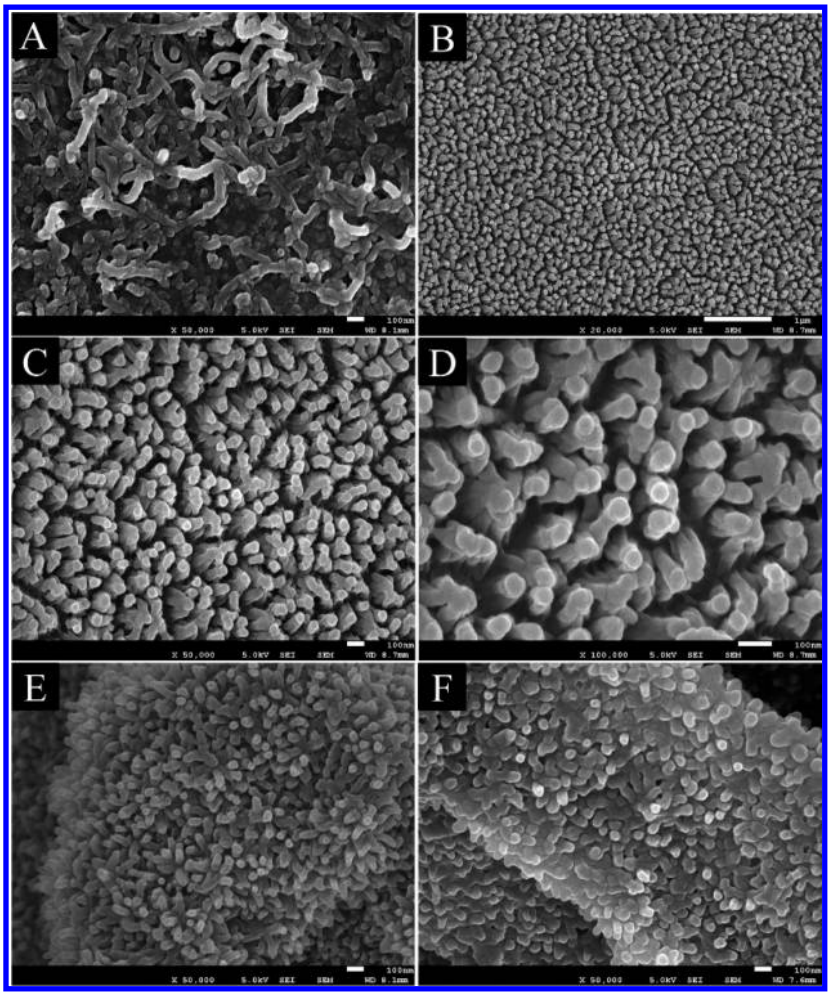

Figure 47. SEM images of electrodes modified with (A) CNTs, (B, C, D) PANi nanowire arrays, and (E, F) PANi/CNT nanocomposites. Reproduced with permission from ref 749. Copyright 2016, Elsevier.

4.1.2.12. Diverse Cations. Potentiometric ion sensors or ion-selective electrodes are an important electrochemical sensor group. These sensors based on polymeric membranes containing neutral or charged carriers (ionophores) are available for the determination of inorganic ions and are of interest in industrial and medical applications.[750] They can be easily miniaturized and represent potentially a low cost alternative. A conductive polymer based on *N*-phenyl-ethyl-enediamine-methacrylamide is deposited by electropolymerization over a thin film onto Au electrode forming an intermediate layer of solid contact.[751] The standard electrode potential, E_0, was 329.1 ± 1.9 mV, and the limit of detection for calcium was 3.2×10^{-6} M (30.2 mV/pCa), with a lifetime of 3 months of constant contact with solutions. This calcium sensor shows a Nernstian response and sufficient selectivity over Na and K ions present at physiological concentrations. CP films doped with metal complexing ligands (MCL) can be made sensitive toward calcium and magnesium, as well as copper, cadmium, lead, or zinc cations.[752] When introduced to the CP layer as doping anions, bulky MCLs are immobilized inside the CP film and preserve their chemical properties known from water chemistry. PPy−Arsenazo films were formed either at constant potential or by cyclic voltammetry. For Mg, the slope was 28.9 mV/pMg (for the first technique) and 27.4 mV/pMg (for the second), but the standard potential values of both films differed by about 100 mV. Induced cadmium sensitivity was almost unchanged during a one-month soaking in 0.01 M $CdCl_2$, and the slope values were equal to 30.5 mV/pCd, 30.1 mV/pCd, and 31.1 mV/pCd after 1 day, 1 week, and 1 month, respectively.[752] Electrochemical oxidation was also successfully applied to induce copper or lead sensitivity of PPy or poly(1-methylpyrrole) films doped with Arsenazo or calcon ligands. For example, after electrochemical oxidation of the PPy−Arsenazo film in a solution of pH = 7, a copper sensitivity with a slope of 24 mV/pCu was induced. Lead sensitivity of the PPy−calcon film was induced by electrochemical oxidation in a solution of the calcon−lead complex at pH = 7. The PPy−xylenol orange films showed slope values with respect to Zn equal to 26.9 mV/pZn. Table 7 depicts a summary of the sensors developed for cation detection.

When introduced to the CP layer as doping anions, bulky metal complexing ligands (MCLs) are immobilized inside the CP film and preserve their chemical properties known from water chemistry. Complexation inside the polymer layer is necessary for inducing preferred cationic sensitivity of the CP films. It was shown also that formation of the complex inside the polymer layer is necessary for inducing preferred open-circuit sensitivity of the CP membrane.

4.1.2.13. Fluoride Anion. High concentrations of fluoride that occur naturally in some groundwater can cause teeth degradation disorders such as fluorosis. At lower concentrations, fluoride can inhibit tooth decay. For the prevention of

DOI: 10.1021/acs.chemrev.7b00482
Chem. Rev. 2018, 118, 4731−4816

Table 7. Sensitivity for Calcium, Magnesium, Copper, Lead, and Zinc Cations

ion/CP matrix electrode	sensitivity	ref
Ca/*N*-phenyl-ethylenediamine-methacrylamide	30.2 mV/pCa	751
Mg/PPy-Arsenazo films	28.9 mV/pMg (potentiostatic) and 27.4 mV/pMg (cyclic voltammetry)	752
Cu/PPy-Arsenazo films	24 mV/pCu	752
Pb/PPy Calcon films	20 mV/pPb	752
Zn/PPy-xylenol orange films	26.9 mV/pZn	752

dental caries, a fluoride concentration between 0.5 and 1.0 ppm in drinking water is considered beneficial. Therefore, the determination of fluoride anion concentrations has emerged as an important goal.[753] A new calix[4]pyrrole compound bearing an electropolymerizable EDOT (Figure 48) was prepared from

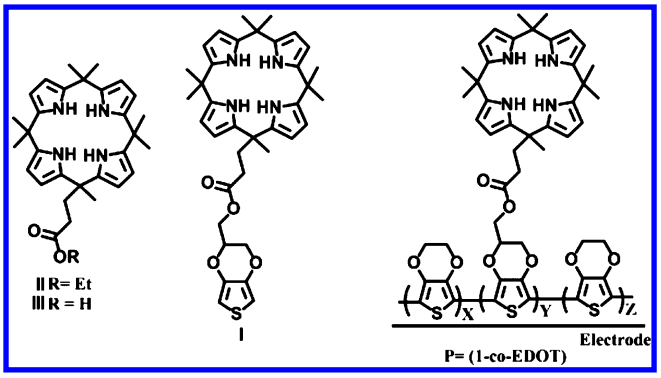

Figure 48. Structures used in the synthesis of P(1-*co*-EDOT). Reproduced with permission from ref 754. Copyright 2014 American Chemical Society.

the carboxylic acid-functionalized CP (**III**) that was, in turn, obtained from its corresponding ester derivative (**II**); esterification then produced the EDOT-functionalized CP (**I**). Electropolymerization of **I** with EDOT gave P(1-*co*-EDOT). This copolymer was deposited on an ITO electrode and used as a fluoride sensor in water. The detection limit for the ITO/P(1-*co*-EDOT) electrode was found to be as low as 0.19 ppm in water.[754]

4.1.2.14. Thiol Derivatives. Widely distributed in living cells, thiols are involved in many biological functions. The presence of sulfur-containing amino acids such as cysteine (CySH) and glutathione (GSH) can be an indication of some clinical conditions and a variety of diseases. Based on this assumption, considerable attention has been drawn to the investigation of the electrochemical behavior of these biological compounds and their determination.[755] Hybrid electrodes, active toward the electrooxidation of thiols by the coimmobilization of native carbon nanotubes (CNTs) and cobalt phthalocyanine (CoPc), were prepared from aqueous solutions where a hydrosoluble pyrrole surfactant was used to obtain homogeneous aqueous dispersions of CNTs and CoPc and to trap both materials on the electrode via the electropolymerization of the pyrrole surfactant. The hybrid electrodes exhibit good electrocatalytic activity toward the oxidation of L-cysteine and glutathione (Figure 49). Their performance in terms of limit of detection (0.01 mM) is compatible with the detection of these thiols in biological samples.[756]

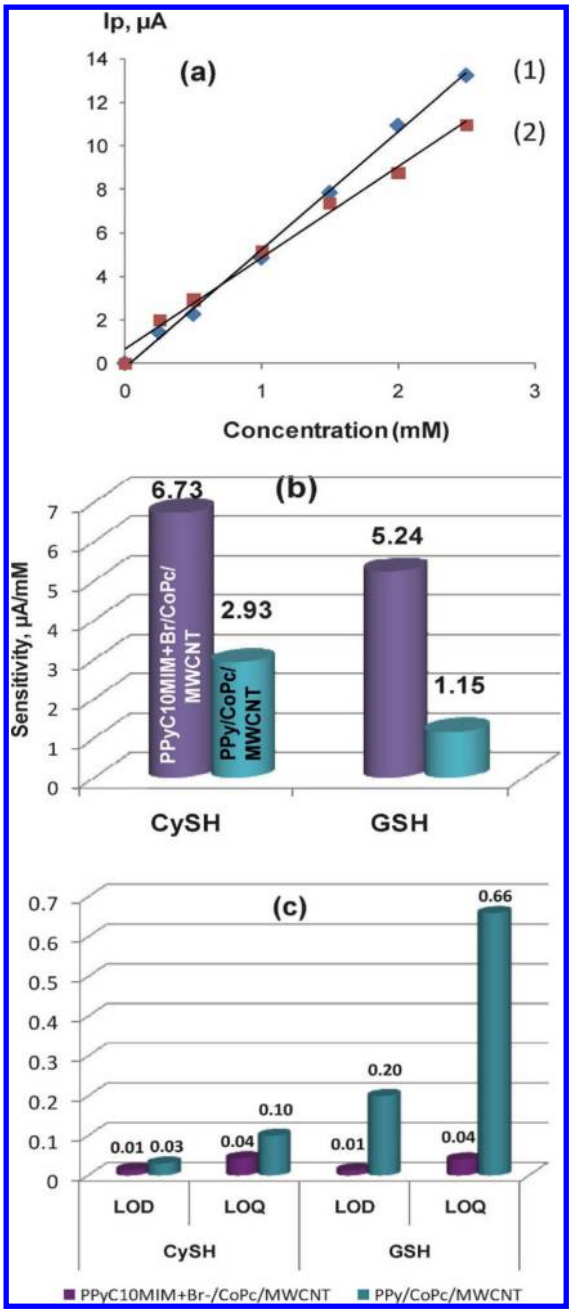

Figure 49. Calibration curves in 0.1 M NaOH deduced from cyclic voltammograms for the detection of (i) CySH and (ii) GSH at $PPyC_{10}MIM^{+}Br$/CoPc/MWCNT GC-modified electrode. (b) Comparison of sensitivity and (c) limit of detection (LOD) and limit of quantitation (LOQ) for the detection of CySH and of GSH obtained at GCEs modified with either $PPyC_{10}MIM^{+}Br$/CoPc/MWCNT or PPy/CoPc/MWCNT films. Reproduced with permission from ref 756. Copyright 2014 John Wiley and Sons.

4.1.2.15. Hydrazine. Hydrazine and its derivatives are widely used in many industrial fields such as rocket fuels, photographic chemicals, insecticides, herbicides, blowing agents, textile dyes, and corrosion inhibitors. However, hydrazine is rather toxic and carcinogenic and can severely injure lungs, liver, kidneys, and brain.[757] Therefore, it is of great importance to develop a sensitive method to monitor the concentration of hydrazine in real samples. PEDOT based sensors, PEDOT/lignosulfonate (PEDOT/LS) composites electrogenerated on a glassy carbon electrode by galvanostatic polymerization,[758] can be combined

DOI: 10.1021/acs.chemrev.7b00482
Chem. Rev. 2018, 118, 4731−4816

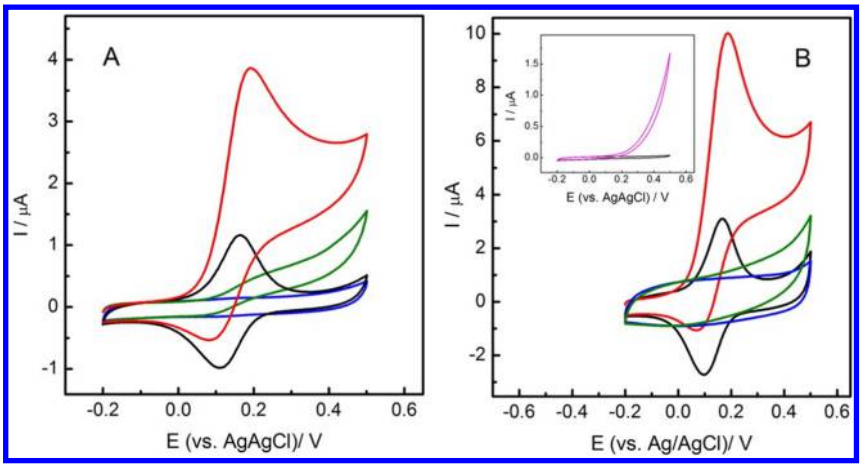

Figure 50. (A) GCE/PEDOT/LS in PBS (pH = 7.0) (black curve), GCE/PEDOT/LS in PBS with 0.5 mM hydrazine (red curve), GCE/PEDOT/ClO_4^- in PBS (blue curve), and GCE/PEDOT/ClO_4^- in PBS with 0.5 mM hydrazine (green curve) and (B) same as panel A for GCE/PPy/LS. The inset in panel B shows the bare GCE electrode (black line) and the bare GCE electrode with 0.5 mM hydrazine. Reproduced with permission from ref 758. Copyright 2016, Elsevier.

to produce materials showing remarkable electrocatalytic activity toward the oxidation of hydrazine. The electrooxidation of hydrazine occurs at a potential of 0.2 V (Figure 50). Amperometric sensitivity values for PEDOT/LS films at optimal thickness were determined to be 137 μA mM^{-1} cm^{-2} with a detection limit of 1.65 μM. The sensor showed high reproducibility and good stability for hydrazine detection in real water samples. A sensitive hydrazine hybrid sensor based on Cu_xO-decorated 3D poly(3,4-ethylene dioxythiophene) (3D-PEDOT) was developed through a facile electrochemical deposition and cyclic voltammetry treatment process.[759] It was found that 3D-PEDOT not only acts as a matrix to increase the loading amount of Cu_xO and enhances the conductivity but also directly contributes to the catalytic oxidation of hydrazine. Owing to the synergistic interaction between 3D-PEDOT and Cu_xO, the 3D-PEDOT−Cu_xO hybrid displayed enhanced catalysis for hydrazine oxidation with a lower overpotential requirement and a higher oxidation current compared to single component Cu_xO or 3D-PEDOT. It also exhibited a 1 order of magnitude wider linear range (0.5 μM to 53 mM), 10-fold lower detection limit (0.2 μM), and higher stability compared to the sensor based on Cu_xO. It was also used for the determination of hydrazine in real water samples with a satisfactory recovery. Once again, the high stability and applicability of PEDOT matrix in sensors are demonstrated, particularly for the case of hydrazine, where, combined with metal oxide nanoparticles, it increases sensitivity.

4.1.3. CP Based Chemical Sensors for Analyses in Gas Phase. *4.1.3.1. Generalities of Gas Sensors.* The electrical responses, such as electronic current or capacitance measurement in a resistivity-type and capacitance-type sensor, play a fundamental role in gas detection. As the sensing material of the detecting device is exposed to the vapor of an analyte, the measurable physical signals such as current, absorbance, or acoustic variables may change.[760] The electrochemical techniques for chemical measurements have, in general, several major advantages compared to other methods as commented previously, and research about electrochemical sensors for volatile organic compounds, carbon dioxide, NO_x, ammonia, and CH_4 is very active nowadays. Some approaches have been developed to control long-term stability and selectivity of gas sensors based on the conducting polymers.[761] Novel sensors can improve the sensing capabilities for gases, for example, those that are used to monitor the environment. In this section, some relevant examples of this kind of sensor, emphasizing versatility of those based on CPs, will be reviewed. A chemiresistive-type sensor (Figure 51) is the most common

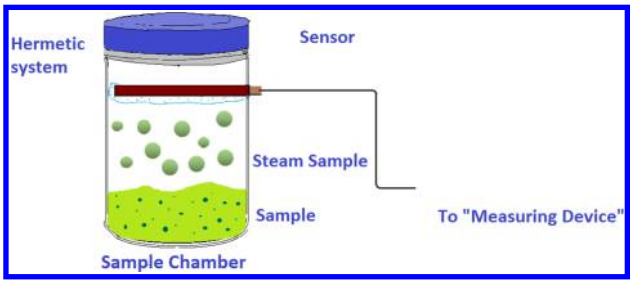

Figure 51. Simple chamber test for a chemiresistive sensor.

kind of sensor available; it usually consists of electrodes coated with conducting polymer, with the resistance of the conducting polymer changing with the chemical environment.

4.1.3.2. Volatile Organic Compounds (Hydrocarbons and Alcohols). There are a variety of toxic volatile organic compounds (VOCs) present during our daily life, including alkanes and benzene derivatives; moreover, some gases produced during metabolism in extremely low concentrations (ppb to ppt) can be used as diagnostic markers for diseases.[762] Nanomaterials are ideal for such sensor arrays because they are easily fabricated and chemically versatile and can be integrated into currently available sensing platforms, like conducting polymers. For electroanalysis, the large surface of CPs makes them very attractive to increase the electroactive surface of electrochemical gas sensors, yielding a better performance. An example about these sensors is the work reported by Kukla et al., where the conducting polymer films (polyaniline, polypyrrole, and poly(3-methylthiophene)) doped with mineral acids or monovalent anions as sensitive layers were deposited on metallic arrays and used for chemical recognition of volatile organic analytes.[763] The changes in film conductivity upon the interaction with saturated vapors of volatile organic compounds (acetone, benzene, xylene, amyl alcohol, ethyl alcohol, isobutyl alcohol, isopropyl alcohol, toluene, and chloroform) confirmed

DOI: 10.1021/acs.chemrev.7b00482
Chem. Rev. 2018, 118, 4731−4816

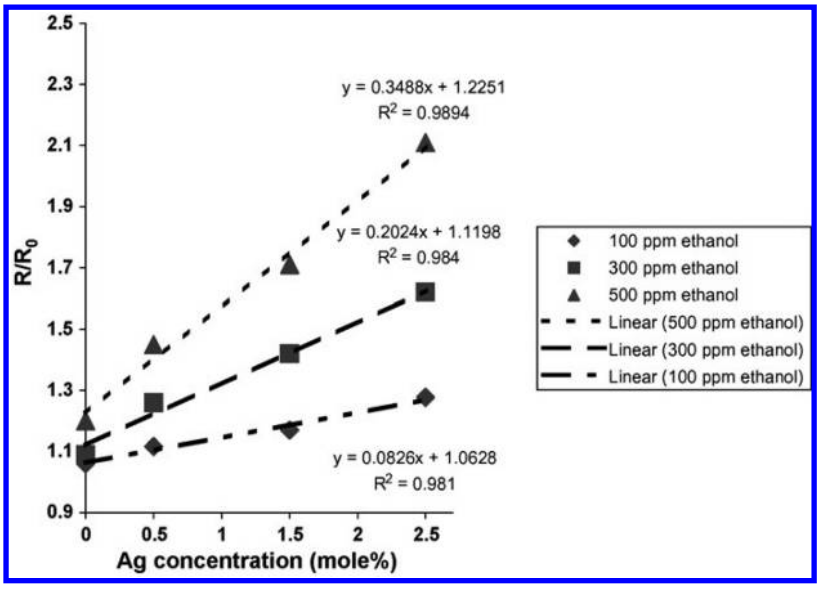

Figure 52. Variations in sensor response toward ethanol vapor as a function of Ag concentration in PANi/Ag nanocomposite. Reproduced with permission from ref 765. Copyright 2009 Elsevier.

the possibility of using CP film-based sensors for detection of these VOCs.[763] Pd−PANi nanohybrids using oxidation polymerization with aniline solution containing Pd nanoparticles were successfully obtained by Athawale et al.[764] These nanohybrids can induce a specific interaction between methanol molecules and imine nitrogen; specifically, the positive charge on the imine nitrogen is reduced by interacting with methanol in the presence of Pd nanoparticles. As a consequence, there is specific selectivity of the nanohybrids toward methanol vapor in gaseous mixtures methanol−ethanol and methanol−isopropanol. The sensitivity was 8.9×10^5 ppm^{-1}, as calculated from the slope of a plot of resistance versus concentration. The linear increase in sensitivity was observed up to 10 ppm methanol, and there after the sensitivity became saturated. Choudhury[765] developed highly specific vapor ethanol sensors using silver/PANi nanohybrids. These nanohybrids were prepared by in situ oxidative polymerization of an aniline monomer in the presence of different contents of silver nanoparticles. The PANi nanohybrids showed superior ethanol sensing capacity when compare to pure PANi. Sensor response increases linearly with increasing Ag concentration as indicated in Figure 52 and showed the maximum sensing ability (0.002 ppm^{-1}) with PANi/Ag-2.5 mol % sensor.

Wang et al.[766] reported a crystalline PEDOT and a PPy-based sensors that were used for vapor ethanol detection; both showed a very good response toward saturated ethanol vapors. The PPy-based sensor showed nonselective response toward both ethanol and ammonia, whereas PEDOT demonstrated very selective response toward ethanol only. The mechanism of change in the resistance of the polymer nanowire is attributed to swelling of the polymer and reduction in the number of charge carriers on the polymer backbone. The electronic properties and gas sensing response of nanowires containing segments of PEDOT:PSS that were synthesized using anodic aluminum oxide (AAO) membranes were studied by Dan et al.[767] This single nanowire based sensor showed very good response to all three gases with linear responses toward methanol up to 50% of its saturation concentration and toward acetone up to about 80% of its saturation concentration with sensitivity of about 6% and 8% per % saturation, respectively. For concentrations higher than these, the sensors showed irreversible resistance changes, whereas for ethanol they showed saturation at higher concentration (Figure 53), sensor response and recovery time of a few seconds, and excellent reproducibility across devices.

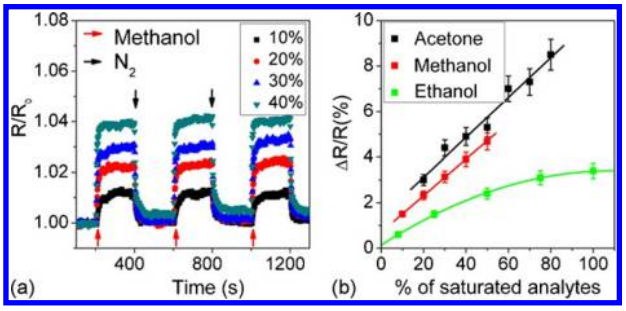

Figure 53. Average of the relative resistance of a set of four nanowire sensors increases with increasing methanol concentration. (b) Relative differential resistance response of the sensors as a function of analyte concentration for acetone, methanol, and ethanol. Lines are drawn as a guide to the eye. Reproduced with permission from ref 767. Copyright 2007 Elsevier.

A highly efficient CH_4 gas sensor was developed by mixing functionalized (MWCNT-COOH) and nonfunctionalized multiwalled carbon nanotubes (MWCNTs) with polyaniline (PANi) yielding conducting nanocomposites (PANi/MWCNTs and PANi/MWCNT-COOH) in a CP matrix.[768] These conducting nanocomposites showed excellent sensing performance toward CH_4 at room temperature, and in both, the response and recovery times were around 5 s. The PANi/MWCNT-based detector had shorter response time (1 s), as well as a higher sensitivity (3.1%) than that of the PANi/MWCNT-COOH-based sensor. Surrounding vapors alter the electronic state of the polymer chains, the number and distribution of charges, affecting interchain charge carrier hopping, and electrostatic interactions with counterions; all these factors influence finally the conductivity of the sensor.

DOI: 10.1021/acs.chemrev.7b00482
Chem. Rev. 2018, 118, 4731−4816

4.1.3.3. Triethylamine. Triethylamine (TEA), as one of the toxic gases released from petrochemicals, harvested fish, and other aging seafood, has caused a serious threat to the environment and human life. The development of highly sensitive sensors for accomplishing rapid and real-time trace detection is necessary.[769] An ingenious sensor based on α-MoO_3/PANi hybrids was fabricated by Bai et al.[770] It was done by loading α-MoO_3 nanorods on poly(ethylene terephthalate) (PET) thin film as a building framework, and then PANi was deposited on the framework via in situ chemical oxidation polymerization (Figure 54). The sensor presented high

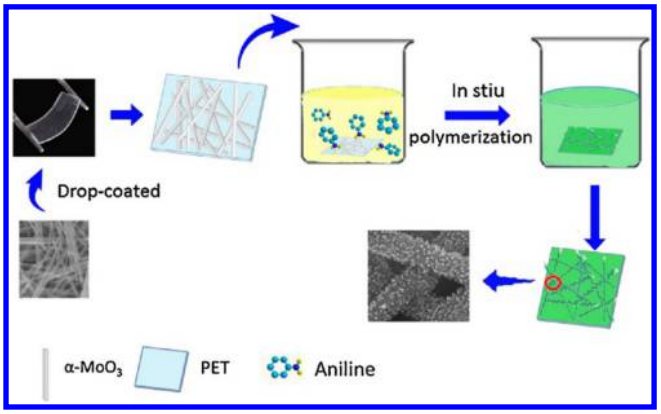

Figure 54. Schematic diagram of fabricating conducting film based on α-MoO_3/PANi hybrids. Reproduced with permission from ref 770. Copyright 2017 Elsevier.

sensitivity, good selectivity to TEA, a linear response from 10 to 100 ppm TEA at room temperature, and a low detection limit of 0.55 ppm. In addition, fabrication is simple and shows flexibility.

4.1.3.4. Ammonia. Rapid detection of ammonia at low concentration is desired in diverse applications like security systems, environmental analysis, explosives, and fertilizer industries, as well as in medical diagnosis.[771] Due to the pair of electrons on nitrogen, ammonia acts as a Lewis base and upon interaction with a p-type conducting polymer, which shows dedoping due to the recombination and loss of positive charge carriers, resulting in an increase in CP resistivity. Doping/dedoping is reversible reaction and the original conductivity can be recovered just by simply removing the analyte gas from the sensor. Several publications on ammonia sensing using this principle have recently been reported and will be discussed in this section.

Among the barriers for these sensors, the poor diffusion of ammonia into the bulk of the CP's matrix required additional investigations to achieve enhanced performance. The use of nanostructures[772] was one approach to overcome this difficulty. High density large area conducting polymer nanostructure fabrication methods were developed. Using a silicon stamp with gratings fabricated by e-beam lithography, polymer gratings on silicon surface were replicated by a technique called nano-imprint lithography (NIL). PPy was deposited on the silicon substrate by immersing the substrate in a monomer solution containing a dopant and a substituted monomer (silanized derivative), which showed improved adhesion with the silicon surface. Subsequent lift off left the conducting polymer nanowire replica with the desired diameter and pitch dictated by gratings on the silicon stamp (Figure 55). The sensor showed excellent response toward ammonia with detection limit of 40 ppm and sensitivity of 0.06% per ppm of ammonia up to 300 ppm concentration due to its behavior as a Lewis base.

The effect of ammonia and water on the conductivity of polyaniline has been investigated along with the polymer adsorption capacity.[773] Films of polyaniline/dodecylbenzene-sulfonate acid (PANi/DBSA) are prepared starting from suspensions of infusible emeraldine base, obtained by using dodecylbenzenesulfonate acid (DBSA) both as a dopant and as a surfactant to aid dispersion. The electrical resistance of PANi/DBSA films exposed to ammonia increases linearly with the NH_3 concentration in the range of 5 to 7 ppm. Wang et al.[766] reported an ammonia sensor based on network of high quality nanowires electrochemically fabricated. These sensors based on polypyrrole showed a very good reproducible response toward 1000 ppm of ammonia with change in the resistance ($\Delta R/R_0$) of about 350%. The sensor also showed very good recovery. Similarly, an array of parallel polypyrrole nanowires connected using gold pads that were deposited with shadow mask method was used to detect ammonia gas. Very fast and reproducible responses of sensors toward ammonia gas were reported[774] by

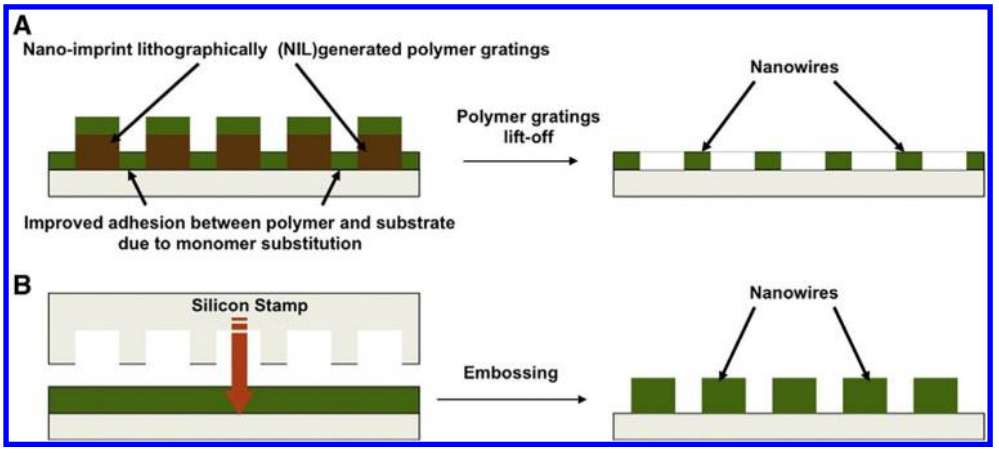

Figure 55. Schematic representation of high density conducting polymer nanowire fabrication methods. (A) High density conducting polymer nanowire fabrication method employing NIL generated polymer gratings for predefined nanowire diameter and pitch. (B) Variation of method in panel A for high density conducting polymer nanowire array fabrication by employing embossing of conducting polymer film using a silicon stamp with predefined features. Reproduced with permission from ref 772. Copyright 2010 Elsevier.

DOI: 10.1021/acs.chemrev.7b00482
Chem. Rev. 2018, 118, 4731−4816

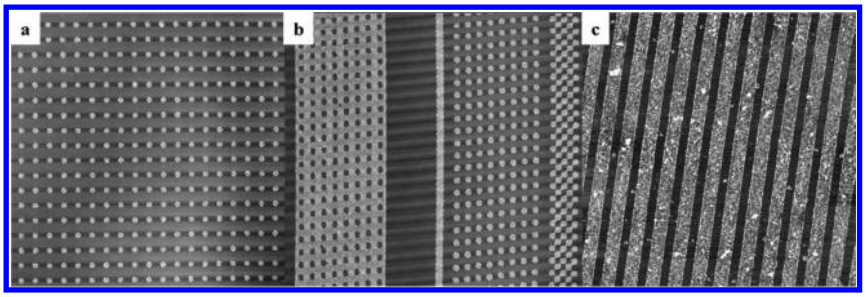

Figure 56. AFM images of conducting polymer dot arrays fabricated using NIL and a lift-off process: (a) 800 nm diameter polypyrrole dots with a center-to-center distance of 3 μm (array size 56 μm × 56 μm); (b) 800 nm diameter polypyrrole hole arrays (left part of the image) with a 2 μm separation (array size 50 μm × 48 μm); (c) PANi nanowires (650 nm wide separated by 400 nm, wire array area 15 μm × 15 μm). Reproduced with permission from ref 774. Copyright 2006, Wiley-VCH Verlag GmbH & Co. KGaA.

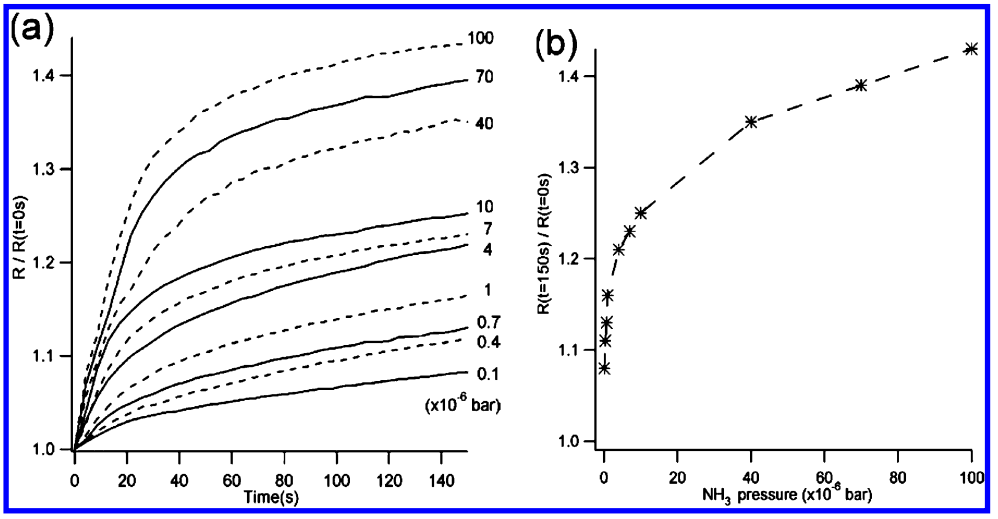

Figure 57. Real-time conducting polymer nanowire device response to ammonia gas for pressures ranging from 0.1 × 10^{-6} to 100 × 10^{-6} bar. The data is normalized by the resistance $R/R(t = 0)$ of the device prior to each exposure. (b) Plot of the normalized resistance of the sensor at exposure time t = 150 s versus ammonia pressure. Reproduced with permission from ref 775. Copyright 2006 Wiley-VCH Verlag GmbH & Co. KGaA.

Dong et al. using high-density conducting-polymer nanostructures fabricated through a combination of nanoimprint lithography (NIL), a copolymer strategy, and a lift-off process (Figure 56). These nanowire arrays function as nanosensors of ammonia. For the same concentration, their response scaled inversely with the nanowire size. Smaller width (300 nm) nanowire showed about twice the response when compared to 5 μm wide nanowires at 240 ppm ammonia concentration, emphasizing the advantage of using nanostructures for improved sensor performance. Kemp et al.[775] reported single polyaniline nanowire deposition between two platinum nanoelectrodes deposited using focused ion beam (FIB) technique. This technique can be used to make chemiresistor type sensor devices, and the effectiveness of these in the detection of ammonia gas at levels as low as 0.1 × 10^{-6} bar has been demonstrated (Figure 57). This device showed reversible response to different ammonia concentrations, while at higher concentration it showed saturation with small irreversibility.

Ammonia sensors were also fabricated from a single conducting polymer nanowire based sensor utilizing chemically polymerized polypyrrole in the pores of alumina template.[776] The sensor showed excellent response toward ammonia with detection limit of 40 ppm and sensitivity of 0.06% per ppm of ammonia up to 300 ppm concentration. Once again the response is based on the interaction between lone-pair electrons of NH_3 with the semiconducting p-type polymer matrix. The sensor sensitivity and detection limit are also influenced by the inherent flaws of sensor architecture, specifically the electrode−polymer contact resistance; therefore sensor design has a crucial role in sensor performance. A single dodecyl sulfate doped polypyrrole nanowire with maskless electrodeposited nickel contacts showed improved sensitivity toward ammonia gas. By securing or anchoring polypyrrole nanowires using selective maskless metal electrodeposition on the contact pads, significant reduction in the noise level of single polypyrrole nanowire sensor was observed. A marked improvement in the sensitivity from about 0.14% to 0.63% per ppm of ammonia was obtained by Hangarter et al.[777]

The use of carbon nanotubes as templates for the electrochemical fabrication of polyaniline nanowires was demonstrated by Zhang et al.[778] These thin nanowire (98 ± 5 nm) based sensors showed excellent sensitivity of 2.44% R/R_0 per ppm of ammonia with an outstanding detection limit of 50 ppb. Polyaniline deposited sensors showed marked improvement (~60 times) over bare carbon nanotube sensors. These polyaniline nanowire sensors showed excellent sensitivity even at higher temperatures. Nanoparticle-doped CPs have shown interesting sensitivity; for example, the electrical response from Pd-encapsulated PPy nanoparticles toward NH_3 was very fast and stable at the range of the 50−200 ppm of NH_3.[779] This nanocomposite of polypyrrole and palladium was fabricated by a facile method involving thermal dynamic refluxing of Pd salt

DOI: 10.1021/acs.chemrev.7b00482
Chem. Rev. 2018, 118, 4731−4816

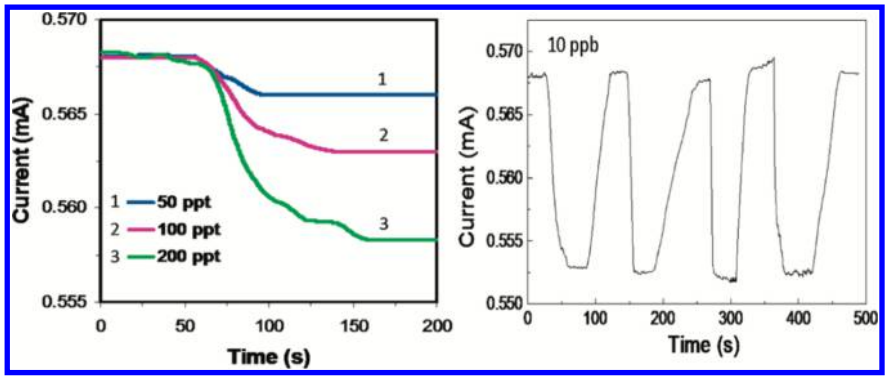

Figure 58. Current responses of a sensor made of TiO_2 microfibers encased with PANi nanograins to different concentrations of NH_3 gas as a function of time (left) and reproducibility of the sensor exposed to 10 ppb NH_3 gas (right). Reproduced with permission from ref 781. Copyright 2010 American Chemical Society.

Table 8. Conducting Polymer Based Sensors for Ammonia and Sensitivity Parameters Reported

sensor element	sensitivity	ref
polyaniline/dodecylbenzenesulfonate acid	linearly with the NH_3 concentration in the range of 5 to 7 ppm	773
nanoimprint lithography (NIL); subsequently, conducting polymer (PPy)	detection limit of 40 ppm and sensitivity of 0.06% per ppm of ammonia	772
array of parallel polypyrrole nanowires connected using gold pads	very good reproducible response toward 1000 ppm of ammonia with change in the resistance ($\Delta R/R_0$) of about 350%.	766
high-density conducting-polymer nanostructures fabricated by nanoimprint lithography (NIL), a copolymer strategy, and a lift-off process	5 μm wide nanowires at 240 ppm ammonia concentration	774
single polyaniline nanowire	0.1×10^{-6} bar	775
polypyrrole in the pores of alumina template	lower detection limit was 40 ppm	776
dodecyl sulfate doped polypyrrole nanowire with maskless electrodeposited nickel	sensitivity from about 0.14% to 0.63% per ppm of ammonia	777
carbon nanotubes as templates for electrochemical fabrication of polyaniline nanowires	detection limit of 50 ppb	778
Pd-encapsulated PPy nanoparticles	fast and stable in the range of 50−200 ppm of NH_3 gas	779
PEDOT nanotube hybrids with silver nanoparticles	1 ppm and less than 1 s	780
PANi and electrospun titania fibers	high response to 50 ppt of NH_3	781
PANi and electrospun titania fibers	high response to 50 ppt	781
poly(3,4-ethylene dioxythiophene)−polystyrene sulfonic acid (PEDOT:PSS) and CNT	1−6 ppm	782

and encapsulation of Pd nanoclusters with PPy by vapor phase polymerization. Gas sensory properties of the nanocomposite greatly depended on the size of Pd nanoparticles and the morphology of the composite film. PEDOT nanotube hybrids were utilized as the chemiresistor in the ammonia sensor with good conductivity and high affinity toward NH_3 by silver nanoparticles,[780] where the highest sensitivity and fastest response time toward NH_3 (1 ppm and less than 1 s) can be obtained with PEDOT nanohybrids owing to the silver nanoparticles dispersed on the surface of PEDOT nanotubes. Gong et al.[781] fabricated unique conducting polymer nanograins using PANi and electrospun titania fibers, leading to the ultrasensitive NH_3 gas sensor. Moreover, the chemoresistive ammonia sensor based on titania/PANi nanohybrids was developed with electric current switches that can be operated by the resistance change from a p−n heterojunction when NH_3 gas is absorbed by PANi nanograins (Figure 58). A high response to 50 ppt of NH_3 gas has been achieved.

Two types of conducting polymers, PEDOT:PSS and PANi with carbon nanotubes, were used and compared for their ammonia gas sensing properties at room temperature.[782] Both sensors exhibit excellent sensitivity but poor recovery from ammonia gas sensing at room temperature. When compared to PANi, a PEDOT:PSS polymer composite was found to be more sensitive (with sensitivity of ~16%) with a faster response time (~15 min). Table 8 summarizes the variety of methods for preparation of ammonia sensors recently reported, as well as the principle of ammonia detection, being a very active field of research nowadays. It involves the interaction of the gas molecules with the conducting polymer and other incorporated materials, being, in most cases, metallic nanostructures whose electrocatalytic activity is very well used. The sensitivity parameters differ greatly, making difficult their comparison among the various sensors, as is done in the case of analytes in solution. In general, it can be seen from the table that the smaller the device, the lower the concentrations of gas that can be detected in a shorter time.

4.1.3.5. Nitric Oxides (NO and NO_2). Nitric oxide (NO) plays an important role in various biological processes. Its production in the central nervous system is linked to the control of certain mechanisms and states like body temperature, sleep, and appetite. The review prepared by Bedioui relates the efforts of sensing this gas by electrochemical techniques and sensors before 2010.[783] Recent work published in the literature in this field uses novel CPs as matrix sensor. Thus, a flexible gas sensor for NO detection uses conducting poly[*N*-9′-heptadecanyl-2,7-carbazole-*alt*-5,5-(4′,7′-di-2-thienyl-2′,1′,3′-benzothiadiazole)] (PCDTBT), which is a highly conjugated polymer, as the sensing material.[784] PCDTBT is highly selective for NO detection with a very good response up to 5 ppm (toxic limit = 25 ppm) (Figure 59). Its long-term environmental stability was confirmed by 35-day measurements that showed it to be a

DOI: 10.1021/acs.chemrev.7b00482
Chem. Rev. 2018, 118, 4731−4816

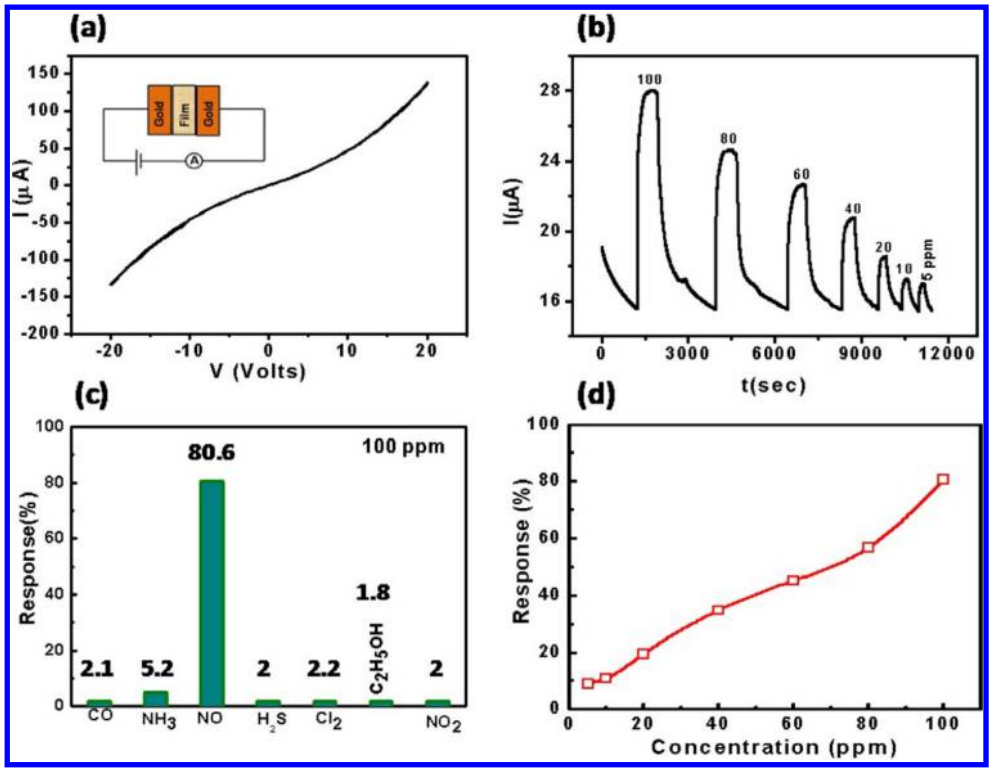

Figure 59. Flexible NO gas sensor based on conducting polymer PCDTBT: (a) Current−voltage characteristics, (b) dynamic response to different NO concentrations, (c) selectivity of the sensor for different gases, and (d) sensitivity of the sensor to commercial-grade NO concentration. Reproduced with permission from ref 768. Copyright 2017 Elsevier.

reliable and effective material for this application. PCDTBT gas measurements under bending conditions displayed improved performance, opening the door for its application as a novel gas sensing material in a flexible NO gas sensor.

Geng and colleagues prepared PPy nanohybrids by means of mechanically mixing PPy with WO_3. Acting as an electrochemical sensor, this composite exhibited a gas sensitivity up to 1000 ppm for NH_3, H_2S and NO_x.[785] H_2S detection was excellent at low temperature (i.e., 90 °C) with PPy/WO_3 sensors demonstrating fast response and recovery time, as well as a linear relationship with H_2S concentration. The sensing mechanism of PPy/WO_3 materials to H_2S may be attributed to a coeffect of a proton−polymer interaction and changes in resistivity due to the semiconducting properties of the PPy/WO_3. Composite resistance increased rapidly with temperature, and their sensitivity toward H_2S disappeared. The same research group prepared PPy/γ-Fe_2O_3 nanohybrids using chemical oxidation of Py with Fe(III) and used them for the detection of NH_3 and H_2S.[786] Using these CP nanohybrids as transducers, a sensitivity difference depending on the different Fe(III)−Py mole ratios was demonstrated. The composite required annealing for H_2S sensing and showed a strong temperature dependence. The maximum sensitivity of these CP nanohybrids toward NH_3 or H_2S was obtained with a Fe(III)/Py mole ratio = 3:1, and the sensitivities obtained for these gases were 48.5 and 31.4 times higher for the first gas as compared to the second one.

The *in situ* chemical oxidative polymerization of thiophene in the presence of SnO_2 gave nanocomposites (PTh/SnO_2), which were applied to NO_x detection.[787] The SnO_2 particles were coated with a PTh shell that was several nanometers thick. Both sensitivity and selectivity can increase by controlling the PTh mass percent (i.e., 1−30%) at different temperatures (Figure 60). The definition of gas sensitivity, S, is the ratio of V_g/V_a, in which V_g and V_a represent the voltage of the sensor in the testing gas and clear air, respectively.

An excellent NO_2 gas sensor was created using PANi/In_2O_3-NP nanofiber composites.[788] Deposition of these nanohybrids on a surface acoustic wave (SAW) lead to fast responses and recovery times with good repeatability at room temperature. The conductivity of PANi/In_2O_3 increased with NO_2 exposure, indicating that NO_2 gas can act as a doping agent for the PANi/

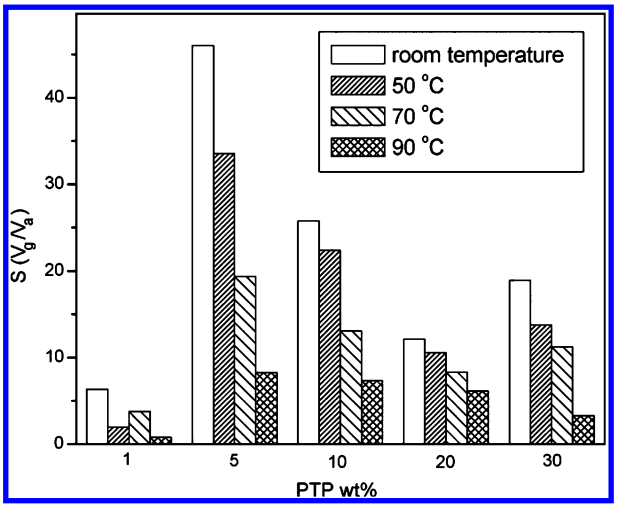

Figure 60. Sensitivity of PTP/SnO_2 composites to 150 ppm of NO_x at different temperatures. S is the ratio of V_g/V_a, in which V_g and V_a represented the voltage of the sensor in testing gas and clear air, respectively. Reproduced with permission from ref 787. Copyright 2008 Elsevier.

DOI: 10.1021/acs.chemrev.7b00482
Chem. Rev. 2018, 118, 4731−4816

In_2O_3 system. Based on this sensing mechanism, the detection limit of the PANi/In_2O_3 nanohybrid was ca. 510 ppb.

A composite made from hydrated tungsten oxide (WO_3)−chitosan-*co*-polyaniline (CHIT-*co*-PANi) was electrochemically prepared on an indium tin oxide (ITO)-coated glass surface using a mineral acid as a supporting electrolyte.[789] The composite electrode exhibited a 3D nanofibrous structure with a nanofiber diameter of 20−100 nm. The modified electrode was used in the amperometric detection of NO_2 gas in acidic media without interferences. The current decreased linearly with an increase in NO_2 gas concentration in the range from 100 to 500 ppb, with a response time of 8 s at a pH = 2.0 and using 0.25 V vs Ag/AgCl.

4.1.3.6. Carbon Monoxide and Carbon Dioxide. The study of potentiometric gas sensors with CO-sensing properties, relies on an anion-conducting polymer (ACP) as the electrolyte and metal oxides (In_2O_3, ZnO, or Co_3O_4) with and without Au nanoparticles as the sensing elements.[790] They showed excellent and rapid CO response with relatively high CO selectivity versus H_2, as well as excellent long-term stability. Au loading (0.5 to 2.0 wt %) in wet synthetic air (at 57% relative humidity, RH) was selected as a condition for CO sensing. All oxide sensors showed relatively small electromotive force changes (i.e., responses) to both CO and H_2. However, In_2O_3 sensors loaded with 2.0 wt % Au and ZnO improved their CO response dramatically against H_2 in the concentration range of 10−3000 ppm. A low cost, easy to build, resistive-type CO_2 gas sensor made of poly(3,4-ethylene dioxythiophene) (PEDOT) and branched polyethylenimine (BPEI) layers was fabricated on an interdigitated electrode.[791] The sensor showed no response (i.e., % of conductivity increase) when the CP film was made of a PEDOT layer without any BPEI. Its response increased to a value of 3.25% upon the addition of a layer of BPEI. Regarding selectivity, it showed a higher response for CO_2 than for O_2. Use of the same PEDOT−BPEI sensor device in 1000 ppm of CO_2 at room temperature and 95% RH for several cycles did not show a decay of its response, proving its reusability. The observed increase in conductivity upon CO_2 exposure was caused by the production of HCO_3^- ions during the reactions between the amine functional groups of BPEI, ambient moisture, and CO_2. This caused a redoping in the underlying p-type PEDOT film.

4.1.3.7. Miscellaneous Gases. Dimethyl methylphosphonate (DMMP) is a nerve gas simulant with a similar chemical structure to sarin gas, which is used as a chemical weapon owing to its extreme potency as a nerve agent.[792] Phosphoryl groups in DMMP cause hydrogen-bond interactions with protons of functionalized CP nanomaterials or nanohybrids. PPy nanohybrids can be produced by electrochemical incorporation in the presence of a cationic surfactant such as cetyltrimethylammonium bromide (CTAB) and copper phthalocyanine (CuPc) to yield multidimensional PPy/(CuPc)/CTAB/$NaClO_4$.[793] Such sensors showed significant frequency shifts in a quartz microbalance at various DMMP concentrations. The highest sensitivity change was achieved at a lower concentration of DMMP vapor (i.e., 5 ppm), but as this increased from 5 to 210 ppm, the sensitivity decreased, which indicates sensor saturation. This modified electrode can be used for the detection of emulators of the nerve agent in field conditions without any interference from other chemical vapors like methanol, acetone, ethanol, benzene, hexane, and toluene.

Hydrogen sulfide (H_2S) from industrial processes is among the most highly toxic and corrosive gases. Low concentrations (i.e., above 250 ppm) can lead to death. It can have potential uses in terrorist attacks since it is colorless, flammable, and heavier than air.[794] Hydrogen sulfide can interact with PANi via a doping mechanism, which may result in a measurable conductivity change. This was demonstrated by incorporating transition metal chlorides ($ZnCl_2$, $CdCl_2$, and $CuCl_2$) into PANi nanofibers, utilized as transistors for 10 ppm H_2S detection.[795] Such hybrid PANi chemical sensors presented measurable resistance changes upon exposure to 10 ppm H_2S (Figure 61).

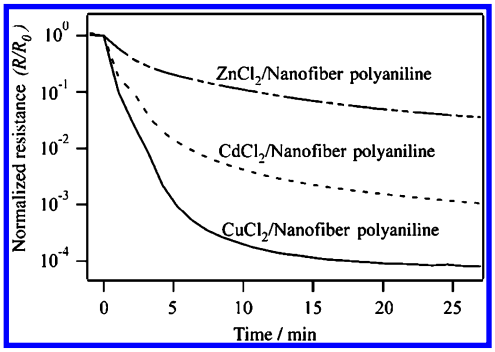

Figure 61. Resistance changes of PANi nanofiber films containing $ZnCl_2$, $CdCl_2$, and $CuCl_2$ on exposure to 10 ppm of H_2S. Reproduced with permission from ref 795. Copyright 2005 Wiley-VCH Verlag GmbH & Co. KGaA.

Chemiresistor sensors were fabricated by potentiostatic electrodeposition of PANi, PPy, and poly(3-methylthiophene) (P-3MTp) in the gap of two planar Au electrodes on a Teflon substrate.[796] The change in electrical resistance was monitored after exposing the electrode array to the headspace of oil samples. Different signals were obtained for each coconut oil sample, and pattern recognition techniques were employed for data analysis. This system can distinguish virgin coconut oil (VCO) from refined, bleached, and deodorized coconut oil (RBDCO), flavored VCO, homemade VCO, and rancid VCO. Vapor diffusion of volatile organic compounds into the polymer matrix causes an increase in the interchain distance and affects electron flow in the polymer chains.

4.1.4. Chiral Conducting Polymer in Sensor and Chiral Applications. *4.1.4.1. Introduction to Chiral Conducting Polymers.* Some conducting polymers, like polypyrrole,[200] polyaniline,[221] and polythiophenes,[523] have attracted much attention due to their well-known chemical stability in the undoped and doped states, high π-conductivity, and facile derivatization. Moreover, their excellent electrochemical stability facilitates tuning the physical and electronic properties of the polymer for use in a wide range of applications in chemistry and organic electronics (see preceding sections). In order to control the properties of the resulting conducting polymers, different synthetic strategies have been used to functionalize them; chirality is not an exception, and in this section the different synthetic strategies used for the introduction of chirality to these conducting materials will be discussed. This chiral material has been called *chiral conducting polymer* (CCP).[797] The chiral interface of electrodes with CCPs deposited on them has been mainly exploited in chiral sensors, while other technological applications have also been described recently and will be discussed in the final part of this sensors section.

DOI: 10.1021/acs.chemrev.7b00482
Chem. Rev. 2018, 118, 4731−4816

The synthetic challenge of preparing new organic molecules to mimic the role of biological molecules has drawn significant interest, and chiral compounds are often required to succeed. The presence of chirality in conjugated polymers offers the possibility of overcoming the inefficiency or high cost of the biological molecules, thus making chiral sensors a promising field of research for electroanalysis. The strategies used to prepare chiral conducting polymers are summarized in Scheme 3. The chirality is introduced in the conducting polymers via

Scheme 3. Strategies for the Preparation of Chiral Conducting Polymers[a]

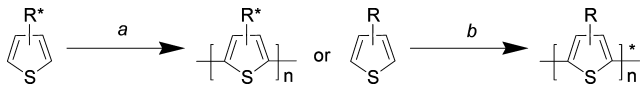

[a](a) Via polymerization of the corresponding chiral monomer precursor; (b) via polymerization of the achiral monomers in a solvent/chiral supporting electrolyte solution. * = chirality.

polymerization of the prepared chiral monomer precursor[798] (a) or via polymerization of the achiral monomers in a solvent/chiral supporting electrolyte solution[799] (b).

In this section, the syntheses and characterization of chiral conducting polythiophenes using both synthetic approaches will be described. The syntheses and applications of other families of chiral conducting polymers, such as polypyrrole and polyaniline derivatives, have been exhaustively described by Kane-Maguire and co-workers,[797] whereas there have been limited reports of chiral polythiophenes[800] and of their environmental stability, which makes them promising materials for technological applications.[801]

4.1.4.2. Chiral Polythiophenes via Electrochemical Oxidation. Several monothiophenes bearing chiral biological molecules were prepared in 1977 by Macco and co-workers.[802,803] In dichloromethane (CH_2Cl_2), the cyclization of a 2-chiral olefin monothiophene (**1**) in the presence of $SnCl_4$ gives a mixture of two asymmetric steroid-based thiophenes, **2** and **3**, with a yield of 50% each (Scheme 4). Other similar substituted

Scheme 4. Synthesis of Steroid Based Thiophenes

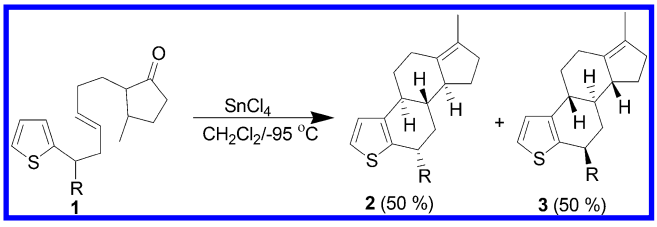

compounds with the *tert*-butyl group (R) have been synthesized. However, the α-substitution of thiophene blocks the polymerization chain of the steroid-thiophene. This example shows the limitation of this synthetic strategy where the α and α' positions need to be unsubstituted to permit the polymerization.

The first chiral conducting materials based on polythiophenes were disseminated by Lemaire and co-workers in 1988.[804] Monothiophene monomers substituted in the 3-position by *R*-(−)- and *S*-(+)-phenylbutanol were prepared (Scheme 5). After a six-step syntheses of thiophene **3**, *R*-(−)- and *S*-(+)-phenylbutanols were added to obtain chiral monothiophenes **5**-*R* and **5**-*S*, respectively.

The electropolymerizations of **5**-*R* and **5**-*S* were performed in nitrobenzene using a platinum anode and aluminum wire as a cathode to give the electroactive polymers poly**5**-*R* and poly**5**-*S*. A compact chiral film with a conductivity of 1 S/cm was deposited on the surface of the electrode. Both undoped chiral films of poly**5**-*R* and poly**5**-*S* showed a maximum absorption at 445 nm and exhibited a high specific rotation, as opposed to their corresponding monomers.

Since then, a wide range of synthetic methods for a variety of conducting polythiophene precursors bearing chiral motifs has been developed.[797] As an example, a series of monothiophenes (**I**), terthiophenes (**II**), and 3,4-ethylene dioxythiophene (**III**)-bearing amino acids (R*) have been prepared (Scheme 6); the synthetic strategies are discussed below.

4.1.4.2.1. Amino Acid-Functionalized Oligo- and Polythiophenes. The condensation reaction of a 3-thiophene carboxylic acid with DL-alanine methyl ester hydrochloride (DL-Ala-OMe, HCl) in the presence of hydroxybenzotriazole (HOBT) and *N*,*N*-dicyclohexylcarbodiimide (DCC) at room temperature in CH_2Cl_2 yields the desired product (**6**), which is then converted to the corresponding alanine-monothiophene **7** in methanol and NaOH/HCl, as shown Scheme 7.[805]

A similar procedure has been used to prepare monothiophenes bearing various amino acids such as L-leucine (Leu)[806] and proline (Pro)[807] as highlighted in Scheme 8 (**8**−**14**). The amino acids are either directly attached to a thiophene or else bridged by a methylene group. The prepared chiral monomers are very stable in the presence of organic solvents and moisture.

Although the electropolymerization using repeated cycling in cyclic voltammetry of the chiral monothiophenes **6**−**14** occurs in acetonitrile (ACN)/tetrabutylammonium hexaphosphate (n-Bu_4NPF_6), no film has been successfully deposited on the surface of the platinum electrode. The high oxidation peak potential (1.6−2.0 V vs Fc^+/Fc) and the poor adhesive properties of their corresponding chiral polymer precluded any deposition of the films on the surface of the platinum electrode. To circumvent this limitation, electro-copolymerization of a proline-thiophene (**14**)[807] was performed in the presence of 2,4-ethylene dioxythiophene (EDOT). EDOT is an ideal candidate for such copolymerization due to its excellent stability in both states, high conductivity, and stable electrochemical properties of its corresponding polymer polyEDOT.[204,808,809] Electropolymerization at different monomer ratios yields a copolymer that combines EDOT and monothiophene **14** features as shown in Scheme 9.

The CO stretch IR absorptions at 1730 and 1635 cm^{-1} observed in Figure 62 (left) correspond to the carboxylate and amide groups of the proline, which confirm the success of the electrochemical copolymerization. Moreover, identical carbonyl CO absorptions are observed in poly**14** obtained by chemical oxidation of **14** using $FeCl_3$ (Figure 62, right).

4.1.4.2.2. Amino Acid-Functionalized Oligo- and Polyterthiophenes. In addition to amino acid-functionalized monothiophenes, several terthiophene monomers bearing alanine and leucine have been prepared in several steps as shown in Scheme 10 for alanine-terthiophene, **17**.[805] Dibrominated 3-thiophene acid with DL-Ala-OMe HCl in CH_2Cl_2 and HOBT/DCC affords dibrominated thiophene−Ala-OMe, **15**, which via Stille cross-coupling reaction gives terthiophene−Ala-OMe **16** (50%). The latter was converted to the corresponding acid in CH_3OH and NaOH/HCl (94%).

DOI: 10.1021/acs.chemrev.7b00482
Chem. Rev. 2018, 118, 4731−4816

Scheme 5. Synthetic Route of 5-*R* and 5-*S* and of Their Corresponding Conducting Polymers

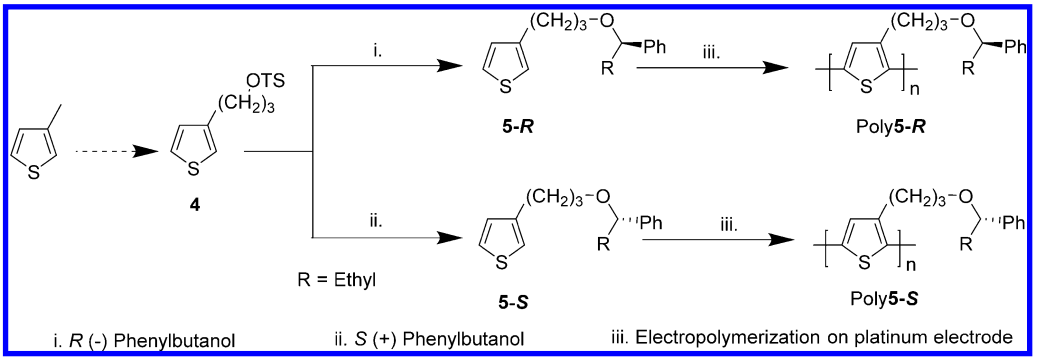

Scheme 6. Monothiophene- (I), Terthiophene- (II), and 3,4-Ethylene Dioxythiophene (III)-Bearing Amino Acids (R*)

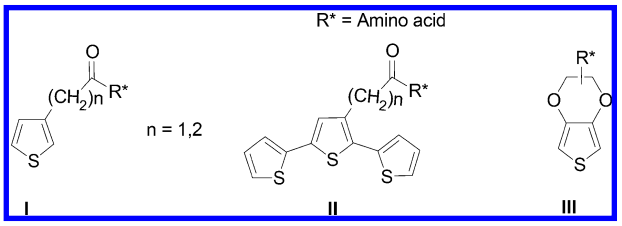

Following this procedure, several terthiophenes (**18**−**22**) bearing DL-alanine[805] and L-leucine[806] have been prepared.

The electrochemical properties of the prepared monomers were examined by cyclic voltammetry, and the $E_{1/2}$ (i.e., the average of oxidation and reduction peak potentials) of all chiral polymers **16**−**23** are summarized in Table 9. It is noteworthy that the conjugation enhancement of amino acid-functionalized terthiophene led to lower oxidation potentials (0.600−0.800 V vs Fc^+/Fc) and therefore to prevention of the overoxidation of the deposited polymer.[810] Moreover, the monomers with a methylene linker exhibited lower oxidation peak potentials than those without it, which can be attributed to the electrodonating behavior of the linker.[811]

The electroactive chiral polymers were obtained successfully by electrochemical oxidation of **16**−**23** using cyclic voltammetry are presented in Scheme 11. These optically active polymers are very stable and their coloration/discoloration is reversible. As an example, the electropolymerization of L-leucine-functionalized terthiophene **23** (0.01 M) was performed in ACN/*n*-Bu_4NPF_6 solution (1 M) through repeated cycling beyond the oxidation potential of the terthiophene component (0.670 V vs Fc^+/Fc).

The ten scan electropolymerization CV curves of **23** are shown in Figure 63 (top-left). The peak current increases with each successive scan, confirming the deposition of a poly**23** film on the surface of the platinum electrode. In a solution of monomer-free ACN/supporting electrolyte, poly**23** displays excellent stability in both doped and undoped states, and the transition is fully reversible. The peak current remains constant and no significant change or degradation of electrochemical behavior was observed over 100 CV scans (Figure 63, top-right).

The optical properties of the chiral polythiophenes **16**−**23** examined on an indium tin oxide (ITO) electrode are similar. They are dark blue in the doped state and orange in undoped states (Figure 63, bottom-left). Moreover, ATR spectra show characteristics of carbonyl stretching absorptions present in the polymers. Although the chiral polymers have been characterized by CV, UV−vis, and IR, the morphology of these polymers should be studied by SEM (scanning electron microscopy). The influence of the chiral center on the geometry of the backbone polymers in the doped and undoped states needs further investigation by circular dichroism (CD). The stable poly**23** chiral polymer has been tested for the detection of bioorganic molecules (Figure 63, bottom-right). Its capacitive current decreased by 30% in the presence of a free D-Ala-OMe (L-Ala-OMe or L-Leu-OMe) as a result of the formation of hydrogen bonds on the surface of the chiral polymers.[812] Similar behavior has been reported for oligonucleotide-functionalized polythiophenes.[813,814]

4.1.4.2.3. Amino Acid-Functionalized PolyEDOT Derivatives. Chiral disubstituted EDOT with chiral alkyl groups and their corresponding optically active polyEDOT was developed by Caras-Quintero and Bäuerle in 2004.[815] They found that the optical properties of the polymer depended on the nature of the chirality present on the backbone polymers. The syntheses of other chiral polyEDOTs bearing L-Ala-Boc[816] (Poly**25**) and L-phenylalanine[817] (Poly**27**) have been achieved and used to detect L-ascorbic acid and 3,4-dihydroxyphenylalanine (Scheme 12).

Poly**25** was deposited on a glassy carbon electrode (GCE) in CH_2Cl_2/*n*-Bu_4NClO_4 (0.1 M) by electropolymerization of **25**, prepared by reaction of **24** and N-(*tert*-butoxycarbonyl)-L-alanine.[816] A similar procedure has been followed for the electrosynthesis of poly**27** using **26** as a precursor.[817]

4.1.4.2.4. Chiral Alkyl Side Chain Polythiophenes. Several polyacetylenes bearing chiral side chains have been prepared via chemical polymerization.[818,819] The analysis using UV−vis and circular dichroism [CD] spectrometers of the resulting chiral

Scheme 7. Condensation Reaction To Obtain (6) along with the Corresponding Conversion to (7) in NaOH/HCl

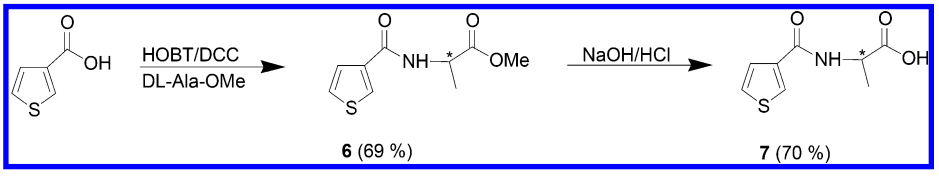

DOI: 10.1021/acs.chemrev.7b00482
Chem. Rev. 2018, 118, 4731−4816

Scheme 8. Chemical Structures of Monothiophenes Bearing Different Amino Acids

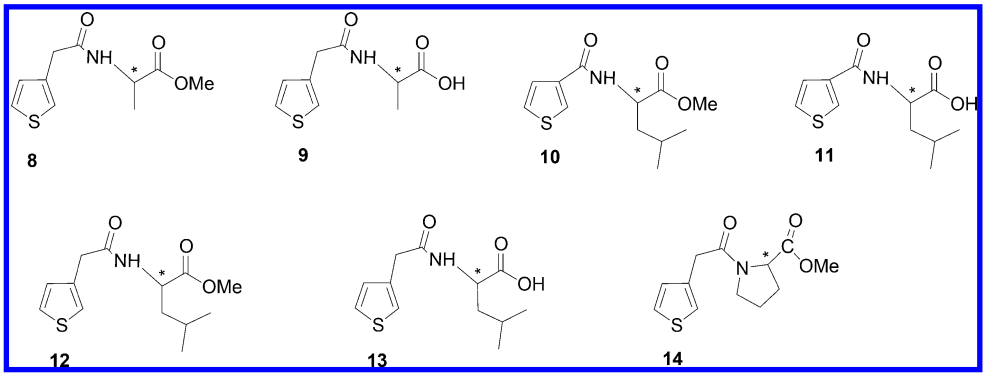

Scheme 9. Electro-copolymerization of 14 and EDOT in ACN

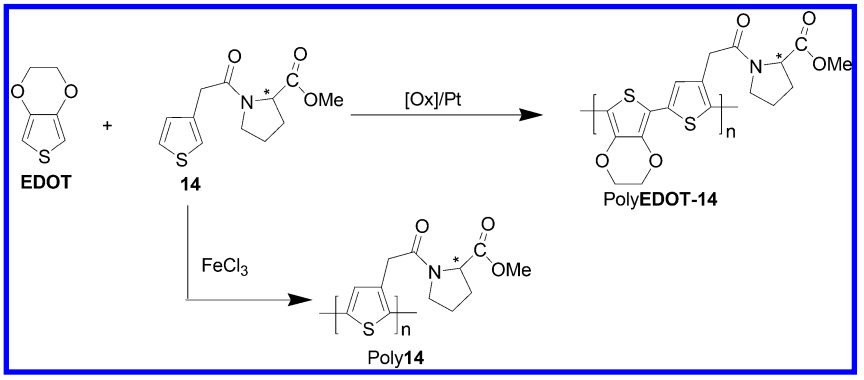

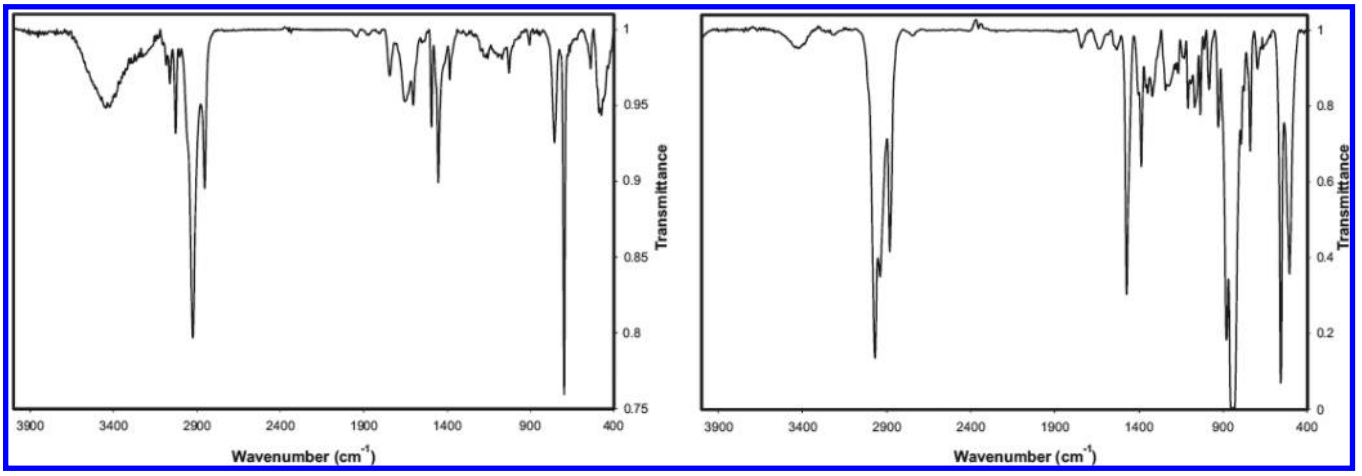

Figure 62. FTIR spectra of poly**14** (left) and poly**EDOT-14** (right). Reproduced with permission from ref 807. Copyright 2011 Elsevier.

conjugated polymers shows that the chirality is present in the side chain and in the polymer backbones. The chiral methyl group induces chirality in the π-conjugated system. Moreover, the intensity of the CD spectra increases when the temperature of the polymer solution decreases, therefore validating that the main chain has a flexible helix structure. Using an electrochemical method, a polyEDOT bridged by a chiral side chain was developed by Akagi and co-workers in 2010.[820] The Stille cross-coupling reaction[821,822] of (*R*)- or (*S*)-dibromobenzoic acid 1-methyl heptyl with 3-tributylstannyl-3,4-ethylene dioxythiophene in the presence of a $Pd(PPh_3)_2Cl_2$ offers either **28**-*R* or **28**-*S* (Scheme 13).

The electrochemical oxidation of 0.01 M **28**-*S* (**28**-*R*) in ACN/*n*-Bu_4NClO_4 (0.1 M) solution using repeated CV cycling between −1 and 1 V (vs Ag/AgCl) facilitates the deposition of poly**28**-*S* (poly**28**-*R*) on a Pt electrode (Figure 64).

Poly**28**-*S* and poly**28**-*R* exhibit similar electrochemical properties, and their oxidation potentials were −0.514 V (vs Ag/AgCl), in agreement with the value found for polyEDOT derivatives bridged by a phenyl group.[823] Since the chiral group is not directly attached to the electroactive species, the chiral groups have no significant effect on the electrochemical properties of poly**28**-*S* and poly**28**-*R*. The doped polymer is green (750 and 1500 nm), and the neutral form is purple (540 nm). The doped state of the polymer backbone is planar due to the quinoid structure (Figure 65a, right), thus limiting the movement of the chiral center, whereas the neutral polymer has a benzenoid structure and therefore the polymer adopts a helical structure similar to that of polyalkylthiophenes (Figure

DOI: 10.1021/acs.chemrev.7b00482
Chem. Rev. 2018, 118, 4731−4816

Scheme 10. Electrosynthesis of Poly16 and Poly17

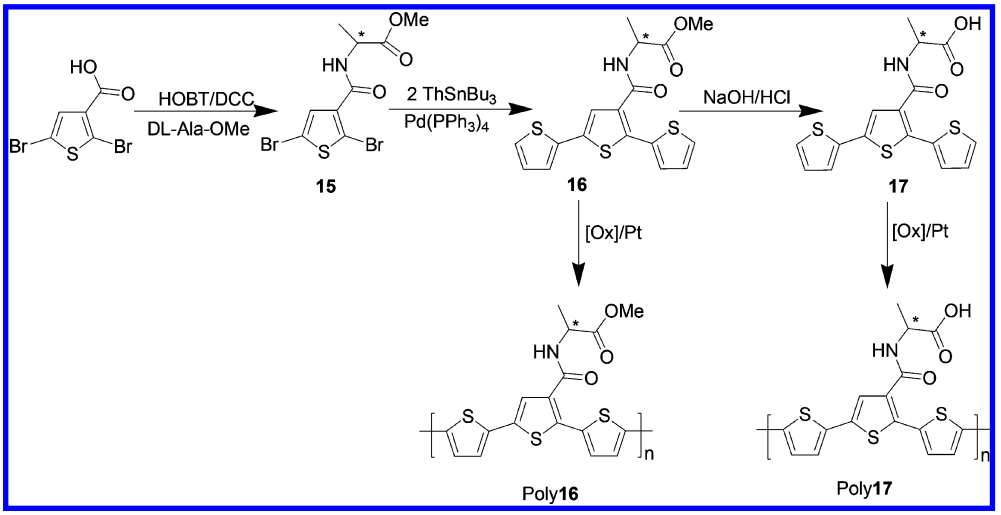

Table 9. Electrochemical Potentials of Amino Acid−Terthiophenes and Their Corresponding Polymers[805,806] in ACN

compound	E_p[a] or [$E_{1/2}$] (V vs Fc^+/Fc) + 0.02 V
16 [poly**16**]	0.720 [0.400]
17 [poly**17**]	0.720 [0.430]
18 [poly**18**]	0.650 [0.350]
19 [poly**19**]	0.610 [0.300]
20 [poly**20**]	0.830 [0.510]
21 [poly**21**]	0.880 [0.480]
22 [poly**22**]	0.660 [0.400]
23 [poly**23**]	0.670 [0.410]

[a]Oxidation peak potential in the first scan using a scan rate of 0.1 V/s. Number in brackets indicates the oxidation potential of the polymer.

65b, left).[824] Furthermore, the oxidized form of poly**28**-*S* shows a weak CD signal because of the planarity of the structure and the intercalation of the dopant (ClO_4^-). The helical structure and the freedom of the chiral centers between the EDOTs in the backbone polymer are at the origin of the CD signals observed for the neutral form. In addition, scanning electron microscopy (SEM) confirms the differences in morphology observed between the neutral and doped forms. The oxidized form of poly**28**-*S* displays a swollen morphology (Figure 65c, right), and the neutral form has a twisted and shrunken morphology (Figure 65c, left). These changes in morphology between the neutral and doped forms are reversible and can be tuned by the electrochemical oxidation/reduction of the polymer.

4.1.4.3. Electrochemical Oxidation of Achiral Thiophene Monomers in Chiral Media. A method in which a chiral nematic liquid crystal (N-LC)* is used to prepare helical polyacetylene with a one-handed screw structure was reported.[825] The results indicate that the chiral liquid crystal plays an essential role in formation of the helical structure, not only at the molecular level but also at the macroscopic level. The addition of a small amount of an optically active molecule as a chiral dopant to the media induces the formation of a chiral nematic liquid crystal with a helical structure. The technique uses as chiral electrolyte a cholesteric liquid crystal (CLC) containing (*R*)- or (*S*)-1-binaphthyl-2,2-bis-*trans*-4-pentylcyclohexyl-phenoxy-1-hexyl ether (PCH506-Binol) as chiral inducer (Scheme 14). In this way, the electrosynthesis of chiral polythiophene poly**29** was achieved.[826,827]

Scheme 11. Chemical Structure of Electroactive Chiral Polymer Precursors

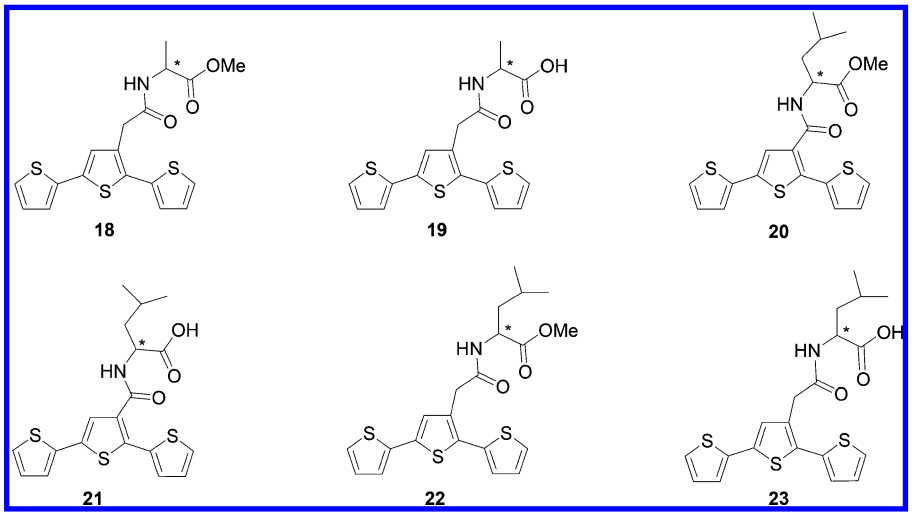

DOI: 10.1021/acs.chemrev.7b00482
Chem. Rev. 2018, 118, 4731−4816

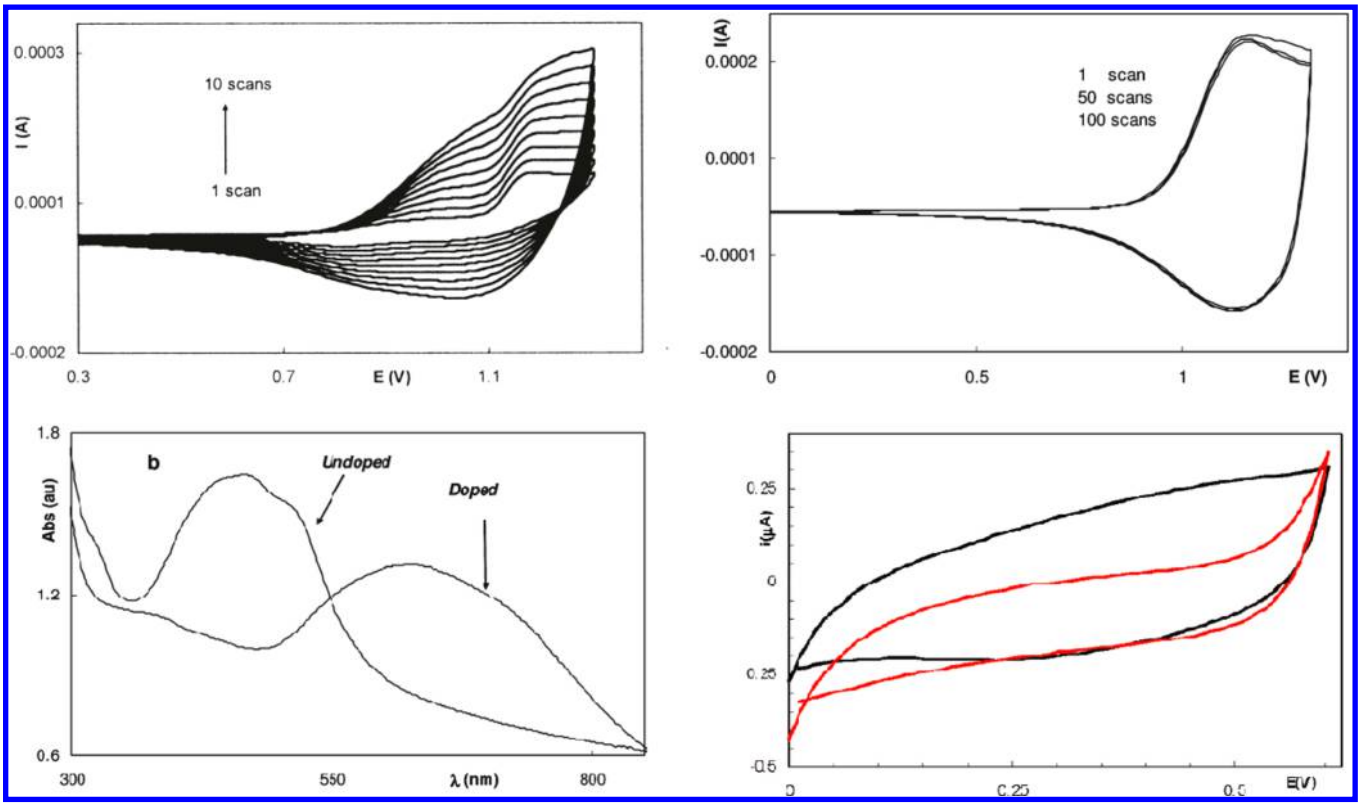

Figure 63. A ten scan electrochemical oxidation of **23** (top left) in ACN (scan rate = 0.1 V/s; WE = Pt electrode; RE = Ag wire; CE = Pt wire). Stability curve of poly**23**. UV−vis spectra of poly**23** in both the doped (blue) and undoped (orange) states. Capacitive current of poly**23** in the absence (black) and presence (orange) of D,L-alanine methyl ester. Reproduced with permission from ref 806. Copyright 2010 American Chemical Society.

Scheme 12. Electrosynthesis of polyEDOT Bearing L-Alanine Derivatives

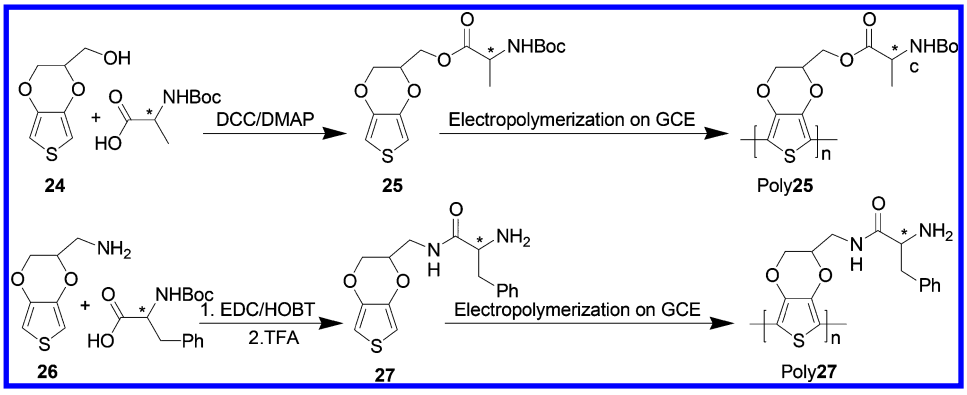

Scheme 13. Electrochemical Synthesis of poly28-*R* and poly28-*S*

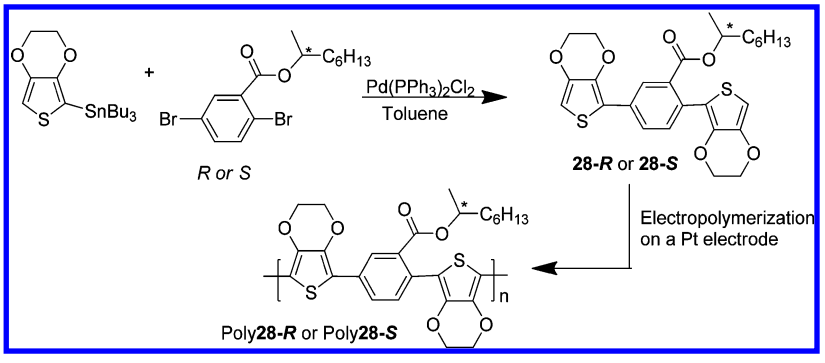

DOI: 10.1021/acs.chemrev.7b00482
Chem. Rev. 2018, 118, 4731−4816

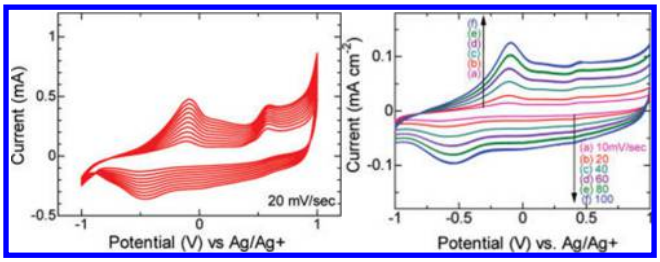

Figure 64. (left) Electrochemical polymerization using cyclic voltammetry for the synthesis of poly**28**-*S* in 0.1 M TBAP in acetonitrile, scan rate: 20 mV/s. (right) Cyclic voltammetry of monomer-free poly**28**-*S* in 0.1 M TBAP/acetonitrile solution: (a) 10, (b) 20, (c) 40, (d) 60, (e) 80, and (f) 100 mV/s. Reproduced with permission from ref 820. Copyright 2011, American Chemical Society.

As example, the electropolymerization of bithiophene **29** was successfully carried out in this media. Due to the low ionic conductivity of the electrolyte, the polymers were prepared potentiostatically using two parallel ITO electrodes separated by a narrow gap; cyclic voltammetry destroyed the macroscopic helical structure of the chiral LC. Both chiral polymers poly**29**-*R* and poly**29**-*S* display similar electrochemical properties. They adhere well to ITO electrode and show a quasi-reversible redox wave in monomer free electrolyte solution. Their CD spectra show that poly**29**-*R* and poly**29**-*S* have the same degree of chirality but opposite sense (Figure 66) and exhibit a Cotton effect similar to chiral polythiophenes prepared via chemical polymerization.[828,829]

Similar behaviors have been observed for polyEDOT prepared by the same method using the same chiral inducer ((*R*)- or (*S*)-PCH506-Binol) and liquid crystal solvent.[830] It was found that none of the chiral molecules or chemicals contained in the electrolyte reacted with the monomer during polymerization as revealed by the analysis of the corresponding chiral polymers. Moreover, the polarized optical microscopy (POM) demonstrates that the resulting chiral conducting polymers have a specific morphology that replicates the LC texture in which it was formed. The (N-LC)* electrolyte plays the role of chiral matrix.

Another strategy for preparing chiral liquid crystals using deoxyribonucleic acid (DNA) as chiral inducer has been developed.[831] DNA in low concentration forms a lyotropic chiral nematic liquid crystal in sodium chloride aqueous solution. This property was used to prepare an asymmetric electrolytic medium for the potentiodynamic electrosynthesis of polyEDOT (Scheme 15).

In order to follow the deposits by CD, ITO electrodes were used. The analysis showed a negative maximum around 500 nm. The conducting polymer obtained presented a honeycomb pattern morphology attributed to an aggregation state of polyEDOT chains in the medium. DNA (N-LC)* provides a sequential pattern equivalent to a molecular mold during electrosynthesis (Figure 67).

A similar approach, using EDOT as monomer, was carried out in aqueous solution containing hydroxypropyl cellulose (HPC) as polymeric lyotropic liquid crystal (LC). Potentiodynamic polymerization of EDOT in the HPC solution afforded an insoluble and infusible chiral thin conducting film on the ITO electrode.[832,833] SEM and circular differential interference contrast (C-DIC) optical micrographs of the obtained polymers showed a multicolored surface and a unique pattern, properties attributed to the LC texture of HPC, that are transferred to the conducting polymer during the electropolymerization (Figure 68A,B). The chiral polyEDOT/HPC exhibits strong CD,

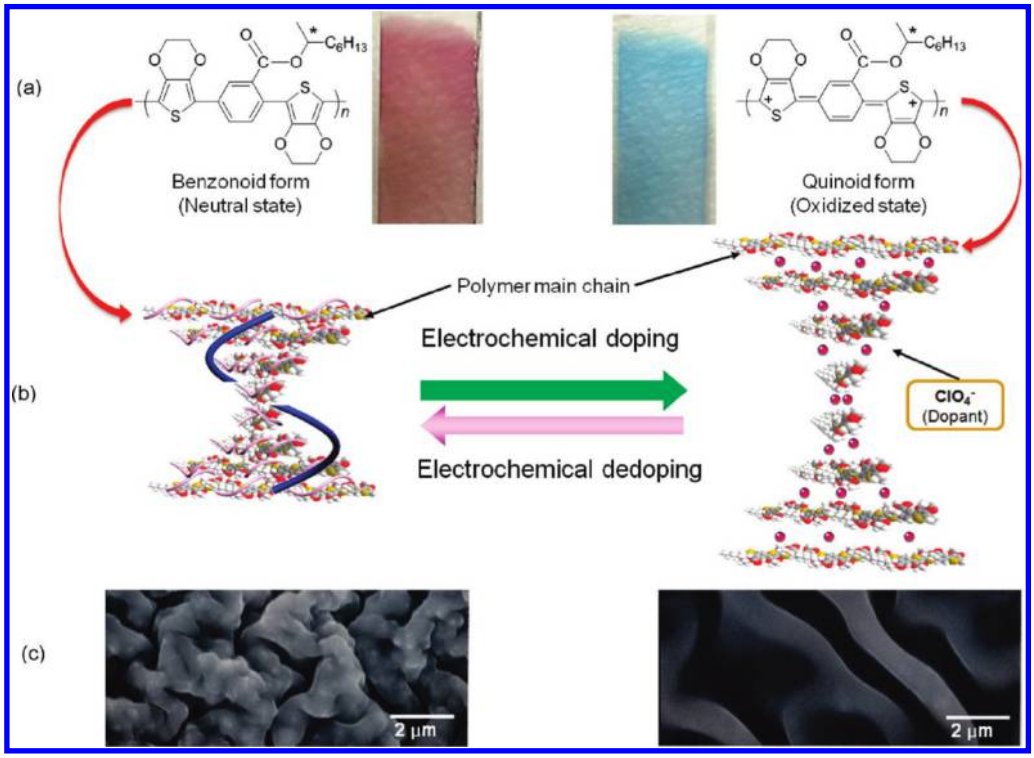

Figure 65. Electrochemical doping and dedoping processes of a chiral polyEDOT derivative, poly**28**-*S* in a TBAP electrolyte system. Changes in (a) electronic structures between neutral and oxidized states and electrochromic color, (b) interchain helical π-stacking structure, and (c) morphology. Reproduced with permission from ref 820. Copyright 2011 American Chemical Society.

DOI: 10.1021/acs.chemrev.7b00482
Chem. Rev. 2018, 118, 4731−4816

Scheme 14. Preparation of Chiral Polythiophene poly29 (*R* or *S*) Using a Liquid Crystal Chiral Electrolyte Containing *R*- or *S*-PCH506-Binol as Chiral Inducer

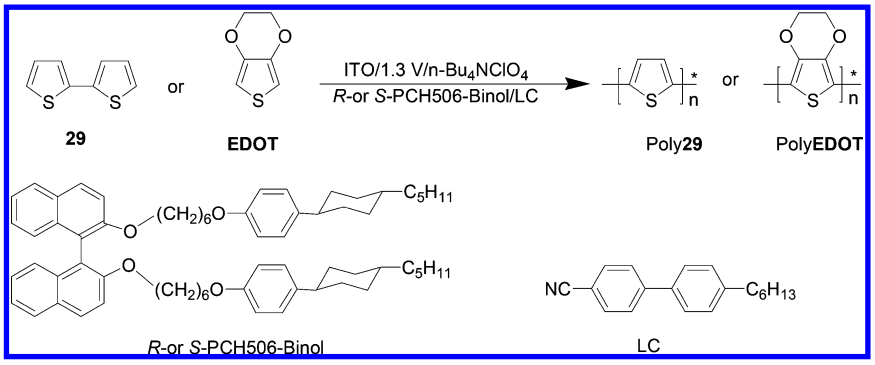

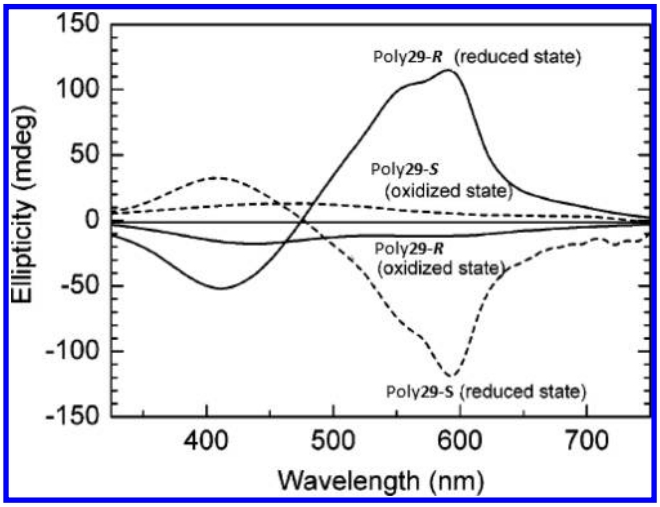

Figure 66. Poly**29**-*R* and poly**29-S** films in oxidized and reduced states. The oxidized and reduced states of the polymer were produced by applications of potential (+1.3 V, oxidized state; 0.1 V, reduced state vs Ag/Ag^{+}) in 0.1 M *n*-Bu_4NClO_4 acetonitrile solution. Reproduced with permission from ref 826. Copyright 2005 American Chemical Society.

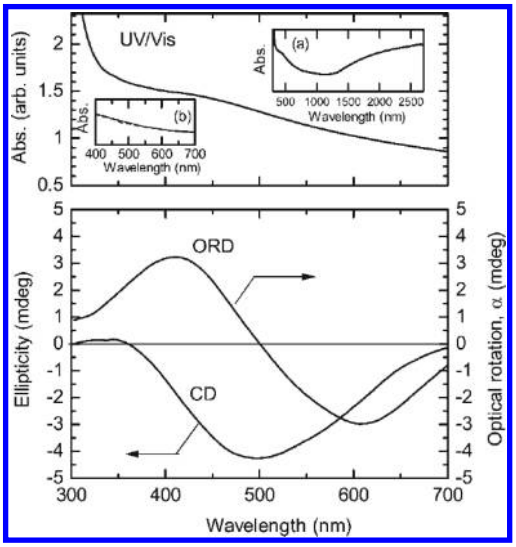

Figure 67. Optical response of chiral PEDOT grown in a DNA (N-LC)*. The ORD spectrum was calculated from the CD spectrum by K−K transformation. Reproduced with permission from ref 831. Copyright 2005, John Wiley and Sons.

Scheme 15. Chiral polyEDOT from DNA as a Chiral Inducer

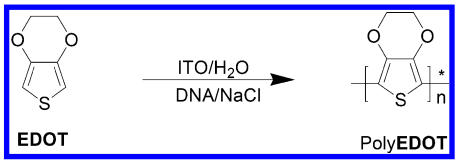

electrochemical stability, and reversible color change between a dark blue for the reduced state and sky blue for the oxidized state (Figure 68C).

Chiral polyEDOT deposited on ITO electrode from the electropolymerization of *ter*-EDOT in the presence of cholesteric liquid crystal (cholesteryl pelargonate) displays a fingerprint surface and a helical molecular arrangement similar to that of cholesteric liquid crystal (CLC) as shown by POM images (Figure 69, left).[834,835] These POM observations were confirmed by the SEM images. Using CLC as chiral inducer, polyEDOT adopts a helical structure produced by transcription from the CLC and aggregates to create fibril surfaces during the electropolymerization process. CD measurements of the polymer films show the presence of the Cotton effect, which is associated with the presence of polarons during the electrochemical oxidation/reduction. ESR signals (Figure 69, right) confirm also the presence of radical resulting from polarons.

Furthermore, Goto and co-workers investigated the structure adopted by the chiral poly**30** during the electropolymerization reaction in the presence of a chiral inducer *R*,*R* or *S*,*S* (Scheme 16) under a magnetic field (4 T).[836]

The electropolymerization of 1,4-di(2-thienyl)benzene, **30**, was carried out in a sandwiched cell with a constant voltage under a magnetic field (**B** = 4 T) to afford either poly**30**-*R* or poly**30**-*S*. Without a magnetic field, POM images reveal that poly**30**-*R* and poly**30**-*S* adopt helical shape of the LC molecules in the identical pathway observed for the electrosynthesis of poly**29** (Figure 70b,d). However, with a 4 T magnetic field, poly**30**-*R* or poly**30**-*S* display strip texture parallel to the applied field (Figure 70e,f).

4.1.4.4. Selected Chiral Polythiophene via Chemical Polymerization. Another method to prepare conjugated materials described in the literature is the chemical oxidation of the parent monomers.[837−839] Using $FeCl_3$ as oxidizing agent, Nilsson and co-workers constructed polythiophenes bearing chiral amino acids (poly**31**), see Scheme 17.[840−842] They stated that the stereochemistry of the side chain does not influence the absorption properties of the polymers.

DOI: 10.1021/acs.chemrev.7b00482
Chem. Rev. 2018, 118, 4731−4816

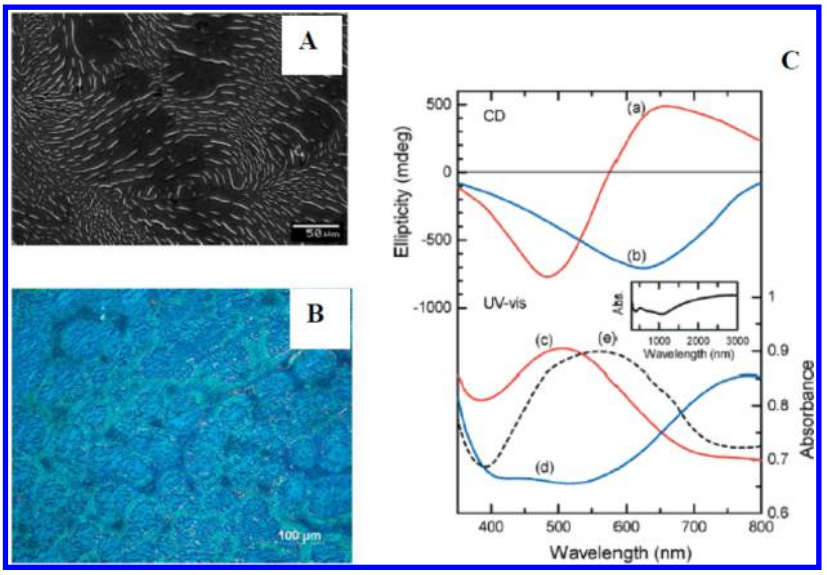

Figure 68. (A) SEM image of polyEDOT*/HPC. (B) Circular differential interference optical image of polyEDOT/HPC. (C) Optical responses of polyEDOT*/HPC. Reproduced with permission from ref 832. Copyright 2006, American Chemical Society.

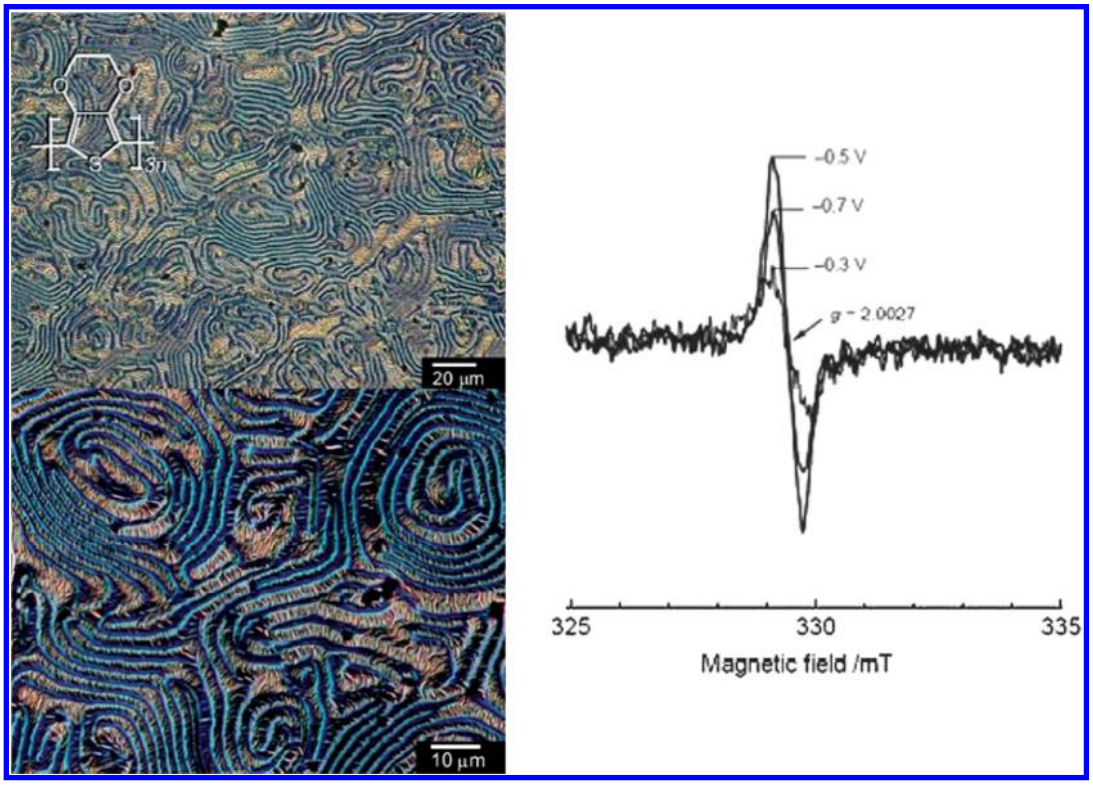

Figure 69. (left) Polarizing optical microscopic (POM) image of chiral polyEDOT* prepared in unoriented cholesteric electrolyte solution at different magnifications. (right) ESR spectra of polyEDOT* at −0.7 V, −0.5 V, and −0.3 V vs Fc/Fc^{+}. Reproduced with permission from ref 835. Copyright 2007, The Royal Society of Chemistry.

(*R*)-(−)-2-(3′-Thienyl)ethyl *N*-(3″,5″-dinitrobenzoyl)-*α*-phenylglycinate and (*S*)-(+)-2-(3′-thienyl)ethyl *N*-(3″,5″-dinitrobenzoyl)-*α*-phenylglycinate are other examples of optically active monothiophenes prepared by reaction of 3-(2′-iodoethyl)thiophene and either (*R*)-(−) or (*S*)-(+)-*N*-(3,5-dinitrobenzoyl)-*α*-phenylglycine in ACN and in the presence of 1,8-bis(dimethylamino)naphthalene as proton sponge (Scheme 18). **32**-*R* and **32**-*S* were obtained with a yield of 51% and 49% and display optical rotation of −76 and +76, respectively.[843]

Chemical oxidation of **32**-*R* and **32**-*S* using $FeCl_3$ offers poly**32**-*R* and poly**32**-*S* with a yield of 60% and 70% postpurification. Both polymers are highly porous and show similar infrared characteristics. The infrared peaks at $\nu(cm^{-1})$ = 1742 and 1652 correspond to the CO present in the ester and amide functionalities, respectively (Figure 71). Moreover, the chirality is maintained for both polymers, and the optical rotation values are −29 for poly**32**-*R* and +28 for poly**32**-*S*, which are surprisingly lower than the ones found for the their parent monomers.

DOI: 10.1021/acs.chemrev.7b00482
Chem. Rev. 2018, 118, 4731−4816

Scheme 16. Electropolymerization of 1,4-Di(2-thienyl)benzene (30) under a Magnetic Field B = 4 T

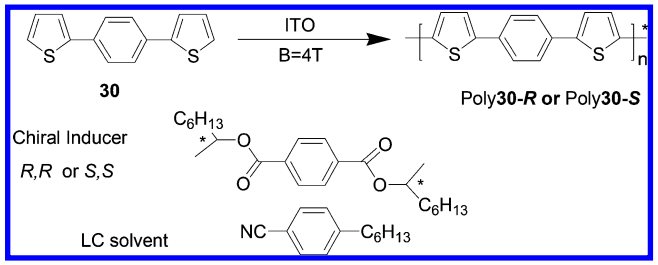

Figure 70. (a) Polarizing optical microscopy (POM) image of (*R*)-CLC electrolyte solution containing the monomer at rt. (b) POM image of poly**30** synthesized in (*R*)-CLC electrolyte solution (poly**30**-*R*). (c) POM image of (*S*)-CLC electrolyte solution containing the monomer at rt. (d) POM image of poly**30** synthesized in (*S*)-CLC electrolyte solution (poly**30**-*S*). (e) POM image of PTBT4T synthesized in (*R*)-CLC electrolyte solution under magnetic field (poly**30**-*R*). (f) POM image of PTBT4T synthesized in (*S*)-CLC electrolyte solution under magnetic field (poly**30**-*S*). Reproduced with permission from ref 836. Copyright 2014 Elsevier.

Scheme 17. Poly31 Molecule

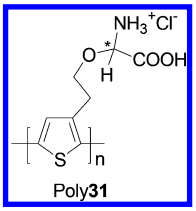

In 2007, Reynolds and co-workers succeeded to incorporate another side chain (2*S*)-ethylhexyl and (2*S*)-methylbutyl on 3,4-propylene dioxythiophene (ProDOT) to form chiral disubstituted ProDOT **33** and **34** by transetherification of the intermediate dialcohols and 3,4-dimethoxythiophene.[844] After dibromination of **33** and **34**, followed by nickel-catalyzed Grignard metathesis polymerization developed by McCullough,[845] chiral poly**33** and poly**34** were synthesized with a yield of 60% and 75%, respectively (Scheme 19). The presence of such chiral substituents increases the solubility of the polymer in organic solvents and can be used to study the aggregation process by CD spectroscopy. The CD spectra of the deposited films present maxima at 501 and 627 nm for poly**33** and at 512 and 637 for poly**34** (Figure 72). These results are similar to the ones found in solution. The chiral polymers poly**33** and poly**34** form helical aggregates similar to chiral alkyl-polythiophene.[846−848] The conductivity of doped spray-coated film with iodine was measured by four-point-method and found to be 0.3 and 4 S/cm for poly**33** and poly**34**, respectively. The band gaps of thin deposited films are 1.98 (poly**32**) and 1.88 eV (poly**34**).

A similar strategy has been followed by Bazan and co-workers to prepare conjugated benzotriazole−thiophene donor−acceptor (D-A) copolymers bearing chiral ethylhexyl side chain.[849] Copolymerization was chosen in order to overcome the poor solubility of the benzotriazole homopolymer, which limits the characterization of its chiral properties in solution. The introduction of chiral side chain ((*S*)-3-bromomethyl)heptane on dibrominated benzotriazole **35** followed by a Stille cross coupling reaction polymerization[850] with bis(Me_3Sn)thiophene in the presence of $Pd(PPh_3)_4$ yields the chiral copolymer poly**36** as depicted in Scheme 20.

The optical property studies of poly**36** show that the UV−vis and CD measurements in dichlorobenzene depend on the temperature. At 25 °C, poly**36** shows an absorption maximum at 572 nm and a second peak at 622 nm. At 110 °C, the peak at 622 nm decreases and was not recovered after cooling for a week (Figure 73a). Moreover, a decrease in CD measurement signals is also observed at 110 °C. However, CD signal is recovered partially after cooling (Figure 73b) suggesting that the aggregation is not fully reversible.

In a related study, two benzothiazole−thiophene conjugated copolymers bearing chiral ethylhexyl side chains, poly**37** and poly**38** (Scheme 21), have been synthesized following similar procedures as those for the synthesis of the copolymer poly**36**.[851] They also found that the optical properties and the aggregation of these donor−acceptor copolymers in solution depend on the temperature.

In poor solvents, the high formation of aggregates in poly**37** enhances the degree of anisotropy, *g*, in comparison to poly**38**. The aggregation is also translated in thin deposited solid film as demonstrated by the CD measurements. However, no CD signal is observed for poly**38** revealing no formation of aggregates in solid thin films explained by the presence of the nitrogen of pyridine that favors the planarity of the backbone polymer.

4.1.4.5. Application of Chiral CPs in Electroanalysis. When a chiral molecule or a bioorganic molecule is attached to the conducting polymer backbone, it is possible to prepare chiral or biological probes activities of which have led to the design of sensors.[852−854] Chiral conducting polymers have shown potential in several applications, including the recognition of bioorganic molecules. For example, luminescent chiral polythiophenes have been used to detect proteins such as insulin.[855] In addition, potentiometric chemosensors based on molecular imprinted polymers (MIP),[657,658] such as functionalized polythiophenes, have been developed to identify cancer biomarkers, for example, neopterin.[856] Using this method, concentrations as low as 0.15 mM of neopterin have been

DOI: 10.1021/acs.chemrev.7b00482
Chem. Rev. 2018, 118, 4731−4816

Scheme 18. Synthetic Route of Poly32-*R* (Poly32-*S*)

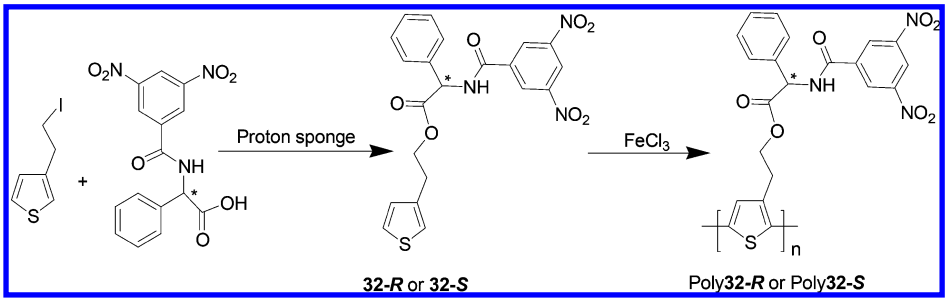

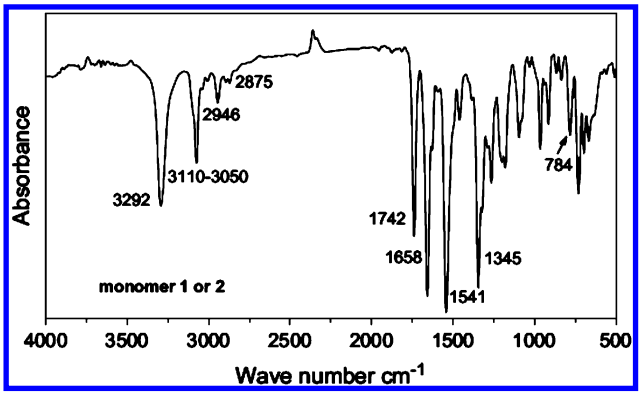

Figure 71. Infrared spectrum of poly**32**-*R* (poly**32**-*S*). Reproduced with permission from ref 843. Copyright 2006, Elsevier.

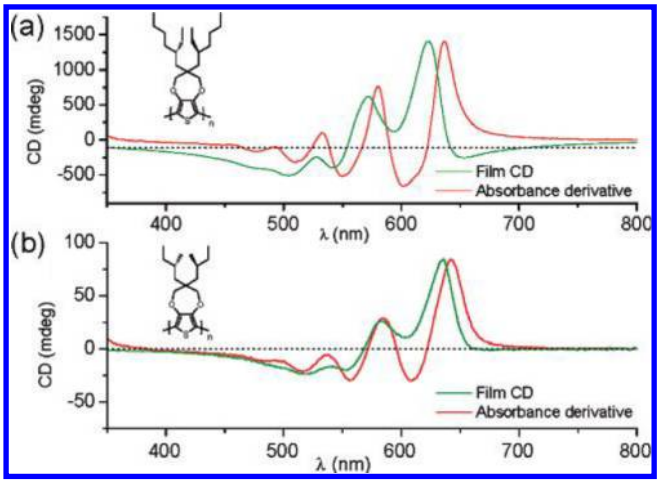

Figure 72. Comparison between CD spectrum and first derivative of the absorption spectrum for of poly**33** (a) and poly**34** (b). Reproduced with permission from ref 844. Copyright 2007 American Chemical Society.

successfully measured in serum samples. Similar, MIPs based on polythiophenes substituted with a fluorophore transducer have also been developed for the detection of explosive and toxic nitroaromatic compounds such as 2,4,6-trinitrophenol (TNP).[857] Other chiral conducting polythiophenes have served as enantioselective chemosensors for the discrimination of alanine and phenylalanine enantiomers.[858,859] The current of the chiral electroactive polymer modified electrode changes in the presence of these target biomolecules, a potential application in biosensors.

A similar strategy has been recently used to discriminate chiral stereoisomers of dihydroxylphenyl alanine (L-DOPA and D-DOPA), and tryptophan.[860,861] The chiral recognition motif was introduced as a side chain on the EDOT molecule; this monomer was then oxidized on a GCE via repeated cyclic voltammetry in the ACN/Bu_4NPF_6 system to form either chiral *R*- or *S*-poly(EDOT). Although *R*- and *S*-poly(EDOT) present similar electrochemical behavior, these chiral conducting polymers display excellent enantioselectivity toward L- and D-DOPA. As observed in cyclic voltammetry (CV), square wave voltammetry (SQV), and differential pulse voltammetry

Scheme 19. Synthesis of Poly33 and Poly34[a]

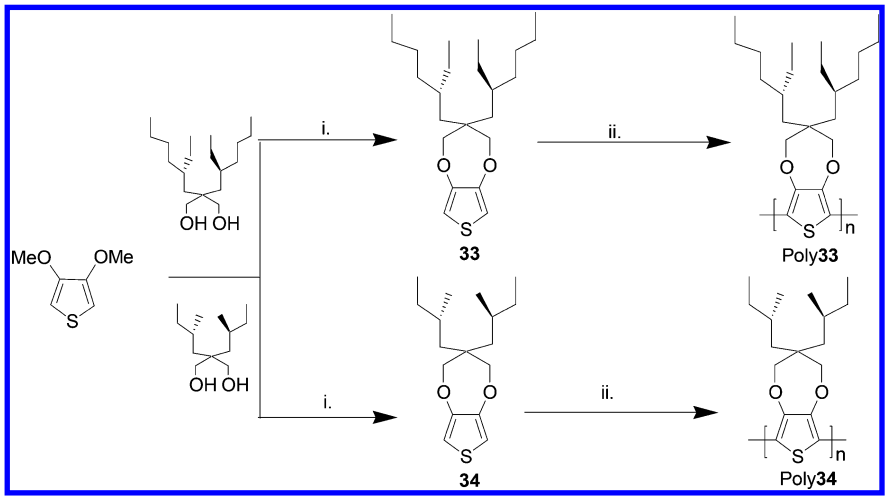

[a]Conditions: (i) pTSA; (ii) NBS, MeMgBr, $Ni(dppp)Cl_2$.

DOI: 10.1021/acs.chemrev.7b00482
Chem. Rev. 2018, 118, 4731−4816

Scheme 20. Synthesis of Poly36

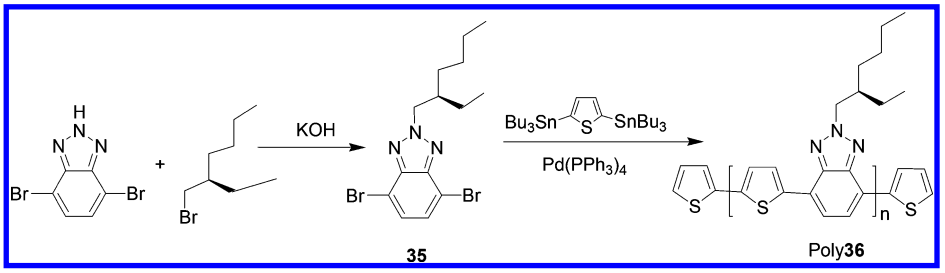

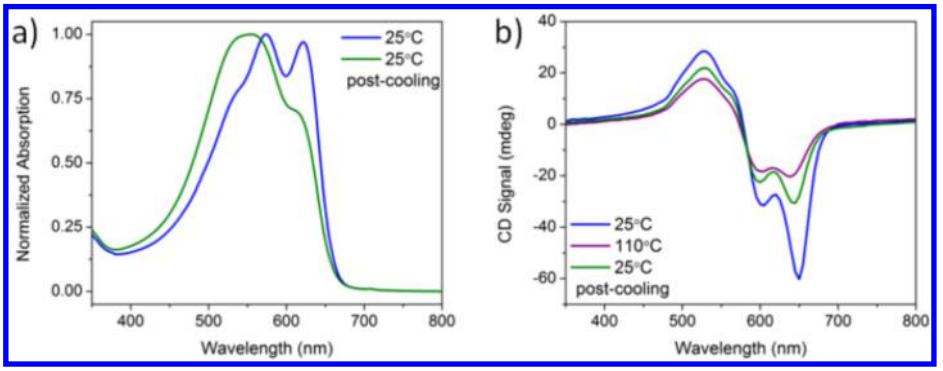

Figure 73. (a) Normalized optical absorption spectra of poly**36** in 0.01 mg mL^{-1} DCB at 25 °C before (blue) and after (green) thermal treatment and (b) CD spectra of poly**36** in 0.01 mg mL^{-1} DCB at 25 °C (blue), 110 °C (purple), and 25 °C 1 week after thermal treatment (green). Reproduced with permission from ref 849. Copyright 2016, American Chemical Society.

Scheme 21. Chemical Structure of Poly37 and Poly38

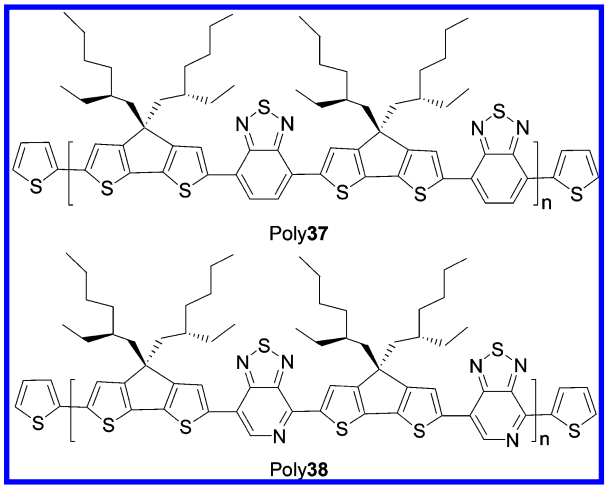

(DPV), the resulting faradaic current from the interaction of *R*-poly(EDOT)/L-DOPA and *S*-poly(EDOT)/D-DOPA is considerably higher in comparison to the resulting faradaic current from *R*-poly(EDOT)/D-DOPA and *S*-poly(EDOT)/L-DOPA interactions. The differences in faradaic current are reasoned to be due to the fact that the right-handed/left-handed or left-handed/right-handed interactions are more favored. Similar observations have been found for the detection of tryptophan[861] and ascorbic acid[862] stereoisomers using similar electrochemical methods.

Furthermore, chiral conducting materials can be also used either as spin filters to improve the efficiency of LED/OLED systems[863] or as electromagnetic protecting materials against electromagnetic pollution.[864] They allow for the injection of selective spin states; as such they can affect the energy consumption of spin-LED and spin-OLED based devices. The spin selectivity was achieved through deposition of a thin layer of chiral conducting polythiophene onto a nickel electrode, which was then magnetized using a permanent magnet in solid state devices. When the magnetic field is up, the resulting cyclic voltammetry (CV) current changes its sign from oxidation to reduction. However, due to the spin filter characteristics of the chiral conducting polythiophene, the sign of the current remains the same when the magnetic field is down. Other chiral conducting materials such as polypyrrole are being tested as electromagnetic protecting materials against electromagnetic pollution.[865]

4.1.5. The Future of CPs in Electroanalysis. From the literature discussed above, it is clear that research on conducting polymers is still growing very quickly, including new synthetic routes, electrode modifications, and material combinations toward high-performance electrodes.[866] The efficient combination of different nanoscale materials with CPs may open new avenues to elaborate enhanced elements for high performance electrochemical sensing platforms.[867] Current developments focus on the possibilities of tailoring their individual and combined 3D structures to produce new improved modified electrodes.[660] In addition, conducting polymer matrix fine-tuning (i.e., main skeleton, reactive or side chains, counterions, and retained solvent) as well as the magnitude of change of the composition-dependent properties[4] like conductivity, volume, color, stored charge, stored ions, ionic diffusivity, and intermolecular forces represent a very important field of research to expand the use of and obtain better analytical performance from these electrochemical sensors. The different CP polymerization methods generate different positions or arrangements of the active sites for interfacial charge transfer, thus providing an interesting way of enhancing interfacial contact between the incorporated materials (e.g., catalysts) and the polymer matrix.[45] A thorough understanding of these properties and their interrelationships

DOI: 10.1021/acs.chemrev.7b00482
Chem. Rev. 2018, 118, 4731−4816

would allow better control of their electrochemical, chemical, and mechanical properties with a consequent beneficial impact on applications, not only in the analytical field but also in other very promising technological areas such as those mentioned in this review.

An additional major advantage of these systems involves the possibility of building miniaturized devices, thus facilitating in situ measurements. Furthermore, the information from such measurements can be obtained in real time[662] and in digital format directly downloadable into computers, which saves laborious work of separate analysis. This considerably reduces processing times and costs and increases the precision and efficiency of the measurements. The electrochemical sensor domain is therefore a multidisciplinary field[868] of rich interaction between different areas like fundamental chemistry, materials, and engineering sciences. Commercial applications require the collaborative work of all these specialists to develop a marketable prototype.

Significant variations are still found for the different sensors depending on their composition and polymerization method.[359] Enhanced electron transfer in the different materials has been claimed as the main reason for this, and therefore properties like charge hopping through the material, or effective charge migration through the polymer are parameters that also require deep study and a better understanding in new CP-based materials. This is important because effective electron transport inside the matrix leads to more efficient electrocatalytic reactions of target analytes.[665] On the other hand, the doping level is also a critical parameter to control since it deeply affects the CPs' electrochemical properties that are associated with the analytical signal used for sensing.[869] Systematic and homogeneous report schedules of these electronic properties in future electrochemical sensor reports would permit a gain in reproducibility among different laboratories. Morphology and roughness values in CPs used as sensors are rarely reported, particularly at the nanometer scale, although the nature of the polymerization method is known to change the ultimate CP structure. These arguments suggest that there is not a "magic recipe" to find the best sensor for a specific application, but the systematic and planned research for optimized experimental parameters during sensor construction are a must.

Chiral conducting materials are attractive bioorganic molecules that can be used as alternatives to biological molecules in sensor devices among other technological applications; therefore, introducing chirality in the polymer backbone is an important topic in this field. Electrochemical methods offer the possibility of preparing modified electrodes with chiral CPs via oxidation of chiral monomers or in a chiral supporting electrolyte/solvent system. In the first approach, the key step to assemble chiral conducting materials is the synthesis of chiral precursors; here although numerous synthetic approaches have been reported, the design of new synthetic methods remains a challenge. The second approach requires chiral conducting polar media to permit the electrochemical reaction to occur; new media like chiral conducting ionic liquids[870] or deep eutectic solvents[871] could be interesting options.

Thus, this section underlines not only the unique physicochemical properties of the components but also their possible synergistic effects, which could lead to numerous electrochemical sensors covering a wide variety of chemical analytes. With current advances in versatile, inexpensive, and reliable techniques for fabricating sensors, CPs will most likely be used as sensory materials to produce the new generation of sensors with commercial applications in a broad range of fields like health care, fitness, and military. Future research may facilitate the development of advanced sensors with applications in the food industry, clinical and point-of-care diagnostics, and the design of biofuel cells.

5. FINAL REMARKS ABOUT CONDUCTING POLYMERS IN THE REVIEWED APPLICATIONS

As have been discussed within this review, catalytic behavior, structural changes, high conductivities, and particular electrochemical and optical properties are among the exceptional attributes of conducting polymers. Additionally, these materials can be economically and conveniently prepared in large scale via chemical or electrochemical approaches. Major advances in material science, in particular, the interesting field of nanoscience and the development of composite compounds, have opened a wide range of possibilities to create and manipulate the morphology and structure of these materials, as well as prepare conducting polymer-based composites with metallic nanoparticles, carbon nanotubes, graphene, and other electrocatalytic compounds incorporated into the structure. Both aspects can increase their performance and give rise to a plethora of possibilities for their use in technological devices. The applications mentioned in this review are just the tip of the iceberg of the vast possibilities for use of conducting polymer based materials in the wide range of promising technological areas. This makes them, for example, one of the future lines of research that will generate new electrocatalysts to increase the performance of known processes or opens the door to the expected flexible organic electronics. Deeper insights into the catalytic mechanisms of the CP-based practical applications like organic and dye-sensitized solar cells, fuel cells, batteries, supercapacitors, photocatalysts, electrochemical water splitting, and environmental applications are required to achieve a full comprehension of the chemistry behind them and propel their use with strong chemical foundations.

A good knowledge of the relationships among polymer components and their bulk properties will permit systematization of their construction. This would open the gate to a vast possibility of applications based on the individual properties of the components and of their mixtures to fine-tune desired properties. Theoretical approaches to predict and explain the properties of pure CPs and their composites also merits exploration with modern computational tools.

Efficient scale-up of the diverse synthetic methods and of stability control are two requirements to achieve large scale applications of conducting polymers. The first one involves optimizing the preparation routes to control the length chain of the polymer, as well as the dispersity and processability of the doping materials with the desired morphology for each application. The second implies that the different monomeric units used in the design of the CPs are by themselves stable enough, so that when bound together the CP preserves its stability. Particularly important is the stability toward water and oxygen to facilitate manipulation in environmental conditions; such factors obviously impact the final price of the desired application.

Fast developments in CP synthesis together with the availability of new techniques for property characterization and the large diversity of monomers that can be used to construct skeletons will permit development of new applications based on CPs with properties adjusted by careful material

DOI: 10.1021/acs.chemrev.7b00482
Chem. Rev. 2018, 118, 4731−4816

selection. The variety of compounds that can be used to dope CPs will also contribute to this objective. Therefore, we believe that these materials will be among those that will facilitate technological change in the near future in diverse chemical industries.

AUTHOR INFORMATION

Corresponding Author

*E-mail: bafrontu@unam.mx.

ORCID

Bernardo A. Frontana-Uribe: 0000-0003-3796-5933

Notes

The authors declare no competing financial interest.

Biographies

Jorge G. Ibanez is a Chemistry and Chemical Engineering professor at Universidad Iberoamericana in Mexico City since 1985. He received a B.Sc. in Chemical Engineering at ITESO (Mexico) and a Ph.D. in Physical Chemistry at the University of Houston (USA). A visiting faculty in countries of five continents, he has received numerous awards and coauthored books on environmental electrochemistry, environmental chemistry, and microscale laboratory experiments, as well as papers and extensive reviews in the general areas of electrochemical remediation, conducting polymers, green electrochemistry, chemical education, and science education for the blind.

Marina E. Rincón is a Senior Researcher at Instituto de Energías Renovables (Renewable Energy Institute) of Universidad Nacional Autónoma de México (UNAM). She has a Ph.D. in Chemistry from the University of California (Santa Barbara) USA and rounded professional experience in academia and industry. She is a Professor in engineering, materials science, and physical chemistry. Her research interests include electrochemical and photoelectrochemical energy conversion and storage, synthesis and characterization of composites based on inorganic and organic semiconductors, and large area metal oxide matrices and low-dimensional nanocarbon materials for energy and environmental applications.

Silvia Gutiérrez Granados is a Chemistry professor at University of Guanajuato (Mexico). She received a B.Sc. and M.Sci. degree in Chemistry at University of Guanajuato and a DEA in Analytical Chemistry and a Ph.D. in Chemistry at the University Pierre and Marie Curie (Université Paris VI) in France. She is a Professor in analytical chemistry, electrochemistry, and electroanalysis. Her recent interests include modified electrodes, electroanalysis, electrochemical sensors, and conducting polymer studies in several applications.

M'hamed Chahma originally from Agadir (Morocco), earned his B.Sc. in Chemistry at Ibn Zohr University. He obtained his Diplome d'Etudes Approfondies (DEA) and his Ph.D. degree in Electrochemistry from Paris Diderot University (Paris 7, France). He was a Postdoctoral Fellow at Virginia Polytechnic Institute and State University (Blacksburg, Virginia) and associated researcher in several Canadian institutions. He joined the department of Chemistry and Biochemistry at Laurentian University (Sudbury, Canada) in 2006, where he has been professor of chemistry since 2013. His research interests lie between physical organic chemistry and surface modifications using conducting polymers.

Oscar A. Jaramillo Quintero received his Ph.D. in Materials Science and Engineering from UNAM in 2016. He joined Instituto de Energías Renovables (Renewable Energy Institute) of UNAM as Catedrático CONACYT-IER since 2017. His research is focused on the nanomaterial synthesis of semiconductor oxides and carbon nanostructures for development and fabrication of electrochemical energy conversion and storage devices, as well as the study of interfacial phenomena in emerging photovoltaics.

Bernardo A. Frontana-Uribe obtained his B.Sc. in Chemistry and M.Sc. degree in Organic Chemistry at the National Autonomous University of Mexico (UNAM). Lately, he got his Ph.D degree in Chemical Sciences in 1999 at the University of Rennes I, France, working on the electrosynthesis of nitrogenated heterocycles. He carried out research investigations at the University of California (Santa Barbara, USA) and University of Freiburg, Germany, where he carried out investigations about conducting polymers. He has been invited professor at the Iberoamerican University and the Institute of Organic Chemistry in Mainz, Germany. He is currently Research Professor at the Institute of Chemistry (UNAM) and the head of the "Electrochemistry and Electrosynthesis Laboratory" at the Center of Sustainable Chemistry UAEM-UNAM in Mexico. During the last years, his research interests have been focused on electrosynthesis, electrochemical transformations of natural products, electrocatalytic properties of conducting polymer electrodes, conducting polymers in organic solar cells, electrochemical water decontamination, and electroassisted crystallization of proteins.

ACKNOWLEDGMENTS

Support from CONACYT-México (Projects 245754, 279953, 270810, and 179356) and UNAM-PAPIIT IN103015 and IN202011) is recognized. O.A.J.-Q thanks CONACYT-México for Postdoctoral fellowship. Hortensia Segura Silva and Citlalit Martinez are recognized for the technical work carried out during the manuscript preparation. B.A.F.-U. thanks PASPA-DGAPA UNAM and CONACYT-Mexico (472389) for the sabbatical year support.

REFERENCES

(1) Hall, N. Twenty-five Years of Conducting Polymers. *Chem. Commun.* **2003**, 1−4.

(2) Swager, T. 50th Anniversary Perspective: Conducting/Semiconducting Conjugated Polymers. A Personal Perspective on the Past and the Future. *Macromolecules* **2017**, *50*, 4867−4886.

(3) Skotheim, T. A.; Reynolds, J., Eds. *Handbook of Conducting Polymers*, 3rd ed.; CRC Press, Boca Raton, FL, USA, 2007.

(4) Otero, T. F.; Martinez, J. G. Electro-chemo-biomimetics from Conducting Polymers: Fundamentals, Materials, Properties and Devices. *J. Mater. Chem. B* **2016**, *4*, 2069−2085.

(5) Heeger, A. Semiconducting Polymers: The Third Generation. *Chem. Soc. Rev.* **2010**, *39*, 2354−2371.

(6) Kularatne, R.; Magurudeniya, H.; Sista, P.; Biewer, M.; Stefan, M. Donor-acceptor Semiconducting Polymers for Organic Solar Cells. *J. Polym. Sci., Part A: Polym. Chem.* **2013**, *51*, 743−768.

(7) Gangopadhyay, P.; Koeckelberghs, G.; Persoons, A. Magneto-optic Properties of Regioregular Polyalkylthiophenes. *Chem. Mater.* **2011**, *23*, 516−521.

(8) Kirova, N.; Brazovskii, S. Electronic Ferroelectricity in Carbon Based Materials. *Synth. Met.* **2016**, *216*, 11−22.

(9) Lim, C.; Cho, M.; Singh, A.; Li, Q.; Kim, W.; Jee, H.; Fillman, K.; Carpenter, S.; Neidig, M. L.; Baev, A.; Swihart, M. T.; Prasad, P. N. Manipulating Magneto-Optic Properties of a Chiral Polymer by Doping with Stable Organic Biradicals. *Nano Lett.* **2016**, *16*, 5451−5455.

(10) Ye, S.; Lu, Y.; Sergey, E. Polypyrrole and Inorganics: Conducting Nanocomposites. In *Dekker Encyclopedia of Nanoscience and Nanotechnology*; Lyshevski, S. E., Ed.; CRC Press: Boca Raton, FL, 2014; pp 3859−3873.

(11) Bobade, R. Polythiophene Composites: A Review of Selected Applications. *J. Polym. Eng.* **2011**, *31*, 209−215.

DOI: 10.1021/acs.chemrev.7b00482
Chem. Rev. 2018, 118, 4731−4816

(12) Wang, L.; Lu, X.; Lei, S.; Song, Y. Graphene-based Polyaniline Nanocomposites: Preparation, Properties and Applications. *J. Mater. Chem. A* **2014**, *2*, 4491−4509.
(13) Meer, S.; Kausar, A.; Iqbal, T. Trends in Conducting Polymer and Hybrids of Conducting Polymer/Carbon Nanotube: A Review. *Polym.-Plast. Technol. Eng.* **2016**, *55*, 1416−1440.
(14) Li, Z.; Zheng, L. P3HT−MWNT Nanocomposites by In-situ Polymerization and Their Properties. In *In-Situ Synthesis of Polymer Nanocomposites*; Mittal, V., Ed.; Wiley-VCH: Weinheim, Germany, 2011; pp 303−329.
(15) Do Nascimento, G. M. Conducting Polymers, Synthesis, Characterization and Applications of Conducting Polymer-clay Nanocomposites. In *Conducting Polymers: Synthesis, Characterization and Applications*, Pimentel-Almeida, L. C., Ed.; Nova Science Publishers: Hauppauge, NY, 2013; pp 155−177.
(16) Jaymand, M. Conductive Polymers/Zeolite (Nano) Composites: Under-exploited Materials. *RSC Adv.* **2014**, *4*, 33935−33954.
(17) García-González, N.; Frontana-Uribe, B. A.; Ordoñez-Regil, E.; Cárdenas, J.; Morales-Serna, J. Evaluation of Fe3+ Fixation into Montmorillonite Clay and its Application in the Polymerization of Ethylenedioxythiophene. *RSC Adv.* **2016**, *6*, 95879−95887.
(18) Aneli, J.; Zaikov, G.; Mukbaniani, O.; Sirghie, C.; Lobo, V.; Islam, R. Physical Principles of the Conductivity of Electrical Conducting Polymer Composites: Review. In *Polymers, Composites and Nanocomposites. Polymer Yearbook − 2011*, Zaikov, G. E., Sirghie, C., Kozlowski, R. M., Eds.; Nova Science Publishers: Hauppauge, NY, 2011; pp 65−88.
(19) Heinze, J.; Frontana-Uribe, B. A.; Ludwigs, S. Electrochemistry of Conducting Polymers Persistent Models and New Concepts. *Chem. Rev.* **2010**, *110*, 4724−4771.
(20) Freund, M.; Deore, B. *Self-Doped Conducting Polymers*; Wiley: Chichester, 2007.
(21) Malinauskas, A. Self-doped Polyanilines. *J. Power Sources* **2004**, *126*, 214−220.
(22) Volkov, A.; Singh, S.; Stavrinidou, E.; Gabrielsson, R.; Franco-Gonzalez, J.; Cruce, A.; Chen, W.; Simon, D.; Berggren, M.; Zozoulenko, I. Spectroelectrochemistry and Nature of Charge Carriers in Self-Doped Conducting Polymer. *Adv. Electron. Mater.* **2017**, *3*, 1700096.
(23) Patil, A.; Ikenoue, Y.; Wudl, F.; Heeger, A. Water Soluble Conducting Polymers. *J. Am. Chem. Soc.* **1987**, *109*, 1858−1859.
(24) Bäuerle, P.; Gaudl, K.; Würthner, F.; Sariciftci, N.; Mehring, M.; Neugebauer, H.; Zhong, C.; Doblhofer, K. Synthesis and Properties of Carboxy-functionalized Poly(3-alkylthienylenes). *Adv. Mater.* **1990**, *2*, 490−494.
(25) Tang, C.; Ang, M.; Choo, K.; Keerthi, V.; Tan, J.; Syafiqah, M.; Kugler, T.; Burroughes, J.; Png, R.; Chua, L.; Ho, P. Doped Polymer Semiconductors with Ultrahigh and Ultralow Work Functions for Ohmic Contacts. *Nature* **2016**, *539*, 536−540.
(26) Mai, C.; Schlitz, R.; Su, G.; Spitzer, D.; Wang, X.; Fronk, S.; Cahill, D.; Chabinyc, M.; Bazan, G. Side-Chain Effects on the Conductivity, Morphology, and Thermoelectric Properties of Self-Doped Narrow-Band-Gap Conjugated Polyelectrolytes. *J. Am. Chem. Soc.* **2014**, *136*, 13478−13481.
(27) Lee, J.; Kang, H.; Kee, S.; Lee, S. H.; Jeong, S. Y.; Kim, G.; Kim, J.; Hong, S.; Back, H.; Lee, K. Long-Term Stable Recombination Layer for Tandem Polymer Solar Cells Using Self-Doped Conducting Polymers. *ACS Appl. Mater. Interfaces* **2016**, *8*, 6144−6151.
(28) Cui, Y.; Yao, H.; Gao, B.; Qin, Y.; Zhang, S.; Yang, B.; He, C.; Xu, B.; Hou, J. Fine-Tuned Photoactive and Interconnection Layers for Achieving over 13% Efficiency in a Fullerene-Free Tandem Organic Solar Cell. *J. Am. Chem. Soc.* **2017**, *139*, 7302−7309.
(29) Subbiah, J.; Mitchell, V. D.; Hui, N. K. C.; Jones, D. J.; Wong, W. W. H. A Green Route to Conjugated Polyelectrolyte Interlayers for High-Performance Solar Cells. *Angew. Chem., Int. Ed.* **2017**, *56*, 8431−8434.
(30) Lim, K.; Ahn, S.; Kim, H.; Choi, M.; Huh, D.; Lee, T. Self-Doped Conducting Polymer as a Hole-Extraction Layer in Organic-Inorganic Hybrid Perovskite Solar Cells. *Adv. Mater. Interfaces* **2016**, *3*, 1500678.
(31) Goncalves, R.; Christinelli, W.; Trench, A.; Cuesta, A.; Pereira, E. Properties Improvement of Poly(o-methoxyaniline) Based Supercapacitors: Experimental and Theoretical Behavior Study of Self-doping Effect. *Electrochim. Acta* **2017**, *228*, 57−65.
(32) Liu, Y.; Duzhko, V. V.; Page, Z. A.; Emrick, T.; Russell, T. P. Conjugated Polymer Zwitterions: Efficient Interlayer Materials in Organic Electronics. *Acc. Chem. Res.* **2016**, *49*, 2478−2488.
(33) Miranda, P.; dos Reis, L.; Taylor, J. Current Synthetic Methodologies for Semiconducting Polymers. In *Conducting Polymers: Synthesis, Properties, and Applications*; Pimentel, L. C., Ed.; Nova Science Publishers: Hauppauge, NY, 2013; Chapter 1, pp 1−25.
(34) Higashihara, T.; Goto, E. Controlled Synthesis of Low-polydisperse Regioregular Poly(3-hexylthiophene) and Related Materials by Zincate-complex Metathesis Polymerization. *Polym. J.* **2014**, *46*, 381−390.
(35) Higashimura, H.; Kobayashi, S. Oxidative Polymerization. *Encyclopedia of Polymer Science and Technology*, 4th ed.; Wiley: New York, 2016; pp 1−37.
(36) Park, T.-J.; Lee, S. H. Deep Eutectic Solvent Systems for $FeCl_3$-catalyzed Oxidative Polymerization of 3-Octylthiophene. *Green Chem.* **2017**, *19*, 910−913.
(37) Lawal, A.; Wallace, G. Vapour Phase Polymerisation of Conducting and Non-conducting Polymers: A Review. *Talanta* **2014**, *119*, 133−143.
(38) Wang, M.; Wang, X.; Moni, P.; Liu, A.; Kim, D. H.; Jo, W. J.; Sojoudi, H.; Gleason, K. K. CVD Polymers for Devices and Device Fabrication. *Adv. Mater.* **2017**, *29*, 1604606.
(39) Atobe, M. Structure Control Synthesis of Polyaniline Materials Using Electrochemical and Chemical Polymerizations in Unique Reaction Fields and Media. In *Trends in Polyaniline Research*, Chowdhury, A., Ohsaka, T., Rahman, A., Islam, M., Eds.; Nova Science Publishers: Hauppauge, NY, 2013; Chapter 4, pp 81−94.
(40) Lee, J.; Kalin, J.; Yuan, T.; Al-Hashimi, M.; Fang, L. Fully Conjugated Ladder Polymers. *Chem. Sci.* **2017**, *8*, 2503−2521.
(41) Martin, D.; Wu, J.; Shaw, C.; King, Z.; Spanninga, S.; Richardson-Burns, S.; Hendricks, J.; Yang, J. The Morphology of Poly(3,4-Ethylenedioxythiophene). *Polym. Rev.* **2010**, *50*, 340−384.
(42) Livi, F.; Carle, J. E.; Bundgaard, E. Thiophene in Conducting Polymers: Synthesis of Poly(thiophene)s and Other Conjugated Polymers Containing Thiophenes, for Application in Polymer Solar Cells. *Top. Heterocycl. Chem.* **2014**, *39*, 203−226.
(43) Chujo, Y., Ed. *Conjugated Polymer Synthesis: Methods and Reactions*; Wiley-VCH: Weinheim, Germany, 2010.
(44) Almeida, L. C., Ed. *Conducting Polymers: Synthesis, Properties and Applications*; Nova Science Publishers: Hauppauge, NY, 2013.
(45) Otero, T. F. *Conducting Polymers: Bioinspired Intelligent Materials and Devices*; Royal Society of Chemistry: London, 2016.
(46) Diaz, A. F.; Kanazawa, K. K.; Gardini, G. P. Electrochemical Polymerization of Pyrrole. *J. Chem. Soc., Chem. Commun.* **1979**, *14*, 635−636.
(47) Sarac, A. Electropolymerization. In *Encyclopedia of Polymer Science and Technology*, 4th ed., Herman, F., Ed.; Wiley: New York, 2014; Vol. *5*, pp 118−144.
(48) Wu, Y.; Zhang, F.; Chen, Q.; Gong, S.; Du, C. Research on Electrochemical Polymerization of Conductive Heteroaromatic Polymers. *Adv. Mater. Res.* **2014**, *900*, 352−356.
(49) Cosnier, S., Karyakin, A., Eds. *Electropolymerization*; Wiley-VCH: Weinheim, Germany, 2010.
(50) Li, H.; Zhang, X. Electropolymerization at Metal Surfaces. In *Encyclopedia of Surface and Colloid Science*, 3rd. ed.; Somasundaran, P., Ed.; CRC Press: Boca Raton, FL, 2016; Vol. *4*, pp 2460−2476.
(51) Inzelt, G. *Conducting Polymers: A New Era in Electrochemistry*; Springer Science & Business Media, 2012.
(52) Genies, E. M.; Bidan, G.; Diaz, A. F. Spectroelectrochemical Study of Polypyrrole Films. *J. Electroanal. Chem. Interfacial Electrochem.* **1983**, *149*, 101−113.

DOI: 10.1021/acs.chemrev.7b00482
Chem. Rev. 2018, 118, 4731−4816

(53) Andrieux, C. P.; Audebert, P.; Hapiot, P.; Savéant, J.-M. Observation of the Cation Radicals of Pyrrole and of some Substituted Pyrroles in Fast-scan Cyclic Voltammetry. Standard Potentials and Lifetimes. *J. Am. Chem. Soc.* **1990**, *112*, 2439−2440.
(54) Audebert, P.; Hapiot, P. Existence of π-Dimers in Solution. *Synth. Met.* **1995**, *75*, 95−102.
(55) Smie, A.; Synowczyk, A.; Heinze, J.; Alle, R.; Tschuncky, P.; Götz, G.; Bäuerle, P. β,β-Disubstituted Oligothiophenes, a New Oligomeric Approach Towards the Synthesis of Conducting Polymers. *J. Electroanal. Chem.* **1998**, *452*, 87−95.
(56) Ruiz, V.; Colina, A.; Heras, A.; Lopez-Palacios, J.; Seeber, R. Bidimensional Spectroelectrochemistry Applied to the Electrosynthesis and Characterization of Conducting Polymers: Study of Poly[4,4′-bis(butylthio)-2,2′-bithiophene]. *Helv. Chim. Acta* **2001**, *84*, 3628−3642.
(57) Raymond, D. E.; Harrison, D. J. Observation of Pyrrole Radical Cations as Transient Intermediates during the Anodic Formation of Conducting Polypyrrole Films. *J. Electroanal. Chem.* **1993**, *361*, 65−76.
(58) Downard, A. J.; Pletcher, D. A Study of the Conditions for the Electrodeposition of Polythiophen in Acetonitrile. *J. Electroanal. Chem. Interfacial Electrochem.* **1986**, *206*, 147−152.
(59) Asavapiriyanont, S.; Chandler, G. K.; Gunawardena, G. A.; Pletcher, D. The Electrodeposition of Polypyrrole Films from Aqueous Solutions. *J. Electroanal. Chem. Interfacial Electrochem.* **1984**, *177*, 229−244.
(60) Randriamahazaka, H.; Sini, G.; Tran Van, F. Electrodeposition Mechanisms and Electrochemical Behavior of Poly(3,4-ethylenedithiathiophene). *J. Phys. Chem. C* **2007**, *111*, 4553−4560.
(61) Villareal, I.; Morales, E.; Acosta, J. L. Nucleation and Growth of $LiCF_3SO_3$-doped Polyalkylthiophene. *Polymer* **2001**, *42*, 3779−3789.
(62) del Valle, M. A.; Cury, P.; Schrebler, R. Solvent Effect on the Nucleation and Growth Mechanisms of Poly(thiophene). *Electrochim. Acta* **2002**, *48*, 397−405.
(63) Bade, K.; Tsakova, V.; Schultze, J. W. Nucleation, Growth and Branching of Polyaniline from Microelectrode Experiments. *Electrochim. Acta* **1992**, *37*, 2255−2261.
(64) Hwang, B. J.; Santhanam, R.; Wu, C. R.; Tsai, Y. W. A Combined Computational/Experimental Study on LiNi1/3Co1/3Mn1/3O2. *J. Solid State Electrochem.* **2003**, *7*, 678−683.
(65) Obretenov, W.; Schmidt, U.; Lorenz, W. J.; Staikov, G.; Budevski, E.; Carnal, D.; Müller, U.; Siegenthaler, H.; Schmidt, E. Underpotential Deposition and Electrocrystallization of Metals. An Atomic View by Scanning Tunneling Microscopy. *J. Electrochem. Soc.* **1993**, *140*, 692−703.
(66) Andrieux, C. P.; Hapiot, P.; Audebert, P.; Guyard, L.; Dinh An, M. N.; Groenendaal, L.; Meijer, E. W. Substituent Effects on the Electrochemical Properties of Pyrroles and Small Oligopyrroles. *Chem. Mater.* **1997**, *9*, 723−729.
(67) Audebert, P.; Catel, J.-M.; Le Coustumer, G.; Duchenet, V.; Hapiot, P. Electrochemistry and Polymerization Mechanisms of Thiophene−Pyrrole−Thiophene Oligomers and Terthiophenes. Experimental and Theoretical Modeling Studies. *J. Phys. Chem. B* **1998**, *102*, 8661−8669.
(68) Bof-Bufon, C. C.; Vollmer, J.; Heinzel, T.; Espindola, P.; John, H.; Heinze, J. Relationship between Chain Length, Disorder, and Resistivity in Polypyrrole Films. *J. Phys. Chem. B* **2005**, *109*, 19191−19199.
(69) Meerholz, K.; Heinze, J. Influence of Chain Length and Defects on the Electrical Conductivity of Conducting Polymers. *Synth. Met.* **1993**, *57*, 5040−5045.
(70) Lukkari, J.; Alanko, M.; Pitkänen, V.; Kleemola, K.; Kankare, J. Photocurrent Spectroscopic Study of the Initiation and Growth of Poly(3-methylthiophene) Films on Electrode Surfaces with Different Adsorption Properties. *J. Phys. Chem.* **1994**, *98*, 8525−8535.
(71) Heinze, J.; Tschuncky, P. Electrochemical Properties. In *Electronic Materials: The Oligomer Approach*; Müllen, K., Wegner, G., Eds.; VCH-Wiley: Weinheim, Germany, 1998; Chapter 9, pp 479−514.
(72) Meerholz, K.; Gregorius, H.; Müllen, K.; Heinze, J. Voltammetric Studies of Solution and Solid-state Properties of Monodisperse Oligo(*p*-phenylenevinylene)s. *Adv. Mater.* **1994**, *6*, 671−677.
(73) Otero, T. F. Biomimetic Conducting Polymers: Synthesis, Materials, Properties, Functions, and Devices. *Polym. Rev.* **2013**, *53*, 311−351.
(74) Miomandre, F.; Audebert, P. Basics and new insights in the electrochemistry of conducting polymers. In *Conducting Polymers: Synthesis, characterization and applications*; Pimentel Almeida, L. C., Ed.; Nova Science Publishers, Inc.: Hauppauge, NY, 2013; pp 53−89.
(75) Hillman, A. R.; Daisley, S. J.; Bruckenstein, S. Ion and Solvent Transfers and Trapping Phenomena During n-Doping of PEDOT Films. *Electrochim. Acta* **2008**, *53*, 3763−3771.
(76) Heinze, J.; Dietrich, M. Cyclic Voltammetry as a Tool for Characterizing Conducting Polymers. *Mater. Sci. Forum* **1989**, *42*, 63−78.
(77) Patra, A.; Bendikov, M.; Chand, S. Poly(3,4-ethylenedioxyselenophene) and Its Derivatives: Novel Organic Electronic Materials. *Acc. Chem. Res.* **2014**, *47*, 1465−1474.
(78) Smela, E.; Gadegaard, N. Surprising Volume Change in PPy(DBS): An Atomic Force Microscopy Study. *Adv. Mater.* **1999**, *11*, 953−957.
(79) Hubbard, A. T.; Anson, F. C. In *Electroanalytical Chemistry*; Bard, A. J., Ed.; Marcel Dekker: New York, 1970; Vol. *4*, pp 129−214.
(80) Shimotani, H.; Diguet, G.; Iwasa, Y. Direct Comparison of Field-effect and Electrochemical Doping in Regioregular Poly(3-hexylthiophene). *Appl. Phys. Lett.* **2005**, *86*, 022104.
(81) Bose, C. S. C.; Basak, S.; Rajeshwar, K. Electrochemistry of Poly-(pyrrole chloride) Films: A Study of Polymerization Efficiency, Ion Transport during Redox and Doping Level Assay by Electrochemical Quartz Crystal Microgravimetry, pH, and Ion-selective Electrode Measurements. *J. Phys. Chem.* **1992**, *96*, 9899−9906.
(82) Harima, Y.; Kunugi, Y.; Yamashita, K.; Shiotani, M. Determination of Mobilities of Charge Carriers in Electrochemically Anion-doped Polythiophene Film. *Chem. Phys. Lett.* **2000**, *317*, 310−314.
(83) Tang, H.; Zhu, L.; Harima, Y.; Yamashita, K. Chronocoulometric Determination of Doping Levels of Polythiophenes: Influences of Overoxidation and Capacitive Processes. *Synth. Met.* **2000**, *110*, 105−113.
(84) Harima, Y.; Eguchi, T.; Yamashita, K. Enhancement of Carrier Mobilities in Poly(3-methylthiophene) Electrochemical Doping. *Synth. Met.* **1998**, *95*, 69−74.
(85) Tóth, P. S.; Endrodi, B.; Janáky, C.; Visy, C. Development of Polymer−dopant Interactions During Electropolymerization, a Key Factor in Determining the Redox Behaviour of Conducting Polymers. *J. Solid State Electrochem.* **2015**, *19*, 2891−2896.
(86) Krische, B.; Zagorska, M. Overoxidation in Conducting Polymers. *Synth. Met.* **1989**, *28*, 257−262.
(87) Deore, B.; Chen, Z.; Nagaoka, T. Potential-induced Enantioselective Uptake of Amino Acid into Molecularly Imprinted Overoxidized Polypyrrole. *Anal. Chem.* **2000**, *72*, 3989−3994.
(88) Damlin, P.; Kvarnström, C.; Petr, A.; Ek, P.; Dunsch, L.; Ivaska, A. In Situ Resonant Raman and ESR Spectroelectrochemical Study of Electrochemically Synthesized Poly(*p*-phenylenevinylene). *J. Solid State Electrochem.* **2002**, *6*, 291−301.
(89) Meana-Esteban, B.; Petr, A.; Kvarnström, C.; Ivaska, A.; Dunsch, L. Poly(2-methoxynaphthalene): A Spectroelectrochemical Study on a Fused Ring Conducting Polymer. *Electrochim. Acta* **2014**, *115*, 10−15.
(90) Holstein, T. Studies of Polaron Motion: Part I. The Molecular-crystal Model. *Ann. Phys.* **1959**, *8*, 325−342.
(91) Brédas, J.; Chance, R.; Silbey, R. Comparative Theoretical Study of the Doping of Conjugated Polymers: Polarons in Polyacetylene and Polyparaphenylene. *Phys. Rev. B: Condens. Matter Mater. Phys.* **1982**, *26*, 5843−5854.
(92) Brédas, J.; Street, G. Polarons, Bipolarons, and Solitons in Conducting Polymers. *Acc. Chem. Res.* **1985**, *18*, 309−315.

DOI: 10.1021/acs.chemrev.7b00482
Chem. Rev. 2018, 118, 4731−4816

(93) Wei, D.; Petr, A.; Kvarnström, C.; Dunsch, L.; Ivaska, A. Charge Carrier Transport and Optical Properties of Poly[N-methyl(aniline)]. *J. Phys. Chem. C* **2007**, *111*, 16571−16576.
(94) Brédas, J.; Marder, S.; André, J. An Introduction to the Electronic Structure of π-Conjugated Molecules and Polymers, and to the Concept of Electronic Bands. In *The WSPC Reference on Organic Electronics: Organic Semiconductors*; Brédas, J., Marder, S., Eds.; World Scientific Publishing Company: Hackensack, NJ, 2016; Vol. *1*, pp 1−18.
(95) Fesser, K.; Bishop, A.; Campbell, D. Optical Absorption from Polarons in a Model of Polyacetylene. *Phys. Rev. B: Condens. Matter Mater. Phys.* **1983**, *27*, 4804−4825.
(96) Brédas, J. L.; Scott, J. C.; Yakushi, K.; Street, G. B. Polarons and Bipolarons in Polypyrrole: Evolution of the Band Structure and Optical Spectrum upon Doping. *Phys. Rev. B: Condens. Matter Mater. Phys.* **1984**, *30*, 1023−1025.
(97) Malgorzata, Z.; Adam, P.; Serge, L. Spectroelectrochemistry and Spectroscopy of Conducting Polymers. In *Handbook of Organic Conductive Molecules and Polymers*; Hari, S. N., Ed.; Wiley: Susex, England, 1997; pp 183−218.
(98) Xia, Y.; Ouyang, J. Transparent Conducting Polymers. In *Organic Optoelectronic Materials. Lecture Notes in Chemistry*; Li, Y., Ed.; Springer International: Germany, 2015; pp 359−392.
(99) Heinze, J. Electrochemistry of Conducting Polymers Persistent Models, New Concepts. PDF file of presentation at the Institute of Chemistry-UNAM, 2007.
(100) Chance, R. R.; Brédas, J. L.; Silbey, R. Bipolaron Transport in Doped Conjugated Polymers. *Phys. Rev. B: Condens. Matter Mater. Phys.* **1984**, *29*, 4491−4495.
(101) Chance, R. R.; Boudreaux, D. S.; Brédas, J. L.; Silbey, R. In *Handbook of Conducting Polymers*; Skotheim, T. A., Ed.; Marcel Dekker: New York, 1986; p 825.
(102) Baranovskii, S. D.; Rubel, O.; Jansson, F.; Österbacka, R. Description of charge transport in disordered organic materials. *Adv. Polym. Sci.* **2009**, *223*, 1−28.
(103) John, H.; Bauer, R.; Espindola, P.; Sonar, P.; Heinze, J.; Müllen, K. 3D-Hybrid Networks with Controllable Electrical Conductivity from the Electrochemical Deposition of Terthiophene-Functionalized Polyphenylene. *Angew. Chem., Int. Ed.* **2005**, *44*, 2447−2451.
(104) Espinoza-Zarria, P. Ph.D. Dissertation. Albert-Ludwigs Universität Friburg, 2006.
(105) Pullen, A. E.; Swager, T. M. Regiospecific Copolyanilines from Substituted Oligoanilines: Electrochemical Comparisons with Random Copolyanilines. *Macromolecules* **2001**, *34*, 812−816.
(106) Ofer, D.; Crooks, R. M.; Wrighton, M. S. Potential Dependence of the Conductivity of Highly Oxidized Polythiophenes, Polypyrroles, and Polyaniline: Finite Windows of High Conductivity. *J. Am. Chem. Soc.* **1990**, *112*, 7869−7879.
(107) Heinze, J. Conducting Polymers. In *Organic Electrochemistry*; Schaffer, H. J., Bard, A. J., Stratmann, M., Eds.; Encyclopedia of Electrochemistry; Wiley-VCH: Weinheim, Germany, 2004; Vol. *8*, Chapter 16, p 607.
(108) Vorotyntsev, M. A.; Heinze, J. Charging Process in Electron Conducting Polymers: Dimerization Mode. *Electrochim. Acta* **2001**, *46*, 3309−3324.
(109) Diaz, A. F.; Logan, J. A. Electroactive Polyaniline Films. *J. Electroanal. Chem. Interfacial Electrochem.* **1980**, *111*, 111−114.
(110) Genies, E. M.; Syed, A. A. Polypyrrole and Poly N-methylpyrrole — An Electrochemical Study in an Aqueous Medium. *Synth. Met.* **1984**, *10*, 21−30.
(111) Yurchenko, O.; Freytag, D.; zur Borg, L.; Zentel, R.; Heinze, J.; Ludwigs, S. Electrochemically Induced Reversible and Irreversible Coupling of Triarylamines. *J. Phys. Chem. B* **2012**, *116*, 30−39.
(112) Heinze, J. Electrochemistry of Conducting Polymers. In *Organic Electrochemistry, Revised and Expanded*, 5th ed.; Hammerich, O., Speiser, B., Eds.; CRC Press: Boca Raton, FL, 2016.
(113) van Haare, J. A. E. H.; Havinga, E. D. E.; van Dongen, J. L. J.; Janssen, R. A. J.; Cornil, J.; Brédas, J. L. Redox States of Long Oligothiophenes: Two Polarons on a Single Chain. *Chem. - Eur. J.* **1998**, *4*, 1509−1522.
(114) Geskin, V. M.; Brédas, J. L. Polaron Pair versus Bipolaron on Oligothiophene Chains: A Theoretical Study of the Singlet and Triplet States. *ChemPhysChem* **2003**, *4*, 498−505.
(115) Salem, L.; Rowland, C. Diradical is Molecule in Which Two Electrons Occupy Two Degenerate or Nearly Degenerate Molecular Orbitals. *Angew. Chem., Int. Ed. Engl.* **1972**, *11*, 92−111.
(116) Sharma, S.; Bendikov, M. α-Oligofurans: A Computational Study. *Chem. - Eur. J.* **2013**, *19*, 13127−13139.
(117) Gu, J.; Wu, W.; Danovich, D.; Hoffmann, R.; Tsuji, Y.; Shaik, S. Valence Bond Theory Reveals Hidden Delocalized Diradical Character of Polyenes. *J. Am. Chem. Soc.* **2017**, *139*, 9302−9316.
(118) André, J.; Delhalle, J.; Brédas, J. *Quantum Chemistry Aided Design of Organic Polymers for Molecular Electronics*; World Scientific Publishing Company: Singapore, 1991.
(119) Beljonne, D.; Brédas, J. L. In *Handbook of Conducting Polymers*, 3rd. ed.; Skotheim, T. A., Reynolds, J. R., Eds.; CRC Press: Boca Raton, FL, 2007; pp 1−3.
(120) Ivanov, M.; Talipov, M.; Boddeda, A.; Abdelwahed, S.; Rathore, R. Hückel Theory + Reorganization Energy = Marcus−Hush Theory: Breakdown of the 1/n Trend in π-Conjugated Polyphenylene Cation Radicals is Explained. *J. Phys. Chem. C* **2017**, *121*, 1552−1561.
(121) Ghosh, S.; Cramer, J.; Truhlar, D.; Gagliardi, L. Generalized-active-space Pair-density Functional Theory: An Efficient Method to Study Large, Strongly Correlated, Conjugated Systems. *Chem. Sci.* **2017**, *8*, 2741−2750.
(122) Kang, S.; Snyder, G. Charge-transport Model for Conducting Polymers. *Nat. Mater.* **2017**, *16*, 252−257.
(123) Burrezo, P.; Zafra, J.; López Navarrete, T.; Casado, J. Quinoidal/Aromatic Transformations in Conjugated Oligomers: Vibrational Raman studies on the Limits of Rupture for π-Bonds. *Angew. Chem., Int. Ed.* **2017**, *56*, 2250−2259.
(124) Coughlin, J.; Zhugayevych, A.; Wang, M.; Bazan, G.; Tretiak, S. Charge Delocalization Characteristics of Regioregular High Mobility Polymers. *Chem. Sci.* **2017**, *8*, 1146−1151.
(125) Lin, J. B.; Jin, Y.; Lopez, S. A.; Druckerman, N.; Wheeler, S. E.; Houk, K. N. Torsional Barriers to Rotation and Planarization in Heterocyclic Oligomers of Value in Organic Electronics. *J. Chem. Theory Comput.* **2017**, *13*, 5624−5638.
(126) Cao, J.; Aoki, K. Percolation Threshold Potentials at Quasi-static Electrochemical Switching of Polyaniline Films. *Electrochim. Acta* **1996**, *41*, 1787−1792.
(127) Aoki, K.; Edo, T.; Cao, J. Potential-step Response of Absorption at Conducting-to-insulating Conversion of Polyaniline Films for Demonstrating the Slow Relaxation. *Electrochim. Acta* **1998**, *43*, 285−289.
(128) Otero, T. F.; Boyano, I. Comparative Study of Conducting Polymers by the ESCR Model. *J. Phys. Chem. B* **2003**, *107*, 6730−6738.
(129) Otero, T. F.; Grande, H.; Rodriguez, J. Conformational Relaxation during Polypyrrole Oxidation: From Experiment to Theory. *Electrochim. Acta* **1996**, *41*, 1863−1869.
(130) Inzelt, G. *Conducting Polymers: A New Era in Electrochemistry*; Springer Science & Business Media, 2012; p 208.
(131) Otero, T. F.; Abadías, R. Poly(3-methylthiophene) Oxidation under Chemical Control. Rate Coefficients Change with Prepolarization Potentials of Reduction. *J. Electroanal. Chem.* **2007**, *610*, 96−101.
(132) Kiefer, R.; Martinez, J. G.; Keskula, A.; Anbarjafari, G.; Aabloo, A.; Otero, T. F. Polymeric Actuators: Solvents Tune Reaction-driven Cation to Reaction-driven Anion Actuation. *Sens. Actuators, B* **2016**, *233*, 328−336.
(133) Trefz, D.; Ruff, A.; Tkachov, R.; Wieland, M.; Goll, M.; Kiriy, A.; Ludwigs, S. Electrochemical Investigations of the n-Type Semiconducting Polymer P(NDI2OD-2) and its Monomer: New Insights in the Reduction Behavior. *J. Phys. Chem. C* **2015**, *119*, 22760−22771.

DOI: 10.1021/acs.chemrev.7b00482
Chem. Rev. 2018, 118, 4731−4816

(134) Otero, T. F.; Martinez, J. G. Structural and Biomimetic Chemical Kinetics: Kinetic Magnitudes Include Structural Information. *Adv. Funct. Mater.* **2013**, *23*, 404−416.
(135) Otero, T. F. Reactions Driving Conformational Movements (Molecular Motors) in Gels: Conformational and Structural Chemical Kinetics. *Phys. Chem. Chem. Phys.* **2017**, *19*, 1718−1730.
(136) Neo, W.; Ye, Q.; Chua, S.-J.; Xu, J. Conjugated Polymer-based Electrochromics: Materials, Device Fabrication and Application Prospects. *J. Mater. Chem. C* **2016**, *4*, 7364−7376.
(137) Xia, Y.; Ouyang, J. Transparent Conducting Polymers. In *Organic Optoelectronic Materials. Lecture Notes in Chemistry*; Li, Y., Ed.; Springer, 2015; Vol. *91*, pp 359−392.
(138) Patra, A.; Bendikov, M.; Chand, S. Poly(3,4-ethylenedioxyselenophene) and Its Derivatives: Novel Organic Electronic Materials. *Acc. Chem. Res.* **2014**, *47*, 1465−1474.
(139) Kline, W.; Lorenzini, R.; Sotzing, G. A Review of Organic Electrochromic Fabric Devices. *Color. Technol.* **2014**, *130*, 73−80.
(140) Shi, H.; Liu, C.; Jiang, Q.; Xu, J. Effective Approaches to Improve the Electrical Conductivity of PEDOT:PSS: A Review. *Adv. Electron. Mater.* **2015**, *1*, 1500017.
(141) Zarras, P.; Irvin, J. Electrically active polymers. In *Encyclopedia of Polymer Science and Technology*; Mark, H. F., Ed.; John Wiley & Sons, Inc., 2014; Vol. *4*, pp 741−789.
(142) Yanilmaz, M.; Sarac, A. S. A Review: Effect of Conductive Polymers on the Conductivities of Electrospun Mats. *Text. Res. J.* **2014**, *84*, 1325−1342.
(143) Roncali, J. Synthetic Principles for Bandgap Control in Linear π-Conjugated Systems. *Chem. Rev.* **1997**, *97*, 173−205.
(144) Holze, R. Optical and Electrochemical Band Gaps in Mono-, Oligo-, and Polymeric Systems: A Critical Reassessment. *Organometallics* **2014**, *33*, 5033−5042.
(145) Ates, M.; Karazehir, T.; Sezai Sarac, A. Conducting Polymers and their Applications. *Curr. Phys. Chem.* **2012**, *2*, 224−240.
(146) Das, T.; Prusty, S. Review on Conducting Polymers and Their Applications. *Polym.-Plast. Technol. Eng.* **2012**, *51*, 1487−1500.
(147) Arias, A.; MacKenzie, J.; McCulloch, I.; Rivnay, J.; Salleo, A. Materials and Applications for Large Area Electronics: Solution-Based Approaches. *Chem. Rev.* **2010**, *110*, 3−24.
(148) Jurchescu, O.; Cicoira, F.; Santato, C. Large-area organic electronics: inkjet printing and spray coating techniques. In *Organic Electronics: Emerging Concepts and Technologies*; Cicoira, F., Santato, C., Eds.; Wiley-VCH: Weinheim, Germany, 2013; pp 319−339.
(149) Tseng, H.; Phan, H.; Luo, C.; Wang, M.; Perez, L.; Patel, S. N.; Ying, L.; Kramer, E.; Nguyen, T.; Bazan, C.; Heeger, A. High-Mobility Field-Effect Transistors Fabricated with Macroscopic Aligned Semiconducting Polymers. *Adv. Mater.* **2014**, *26*, 2993−2998.
(150) Schmatz, B.; Yuan, Z.; Lang, A. W.; Hernandez, J. L.; Reichmanis, E.; Reynolds, J. R. Aqueous Processing for Printed Organic Electronics: Conjugated Polymers with Multistage Cleavable Side Chains. *ACS Cent. Sci.* **2017**, *3*, 961−967.
(151) Guimard, N. K.; Gomez, N.; Schmidt, C. E. Conducting Polymers in Biomedical Engineering. *Prog. Polym. Sci.* **2007**, *32*, 876−921.
(152) Kaur, G.; Adhikari, R.; Cass, P.; Bown, M.; Gunatillake, P. Electrically Conductive Polymers and Composites for Biomedical Applications. *RSC Adv.* **2015**, *5*, 37553−37567.
(153) Isaksson, J.; Kjall, P.; Nilsson, D.; Robinson, N. D.; Berggren, M. A.; Richter-Dahlfors. Electronic Control of Ca^{2+} Signalling in Neuronal Cells Using an Organic Electronic Ion Pump. *Nat. Mater.* **2007**, *6*, 673.
(154) Wong, J. Y.; Langer, R.; Ingber, D. E. Electrically Conducting Polymers can Non-invasively Control the Shape and Growth of Mammalian Cells. *Proc. Natl. Acad. Sci. U. S. A.* **1994**, *91*, 3201−3204.
(155) Schmidt, C. E.; Shastri, V. R.; Vacanti, J. P.; Langer, R. Stimulation of Neurite Outgrowth Using an Electrically Conducting Polymer. *Proc. Natl. Acad. Sci. U. S. A.* **1997**, *94*, 8948−8953.
(156) Sivaraman, K. M.; Özkale, B.; Ergeneman, O.; Lühmann, T.; Fortunato, G.; Zeeshan, M. A.; Nelson, B. J.; Pané, S. Redox Cycling for Passive Modification of Polypyrrole Surface Properties: Effects on Cell Adhesion and Proliferation. *Adv. Healthcare Mater.* **2013**, *2*, 591−598.
(157) Qazi, T. H.; Rai, R.; Boccaccini, A. R. Tissue Engineering of Electrically Responsive Tissues Using Polyaniline Based Polymers: A Review. *Biomaterials* **2014**, *35*, 9068−9086.
(158) Bendrea, A.-D.; Cianga, L.; Cianga, I. Review Paper: Progress in the Field of Conducting Polymers for Tissue Engineering Applications. *J. Biomater. Appl.* **2011**, *26*, 3−84.
(159) Balint, R.; Cassidy, N.; Cartmell, S. Conductive Polymers: Towards a Smart Biomaterial for Tissue Engineering. *Acta Biomater.* **2014**, *10*, 2341−2353.
(160) Marzocchi, M.; Gualandi, I.; Calienni, M.; Zironi, I.; Scavetta, E.; Castellani, G.; Fraboni, B. Physical and Electrochemical Properties of PEDOT:PSS as a Tool for Controlling Cell Growth. *ACS Appl. Mater. Interfaces* **2015**, *7*, 17993−18003.
(161) Inal, S.; Hama, A.; Ferro, M.; Pitsalidis, C.; Oziat, J.; Iandolo, D.; Pappa, A.-M.; Hadida, M.; Huerta, M.; Marchat, D.; Mailley, P.; Owens, R. M. Conducting Polymer Scaffolds for Hosting and Monitoring 3D Cell Culture. *Adv. Biosyst.* **2017**, *1*, 1700052.
(162) Weng, B.; Diao, J.; Xu, Q.; Liu, Y.; Li, C.; Ding, A.; Chen, J. Bio-Interface of Conducting Polymer-Based Materials for Neuroregeneration. *Adv. Mater. Interfaces* **2015**, *2*, 1500059.
(163) Pires, F.; Ferreira, Q.; Rodrigues, C. A. V.; Morgado, J.; Ferreira, F. C. Neural Stem Cell Differentiation by Electrical Stimulation using a Cross-Linked PEDOT Substrate: Expanding the Use of Biocompatible Conjugated Conductive Polymers for Neural Tissue Engineering. *Biochim. Biophys. Acta, Gen. Subj.* **2015**, *1850*, 1158−1168.
(164) Cui, X.; Wiler, J.; Dzaman, M.; Altschuler, R. A.; Martin, D. C. In Vivo Studies of Polypyrrole/Peptide Coated Neural Probes. *Biomaterials* **2003**, *24*, 777−787.
(165) Smith, J.; Lamprou, D. Polymer Coatings for Biomedical Applications: A Review. *Trans. Inst. Met. Finish.* **2014**, *92*, 9−19.
(166) Liao, C.; Zhang, M.; Yao, M. Y.; Hua, T.; Li, L.; Yan, F. Flexible Organic Electronics in Biology: Materials and Devices. *Adv. Mater.* **2015**, *27*, 7493−7527.
(167) Jimison, L.; Rivnay, J.; Owens, R. Conducting polymers to control and monitor cells. In *Organic Electronics: Emerging Concepts and Technologies*; Cicoira, F., Santato, C., Eds.; Wiley-VCH: Weinheim, Germany, 2013; pp 27−67.
(168) Perez-Madrigal, M. M.; Armelin, E.; Puiggali, J.; Aleman, C. Insulating and Semiconducting Polymeric Free-standing Nanomembranes with Biomedical Applications. *J. Mater. Chem. B* **2015**, *3*, 5904−5932.
(169) Green, R.; Abidian, M. Conducting Polymers for Neural Prosthetic and Neural Interface Applications. *Adv. Mater.* **2015**, *27*, 7620−7637.
(170) Fang, Y.; Li, X.; Fang, Y. Organic Bioelectronics for Neural Interfaces. *J. Mater. Chem. C* **2015**, *3*, 6424−6430.
(171) Jin, G.; Li, K. The Electrically Conductive Scaffold as the Skeleton of Stem Cell Niche in Regenerative Medicine. *Mater. Sci. Eng., C* **2014**, *45*, 671−681.
(172) Ostrovsky, S.; Hahnewald, S.; Kiran, R.; Mistrik, P.; Hessler, R.; Tscherter, A.; Senn, P.; Kang, J.; Kim, J.; Roccio, M.; Lellouche, J. P. Conductive Hybrid Carbon Nanotube (CNT)-polythiophene Coatings for Innovative Auditory Neuron-multi-electrode Array Interfacing. *RSC Adv.* **2016**, *6*, 41714−41723.
(173) Sista, P.; Ghosh, K.; Martinez, J.; Rocha, R. Polythiophenes in Biological Applications. *J. Nanosci. Nanotechnol.* **2014**, *14*, 250−272.
(174) Olad, A.; Azhar, F. Biomedical applications of polyaniline. In *Trends in Polyaniline Research*; Chowdhury, A., Ohsaka, T., Rahman, A., Islam, M., Eds.; Nova Science Publishers, Inc.: Hauppauge, NY, 2013; pp 361−383.
(175) Otero, T. F.; Martinez, J. G.; Arias-Pardilla, J. Biomimetic Electrochemistry from Conducting Polymers. A Review of Artificial Muscles, Smart Membranes, Smart Drug Delivery and Computer/Neuron Interfaces. *Electrochim. Acta* **2012**, *84*, 112−128.
(176) Wei, M.; Gao, Y.; Li, X.; Serpe, M. J. Stimuli-responsive Polymers and their Applications. *Polym. Chem.* **2017**, *8*, 127−143.

DOI: 10.1021/acs.chemrev.7b00482
Chem. Rev. 2018, 118, 4731−4816

(177) Sharma, M.; Svirskis, D.; Garg, S. Advances in Drug-delivery Systems Based on Intrinsically Conducting Polymers. *RSC Smart Mater.* **2013**, *1*, 283−303.
(178) Svirskis, D.; Travas-Sejdic, J.; Rodgers, A.; Garg, S. Electrochemically Controlled Drug Delivery Based on Intrinsically Conducting Polymers. *J. Controlled Release* **2010**, *146*, 6−15.
(179) Alshammary, B.; Walsh, F. C.; Herrasti, P.; Ponce de Leon, C. Electrodeposited Conductive Polymers for Controlled Drug Release: Polypyrrole. *J. Solid State Electrochem.* **2016**, *20*, 839−859.
(180) Svirskis, D.; Wright, B. E.; Travas-Sejdic, J.; Rodgers, A.; Garg, S. Evaluation of Physical Properties and Performance over Time of an Actuating Polypyrrole Based Drug Delivery System. *Sens. Actuators, B* **2010**, *151*, 97−102.
(181) George, P. M.; Lavan, D. A.; Burdick, J. A.; Chen, C. Y.; Liang, E.; Langer, R. Electrically Controlled Drug Delivery from Biotin-Doped Conductive Polypyrrole. *Adv. Mater.* **2006**, *18*, 577−581.
(182) Thompson, B. C.; Moulton, S. E.; Richardson, R. T.; Wallace, G. G. Effect of the Dopant Anion in Polypyrrole on Nerve Growth and Release of a Neurotrophic Protein. *Biomaterials* **2011**, *32*, 3822−3831.
(183) Barthus, R. C.; Lira, L. M.; de Torresi, S. I. C. Conducting Polymer-hydrogel Blends for Electrochemically Controlled Drug Release Devices. *J. Braz. Chem. Soc.* **2008**, *19*, 630−636.
(184) Wadhwa, R.; Lagenaur, C. F.; Cui, V. J. Electrochemically Controlled Release of Dexamethasone from Conducting Polymer Polypyrrole Coated Electrode. *J. Controlled Release* **2006**, *110*, 531−541.
(185) Luo, X.; Cui, X. T. Sponge-like Nanostructured Conducting Polymers for Electrically Controlled Drug Release. *Electrochem. Commun.* **2009**, *11*, 1956−1959.
(186) Uppalapati, D.; Boyd, B. J.; Garg, S.; Travas-Sejdic, J.; Svirskis, D. Conducting Polymers with Defined Micro- or Nanostructures for Drug Delivery. *Biomaterials* **2016**, *111*, 149−162.
(187) Zhao, Y.; Tavares, A. C.; Gauthier, M. A. Nano-engineered Electro-responsive Drug Delivery Systems. *J. Mater. Chem. B* **2016**, *4*, 3019−3030.
(188) Paun, I. A.; Zamfirescu, M.; Luculescu, C. R.; Acasandrei, A. M.; Mustaciosu, C. C.; Mihailescu, M.; Dinescu, M. Electrically Responsive Microreservoires for Controllable Delivery of Dexamethasone in Bone Tissue Engineering. *Appl. Surf. Sci.* **2017**, *392*, 321−331.
(189) Conzuelo, L. V.; Arias-Pardilla, J.; Cauich-Rodríguez, J. V.; Smit, M. A.; Otero, T. F. Sensing and Tactile Artificial Muscles from Reactive Materials. *Sensors* **2010**, *10*, 2638−2674.
(190) Otero, T. F. Coulovoltammetric and Dynamovoltammetric Responses from Conducting Polymers and Bilayer Muscles as Tools to Identify Reaction-driven Structural Changes. A Review. *Electrochim. Acta* **2016**, *212*, 440−457.
(191) Kaneto, K. Research Trends of Soft Actuators based on Electroactive Polymers and Conducting Polymers. *J. Phys.: Conf. Ser.* **2016**, *704*, 012004.
(192) Kaneto, K.; Suematsu, H.; Yamato, K. Conducting Polymer Soft Actuators Based on Polypyrrole-Training Effect and Fatigue. In *Artificial Muscle Actuators Using Electroactive Polymers*; Vincenzini, P., Bar-Cohen, Y., Carpi, F., Eds.; Trans Tech Publications: Stafa-Zuerich, Switzerland, 2009; Vol. *61*, pp 122−130.
(193) Fuchiwaki, M.; Martinez, J. G.; Otero, T. F. Polypyrrole Asymmetric Bilayer Artificial Muscle: Driven Reactions, Cooperative Actuation, and Osmotic Effects. *Adv. Funct. Mater.* **2015**, *25*, 1535−1541.
(194) Fuchiwaki, M.; Martinez, J. G.; Otero, T. F. Asymmetric Bilayer Muscles. Cooperative and Antagonist Actuation. *Electrochim. Acta* **2016**, *195*, 9−18.
(195) García-Córdova, F.; Valero, L.; Ismail, Y. A.; Otero, T. F. Biomimetic Polypyrrole Based all Three-in-one Triple Layer Sensing Actuators Exchanging Cations. *J. Mater. Chem.* **2011**, *21*, 17265−17272.
(196) Kiefer, R.; Keskula, A.; Martinez, J. G.; Anbarjafari, G.; Torop, J.; Otero, T. F. Interpenetrated Triple Polymeric Layer as Electrochemomechanical Actuator: Solvent Influence and Diffusion Coefficient of Counterions. *Electrochim. Acta* **2017**, *230*, 461−469.
(197) Romero, I. S.; Bradshaw, N. P.; Larson, J. D.; Severt, S. Y.; Roberts, S. J.; Schiller, M. L.; Leger, J. M.; Murphy, A. R. Biocompatible Electromechanical Actuators Composed of Silk-conducting Polymer Composites. *Adv. Funct. Mater.* **2014**, *24*, 3866−3873.
(198) Ismail, Y. A.; Martinez, J. G.; Otero, T. F. Fibroin/Polyaniline Microfibrous Mat. Preparation and Electrochemical Characterization as Reactive Sensor. *Electrochim. Acta* **2014**, *123*, 501−510.
(199) Zhao, S.; Li, J.; Cao, D.; Zhang, G.; Li, J.; Li, K.; Yang, Y.; Wang, W.; Jin, Y.; Sun, R.; Wong, C.-P. Recent Advancements in Flexible and Stretchable Electrodes for Electromechanical Sensors: Strategies, Materials, and Features. *ACS Appl. Mater. Interfaces* **2017**, *9*, 12147−12164.
(200) Ward, M.; Baker, P.; Iwuoha, E.; Aubert, P.-H.; Plesse, C. Polypyrrole Derivatives in the Design of Electrochemically Driven Actuators. *Mini-Rev. Org. Chem.* **2015**, *12*, 414−423.
(201) Jonas, F.; Krafft, W.; Muys, B. Poly(3,4-ethylenedioxythiophene): Conductive Coatings, Technical Applications and Properties. *Macromol. Symp.* **1995**, *100*, 169−173.
(202) Bayer, A. G., Eur. Patent 440 957, 1991. Agfa Gevaert, Eur. Patent 564 911, 1993.
(203) http://www.agfa.com/specialty-products/solutions/conductive-materials/orgacon-antistatic-films/ consulted 10/12/2017.
(204) Groenendaal, L.; Jonas, F.; Freitag, D.; Pielartzik, H.; Reynolds, J. Poly(3,4-ethylenedioxythiophene) and its Derivatives: Past, Present, and Future. *Adv. Mater.* **2000**, *12*, 481−494.
(205) Loevenich, W. PEDOT-Properties and Applications. *Polym. Sci., Ser. C* **2014**, *56*, 135−143.
(206) Yang, X.; Li, Y.; Wang, X. Intrinsically Conducting Polymers and Their Composites for Anticorrosion and Antistatic Applications. In *Semiconducting Polymer Composites: Principles, Morphologies, Properties and Applications*; Yang, X., Ed.; Wiley-VCH Verlag: Weinheim, Germany, 2012, Chapter 10.
(207) Ala, O.; Fan, Q. Applications of Conducting Polymers in Electronic Textiles. *Res. J. Text. Apparel* **2009**, *13*, 51−68.
(208) Abu-Thabit, N. Y.; Makhlouf, A. S. H. Recent Advances in Polyaniline (PANi)-based Organic Coatings for Corrosion Protection. In *Handbook of Smart Coatings for Materials Protection*; Makhlouf, A. S. H., Ed.; Woodhead Publishing: U.K., 2014; pp 459−486.
(209) Tian, Z.; Yu, H.; Wang, L.; Saleem, M.; Ren, F.; Ren, P.; Chen, Y.; Sun, R.; Sun, Y.; Huang, L. Recent Progress in the Preparation of Polyaniline Nanostructures and Their Applications in Anticorrosive Coatings. *RSC Adv.* **2014**, *4*, 28195−28208.
(210) Nautiyal, A.; Qiao, M.; Cook, J. E.; Zhang, X.; Huang, T.-S. High Performance Polypyrrole Coating for Corrosion Protection and Biocidal Applications. *Appl. Surf. Sci.* **2018**, *427*, 922−930.
(211) Ates, M. A Review on Conducting Polymer Coatings for Corrosion Protection. *J. Adhes. Sci. Technol.* **2016**, *30*, 1510−1536.
(212) Spinks, G. M.; Dominis, A. J.; Wallace, G. G.; Tallman, D. E. Electroactive Conducting Polymers for Corrosion Control. *J. Solid State Electrochem.* **2002**, *6*, 85−100.
(213) Tallman, D. E.; Spinks, G.; Dominis, A.; Wallace, G. Electroactive Conducting Polymers for Corrosion Control. Part 1. General Introduction and a Review of Non-ferrous Metals. *J. Solid State Electrochem.* **2002**, *6*, 73−84.
(214) Hoang, T. K. A.; Doan, T. N. L.; Sun, K. E. K.; Chen, P. Corrosion Chemistry and Protection of Zinc & Zinc Alloys by Polymer-containing Materials for Potential use in Rechargeable Aqueous Batteries. *RSC Adv.* **2015**, *5*, 41677−41691.
(215) Upadhyay, V.; Battocchi, D. Localized Electrochemical Characterization of Organic Coatings: A Brief Review. *Prog. Org. Coat.* **2016**, *99*, 365−377.
(216) Perrin, F. X.; Oueiny, C. Polyaniline Thermoset Blends and Composites. *React. Funct. Polym.* **2017**, *114*, 86−103.
(217) Zeybek, B.; Aksun, E.; Uge, A. Investigation of Corrosion Protection Performance of Poly(N-methylpyrrole)-dodecylsulfate/Multi-walled Carbon Nanotubes Composite Coatings on the Stainless Steel. *Mater. Chem. Phys.* **2015**, *163*, 11−23.

DOI: 10.1021/acs.chemrev.7b00482
Chem. Rev. 2018, 118, 4731−4816

(218) Lyon, S.; Bingham, R.; Mills, D. Advances in Corrosion Protection by Organic Coatings: What we Know and what we Would Like to Know. *Prog. Org. Coat.* **2017**, *102*, 2−7.
(219) Abdolahi, A.; Hamzah, E.; Ibrahim, Z.; Hashim, S. Application of Environmentally-Friendly Coatings Toward Inhibiting the Microbially Influenced Corrosion (MIC) of Steel: A Review. *Polym. Rev.* **2014**, *54*, 702−745.
(220) Deshpande, P.; Jadhav, N.; Gelling, V.; Sazou, D. Conducting Polymers for Corrosion Protection: A Review. *J. Coat. Technol. Res.* **2014**, *11*, 473−494.
(221) Olad, A.; Rashidzadeh, A.; Takeo, E. Anticorrosive properties of polyaniline. In *Trends in Polyaniline Research*; Chowdhury, A., Ohsaka, T., Rahman, A., Islam, M., Eds.; Nova Science Publishers, Inc.: Hauppauge, NY, 2013; pp 319−337.
(222) Riaz, U.; Nwaoha, C.; Ashraf, S. M. Recent Advances in Corrosion Protective Composite Coatings Based on Conducting Polymers and Natural Resource Derived Polymer. *Prog. Org. Coat.* **2014**, *77*, 743−756.
(223) Monk, P.; Mortimer, R.; Rosseinsky, D. *Electrochromism and Electrochromic Devices*; Cambridge University Press: Cambridge, 2007.
(224) Kalagi, S. S.; Patil, P. S. Secondary Electrochemical Doping Level Effects on Polaron and Bipolaron Bands Evolution and Interband Transition Energy from Absorbance Spectra of PEDOT:PSS Thin Films. *Synth. Met.* **2016**, *220*, 661−666.
(225) Mortimer, R. J. Organic Electrochromic Materials. *Electrochim. Acta* **1999**, *44*, 2971−2981.
(226) Monk, P. M. S.; Mortimer, R. J.; Rosseinsky, D. R. *Electrochromism*; VCH: Weinheim, Germany, 1995.
(227) Garnier, F.; Tourillon, G.; Gazard, M.; Dubois, J. C. Organic Conducting Polymers Derived from Substituted Thiophenes as Electrochromic Material. *J. Electroanal. Chem. Interfacial Electrochem.* **1983**, *148*, 299−303.
(228) Yashima, H.; Kobayashi, M.; Lee, K. B.; Chung, D.; Heeger, A. J.; Wudl, F. Electrochromic Switching of the Optical Properties of Polyisothianaphthene. *J. Electrochem. Soc.* **1987**, *134*, 46−52.
(229) Kitani, A.; Yano, J.; Sasaki, K. ECD Materials for the Three Primary Colors Developed by Polyanilines. *J. Electroanal. Chem. Interfacial Electrochem.* **1986**, *209*, 227−232.
(230) Argun, A. A.; Aubert, P. H.; Thompson, B. C.; Schwendeman, S. I.; Gaupp, C. L.; Hwang, J.; Pinto, N. J.; Tanner, D. B.; MacDiarmid, A. G.; Reynolds, J. R. Multicolored Electrochromism in Polymers: Structures and Devices. *Chem. Mater.* **2004**, *16*, 4401−4412.
(231) Mortimer, R. J. Electrochromic Materials. *Annu. Rev. Mater. Res.* **2011**, *41*, 241−268.
(232) Beaujuge, P. M.; Reynolds, J. R. Color Control in π-Conjugated Organic Polymers for Use in Electrochromic Devices. *Chem. Rev.* **2010**, *110*, 268−320.
(233) Amb, C. M.; Dyer, A. L.; Reynolds, J. R. Navigating the Color Palette of Solution-Processable Electrochromic Polymers. *Chem. Mater.* **2011**, *23*, 397−415.
(234) Sonmez, G. Polymeric Electrochromics. *Chem. Commun.* **2005**, 5251−5259.
(235) Alesanco, Y.; Vinuales, A.; Palenzuela, J.; Odriozola, I.; Cabanero, G.; Rodriguez, J.; Tena-Zaera, R. Multicolor Electrochromics: Rainbow-Like Devices. *ACS Appl. Mater. Interfaces* **2016**, *8*, 14795−14801.
(236) Gunbas, G.; Toppare, L. Electrochromic Conjugated Polyheterocycles and Derivatives - Highlights from the Last Decade towards Realization of Long Lived Aspirations. *Chem. Commun.* **2012**, *48*, 1083−1101.
(237) Lv, X.; Li, W.; Ouyang, M.; Zhang, Y.; Wright, D. S.; Zhang, C. Polymeric Electrochromic Materials with Donor−acceptor Structures. *J. Mater. Chem. C* **2017**, *5*, 12−28.
(238) Luo, J.; Ma, Y.; Pei, J.; Song, Y. Recent Progress on Organic and Polymeric Electrochromic Materials. *Curr. Phys. Chem.* **2011**, *1*, 216−231.
(239) Vasilyeva, S. V.; Unur, E.; Walczak, R. M.; Donoghue, E. P.; Rinzler, A. G.; Reynolds, J. R. Color Purity in Polymer Electrochromic Window Devices on Indium-Tin Oxide and Single-Walled Carbon Nanotube Electrodes. *ACS Appl. Mater. Interfaces* **2009**, *1*, 2288−2297.
(240) Camurlu, P. Polypyrrole Derivatives for Electrochromic Applications. *RSC Adv.* **2014**, *4*, 55832−55845.
(241) Mortimer, R. J.; Dyer, A. L.; Reynolds, J. R. Electrochromic Organic and Polymeric Materials for Display Applications. *Displays* **2006**, *27*, 2−18.
(242) Kai, H.; Suda, W.; Ogawa, Y.; Nagamine, K.; Nishizawa, M. Intrinsically Stretchable Electrochromic Display by a Composite Film of Poly(3,4-ethylenedioxythiophene) and Polyurethane. *ACS Appl. Mater. Interfaces* **2017**, *9*, 19513−19518.
(243) Jensen, J.; Hoesel, M.; Dyer, A. L.; Krebs, F. C. Development and Manufacture of Polymer-based Electrochromic Devices. *Adv. Funct. Mater.* **2015**, *25*, 2073−2090.
(244) Ahmad, S.; Ikeda, T. Electroactive Coatings: For Electrically Controlled On-Demand Power Windows. *Nanosci. Nanotechnol. Lett.* **2013**, *5*, 3−12.
(245) Argun, A. A.; Cirpan, A.; Reynolds, J. R. The First Truly All-Polymer Electrochromic Devices. *Adv. Mater.* **2003**, *15*, 1338−1341.
(246) Gavim, A. E. X.; Santos, G. H.; de Souza, E. H.; Rodrigues, P. C.; Floriano, J. B.; Kamikawachi, R. C.; de Deus, J. F.; Macedo, A. G. Influence of Electrolyte Distribution in PEDOT:PSS Based Flexible Electrochromic Devices. *Chem. Phys. Lett.* **2017**, *689*, 212−218.
(247) Singh, R.; Tharion, J.; Murugan, S.; Kumar, A. ITO-Free Solution-Processed Flexible Electrochromic Devices Based on PEDOT:PSS as Transparent Conducting Electrode. *ACS Appl. Mater. Interfaces* **2017**, *9*, 19427−19435.
(248) Jensen, J.; Hoesel, M.; Kim, I.; Yu, J.-S.; Jo, J.; Krebs, F. C. Fast Switching ITO Free Electrochromic Devices. *Adv. Funct. Mater.* **2014**, *24*, 1228−1233.
(249) Cai, G. F.; Darmawan, P.; Cui, M. Q.; Wang, J. X.; Chen, J. W.; Magdassi, S.; Lee, P. S. Highly Stable Transparent Conductive Silver Grid/PEDOT:PSS Electrodes for Integrated Bifunctional Flexible Electrochromic Supercapacitors. *Adv. Energy Mater.* **2016**, *6*, 1501882.
(250) Yu, L.; Shearer, C.; Shapter, J. Recent Development of Carbon Nanotube Transparent Conductive Films. *Chem. Rev.* **2016**, *116*, 13413−13453.
(251) Shen, E. D.; Osterholm, A. M.; Reynolds, J. R. Out of Sight but not Out of Mind: The Role of Counter Electrodes in Polymer-based Solid-state Electrochromic Devices. *J. Mater. Chem. C* **2015**, *3*, 9715−9725.
(252) Kline, W. M.; Lorenzini, R. G.; Sotzing, G. A. A Review of Organic Electrochromic Fabric Devices. *Color. Technol.* **2014**, *130*, 73−80.
(253) Alkire, R., Kolb, D., Lipkowski, J., Eds. *Electrocatalysis: Theoretical Foundations and Model Experiments*; Wiley-VCH: Weinheim, Germany, 2014.
(254) Francke, R.; Little, R. Redox Catalysis in Organic Electrosynthesis: Basic Principles and Recent Developments. *Chem. Soc. Rev.* **2014**, *43*, 2492−2521.
(255) Costentin, C.; Robert, M.; Saveant, J.-M. Catalysis of the Electrochemical Reduction of Carbon Dioxide. *Chem. Soc. Rev.* **2013**, *42*, 2423−2436.
(256) Frontana-Uribe, B. A.; Little, R.; Ibanez, J. G.; Palma, A.; Vasquez-Medrano, R. C. Organic Electrosynthesis: A Promising Green Methodology in Organic Chemistry. *Green Chem.* **2010**, *12*, 2099−2119.
(257) Yan, M.; Kawamata, Y.; Baran, P. S. Synthetic Organic Electrochemical Methods since 2000: On the Verge of a Renaissance. *Chem. Rev.* **2017**, *117*, 13230−13319.
(258) Xiang, Z.; Cao, D.; Dai, L. Well-defined Two Dimensional Covalent Organic Polymers: Rational Design, Controlled Syntheses, and Potential Applications. *Polym. Chem.* **2015**, *6*, 1896−1911.
(259) Peng, P.; Zhou, Z.; Guo, J.; Xiang, Z. Well-Defined 2D Covalent Organic Polymers for Energy Electrocatalysis. *ACS Energy Lett.* **2017**, *2*, 1308−1314.
(260) Ding, S.-Y.; Wang, W. Covalent Organic Frameworks (COFs): From Design to Applications. *Chem. Soc. Rev.* **2013**, *42*, 548−568.

DOI: 10.1021/acs.chemrev.7b00482
Chem. Rev. 2018, 118, 4731−4816

(261) Qian, Y.; Khan, I. A.; Zhao, D. Electrocatalysts Derived from Metal-Organic Frameworks for Oxygen Reduction and Evolution Reactions in Aqueous Media. *Small* **2017**, *13*, 1701143.
(262) Inzelt, G. *Conducting Polymers: A New Era in Electrochemistry*; Springer Science & Business Media, 2012; p 250.
(263) Bullock, R. M.; Das, A. K.; Appel, A. M. Surface Immobilization of Molecular Electrocatalysts for Energy Conversion. *Chem. - Eur. J.* **2017**, *23*, 7626−7641.
(264) Wang, L.; Fan, K.; Daniel, Q.; Duan, L.; Li, F.; Philippe, B.; Rensmo, H.; Chen, H.; Sun, J.; Sun, L. Electrochemical Driven Water Oxidation by Molecular Catalysts In Situ Polymerized on the Surface of Graphite Carbon Electrode. *Chem. Commun.* **2015**, *51*, 7883−7886.
(265) Beley, M.; Gros, P. C. Ruthenium Polypyridine Complexes Bearing Pyrroles and π-Extended Analogues. Synthesis, Spectroelectronic, Electrochemical, and Photovoltaic Properties. *Organometallics* **2014**, *33*, 4590−4606.
(266) Bidan, G.; Billon, M.; Calvo-Muñoz, M. L.; Dupont-Fillard, A. Bio-Assemblies onto Conducting Polymer Support: Implementation of DNA-Chips. *Mol. Cryst. Liq. Cryst.* **2004**, *418*, 255−270.
(267) Ahlers, M.; Mueller, W.; Reichert, A.; Ringsdorf, H.; Venzmer, J. Specific Interactions of Proteins with Functional Lipid Monolayers—Ways of Simulating Biomembrane Processes. *Angew. Chem., Int. Ed. Engl.* **1990**, *29*, 1269−1285.
(268) Rodriguez, L. M. T.; Billon, M.; Roget, A.; Bidan, G. Electrosynthesis of a Biotinylated Polypyrrole Film and Study of the Avidin Recognition by QCM. *J. Electroanal. Chem.* **2002**, *523*, 70−78.
(269) Cosnier, S.; Lepellec, A. Poly(pyrrole−biotin): A New Polymer for Biomolecule Grafting on Electrode Surfaces. *Electrochim. Acta* **1999**, *44*, 1833−1836.
(270) Mouffouk, F.; Brown, S. J.; Demetriou, A. M.; Higgins, S. J.; Nichols, R. J.; Rajapakse, R. M. G.; Reeman, S. Electrosynthesis and Characterization of Biotin-functionalized Poly(terthiophene) Copolymers, and their Response to Avidin. *J. Mater. Chem.* **2005**, *15*, 1186−1196.
(271) Mouffouk, F.; Higgins, S. J. A Biotin-functionalised Poly(3,4-ethylenedioxythiophene)-coated Microelectrode which Responds Electrochemically to Avidin Binding. *Electrochem. Commun.* **2006**, *8*, 15−20.
(272) Nguyen Cong, H.; El Abbassi, K.; Gautier, J. L.; Chartier, P. Oxygen Reduction on Oxide/Polypyrrole Composite Electrodes: Effect of Doping Anions. *Electrochim. Acta* **2005**, *50*, 1369−1376.
(273) Gautier, J. L.; Marco, J. F.; Gracia, M.; Gancedo, J. R.; de la Garza Guadarrama, V. G.; Nguyen-Cong, H.; Chartier, P. $Ni_{0.3}Co_{2.7}O_4$ Spinel Particles/Polypyrrole Composite Electrode: Study by X-ray Photoelectron Spectroscopy. *Electrochim. Acta* **2002**, *48*, 119−125.
(274) Simon, E.; Sablé, E.; Handel, H.; L'Her, M. Electrodes Modified by Conducting Polymers Bearing Redox Sites: Ni- and Co-cyclam Complexes on Polypyrrole. *Electrochim. Acta* **1999**, *45*, 855−863.
(275) Lamy, C.; Léger, J.-M.; Garnier, F. In *Handbook of Organic Conductive Molecules and Polymers*, Nalwa, H. S., Ed.; Wiley: Chichester, 1997; Vol. 3, p 471.
(276) Dong, Y.-T.; Feng, J.-X.; Li, G.-R. Transition Metal Ion-Induced High Electrocatalytic Performance of Conducting Polymer for Oxygen and Hydrogen Evolution Reactions. *Macromol. Chem. Phys.* **2017**, *218*, 1700359.
(277) Blasco-Ahicart, M.; Soriano-Lopez, J.; Galan-Mascaros, J. R. Conducting Organic Polymer Electrodes with Embedded Polyoxometalate Catalysts for Water Splitting. *ChemElectroChem* **2017**, *4*, 3296.
(278) Cao, X.; Yan, W.; Jin, C.; Tian, J.; Ke, K.; Yang, R. Surface Modification of MnCo2O4 with Conducting Polypyrrole as a Highly Active Bifunctional Electrocatalyst for Oxygen Reduction and Oxygen Evolution Reaction. *Electrochim. Acta* **2015**, *180*, 788−794.
(279) Zhou, Q.; Shi, G. Conducting Polymer-Based Catalysts. *J. Am. Chem. Soc.* **2016**, *138*, 2868−2876.
(280) Wang, Z.; Xu, D.; Xu, J.; Zhang, X. Oxygen Electrocatalysts in Metal-air Batteries: From Aqueous to Nonaqueous Electrolytes. *Chem. Soc. Rev.* **2014**, *43*, 7746−7786.
(281) Song, F.; Li, W.; Han, G.; Sun, Y. Electropolymerization of Aniline on Nickel-Based Electrocatalysts Substantially Enhances Their Performance for Hydrogen Evolution. *ACS Appl. Energy Mater.* **2018**, *1*, 3−8.
(282) Ashassi-Sorkhabi, H.; Rezaei-Moghadam, B.; Asghari, E.; Bagheri, R.; Hosseinpour, Z. Fabrication of Bridge Like Pt@MWCNTs/CoS_2 Electrocatalyst on Conductive Polymer Matrix for Electrochemical Hydrogen Evolution. *Chem. Eng. J.* **2017**, *308*, 275−288.
(283) Ng, C. H.; Winther-Jensen, O.; Ohlin, C. A.; Winther-Jensen, B. Exploration and Optimisation of Poly(2,2′-bithiophene) as a Stable Photo-electrocatalyst for Hydrogen Production. *J. Mater. Chem. A* **2015**, *3*, 11358−11366.
(284) McQuade, D. T.; Pullen, A. E.; Swager, T. M. Conjugated Polymer-Based Chemical Sensors. *Chem. Rev.* **2000**, *100*, 2537−2574.
(285) Potyrailo, R. A. Polymeric Sensor Materials: Toward an Alliance of Combinatorial and Rational Design Tools? *Angew. Chem., Int. Ed.* **2006**, *45*, 702−723.
(286) Liu, B.; Bazan, G. C. Optimization of the Molecular Orbital Energies of Conjugated Polymers for Optical Amplification of Fluorescent Sensors. *J. Am. Chem. Soc.* **2006**, *128*, 1188−1196.
(287) Ramanavicius, A.; Ramanavičienė, A.; Malinauskas, A. Electrochemical Sensors Based on Conducting Polymer—Polypyrrole. *Electrochim. Acta* **2006**, *51*, 6025−6037.
(288) Yang, G.; Kampstra, K. L.; Abidian, M. R. High Performance Conducting Polymer Nanofiber Biosensors for Detection of Biomolecules. *Adv. Mater.* **2014**, *26*, 4954−4960.
(289) Pal, R. K.; Kundu, S. C.; Yadavalli, V. K. Biosensing Using Photolithographically Micropatterned Electrodes of PEDOT:PSS on ITO substrates. *Sens. Actuators, B* **2017**, *242*, 140−147.
(290) Zhan, R.; Fang, Z.; Liu, B. Naked-Eye Detection and Quantification of Heparin in Serum with a Cationic Polythiophene. *Anal. Chem.* **2010**, *82*, 1326−1333.
(291) Peng, P.; Zhou, Z.; Guo, J.; Xiang, Z. Well-Defined 2D Covalent Organic Polymers for Energy Electrocatalysis. *ACS Energy Lett.* **2017**, *2*, 1308−1314.
(292) Sakaushi, K.; Antonietti, M. Carbon and Nitrogen-Based Organic Frameworks. *Acc. Chem. Res.* **2015**, *48*, 1591−1600.
(293) Tian, X. L.; Xu, Y. Y.; Zhang, W.; Wu, T.; Xia, B. Y.; Wang, X. Unsupported Platinum-Based Electrocatalysts for Oxygen Reduction Reaction. *ACS Energy Lett.* **2017**, *2*, 2035−2043.
(294) Lamy, C.; Leger, J.; Garnier, F. Electrocatalytic Properties of Conductive Polymers. In *Handbook of Organic Conductive Molecules and Polymers*; Nalwa, H., Ed.; Wiley: Sussex, England, 1997; Vol. 3, pp 470−496.
(295) Singh, S. K.; Crispin, X.; Zozoulenko, I. V. Oxygen Reduction Reaction in Conducting Polymer PEDOT: Density Functional Theory Study. *J. Phys. Chem. C* **2017**, *121*, 12270−12277.
(296) Meller, G., Grasser, T., Eds. *Organic Electronics*; Springer: Germany, 2010.
(297) Zaki, T. *Short-Channel Organic Thin-Film Transistors*; Springer: Germany, 2015.
(298) Clemens, W., Lupo, D., Hecker, K., Breitung, S., Eds. *OE-A Roadmap for Organic and Printed Electronics*. White Paper, 4th. ed. Organic Electronics Association, 2011, http://www.oe-a.org/en_GB/.
(299) Manna, E.; Xiao, T.; Shinar, J.; Shinar, R. Organic Photodetectors in Analytical Applications. *Electronics* **2015**, *4*, 688−722.
(300) Elkington, D.; Cooling, N.; Belcher, W.; Dastoor, P. C.; Zhou, X. Organic Thin-film Transistor (OTFT)-based Sensors. *Electronics* **2014**, *3*, 234−254.
(301) Liao, C.; Yan, F. Organic Semiconductors in Organic Thin-Film Transistor-Based Chemical and Biological Sensors. *Polym. Rev.* **2013**, *53*, 352−406.
(302) Shinar, R.; Shinar, J. *Organic Electronics in Sensors and Biotechnology*; McGraw-Hill: New York, USA, 2009.
(303) Wang, M.; Wang, X.; Moni, P.; Liu, A.; Kim, D. H.; Jo, W. J.; Sojoudi, H.; Gleason, K. K. CVD Polymers for Devices and Device Fabrication. *Adv. Mater.* **2017**, *29*, 1604606.

DOI: 10.1021/acs.chemrev.7b00482
Chem. Rev. 2018, 118, 4731−4816

(304) Qu, G.; Kwok, J. J.; Diao, Y. Flow-Directed Crystallization for Printed Electronics. *Acc. Chem. Res.* **2016**, *49*, 2756−2764.
(305) Klauk, H. Organic Thin-film Transistors. *Chem. Soc. Rev.* **2010**, *39*, 2643−2666.
(306) LOPEC. What is Printed Electronics? https://www.youtube.com/watch?v=S9e-9skrnsU (accessed 14 Dec 2017).
(307) Zhang, C.; Zang, Y.; Gann, E.; McNeill, C. R.; Zhu, X.; Di, C.-a.; Zhu, D. Two-Dimensional π-Expanded Quinoidal Terthiophenes Terminated with Dicyanomethylenes as n-Type Semiconductors for High-Performance Organic Thin-Film Transistors. *J. Am. Chem. Soc.* **2014**, *136*, 16176−16184.
(308) Ko, S.; Verploegen, E.; Hong, S.; Mondal, R.; Hoke, E. T.; Toney, M. F.; McGehee, M. D.; Bao, Z. 3,4-Disubstituted Polyalkylthiophenes for High-Performance Thin-Film Transistors and Photovoltaics. *J. Am. Chem. Soc.* **2011**, *133*, 16722−16725.
(309) Liu, P.; Wu, Y.; Pan, H.; Ong, B. S.; Zhu, S. High-Performance Polythiophene Thin-Film Transistors Processed with Environmentally Benign Solvent. *Macromolecules* **2010**, *43*, 6368−6373.
(310) Nejati, S.; Minford, T. E.; Smolin, Y. Y.; Lau, K. K. S. Enhanced Charge Storage of Ultrathin Polythiophene Films within Porous Nanostructures. *ACS Nano* **2014**, *8*, 5413−5422.
(311) Krebs, F. C. Fabrication and Processing of Polymer Solar Cells: A Review of Printing and Coating Techniques. *Sol. Energy Mater. Sol. Cells* **2009**, *93*, 394−412.
(312) Angmo, D.; Hosel, M.; Krebs, F. C. Roll-to-roll Processing of Polymer Solar Cells. In *Organic Photovoltaics*, 2nd ed.; Brabec, C. J., Scherf, U., Dyakonov, V., Eds.; Wiley-VCH: Germany, 2014; pp 561−586.
(313) Choi, J.-Y.; Das, S.; Theodore, N. D.; Kim, I.; Honsberg, C.; Choi, H. W.; Alford, T. L. Advances in 2D/3D Printing of Functional Nanomaterials and Their Applications. *ECS J. Solid State Sci. Technol.* **2015**, *4*, P3001−P3009.
(314) Forrest, S. The Path to Ubiquitous and Low-cost Organic Electronic Appliances on Plastic. *Nature* **2004**, *428*, 911−918.
(315) Kaloni, T. P.; Giesbrecht, P. K.; Schreckenbach, G.; Freund, M. S. Polythiophene: From Fundamental Perspectives to Applications. *Chem. Mater.* **2017**, *29*, 10248.
(316) Gupta, S. K.; Jha, P.; Singh, A.; Chehimi, M. M.; Aswal, D. K. Flexible Organic Semiconductor Thin Films. *J. Mater. Chem. C* **2015**, *3*, 8468−8479.
(317) Ogawa, S. *Organic Electronics Materials and Devices*; Springer: Germany, 2015.
(318) Chiba, T.; Pu, Y.-J.; Kido, J. Solution-processable Electron Injection Materials for Organic Light-emitting Devices. *J. Mater. Chem. C* **2015**, *3*, 11567−11576.
(319) Song, T.-B.; Li, N. Emerging Transparent Conducting Electrodes for Organic Light Emitting Diodes. *Electronics* **2014**, *3*, 190−204.
(320) Ahn, S.; Jeong, S.-H.; Han, T.-H.; Lee, T.-W. Conducting Polymers as Anode Buffer Materials in Organic and Perovskite Optoelectronics. *Adv. Opt. Mater.* **2017**, *5*, 1600512.
(321) Yan, W.; Ye, S.; Li, Y.; Sun, W.; Rao, H.; Liu, Z.; Bian, Z.; Huang, C. Hole-Transporting Materials in Inverted Planar Perovskite Solar Cells. *Adv. Energy Mater.* **2016**, *6*, 1600474.
(322) Tang, C. W.; Van Slyke, S. A. Organic Electroluminescent Diodes. *Appl. Phys. Lett.* **1987**, *51*, 913−915.
(323) Tsujimura, T. *OLED Displays*; Wiley: New Jersey, USA, 2012.
(324) Chiba, T.; Pu, Y.-J.; Kido, J. Solution-processable Electron Injection Materials for Organic Light-emitting Devices. *J. Mater. Chem. C* **2015**, *3*, 11567−11576.
(325) Tsumura, A.; Koezuka, H.; Ando, T. Macromolecular Electronic Device: Field Effect Transistor with a Polythiophene Thin Film. *Appl. Phys. Lett.* **1986**, *49*, 1210−1212.
(326) Klauk, H. Organic Thin-film Transistors. *Chem. Soc. Rev.* **2010**, *39*, 2643−2666.
(327) Kaushik, B. K.; Kumar, B.; Prajapati, S.; Mittal, P. *Organic Thin-Film Transistor Applications: Materials to Circuits*; CRC Press: Boca Raton, FL, USA, 2016.
(328) Kagan, C. R., Andry, P., Eds. *Thin-Film Transistors*; Marcel Dekker: New York, 2003; pp 1−34.
(329) Kumar, B.; Kaushik, B.; Negi, Y. S. Organic Thin Film Transistors: Structures, Models, Materials, Fabrication, and Applications: A Review. *Polym. Rev.* **2014**, *54*, 33−111.
(330) Shen, Y.; Hosseini, A.; Wong, M.; Malliaras, G. How to Make Ohmic Contacts to Organic Semiconductors. *ChemPhysChem* **2004**, *5*, 16−25.
(331) Facchetti, A. Polymers Make Charge Flow Easy. *Nature* **2016**, *539*, 499−500.
(332) Charlot, B.; Sassine, G.; Garraud, A.; Sorli, B.; Giani, A.; Combette, P. Micropatterning PEDOT:PSS Layers. *Microsyst. Technol.* **2013**, *19*, 895−903.
(333) Martin, D.; Wu, J.; Shaw, C.; King, Z.; Spanninga, S.; Richardson-Burns, S.; Hendricks, J.; Yang, J. The Morphology of Poly(3,4-Ethylenedioxythiophene). *Polym. Rev.* **2010**, *50*, 340−384.
(334) Dong, B.; Chi, L. Conducting Polymeric Nano/Microstructures: From Fabrication to Sensing Applications. *ACS Symp. Ser.* **2015**, *1215*, 181−197.
(335) Tseng, H.; Phan, H.; Luo, C.; Wang, M.; Perez, L.; Patel, S.; Ying, L.; Kramer, E.; Nguyen, T.; Bazan, G.; Heeger, A. High-Mobility Field-Effect Transistors Fabricated with Macroscopic Aligned Semiconducting Polymers. *Adv. Mater.* **2014**, *26*, 2993−2998.
(336) Chandran, G. T.; Li, X.; Ogata, A.; Penner, R. M. Electrically Transduced Sensors Based on Nanomaterials (2012 - 2016). *Anal. Chem.* **2017**, *89*, 249−275.
(337) Kim, S.; Kwon, J.; Nam, J.; Kim, W.; Park, J. Long-term Stability of Conducting Polymers in Iodine/iodide Electrolytes: Beyond Conventional Platinum Catalysts. *Electrochim. Acta* **2017**, *227*, 95−100.
(338) Kim, S.; Lee, S. J.; Cho, S.; Shin, S.; Jeong, U.; Myoung, J.-M. Improved Stability of Transparent PEDOT:PSS/Ag Nanowire Hybrid Electrodes by Using Non-ionic Surfactants. *Chem. Commun.* **2017**, *53*, 8292−8295.
(339) Fielding, L.; Hillier, J.; Burchell, M.; Armes, S. Space Science Applications for Conducting Polymer Particles: Synthetic Mimics for Cosmic Dust and Micrometeorites. *Chem. Commun.* **2015**, *51*, 16886−16899.
(340) Gueye, M. N.; Carella, A.; Demadrille, R.; Simonato, J.-P. All-Polymeric Flexible Transparent Heaters. *ACS Appl. Mater. Interfaces* **2017**, *9*, 27250−27256.
(341) Gayner, C.; Kar, K. K. Recent Advances in Thermoelectric Materials. *Prog. Mater. Sci.* **2016**, *83*, 330−382.
(342) Shi, H.; Liu, C.; Jiang, Q.; Xu, J. Effective Approaches to Improve the Electrical Conductivity of PEDOT:PSS: A Review. *Adv. Electron. Mater.* **2015**, *1*, 1500017.
(343) Ouyang, J. Secondary Doping Methods to Significantly Enhance the Conductivity of PEDOT:PSS for its Application as Transparent Electrode of Optoelectronic Devices. *Displays* **2013**, *34*, 423−436.
(344) Xia, Y.; Sun, Y.; Ouyang, J. Solution-Processed Metallic Conducting Polymer Films as Transparent Electrode of Optoelectronic Devices. *Adv. Mater.* **2012**, *24*, 2436−2440.
(345) Burke, A.; Miller, M. The Power Capability of Ultracapacitors and Lithium Batteries for Electric and Hybrid Vehicle Applications. *J. Power Sources* **2011**, *196*, 514−522.
(346) Bauman, J.; Kazerani, M. A Comparative Study of Fuel-Cell−Battery, Fuel-Cell−Ultracapacitor, and Fuel-Cell−Battery−Ultracapacitor Vehicles. *IEEE Trans. Veh. Technol.* **2008**, *57*, 760−769.
(347) Conway, B. E.; Birss, V.; Wojtowicz, J. The Role and Utilization of Pseudocapacitance for Energy Storage by Supercapacitors. *J. Power Sources* **1997**, *66*, 1−14.
(348) Dubal, D. P.; Ayyad, O.; Ruiz, V.; Gomez-Romero, P. Hybrid Energy Storage: The Merging of Battery and Supercapacitor Chemistries. *Chem. Soc. Rev.* **2015**, *44*, 1777−1790.
(349) Amatucci, G. G.; Badway, F.; Du Pasquier, A.; Zheng, T. An Asymmetric Hybrid Nonaqueous Energy Storage Cell. *J. Electrochem. Soc.* **2001**, *148*, A930−A939.

DOI: 10.1021/acs.chemrev.7b00482
Chem. Rev. 2018, 118, 4731−4816

(350) Cericola, D.; Kötz, R. Hybridization of Rechargeable Batteries and Electrochemical Capacitors: Principles and Limits. *Electrochim. Acta* **2012**, *72*, 1−17.
(351) Laheäär, A.; Przygocki, P.; Abbas, Q.; Béguin, F. Appropriate Methods for Evaluating the Efficiency and Capacitive Behavior of Different Types of Supercapacitors. *Electrochem. Commun.* **2015**, *60*, 21−25.
(352) Brousse, T.; Belanger, D.; Long, J. W. To Be Or Not to Be Pseudocapacitive? *J. Electrochem. Soc.* **2015**, *162*, A5185−A5189.
(353) Burke, A.; Miller, M. Testing of Electrochemical Capacitors: Capacitance, Resistance, Energy Density, and Power Capability. *Electrochim. Acta* **2010**, *55*, 7538−7548.
(354) Zhao, S.; Wu, F.; Yang, L.; Gao, L.; Burke, A. F. A Measurement Method for Determination of DC Internal Resistance of Batteries and Supercapacitors. *Electrochem. Commun.* **2010**, *12*, 242−245.
(355) Snook, G. A.; Chen, G. Z. The Measurement of Specific Capacitances of Conducting Polymers Using the Quartz Crystal Microbalance. *J. Electroanal. Chem.* **2008**, *612*, 140−146.
(356) Akinwolemiwa, B.; Peng, C.; Chen, G. Z. Redox Electrolytes in Supercapacitors. *J. Electrochem. Soc.* **2015**, *162*, A5054−A5059.
(357) Acevedo Peña, P.; Haro, M.; Rincón, M. E.; Bisquert, J.; Garcia Belmonte, G. Facile Kinetics of Li-ion Intake Causes Superior Rate Capability in MWCNT@TiO_2 Nanocomposite Battery Anodes. *J. Power Sources* **2014**, *268*, 397−403.
(358) Xu, Y.; Wang, J.; Sun, W.; Wang, S. Capacitance Properties of Poly(3,4-ethylenedioxythiophene)/Polypyrrole Composites. *J. Power Sources* **2006**, *159*, 370−373.
(359) Le, T.-H.; Kim, Y.; Yoon, H. Electrical and Electrochemical Properties of Conducting Polymers. *Polymers* **2017**, *9*, 150.
(360) Park, H. W.; Kim, T.; Huh, J.; Kang, M.; Lee, J. E.; Yoon, H. Anisotropic Growth Control of Polyaniline Nanostructures and Their Morphology-Dependent Electrochemical Characteristics. *ACS Nano* **2012**, *6*, 7624−7633.
(361) Chen, W.; Rakhi, R. B.; Alshareef, H. N. Morphology-Dependent Enhancement of the Pseudocapacitance of Template-Guided Tunable Polyaniline Structures. *J. Phys. Chem. C* **2013**, *117*, 15009−15019.
(362) Wang, Z. L.; He, X. J.; Ye, S. H.; Tong, Y. X.; Li, G. R. Design of Polypyrrole/polyaniline Double-walled Nanotube Arrays for Electrochemical Energy Storage. *ACS Appl. Mater. Interfaces* **2014**, *6*, 642−647.
(363) Chen, W.; Rakhi, R. B.; Alshareef, H. N. Facile Synthesis of Polyaniline Nanotubes Using Reactive Oxide Templates for High Density Pseudocapacitors. *J. Mater. Chem. A* **2013**, *1*, 3315−3324.
(364) Wang, K.; Huang, J.; Wei, Z. Conducting Polyaniline Nanowire Arrays for High Performance Supercapacitors. *J. Phys. Chem. C* **2010**, *114*, 8062−8067.
(365) Shi, Ye; Yu, G. *Chem. Mater.* **2016**, *28*, 2466−2477.
(366) Lee, Y.; Noh, S.; Kim, M. S.; Kong, H. J.; Im, K.; Kwon, O. S.; Kim, S.; Yoon, H. The Effect of Nanoparticle Packing on Capacitive Electrode Performance. *Nanoscale* **2016**, *8*, 11940−11948.
(367) Snook, G. A.; Kao, P.; Best, A. S. Conducting-Polymer-Based Supercapacitor Devices and Electrodes. *J. Power Sources* **2011**, *196*, 1−12.
(368) Chae, J. H.; Ng, K. C.; Chen, G. Z. Nanostructured Materials for the Construction of Asymmetrical Supercapacitors. *Proc. Inst. Mech. Eng., Part A* **2010**, *224*, 479−503.
(369) Ghenaatian, H. R.; Mousavi, M. F.; Rahmanifar, M. S. High Performance Hybrid Supercapacitor based on Two Nanostructured Conducting Polymers: Self-Doped Polyaniline and Polypyrrole Nanofibers. *Electrochim. Acta* **2012**, *78*, 212−222.
(370) Mi, H.; Zhang, X.; Ye, X.; Yang, S. Preparation and Enhanced Capacitance of Core-Shell Polypyrrole/Polyaniline Composite Electrode for Supercapacitors. *J. Power Sources* **2008**, *176*, 403−409.
(371) Liu, J.; Zhou, M.; Fan, L.-Z.; Li, P.; Qu, X. Porous Polyaniline Exhibits Highly Enhanced Electrochemical Capacitance Performance. *Electrochim. Acta* **2010**, *55*, 5819−5822.
(372) Zhang, J.; Kong, L.-B.; Li, H.; Luo, Y.-C.; Kang, L. Synthesis of Polypyrrole Film by Pulse Galvanostatic Method and Its Application as Supercapacitor Electrode Materials. *J. Mater. Sci.* **2010**, *45*, 1947−1954.
(373) Pan, L.; Qiu, H.; Dou, C.; Li, Y.; Pu, L.; Xu, J.; Shi, Y. Conducting Polymer Nanostructures: Template Synthesis and Applications in Energy Storage. *Int. J. Mol. Sci.* **2010**, *11*, 2636−2657.
(374) Lu, Q.; Zhao, Q.; Zhang, H.; Li, J.; Wang, X.; Wang, F. Water Dispersed Conducting Polyaniline Nanofibers for High-Capacity Rechargeable Lithium—Oxygen Battery. *ACS Macro Lett.* **2013**, *2*, 92−95.
(375) Pacheco-Catalán, D. E.; Smit, M. A.; Morales, E. Characterization of Composite Mesoporous Carbon/Conducting Polymer Electrodes Prepared by Chemical Oxidation of Gas-Phase Absorbed Monomer for Electrochemical Capacitors. *Inter. J. Electrochem. Science* **2011**, *6*, 78−90.
(376) Bose, S.; Kim, N. H.; Kuila, T.; Lau, K.-T.; Lee, J. H. Electrochemical Performance of a Graphene−Polypyrrole Nanocomposite as a Supercapacitor Electrode. *Nanotechnology* **2011**, *22*, 295202.
(377) Kim, J.-H.; Lee, Y.-S.; Sharma, A. K.; Liu, C. G. Polypyrrole/Carbon Composite Electrode for High-Power Electrochemical Capacitors. *Electrochim. Acta* **2006**, *52*, 1727−1732.
(378) Wang, H.; Hao, Q.; Yang, X.; Lu, L.; Wang, X. Graphene Oxide Doped Polyaniline for Supercapacitors. *Electrochem. Commun.* **2009**, *11*, 1158−1161.
(379) Zhang, K.; Zhang, L. L.; Zhao, X. S.; Wu, J. Graphene/Polyaniline Nanofiber Composites as Supercapacitor Electrodes. *Chem. Mater.* **2010**, *22*, 1392−1401.
(380) Chini, M. K.; Chatterjee, S. Hydrothermally Reduced Nano Porous Graphene-Polyaniline Nanofiber Composites for Supercapacitor. *FlatChem* **2017**, *1*, 1−5.
(381) Wang, H.; Hao, Q.; Yang, X.; Lu, L.; Wang, X. A Nanostructured Graphene/Polyaniline Hybrid Material for Supercapacitors. *Nanoscale* **2010**, *2*, 2164−2170.
(382) Huang, Z. H.; Song, Y.; Xu, X. X.; Liu, X. X. Ordered Polypyrrole Nanowire Arrays Grown on Carbon Cloth Substrate for a High-Performance Pseudocapacitor Electrode. *ACS Appl. Mater. Interfaces* **2015**, *7*, 25506−25513.
(383) Xu, D.; Xu, Q.; Wang, K.; Chen, J.; Chen, Z. Fabrication of Free-Standing Hierarchical Carbon Nanofiber/Graphene Oxide/Polyaniline Films for Supercapacitors. *ACS Appl. Mater. Interfaces* **2014**, *6*, 200−209.
(384) Gupta, S.; Price, C. Investigating Graphene/Conducting Polymer Hybrid Layered Composites as Pseudocapacitors: Interplay of Heterogeneous Electron Transfer, Electric Double Layers and Mechanical Stability. *Composites, Part B* **2016**, *105*, 46−59.
(385) Lee, T.; Yun, T.; Park, B.; Sharma, B.; Song, H.-K.; Kim, B.-S. Hybrid Multilayer Thin Film Supercapacitor of Graphene Nanosheets with Polyaniline: Importance of Establishing Intimate Electronic Contact through Nanoscale Blending. *J. Mater. Chem.* **2012**, *22*, 21092−21099.
(386) Conway, B. E. Capacitance Behavior of Films of Conducting, Electrochemically Reactive Polymers. In *Electrochemical Supercapacitors*; Conway, B. E., Ed.; Springer: Berlin, Germany, 1999; pp 299−334.
(387) Li, J.; Cui, L.; Zhang, X. Preparation and Electrochemistry of One-Dimensional Nanostructured MnO_2/PPy Composite for Electrochemical Capacitor. *Appl. Surf. Sci.* **2010**, *256*, 4339−4343.
(388) Zhao, X.; Johnston, C.; Crossley, A.; Grant, P. S. Printable Magnetite and Pyrrole Treated Magnetite Based Electrodes for Supercapacitors. *J. Mater. Chem.* **2010**, *20*, 7637−7644.
(389) Zou, W.-Y.; Wang, W.; He, B.-L.; Sun, M.-L.; Yin, Y.-S. Supercapacitive Properties of Hybrid Films of Manganese Dioxide and Polyaniline Based on Active Carbon in Organic Electrolyte. *J. Power Sources* **2010**, *195*, 7489−7493.
(390) Zou, B.-X.; Liang, Y.; Liu, X.-X.; Diamond, D.; Lau, K.-T. Electrodeposition and Pseudocapacitive Properties of Tungsten Oxide/Polyaniline Composite. *J. Power Sources* **2011**, *196*, 4842−4848.

DOI: 10.1021/acs.chemrev.7b00482
Chem. Rev. 2018, 118, 4731−4816

(391) Estaline Amitha, F.; Leela Mohana Reddy, A.; Ramaprabhu, S. A Non-Aqueous Electrolyte-Based Asymmetric Supercapacitor with Polymer and Metal Oxide/Multiwalled Carbon Nanotube Electrodes. *J. Nanopart. Res.* **2009**, *11*, 725−729.
(392) Ye, F.; Zhao, B.; Ran, R.; Shao, Z. A Polyanilinne-Coated Mechanochemically, Synthesized Tin Oxide/Graphene Nanocomposite for High Power and High Energy Lithium-Ion Batteries. *J. Power Sources* **2015**, *290*, 61−70.
(393) Fan, X.; Wang, X.; Li, G.; Yu, A.; Chen, Z. High-Performance Flexible Electrode Based on Electrodeposition of Polypyrrole/MnO_2 on Carbon Cloth for Supercapacitors. *J. Power Sources* **2016**, *326*, 357−364.
(394) Guan, C.; Wang, J. Recent Development of Advanced Electrode Materials by Atomic Layer Deposition for Electrochemical Energy Storage. *Adv. Sci.* **2016**, *3*, 1500405.
(395) Xia, C.; Chen, W.; Wang, X.; Hedhili, M. N.; Wei, N.; Alshareef, H. N. Supercapacitors: Highly Stable Supercapacitors with Conducting Polymer Core-Shell Electrodes for Energy Storage Applications. *Adv. Energy Mater.* **2015**, *5*, 1401805.
(396) Genovese, M.; Lian, K. Polyocometalate Modified Inorganic-Organic Nanocomposite Materials for Energy Storage Applications: A Review. *Curr. Opin. Solid State Mater. Sci.* **2015**, *19*, 126−137.
(397) Suppes, G. M.; Deore, B. A.; Freund, M. S. Porous Conducting Polymer/Heteropolyoxometalate Hybrid Material for Electrochemical Supercapacitor Applications. *Langmuir* **2008**, *24*, 1064−1069.
(398) Chithra lekha, P.; Subramanian, S.; Pathinettam Padiyan, D. Investigation of Pseudocapacitance Effect and Frequency Dependence of AC Impedance in Polyaniline-Polyoxometalate Hybrids. *J. Mater. Sci.* **2009**, *44*, 6040−6053.
(399) Balamurugan, A.; Chen, S. M. Silicomolybdate-Doped PEDOT Modified Electrode: Electrocatalytic Reduction of Bromate and Oxidation of Ascorbic Acid. *Electroanalysis* **2007**, *19*, 1616−1622.
(400) Yang, H.; Song, T.; Liu, L.; Devadoss, A.; Xia, F.; Han, H.; Park, H.; Sigmund, W.; Kwon, K.; Paik, U. Polyaniline/Polyoxometalate Hybrid Nanofibers as Cathode for Lithium Ion Batteries with Improved Lithium Storage Capacity. *J. Phys. Chem. C* **2013**, *117*, 17376−17381.
(401) Cuentas-Gallegos, A. K.; Pacheco-Catalán, D.; Miranda-Hernández, M. Environmentally Friendly Supercapacitors. In *Materials for Sustainable Energy Applications: Conversion, Storage, Transmission, and Comsuption*; Moya, X., Muñoz-Rojas, D., Eds.; CRC Press, Taylor & Francis Group, 2016; pp 351−492.
(402) Cuentas Gallegos, A. K.; Rincón, M. E. Carbon Nanofiber and PEDOT-PSS Bilayer Systems as Electrodes for Symmetric and Asymmetric Electrochemical Capacitor Cells. *J. Power Sources* **2006**, *162*, 743−747.
(403) Hussain, A. M. P.; Kumar, A. Enhanced Electrochemical Stability of All-Polymer Redox Supercapacitors with Modified Polypyrrole Electrodes. *J. Power Sources* **2006**, *161*, 1486−1492.
(404) Bhat, D.; Selva Kumar, M. *n*- and *p*-Doped Poly(3,4-ethylenedioxythiophene) Electrode Materials for Symmetric Redox Supercapacitors. *J. Mater. Sci.* **2007**, *42*, 8158−8162.
(405) Conte, M. Supercapacitors Technical Requirements for New Applications. *Fuel Cells* **2010**, *10*, 806−818.
(406) Leela Mohana Reddy, A.; Estaline Amitha, F.; Jafri, I.; Ramaprabhu, S. Asymmetric Flexible Supercapacitor Stack. *Nanoscale Res. Lett.* **2008**, *3*, 145−151.
(407) Qu, Q. T.; Shi, Y.; Li, L. L.; Guo, W. L.; Wu, Y. P.; Zhang, H. P.; Guan, S. Y.; Holze, R. V_2O_5 $0.6H_2O$ Nanoribbons as Cathode Material for Asymmetric Supercapacitor in K_2SO_4 Solution. *Electrochem. Commun.* **2009**, *11*, 1325−1328.
(408) Machida, K.; Suematsu, S.; Ishimoto, S.; Tamamitsu, K. High-Voltage Asymmetric Electrochemical Capacitor Based on Polyfluorene Nanocomposite and Activated Carbon. *J. Electrochem. Soc.* **2008**, *155*, A970−A974.
(409) Hung, P.-J.; Chang, K.-H.; Lee, Y.-F.; Hu, C.-C.; Lin, K.-M. Ideal Asymmetric Supercapacitors Consisting of Polyaniline Nanofibers and Graphene Nanosheets with Proper Complementary Potential Windows. *Electrochim. Acta* **2010**, *55*, 6015−6021.
(410) Wolfart, F.; Hryniewicz, B. N.; Góes, M. S.; Correa, C. M.; Torresi, R.; Minadeo, M. A. O. S.; Córdoba de Torresi, S. I.; Oliveira, R. D.; Marchesi, L. F.; Vidotti, M. Conducting Polymers Revisited: Applications in Energy, Electrochromism and Molecular Recognition. *J. Solid State Electrochem.* **2017**, *21*, 2489−2515.
(411) Long, J. W.; Bélanger, D.; Brousse, T.; Sugimoto, W.; Sassin, M. B.; Crosnier, O. Asymmetric Electrochemical Capacitors − Stretching the Limits of Aqueous Electrolytes. *MRS Bull.* **2011**, *36*, 513−522.
(412) Liang, R. L.; Cao, H. Q.; Qian, D.; Zhang, J. X.; Qu, M. Z. Designed Synthesis of SnO_2-Polyaniline-Reduced Graphene Oxide Nanocomposites as an Anode Material for Lithium-Ion Batteries. *J. Mater. Chem.* **2011**, *21*, 17654−17657.
(413) Dubal, D. P.; Caban-Huertas, Z.; Holze, R.; Gomez-Romero, P. Growth of Polypyrrole Nanostructures Through Reactive Templates for Energy Storage Applications. *Electrochim. Acta* **2016**, *191*, 346−354.
(414) Park, K. S.; Schougaard, S. B.; Goodenough, J. B. Conducting-Polymer/Iron-Redox-Couple Composite Cathodes for Lithium Secondary Batteries. *Adv. Mater.* **2007**, *19*, 848−851.
(415) Qie, L.; Yuan, L. X.; Zhang, W. X.; Chen, W. M.; Huang, Y. H. Revisit of Polypyrrole as Cathode Material for Lithium-Ion Battery. *J. Electrochem. Soc.* **2012**, *159*, A1624.
(416) Abdelhamid, M.; O'Mullane, A.; Snook, G. A. Storing Energy in Plastics: A Review on Conducting Polymers & their Role in Electrochemical Energy Storage. *RSC Adv.* **2015**, *5*, 11611−11626.
(417) Sun, K.; Zhang, S.; Li, P.; Xia, Y.; Zhang, X.; Du, D.; Isikgor, F. H.; Ouyang, J. Review on Application of PEDOTs and PEDOT:PSS in Energy Conversion and Storage Devices. *J. Mater. Sci.: Mater. Electron.* **2015**, *26*, 4438−4462.
(418) Wang, X.; Jiang, K.; Shen, G. Flexible Fiber Energy Storage and Integrated Devices: Recent Progress and Perspectives. *Mater. Today* **2015**, *18*, 265−272.
(419) Lee, J. A.; Shin, M. K.; Kim, S. H.; Cho, H. U.; Spinks, G. M.; Wallace, G. G.; Lima, M. D.; Lepró, X.; Kozlov, M. E.; Baughman, R. H.; Kim, S. J. Ultrafast Charge and Discharge Biscrolled Yarn Supercapacitors for Textiles and Microdevices. *Nat. Commun.* **2013**, *4*, 1970.
(420) Yu, D.; Goh, K.; Wang, H.; Wei, L.; Jiang, W.; Zhang, Q.; Dai, L.; Chen, Y. Scalable Synthesis of Hierarchically Structured Carbon Nanotube−Graphene Fibres for Capacitive Energy Storage. *Nat. Nanotechnol.* **2014**, *9*, 555−562.
(421) Liu, N.; Ma, W.; Tao, J.; Zhang, X.; Su, J.; Li, L.; Yang, C.; Gao, Y.; Golberg, D.; Bando, Y. Cable-Type Supercapacitors of Three-Dimensional Cotton Thread Based Multi-Grade Nanostructures for Wearable Energy Storage. *Adv. Mater.* **2013**, *25*, 4925−4931.
(422) Fu, Y.; Wu, H.; Ye, S.; Cai, X.; Yu, X.; Hou, S.; Kafafy, H.; Zou, D. Integrated Power Fiber for Energy Conversion and Storage. *Energy Environ. Sci.* **2013**, *6*, 805−812.
(423) Zhang, Z.; Chen, X.; Chen, P.; Guan, G.; Qiu, L.; Lin, H.; Yang, Z.; Bai, W.; Luo, Y.; Peng, H. Integrated Polymer Solar Cell and Electrochemical Supercapacitor in a Flexible and Stable Fiber Format. *Adv. Mater.* **2014**, *26*, 466−470.
(424) Li, Z.; Ye, B.; Hu, X.; Ma, X.; Zhang, X.; Deng, Y. Facile Electropolymerized-PANi as Counter Electrode for Low Cost Dye-Sensitized Solar Cell. *Electrochem. Commun.* **2009**, *11*, 1768−1771.
(425) Chal, P.; Shit, A.; Nandi, A. K. Dye-Sensitized Solar Cell from a New Organic n-Type Semiconductor/Polyaniline Composite: Insight from Impedance Spectroscopy. *J. Mater. Chem. C* **2016**, *4*, 272−285.
(426) Yoon, J.-H.; Kim, D.-M.; Yoon, S.-S.; Won, M.-S.; Shim, Y.-B. Comparison of Solar Cell Performance of Conducting Polymer Dyes with Different Functional Groups. *J. Power Sources* **2011**, *196*, 8874−8880.
(427) Zhang, W.; Zhu, R.; Liu, X.-Z.; Liu, B.; Ramakrishna, S. Conjugated Polymer-Sensitized Solar Cells Based On Electrospun TiO_2 Nanofiber Electrode. *Int. J. Nanosci.* **2009**, *8*, 227−230.
(428) Koczkur, K.; Yi, Q.; Chen, A. Nanoporous Pt-Ru Networks and their Electrocatalytical Properties. *Adv. Mater.* **2007**, *19*, 2648−2652.

DOI: 10.1021/acs.chemrev.7b00482
Chem. Rev. 2018, 118, 4731−4816

(429) Briscoe, J.; Dunn, S. The Future of Using Earth-Abundant Elements in Counter Electrodes for Dye-Sensitized Solar Cells. *Adv. Mater.* **2016**, *28*, 3802−3813.
(430) Tang, Q.; Duan, J.; Duan, Y.; He, B.; Yu, L. Recent Advances in Alloy Counter Electrodes for Dye-Sensitized Solar Cells. A Critical Review. *Electrochim. Acta* **2015**, *178*, 886−899.
(431) Theerthagiri, J.; Senthil, A.; Madhavan, J.; Maiyalagan, T. Recent Progress in Non-Platinum Counter Electrode Materials for Dye-Sensitized Solar Cells. *ChemElectroChem* **2015**, *2*, 928−945.
(432) Saranya, K.; Rameez, M.; Subramania, A. Developments in Conducting Polymer Based Counter Electrodes for Dye-Sensitized Solar Cells - An Overview. *Eur. Polym. J.* **2015**, *66*, 207−227.
(433) Tai, Q.; Zhao, X. Pt-free Transparent Counter Electrodes for Cost-effective Bifacial Dye-sensitized Solar Cells. *J. Mater. Chem. A* **2014**, *2*, 13207−13218.
(434) Thomas, S.; Deepak, T. G.; Anjusree, G. S.; Arun, T. A.; Nair, S. V.; Nair, S. A Review on Counter Electrode Materials in Dye-sensitized Solar Cells. *J. Mater. Chem. A* **2014**, *2*, 4474−4490.
(435) Saranya, K.; Rameez, M.; Subramania, A. Developments in Conducting Polymer Based Counter Electrodes for Dye-Sensitized Solar Cells − An Overview. *Eur. Polym. J.* **2015**, *66*, 207−227.
(436) Ye, M.; Wen, X.; Wang, M.; Iocozzia, J.; Zhang, N.; Lin, C.; Lin, Z. Recent Advances in Dye-Sensitized Solar Cells: From Photoanodes, Sensitizers and Electrolytes to Counter Electrodes. *Mater. Today* **2015**, *18*, 155−162.
(437) Li, Q.; Wu, J.; Tang, Q.; Lan, Z.; Li, P.; Lin, J.; Fan, L. Application of Microporous Polyaniline Counter Electrode for Dye-Sensitized Solar Cells. *Electrochem. Commun.* **2008**, *10*, 1299−1302.
(438) Lin, J.-Y.; Wang, W.-Y.; Lin, Y.-T. Characterization of Polyaniline Counter Electrodes for Dye-Sensitized Solar Cells. *Surf. Coat. Technol.* **2013**, *231*, 171−175.
(439) Zhang, J.; Hreid, T.; Li, X.; Guo, W.; Wang, L.; Shi, W.; Su, H.; Yuan, Z. Nanostructured Polyaniline Counter Electrode for Dye-Sensitised Solar Cells: Fabrication and Investigation of Its Electrochemical Formation Mechanism. *Electrochim. Acta* **2010**, *55*, 3664−3668.
(440) Qin, Q.; Guo, Y. Preparation and Characterization of Nano-Polyaniline Film on ITO Conductive Glass by Electrochemical Polymerization. *J. Nanomater.* **2012**, *2012*, 1−6.
(441) Park, K.-H.; Kim, S. J.; Gomes, R.; Bhaumik, A. High Performance Dye-Sensitized Solar Cell by Using Porous Polyaniline Nanotubes as Counter Electrode. *Chem. Eng. J.* **2015**, *260*, 393−398.
(442) He, Z.; Liu, J.; Khoo, S. Y.; Tan, T. T. Y. Electropolymerization of Uniform Polyaniline Nanorod Arrays on Conducting Oxides as Counter Electrodes in Dye-Sensitized Solar Cells. *ChemSusChem* **2016**, *9*, 172−176.
(443) Sun, W.; Peng, T.; Liu, Y.; Xu, S.; Yuan, J.; Guo, S.; Zhao, X.-Z. Hierarchically Porous Hybrids of Polyaniline Nanoparticles Anchored on Reduced Graphene Oxide Sheets as Counter Electrodes for Dye-Sensitized Solar Cells. *J. Mater. Chem. A* **2013**, *1*, 2762−2768.
(444) Ghani, S.; Sharif, R.; Bashir, S.; Ashraf, A.; Shahzadi, S.; Zaidi, A. A.; Rafique, S.; Zafar, N.; Kamboh, A. H. Dye-Sensitized Solar Cells with High-Performance Electrodeposited Gold/Polyaniline Composite Counter Electrodes. *Mater. Sci. Semicond. Process.* **2015**, *31*, 588−592.
(445) He, B.; Tang, Q.; Wang, M.; Chen, H.; Yuan, S. Robust Polyaniline−Graphene Complex Counter Electrodes for Efficient Dye-Sensitized Solar Cells. *ACS Appl. Mater. Interfaces* **2014**, *6*, 8230−8236.
(446) Xia, J.; Chen, L.; Yanagida, S. Application of Polypyrrole as a Counter Electrode for a Dye-Sensitized Solar Cell. *J. Mater. Chem.* **2011**, *21*, 4644−4649.
(447) Rafique, S.; Sharif, R.; Rashid, I.; Ghani, S. Facile Fabrication of Novel Silver-Polypyrrole-Multiwall Carbon Nanotubes Nanocomposite for Replacement of Platinum in Dye-Sensitized Solar Cell. *AIP Adv.* **2016**, *6*, 085018.
(448) Muto, T.; Ikegami, M.; Miyasaka, T. Polythiophene-Based Mesoporous Counter Electrodes for Plastic Dye-Sensitized Solar Cells. *J. Electrochem. Soc.* **2010**, *157*, B1195−B1200.
(449) Erten-Ela, S.; Cogal, S.; Cogal, G. C.; Oksuz, A. U. Highly Conductive Polymer Materials Based Multi-Walled Carbon Nanotubes as Counter Electrodes for Dye-Sensitized Solar Cells. *Fullerenes, Nanotubes, Carbon Nanostruct.* **2016**, *24*, 380−384.
(450) Xia, J.; Masaki, N.; Jiang, K.; Yanagida, S. The Influence of Doping Ions on Poly(3,4-Ethylenedioxythiophene) as a Counter Electrode of a Dye-Sensitized Solar Cell. *J. Mater. Chem.* **2007**, *17*, 2845−2850.
(451) Seo, H.; Son, M.-K.; Itagaki, N.; Koga, K.; Shiratani, M. Polymer Counter Electrode of Poly(3,4-ethylenedioxythiophene):Poly(4-styrenesulfonate) Containing TiO_2 Nano-particles for Dye-Sensitized Solar Cells. *J. Power Sources* **2016**, *307*, 25−30.
(452) Dinari, M.; Momeni, M. M.; Goudarzirad, M. Dye-Sensitized Solar Cells Based on Nanocomposite of Polyaniline/Graphene Quantum Dots. *J. Mater. Sci.* **2016**, *51*, 2964−2971.
(453) Lee, C.-P.; Lin, C.-A.; Wei, T.-C.; Tsai, M.-L.; Meng, Y.; Li, C.-T.; Ho, K.-C.; Wu, C.-I; Lau, S.-P.; He, J.-H. Economical Low-Light Photovoltaics by Using the Pt-Free Dye-Sensitized Solar Cell with Graphene Dot/PEDOT:PSS Counter Electrodes. *Nano Energy* **2015**, *18*, 109−117.
(454) Jeong, G.-H.; Kim, S.-J.; Ko, H.-S.; Han, E.-M.; Park, K. H. Electrochemical Properties of Graphene/PEDOT:PSS Counter Electrode in Dye-sensitized Solar Cells. *Mol. Cryst. Liq. Cryst.* **2015**, *620*, 117−122.
(455) Docampo, P.; Hey, A.; Guldin, S.; Gunning, R.; Steiner, U.; Snaith, H. J. Pore Filling of Spiro-OMeTAD in Solid-State Dye-Sensitized Solar Cells Determined *via* Optical Reflectometry. *Adv. Funct. Mater.* **2012**, *22*, 5010−5019.
(456) Nguyen, W. H.; Bailie, C. D.; Unger, E. L.; McGehee, M. D. Enhancing the Hole-Conductivity of Spiro-OMeTAD without Oxygen or Lithium Salts by Using Spiro(TFSI)2 in Perovskite and Dye-Sensitized Solar Cells. *J. Am. Chem. Soc.* **2014**, *136*, 10996−11001.
(457) Le Ouay, B.; Boudot, M.; Kitao, T.; Yanagida, T.; Kitagawa, S.; Uemura, T. Nanostructuration of PEDOT in Porous Coordination Polymers for Tunable Porosity and Conductivity. *J. Am. Chem. Soc.* **2016**, *138*, 10088−10091.
(458) Zuber, K.; Fabretto, M.; Hall, C.; Murphy, P. Improved PEDOT Conductivity *via* Suppression of Crystallite Formation in Fe(III) Tosylate During Vapor Phase Polymerization. *Macromol. Rapid Commun.* **2008**, *29*, 1503−1508.
(459) Ouyang, J.; Chu, C.-W.; Chen, F.-C.; Xu, Q.; Yang, Y. High-Conductivity Poly(3,4-ethylenedioxythiophene):Poly(styrene sulfonate) Film and Its Application in Polymer Optoelectronic Devices. *Adv. Funct. Mater.* **2005**, *15*, 203−208.
(460) Jin Bae, E.; Hun Kang, Y.; Jang, K.-S.; Yun Cho, S. Enhancement of Thermoelectric Properties of PEDOT:PSS and Tellurium-PEDOT:PSS Hybrid Composites by Simple Chemical Treatment. *Sci. Rep.* **2016**, *6*, 18805.
(461) Obrzut, J.; Page, K. A. Electrical Conductivity and Relaxation in Poly(3-Hexylthiophene). *Phys. Rev. B: Condens. Matter Mater. Phys.* **2009**, *80*, 195211.
(462) Kang, H. C.; Geckeler, K. E. Enhanced Electrical Conductivity of Polypyrrole Prepared by Chemical Oxidative Polymerization: Effect of the Preparation Technique and Polymer Additive. *Polymer* **2000**, *41*, 6931−6934.
(463) Qi, G.; Huang, L.; Wang, H. Highly Conductive Free Standing Polypyrrole Films Prepared by Freezing Interfacial Polymerization. *Chem. Commun.* **2012**, *48*, 8246−8248.
(464) Zhang, Y.; Rutledge, G. C. Electrical Conductivity of Electrospun Polyaniline and Polyaniline-Blend Fibers and Mats. *Macromolecules* **2012**, *45*, 4238−4246.
(465) Song, L.; Wang, W.; Körstgens, V.; González, D. M.; Yao, Y.; Minar, N. R.; Feckl, J. M.; Peters, K.; Bein, T.; Fattakhova-Rohlfing, D.; Santoro, G.; Roth, S. V.; Müller-Buschbaum, P. Spray Deposition of Titania Films with Incorporated Crystalline Nanoparticles for All-Solid-State Dye-Sensitized Solar Cells Using P3HT. *Adv. Funct. Mater.* **2016**, *26*, 1498−1506.
(466) Rani, S.; Mehra, R. M. ZnO Solid-State Dye Sensitized Solar Cells Using Composite Electrolyte of Poly(3-hexylthiophene-2,5-diyl)

DOI: 10.1021/acs.chemrev.7b00482
Chem. Rev. 2018, 118, 4731−4816

and Carbon Nanotubes. *J. Renewable Sustainable Energy* **2009**, *1*, 033109−033112.
(467) Sadoughi, G.; Sivaram, V.; Gunning, R.; Docampo, P.; Bruder, I.; Pschirer, N.; Irajizad, A.; Snaith, H. J. Enhanced Electronic Contacts in SnO_2−Dye−P3HT based Solid State Dye Sensitized Solar Cells. *Phys. Chem. Chem. Phys.* **2013**, *15*, 2075−2080.
(468) Dorman, J. A.; Weickert, J.; Reindl, J. B.; Putnik, M.; Wisnet, A.; Noebels, M.; Scheu, C.; Schmidt-Mende, L. Control of Recombination Pathways in TiO_2 Nanowire Hybrid Solar Cells Using Sn^{4+} Dopants. *J. Phys. Chem. C* **2014**, *118*, 16672−16679.
(469) Liu, Q.; Li, C.; Jiang, K.; Song, Y.; Pei, J. A High-Efficiency Solid-State Dye-Sensitized Solar Cell with P3HT Polymer as a Hole Conductor and an Assistant Sensitizer. *Particuology* **2014**, *15*, 71−76.
(470) Zhang, W.; Zhu, R.; Li, F.; Wang, Q.; Liu, B. High-Performance Solid-State Organic Dye Sensitized Solar Cells with P3HT as Hole Transporter. *J. Phys. Chem. C* **2011**, *115*, 7038−7043.
(471) Park, Y. R.; Lee, Y.-J.; Yu, C.-J.; Kim, J.-H. Investigations of the Polymer Alignment, the Nonradiative Resonant Energy Transfer, and the Photovoltaic Response of Poly(3-hexylthiophene)/TiO_2 Hybrid Solar Cells. *J. Appl. Phys.* **2010**, *108*, 044508.
(472) Park, B.-W.; Yang, L.; Johansson, E. M. J.; Vlachopoulos, N.; Chams, A.; Perruchot, C.; Jouini, M.; Boschloo, G.; Hagfeldt, A. Neutral, Polaron, and Bipolaron States in PEDOT Prepared by Photoelectrochemical Polymerization and the Effect on Charge Generation Mechanism in the Solid-State Dye-Sensitized Solar Cell. *J. Phys. Chem. C* **2013**, *117*, 22484−22491.
(473) Zhang, J.; Vlachopoulos, N.; Jouini, M.; Johansson, M. B.; Zhang, X.; Nazeeruddin, M. K.; Boschloo, G.; Johansson, E. M. J.; Hagfeldt, A. Efficient Solid-State Dye Sensitized Solar Cells: The Influence of Dye Molecular Structures for the In-Situ Photoelectrochemically Polymerized PEDOT as Hole Transporting Material. *Nano Energy* **2016**, *19*, 455−470.
(474) Yamada, K.; Hayakawa, Y.; Okada, T.; Yamamoto, K.; Sonoda, T.; Nakamura, H.; Yamane, H. Effect of Polymeric p-Type Semiconductor on Photovoltaic Properties in Dye-Sensitized Solar Cell. *Mol. Cryst. Liq. Cryst.* **2012**, *567*, 1−8.
(475) Yang, L.; Cappel, U. B.; Unger, E. L.; Karlsson, M.; Karlsson, K. M.; Gabrielsson, E.; Sun, L. C.; Boschloo, G.; Hagfeldt, A.; Johansson, E. M. J. Comparing Spiro-OMeTAD and P3HT Hole Conductors in Efficient Solid State Dye-Sensitized Solar Cells. *Phys. Chem. Chem. Phys.* **2012**, *14*, 779−789.
(476) Yuan, S.; Tang, Q.; He, B.; Yang, P. Efficient Quasi-Solid-State Dye-Sensitized Solar Cells Employing Polyaniline and Polypyrrole Incorporated Microporous Conducting Gel Electrolytes. *J. Power Sources* **2014**, *254*, 98−105.
(477) Snaith, H. J.; Humphry-Baker, R.; Chen, P.; Cesar, I.; Zakeeruddin, S. M.; Gratzel, M. Charge Collection and Pore Filling in Solid-State Dye-Sensitized Solar Cells. *Nanotechnology* **2008**, *19*, 424003.
(478) Zhang, W.; Cheng, Y.; Yin, X.; Liu, B. Solid-State Dye-Sensitized Solar Cells with Conjugated Polymers as Hole-Transporting Materials. *Macromol. Chem. Phys.* **2011**, *212*, 15−23.
(479) Kim, Y.; Sung, Y.-E.; Xia, J.-B.; Lira-Cantu, M.; Masaki, N.; Yanagida, S. Solid-State Dye-Sensitized TiO_2 Solar Cells Using Poly(3,4-ethylenedioxythiophene) as Substitutes of Iodine/Iodide Electrolytes and Noble Metal Catalysts on FTO Counter Electrodes. *J. Photochem. Photobiol., A* **2008**, *193*, 77−80.
(480) Liu, X.; Zhang, W.; Uchida, S.; Cai, L.; Liu, B.; Ramakrishna, S. An Efficient Organic-Dye-Sensitized Solar Cell with In Situ Polymerized Poly(3,4-ethylenedioxythiophene) as a Hole-Transporting Material. *Adv. Mater.* **2010**, *22*, E150−E155.
(481) Zhang, J.; Vlachopoulos, N.; Hao, Y.; Holcombe, T. W.; Boschloo, G.; Johansson, E. M. J.; Grätzel, M.; Hagfeldt, A. Efficient Blue-Colored Solid-State Dye-Sensitized Solar Cells: Enhanced Charge Collection by Using an in Situ Photoelectrochemically Generated Conducting Polymer Hole Conductor. *ChemPhysChem* **2016**, *17*, 1441−1445.
(482) Song, I. Y.; Kim, M.; Park, T. Effect of Ion-Chelating Chain Lengths in Thiophene-Based Monomers on in Situ Photoelectrochemical Polymerization and Photovoltaic Performances. *ACS Appl. Mater. Interfaces* **2015**, *7*, 11482−11489.
(483) Gevaerts, V. S.; Koster, L. J. A.; Wienk, M. M.; Janssen, R. A. J. Discriminating between Bilayer and Bulk Heterojunction Polymer:-Fullerene Solar Cells Using the External Quantum Efficiency. *ACS Appl. Mater. Interfaces* **2011**, *3*, 3252−3255.
(484) Li, S.; Yan, J.; Li, C.-Z.; Liu, F.; Shi, M.; Chen, H.; Russell, T. P. A Non-Fullerene Electron Acceptor Modified by Thiophene-2-Carbonitrile for Solution-Processed Organic Solar Cells. *J. Mater. Chem. A* **2016**, *4*, 3777−3783.
(485) Kesters, J.; Verstappen, P.; Raymakers, J.; Vanormelingen, W.; Drijkoningen, J.; D'Haen, J.; Manca, J.; Lutsen, L.; Vanderzande, D.; Maes, W. Enhanced Organic Solar Cell Stability by Polymer (PCPDTBT) Side Chain Functionalization. *Chem. Mater.* **2015**, *27*, 1332−1341.
(486) Xu, Z.; Chen, L. M.; Chen, M. H.; Li, G.; Yang, Y. Energy Level Alignment of Poly(3-hexylthiophene): [6,6]-phenyl C61 Butyric Acid Methyl Ester Bulk Heterojunction. *Appl. Phys. Lett.* **2009**, *95*, 013301.
(487) Oehzelt, M.; Akaike, K.; Koch, N.; Heimel, G. Energy-Level Alignment at Organic Heterointerfaces. *Sci. Adv.* **2015**, *1*, e1501127.
(488) Glen, T. S.; Scarratt, N. W.; Yi, H.; Iraqi, A.; Wang, T.; Kingsley, J.; Buckley, A. R.; Lidzey, D. G.; Donald, A. M. Dependence on Material Choice of Degradation of Organic Solar Cells Following Exposure to Humid Air. *J. Polym. Sci., Part B: Polym. Phys.* **2016**, *54*, 216−224.
(489) Savva, A.; Burgués-Ceballos, I.; Papazoglou, G.; Choulis, S. A. High-Performance Inverted Organic Photovoltaics without Hole-Selective Contact. *ACS Appl. Mater. Interfaces* **2015**, *7*, 24608−24615.
(490) Xu, T.; Yu, L. How to Design Low Bandgap Polymers for Highly Efficient Organic Solar Cells. *Mater. Today* **2014**, *17*, 11−15.
(491) Wang, D. H.; Kyaw, A. K. K.; Pouliot, J.-R.; Leclerc, M.; Heeger, A. J. Enhanced Power Conversion Efficiency of Low Band-Gap Polymer Solar Cells by Insertion of Optimized Binary Processing Additives. *Adv. Energy Mater.* **2014**, *4*, 1300835.
(492) Kadem, B.; Cranton, W.; Hassan, A. Metal Salt Modified PEDOT: PSS as Anode Buffer Layer and Its Effect on Power Conversion Efficiency of Organic Solar Cells. *Org. Electron.* **2015**, *24*, 73−79.
(493) Duraisamy, N.; Muhammad, N. M.; Hyun, M.-T.; Choi, K.-H. Structural and Electrical Properties of P3HT:PCBM/PEDOT:PSS Thin Films Deposited Through Electrohydrodynamic Atomization Technique. *Mater. Lett.* **2013**, *92*, 227−230.
(494) Huang, Y.-C.; Tsao, C.-S.; Cha, H.-C.; Chuang, C.-M.; Su, C.-J.; Jeng, U.-S.; Chen, C.-Y. Correlation between Hierarchical Structure and Processing Control of Large-area Spray-coated Polymer Solar Cells toward High Performance. *Sci. Rep.* **2016**, *6*, 20062.
(495) Heo, S. W.; Baek, K. H.; Song, H. J.; Lee, T. H.; Moon, D. K. Improved Performance of P3HT:PCBM-Based Solar Cells Using Nematic Liquid Crystals as a Processing Additive under Low Processing Temperature conditions. *Macromol. Mater. Eng.* **2014**, *299*, 353−360.
(496) van Bavel, S. S.; Bärenklau, M.; de With, G.; Hoppe, H.; Loos, J. P3HT/PCBM Bulk Heterojunction Solar Cells: Impact of Blend Composition and 3D Morphology on Device Performance. *Adv. Funct. Mater.* **2010**, *20*, 1458−1463.
(497) Kadem, B.; Hassan, A.; Cranton, W. Efficient P3HT:PCBM Bulk Heterojunction Organic Solar Cells; Effect of Post Deposition Thermal Treatment. *J. Mater. Sci.: Mater. Electron.* **2016**, *27*, 7038−7048.
(498) Verploegen, E.; Miller, C. E.; Schmidt, K.; Bao, Z.; Toney, M. F. Manipulating the Morphology of P3HT−PCBM Bulk Heterojunction Blends with Solvent Vapor Annealing. *Chem. Mater.* **2012**, *24*, 3923−3931.
(499) T. N., A.; K. M., A.; Krishna Pai, R. Hexagonal Columnar Liquid Crystals as a Processing Additive to a P3HT:PCBM Photoactive Layer. *New J. Chem.* **2015**, *39*, 8439−8445.

DOI: 10.1021/acs.chemrev.7b00482
Chem. Rev. 2018, 118, 4731−4816

(500) Long, Y.; Ward, A. J.; Ruseckas, A.; Samuel, I. D. W. Effect of a High Boiling Point Additive on the Morphology of Solution-Processed P3HT-Fullerene Blends. *Synth. Met.* **2016**, *216*, 23−30.
(501) Chen, W.-C.; Xiao, M.-J.; Yang, C.-P.; Duan, L.-R.; Yang, R.-Q. Efficient P3HT:PC61BM Solar Cells Employing 1,2,4-trichlorobenzene as the Processing Additives. *Chin. J. Polym. Sci.* **2017**, *35*, 302−308.
(502) Ng, A.; Liu, X.; To, C.-H.; Djurišić, A. B.; Zapien, J. A.; Chan, W. K. Annealing of P3HT:PCBM Blend Film-The Effect on Its Optical Properties. *ACS Appl. Mater. Interfaces* **2013**, *5*, 4247−4259.
(503) Zhang, W.; Hu, R.; Li, D.; Huo, M.-M.; Ai, X.-C.; Zhang, J. P. Primary Dynamics of Exciton and Charge Photogeneration in Solvent Vapor Annealed P3HT/PCBM Films. *J. Phys. Chem. C* **2012**, *116*, 4298−4310.
(504) Liao, H.-C.; Tsao, C.-S.; Huang, Y.-C.; Jao, M.-H.; Tien, K.-Y.; Chuang, C.-M.; Chen, C.-Y.; Su, C.-J.; Jeng, U.-S.; Chen, Y.-F.; Su, W.-F. Insights into Solvent Vapor Annealing on the Performance of Bulk Heterojunction Solar Cells by a Quantitative Nanomorphology Study. *RSC Adv.* **2014**, *4*, 6246−6253.
(505) Huang, Y.-C.; Chia, H.-C.; Chuang, C.-M.; Tsao, C.-S.; Chen, C.-Y.; Su, W.-F. Facile Hot Solvent Vapor Annealing for High Performance Polymer Solar Cell Using Spray Process. *Sol. Energy Mater. Sol. Cells* **2013**, *114*, 24−30.
(506) Tang, H.; Lu, G.; Li, L.; Li, J.; Wang, Y.; Yang, X. Precise construction of PCBM Aggregates for Polymer Solar Cells *via* Multi-Step Controlled Solvent Vapor Annealing. *J. Mater. Chem.* **2010**, *20*, 683−688.
(507) Sowjanya Pali, L. S.; Ganesan, P.; Garg, A. Inverted P3HT:PCBM Organic Solar Cells on Low Carbon Steel Substrates. *Sol. Energy* **2016**, *133*, 339−348.
(508) Fukuda, T.; Toda, A.; Takahira, K.; Suzuki, K.; Liao, Y.; Hirahara, M.; Saito, M.; Osaka, I. Molecular Ordering of Spin-Coated and Electrosprayed P3HT:PCBM Thin Films and Their Applications to Photovoltaic Cell. *Thin Solid Films* **2016**, *612*, 373−380.
(509) Gupta, S. K.; Jindal, R.; Garg, A. Microscopic Investigations into the Effect of Surface Treatment of Cathode and Electron Transport Layer on the Performance of Inverted Organic Solar Cells. *ACS Appl. Mater. Interfaces* **2015**, *7*, 16418−16427.
(510) Chen, C.-Y.; Tsao, C. S.; Huang, Y. C.; Liu, H. W.; Chiu, W. Y.; Chuang, C. M.; Jeng, U. S.; Su, C. J.; Wu, W. R.; Su, W. F.; Wang, L. Mechanism and Control of Structural Evolution of Polymer Solar Cell from Bulk Heterojunction to Thermally Unstable Hierarchical Structure. *Nanoscale* **2013**, *5*, 7629−7638.
(511) Kim, Y.; Kim, G.; Lee, J.; Lee, K. Morphology Controlled Bulk-Heterojunction Layers of Fully Electro-Spray Coated Organic Solar Cells. *Sol. Energy Mater. Sol. Cells* **2012**, *105*, 272−279.
(512) Duraisamy, N.; Muhammad, N. M.; Hyun, M.-T.; Choi, K.-H. Structural and Electrical properties of P3HT:PCBM/PEDOT:PSS Thin Films Deposited Through Electrohydrodynamic Atomization Technique. *Mater. Lett.* **2013**, *92*, 227−230.
(513) Lei, T.; Wang, J.-Y.; Pei, J. Design, Synthesis, and Structure-Property Relationships of Isoindigo-Based Conjugated Polymers. *Acc. Chem. Res.* **2014**, *47*, 1117−1126.
(514) Cheng, Y.-J.; Yang, S.-H.; Hsu, C.-S. Synthesis of Conjugated Polymers for Organic Solar Cell Applications. *Chem. Rev.* **2009**, *109*, 5868−5923.
(515) Yuen, J. D.; Wudl, F. Strong Acceptors in Donor-Acceptor Polymers for High Performance Thin Film Transistors. *Energy Environ. Sci.* **2013**, *6*, 392−406.
(516) Nielsen, C. B.; Turbiez, M.; McCulloch, I. Recent Advances in the Development of Semiconducting DPP-Containing Polymers for Transistor Applications. *Adv. Mater.* **2013**, *25*, 1859−1880.
(517) Zhan, X.; Facchetti, A.; Barlow, S.; Marks, T. J.; Ratner, M. A.; Wasielewski, M. R.; Marder, S. R. Rylene and Related Diimides for Organic Electronics. *Adv. Mater.* **2011**, *23*, 268−284.
(518) Xu, T.; Yu, L. How to Design Low Band Gap Polymers for Highly Efficient Organic Solar Cells. *Mater. Today* **2014**, *17*, 11−15.
(519) Deng, Y.; Liu, J.; Wang, J.; Liu, L.; Li, W.; Tian, H.; Zhang, X.; Xie, Z.; Geng, Y.; Wang, F. Dithienocarbazole and Isoindigo Based Amorphous Low Bandgap Conjugated Polymers for Efficient Polymer Solar Cells. *Adv. Mater.* **2014**, *26*, 471−476.
(520) Wang, E.; Ma, Z.; Zhang, Z.; Vandewal, K.; Henriksson, P.; Inganäs, O.; Zhang, F.; Andersson, M. R. An Easily Accessible Isoindigo-Based Polymer for High-Performance Polymer Solar Cells. *J. Am. Chem. Soc.* **2011**, *133*, 14244−14247.
(521) Meager, I.; Ashraf, R. S.; Mollinger, S.; Schroeder, B. C.; Bronstein, H.; Beatrup, D.; Vezie, M. S.; Kirchartz, T.; Salleo, A.; Nelson, J.; McCulloch, I. Photocurrent Enhancement from Diketopyrrolopyrrole Polymer Solar Cells through Alkyl-Chain Branching Point Manipulation. *J. Am. Chem. Soc.* **2013**, *135*, 11537−11540.
(522) Livi, F.; Carle, J.; Bundgaard, E. Thiophene in Conducting Polymers: Synthesis of Poly(thiophene)s and Other Conjugated Polymers Containing Thiophenes, for Application in Polymer Solar Cells. In *Thiophenes*; Joule, J. A., Ed.; Topics in Heterocyclic Chemistry, Springer-Verlag: Berlin Heidelberg, 2015; Vol. *39*, p 203−226.
(523) Mehmood, U.; Al-Ahmed, A.; Hussein, I. A. Review on recent advances in polythiophene based photovoltaic devices. *Renewable Sustainable Energy Rev.* **2016**, *57*, 550−561.
(524) Meyer, F. Fluorinated Conjugated Polymers in Organic Bulk Heterojunction Photovoltaic Solar Cells. *Prog. Polym. Sci.* **2015**, *47*, 70−91.
(525) Yu, Y.; Teran, G.; Caicedo, J.; Gonzalez, I.; Lira, M. In *Conducting Polymers: Synthesis, characterization and applications*; Pimentel, L., Ed.; Nova Science Publishers, Inc.: Hauppauge, NY, 2013; pp 315−343.
(526) Jeffries-El, M.; Kobilka, B. M.; Hale, B. J. Optimizing the Performance of Conjugated Polymers in Organic Photovoltaic Cells by Traversing Group 16. *Macromolecules* **2014**, *47*, 7253−7271.
(527) McCarthy, J. E.; Hanley, C. A.; Brennan, L. J.; Lambertini, V. G.; Gun'ko, Y. K. Fabrication of Highly Transparent and Conducting PEDOT:PSS Films Using a Formic Acid Treatment. *J. Mater. Chem. C* **2014**, *2*, 764−770.
(528) Zhang, F. J.; Vollmer, A.; Zhang, J.; Xu, Z.; Rabe, J. P.; Koch, N. Energy Level Alignment and Morphology of Interfaces Between Molecular and Polymeric Organic Semiconductors. *Org. Electron.* **2007**, *8*, 606−614.
(529) Kim, S.; Kim, S. Y.; Chung, M. H.; Kim, J.; Kim, J. H. A One-Step Roll-To-Roll Process of Stable AgNW/PEDOT:PSS Solution Using Imidazole as a Mild Base for Highly Conductive and Transparent Films: Optimizations and Mechanisms. *J. Mater. Chem. C* **2015**, *3*, 5859−5868.
(530) De Jong, M. P.; Van Ijzendoorn, L. J.; De Voigt, M. J. A. Stability of the Interface Between Indium-Tin-Oxide and Poly (3, 4-ethylenedioxythiophene)/Poly (styrenesulfonate) in Polymer Light-Emitting Diodes. *Appl. Phys. Lett.* **2000**, *77*, 2255−2257.
(531) Grossiord, N.; Kroon, J. M.; Andriessen, R.; Blom, P. W. M. Degradation Mechanisms in Organic Photovoltaic Devices. *Org. Electron.* **2012**, *13*, 432−456.
(532) Zhang, Y.; Chen, L.; Hu, X.; Zhang, L.; Chen, Y. Low Work-function Poly(3,4-ethylenedioxylenethiophene): Poly(styrene sulfonate) as Electron-transport Layer for High-efficient and Stable Polymer Solar Cells. *Sci. Rep.* **2015**, *5*, 12839.
(533) Park, Y.; Soon Choi, K. S.; Young Kim, S. Y. Graphene Oxide/PEDOT:PSS and Reduced Graphene Oxide/PEDOT:PSS Hole Extraction Layers in Organic Photovoltaic Cells. *Phys. Status Solidi A* **2012**, *209*, 1363−1368.
(534) Palma-Cando, A. U.; Frontana-Uribe, B. A.; Maldonado, J. L.; Hernández, M. R. Control of Thickness of PEDOT Electrodeposits on Glass/ITO Electrodes from Organic Solutions and its Use as Anode in Organic Solar Cells. *Procedia Chem.* **2014**, *12*, 92−99.
(535) Del-Oso, J. A.; Frontana-Uribe, B. A.; Maldonado, J.-L.; Rivera, M.; Tapia-Tapia, M.; Roa-Morales, G. Electrochemical deposition of poly[ethylene-dioxythiophene] (PEDOT) films on ITO electrodes for organic photovoltaic cells: control of morphology, thickness, and electronic properties. *J. Solid State Electrochem.* **2018**, DOI: 10.1007/s10008-018-3909-z.

DOI: 10.1021/acs.chemrev.7b00482
Chem. Rev. 2018, 118, 4731−4816

(536) Frohne, H.; Shaheen, S. E.; Brabec, C. J.; Müller, D. C.; Sariciftci, N. S.; Meerholz, K. Influence of the Anodic Work Function on the Performance of Organic Solar Cells. *ChemPhysChem* **2002**, *3*, 795−799.
(537) Rider, D. A.; Harris, K. D.; Wang, D.; Bruce, J.; Fleischauer, M. D.; Tucker, R. T.; Brett, M. J.; Buriak, J. B. Thienylsilane-modified Indium Tin Oxide as an Anodic Interface in Polymer/Fullerene Solar Cells. *ACS Appl. Mater. Interfaces* **2009**, *1*, 279−288.
(538) Vlamidis, Y.; Lanzi, M.; Salatelli, E.; Gualandi, I.; Fraboni, B.; Setti, L.; Tonelli, D. Electrodeposition of PEDOT Perchlorate as an Alternative Route to PEDOT: PSS for the Development of Bulk Heterojunction Solar Cells. *J. Solid State Electrochem.* **2015**, *19*, 1685−1693.
(539) Nasybulin, E.; Wei, S.; Cox, M.; Kymissis, I.; Levon, K. Morphological and Spectroscopic Studies of Electrochemically Deposited Poly(3, 4-ethylenedioxythiophene)(PEDOT) Hole Extraction Layer for Organic Photovoltaic. *J. Phys. Chem. C* **2011**, *115*, 4307−4314.
(540) Fan, X.; Wang, J.; Wang, H.; Liu, X.; Wang, H. Bendable ITO-free Organic Solar Cells with Highly Conductive and Flexible PEDOT:PSS Electrodes on Plastic Substrates. *ACS Appl. Mater. Interfaces* **2015**, *7*, 16287−16295.
(541) dos Reis Benatto, G. A.; Roth, B.; Corazza, M.; Søndergaard, R. R.; Gevorgyan, S. A.; Jørgensen, M.; Krebs, F. C. Roll-To-Roll Printed Silver Nanowires for Increased Stability of Flexible ITO-Free Organic Solar Cell Modules. *Nanoscale* **2016**, *8*, 318−326.
(542) Na, S.-I.; Kim, S.-S.; Jo, J.; Kim, D.-Y. Efficient and Flexible ITO-Free Organic Solar Cells Using Highly Conductive Polymer Anodes. *Adv. Mater.* **2008**, *20*, 4061−4067.
(543) He, M.; Zheng, D.; Wang, M.; Lin, C.; Lin, Z. High Efficiency Perovskite Solar Cells: from Complex Nanostructure to Planar Heterojunction. *J. Mater. Chem. A* **2014**, *2*, 5994−6003.
(544) Lim, K.-G.; Ahn, S.; Kim, H.; Choi, M.-R.; Huh, D. H.; Lee, T.-W. Self-Doped Conducting Polymer as a Hole-Extraction Layer in Organic−Inorganic Hybrid Perovskite Solar Cells. *Adv. Mater. Interfaces* **2016**, *3*, 1500678.
(545) Li, Y.; Meng, L.; Yang, Y. M.; Xu, G.; Hong, Z.; Chen, Q.; You, J.; Li, G.; Yang, Y.; Li, Y. High-Efficiency Robust Perovskite Solar Cells on Ultrathin Flexible Substrates. *Nat. Commun.* **2016**, *7*, 10214.
(546) Kim, G.-W.; Kang, G.; Kim, J.; Lee, G.-Y.; Kim, H. I.; Pyeon, L.; Lee, J.; Park, T. Dopant-Free Polymeric Hole Transport Materials for Highly Efficient and Stable Perovskite Solar Cells. *Energy Environ. Sci.* **2016**, *9*, 2326−2333.
(547) Yan, W.; Li, Y.; Li, Y.; Ye, S.; Liu, Z.; Wang, S.; Bian, Z.; Huang, C. High-Performance Hybrid Perovskite Solar Cells with Open Circuit Voltage Dependence on Hole-Transporting Materials. *Nano Energy* **2015**, *16*, 428−437.
(548) Ameen, S.; Akhtar, M. S.; Seo, H. K.; Shin, H. S. Photocurrent Induced by Conducting Channels of Hole Transporting Layer to Adjacent Photoactive Perovskite Sensitized TiO_2 Thin Film: Solar Cell Paradigm. *Langmuir* **2014**, *30*, 12786−12794.
(549) Xiao, Y.; Han, G.; Chang, Y.; Zhou, H.; Li, M.; Li, Y. An All-Solid-State Perovskite-Sensitized Solar Cell Based on the Dual Function Polyaniline as the Sensitizer and p-Type Hole-Transporting Material. *J. Power Sources* **2014**, *267*, 1−8.
(550) Wu, Y.; Wang, J.; Qiu, X.; Yang, R.; Lou, H.; Bao, X.; Li, Y. Highly Efficient Inverted Perovskite Solar Cells With Sulfonated Lignin Doped PEDOT as Hole Extract Layer. *ACS Appl. Mater. Interfaces* **2016**, *8*, 12377−12383.
(551) Guo, Y.; Sato, W.; Inoue, K.; Zhang, W.; Yu, G.; Nakamura, E. n-Type Doping for Efficient Polymeric Electron-Transporting Layers in Perovskite Solar Cells. *J. Mater. Chem. A* **2016**, *4*, 18852−18856.
(552) Rajamanickam, N.; Kumari, S.; Vendra, V. K.; Lavery, B. W.; Spurgeon, J.; Druffel, T.; Sunkara, M. K. Stable and Durable $CH_3NH_3PbI_3$ Perovskite Solar Cells at Ambient Conditions. *Nanotechnology* **2016**, *27*, 235404.
(553) Manshor, N. A.; Wali, Q.; Wong, K. K.; Muzakir, S. K.; Fakharuddin, A.; Schmidt-Mende, L.; Jose, R. Humidity versus Photo-Stability of Metal Halide Perovskite Films in a Polymer Matrix. *Phys. Chem. Chem. Phys.* **2016**, *18*, 21629−21639.
(554) Muckley, E. S.; Jacobs, C. B.; Vidal, K.; Mahalik, J. P.; Kumar, R.; Sumpter, B. G.; Ivanov, I. N. New Insights on Electro-Optical Response of Poly(3,4 ethylenedioxythiophene):Poly(styrenesulfonate) Film to Humidity. *ACS Appl. Mater. Interfaces* **2017**, *9*, 15880−15886.
(555) Liu, Y.; Hong, Z.; Chen, Q.; Chang, W.; Zhou, H.; Song, T.-B.; Young, E.; Yang, Y. M.; You, J.; Li, G.; Yang, Y. Integrated Perovskite/Bulk-Heterojunction toward Efficient Solar Cells. *Nano Lett.* **2015**, *15*, 662−668.
(556) Chiang, C.-H.; Wu, C.-G. Bulk Heterojunction Perovskite−PCBM Solar Cells With High Fill Factor. *Nat. Photonics* **2016**, *10*, 196−200.
(557) Yan, W.; Ye, S.; Li, Y.; Sun, W.; Rao, H.; Liu, Z.; Bian, Z.; Huang, C. Hole-Transporting Materials in Inverted Planar Perovskite Solar Cells. *Adv. Energy Mater.* **2016**, *6*, 1600474.
(558) Lee, K.; Cho, K. H.; Ryu, J.; Yun, J.; Yu, H.; Lee, J.; Na, W.; Jang, J. Low-Cost and Efficient Perovskite Solar Cells Using a Surfactant-Modified Polyaniline:Poly(styrenesulfonate) Hole Transport Material. *Electrochim. Acta* **2017**, *224*, 600−607.
(559) Su, P.-Y.; Huang, L.-B.; Liu, J.-M.; Chen, Y.-F.; Xiao, L.-M.; Kuang, D. B.; Mayor, M.; Su, C.-Y. A Multifunctional Poly-N-Vinylcarbazole Interlayer in Perovskite Solar Cells for High Stability and Efficiency: a Test with New Triazatruxene-based Hole Transporting Materials. *J. Mater. Chem. A* **2017**, *5*, 1913−1918.
(560) Wang, H.; Rahaq, Y.; Kumar, V. A Composite Light-Harvesting Layer from Photoactive Polymer and Halide Perovskite for Planar Heterojunction Solar Cells. *Sci. Rep.* **2016**, *6*, 29567.
(561) Chiang, C.-H.; Chen, S.-C.; Wu, C.-G. Preparation of Highly Concentrated and Stable Conducting Polymer Solutions and their Application in High-Efficiency Dye-Sensitized Solar Cell. *Org. Electron.* **2013**, *14*, 2369−2378.
(562) Jeon, S. S.; Kim, C.; Ko, J.; Im, S. S. Spherical Polypyrrole Nanoparticles as a Highly Efficient Counter Electrode for Dye-Sensitized Solar Cells. *J. Mater. Chem.* **2011**, *21*, 8146−8151.
(563) Janek, J.; Zeier, W. G. A Solid Future for Battery Development. *Nature Energy* **2016**, *1*, No. 16141.
(564) Adelhelm, P.; Janek, J. Zukunftstechnologien. In *Handbuch Lithium-Ionen-Batterien*; Korthauer, R., Ed.; Springer-Verlag, Berlin, Heidelberg, 2013; pp 199−217.
(565) Pang, Q.; Liang, X.; Kwok, C. Y.; Nazar, L. F. Advances in Lithium-Sulfur Batteries based on Multifunctional Cathodes and Electrolytes. *Nature Energy* **2016**, *1*, No. 16132.
(566) Li, W.; Zhang, Q.; Zheng, G.; Seh, Z. W.; Yao, H.; Cui, Y. Understanding the Role of Different Conductive Polymers in Improving the Nanostructured Sulfur Cathode Performance. *Nano Lett.* **2013**, *13*, 5534−5540.
(567) Seh, Z. W.; Wang, H.; Hsu, P.-C.; Zhang, Q.; Li, W.; Zheng, G.; Yao, H.; Cui, Y. Facile Synthesis of Li_2S-Polypyrrole Composite Structures for High-Performance Li_2S Cathodes. *Energy Environ. Sci.* **2014**, *7*, 672−676.
(568) Gupta, D.; Wienk, M. M.; Janssen, R. A. J. Efficient Polymer Solar Cells on Opaque Substrates with a Laminated PEDOT:PSS Top Electrode. *Adv. Energy Mater.* **2013**, *3*, 782−787.
(569) Li, Z.; Kulkarni, S. A.; Boix, P. P.; Shi, E.; Cao, A.; Fu, K.; Batabyal, S. K.; Zhang, J.; Xiong, Q.; Wong, L. H.; Mathews, N.; Mhaisalkar, S. G. Laminated Carbon Nanotube Networks for Metal Electrode-free Efficient Perovskite Solar Cells. *ACS Nano* **2014**, *8*, 6797−6804.
(570) Li, M.; Gao, K.; Wan, X.; Zhang, Q.; Kan, B.; Xia, R.; Liu, F.; Yang, X.; Feng, H.; Ni, W.; Peng, J.; Zhang, H.; Liang, Z.; Yip, H.-L.; Peng, X.; Cao, Y.; Chen, Y.; Wang, Y. Solution-Processed Organic Tandem Solar Cells with Power Conversion Efficiencies > 12%. *Nat. Photonics* **2017**, *11*, 85−90.
(571) Li, N.; Baran, D.; Spyropoulos, G. D.; Zhang, H.; Berny, S.; Turbiez, M.; Ameri, T.; Krebs, F. C.; Brabec, C. J. Environmentally Printing Efficient Organic Tandem Solar Cells with High Fill Factors: A Guideline Towards 20% Power Conversion Efficiency. *Adv. Energy Mater.* **2014**, *4*, 1400084.

DOI: 10.1021/acs.chemrev.7b00482
Chem. Rev. 2018, 118, 4731−4816

(572) Hong, Z.; Dou, L.; Li, G.; Yang, Y. Tandem Solar Cell—Concept and Practice in Organic Solar Cells. In *Progress in High-Efficient Solution Process Organic Photovoltaic Devices*; Yang, Y., Li, G., Eds.; Topics in Applied Physics series 130; Springer-Verlag: Berlin, Heidelberg, 2015; pp 315—346.
(573) Kolesov, V. A.; Fuentes-Hernandez, C.; Chou, W.-F.; Aizawa, N.; Larrain, F. A.; Wang, M.; Perrotta, A.; Choi, S.; Graham, S.; Bazan, G. C.; Nguyen, T.-Q.; Marder, S. R.; Kippelen, B. Solution-Based Electrical Doping of Semiconducting Polymer Films Over a Limited Depth. *Nat. Mater.* **2017**, *16*, 474—480.
(574) Chen, H.-W.; Huang, T.-Y.; Chang, T.-H.; Sanehira, Y.; Kung, C.-W.; Chu, C.-W.; Ikegami, M.; Miyasaka, T.; Ho, K.-C. Efficiency Enhancement of Hybrid Perovskite Solar Cells with MEH-PPV Hole-Transporting Layers. *Sci. Rep.* **2016**, *6*, 34319.
(575) Alatorre, M. A.; Gutiérrez, S.; Páramo, U.; Ibanez, J. G. Reduction of Hexavalent Chromium by Polypyrrole Deposited on Different Carbon Substrates. *J. Appl. Electrochem.* **1998**, *28*, 551—557.
(576) Hepel, M.; Xingmin, Z.; Stephenson, R.; Perkins, S. Use of Electrochemical Quartz Crystal Microbalance Technique to Track Electrochemically Assisted Removal of Heavy Metals from Aqueous Solutions by Cation-Exchange Composite Polypyrrole-Modified Electrodes. *Microchem. J.* **1997**, *56*, 79—92.
(577) Wang, J.; Deng, B.; Chen, H.; Wang, X.; Zheng, J. Removal of Aqueous Hg(II) by Polyaniline: Sorption Characteristics and Mechanisms. *Environ. Sci. Technol.* **2009**, *43*, 5223—5228.
(578) Bhaumik, M.; Maity, A.; Srinivasu, V. V.; Onyango, M. S. Removal of Hexavalent Chromium from Aqueous Solution Using Polypyrrole-Polyaniline Nanofibers. *Chem. Eng. J.* **2012**, *181—182*, 323—333.
(579) Kumar, P. A.; Chakraborty, S.; Ray, M. Removal and Recovery of Chromium from Wastewater Using Short Chain Polyaniline Synthesized on Jute Fiber. *Chem. Eng. J.* **2008**, *141*, 130—140.
(580) Baba, A.; Tian, S.; Stefani, F.; Xia, C.; Wang, Z.; Advincula, R. C.; Johannsmann, D.; Knoll, W. Doping/Dedoping Properties of Polyaniline Thin Films as Studied by Electrochemical-Surface Plasmon Spectroscopy and by the Quartz Crystal Microbalance. *J. Electroanal. Chem.* **2004**, *562*, 95—103.
(581) Hepel, M.; Dentrone, L. Controlled Incorporation of Heavy Metals from Aqueous Solutions and Their Electrorelease Using Composite Polypyrrole Films. *Electroanalysis* **1996**, *8*, 996—1005.
(582) Hepel, M.; Stephenson, R. Removal of Residual Nickel Ions from Aqueous Solutions Using Conductive Polymer Films. Presented at the 15th AESF/EPA Pollution Prevention & Control Conference, Jan. 24—27, Kissimee, FL, USA. 1994.
(583) Silk, T.; Tamm, J. Voltammetric Study of the Influence of Cations on the Redox Switching Process of Halogenide-Doped Polypyrrole. *Electrochim. Acta* **1996**, *41*, 1883—1885.
(584) Ruotolo, L. A. M.; Gubulin, J. C. A Factorial-Design Study of the Variables Affecting the Electrochemical Reduction of Cr(VI) at Polyaniline-Modified Electrodes. *Chem. Eng. J.* **2005**, *110*, 113—121.
(585) Muhammad Ekramul Mahmud, H. N.; Huq, A. K. O.; Yahya, R. B. The removal of heavy metal ions from wastewater/aqueous solution using polypyrrole-based adsorbents: A review. *RSC Adv.* **2016**, *6*, 14778—14791.
(586) Lin, Y.; Cui, X.; Bontha, J. Electrically Controlled Anion Exchange Based on Polypyrrole and Carbon Nanotubes Nanocomposite for Perchlorate Removal. *Environ. Sci. Technol.* **2006**, *40*, 4004—4009.
(587) Weidlich, C.; Mangold, K. M.; Jüttner, K. Electrochemistry of Electrocactive Materials. EQCM Study of the Ion Exchange Behaviour of Polypyrrole with Different Counterions in Different Electrolytes. *Electrochim. Acta* **2005**, *50*, 1547—1552.
(588) Careem, M. A.; Velmurugu, Y.; Skaarup, S.; West, K. A Voltammetry Study on the Diffusion of Counter Ions in Polypyrrole Films. *J. Power Sources* **2006**, *159*, 210—214.
(589) Suarez, M. F.; Compton, R. G. In Situ Atomic Force Microscopy Study of Polypyrrole Synthesis and the Volume Changes Induced by Oxidation and Reduction of the Polymer. *J. Electroanal. Chem.* **1999**, *462*, 211—221.
(590) Sadki, S.; Schottland, P.; Brodie, N.; Sabouraud, G. The Mechanisms of Pyrrole Electropolymerization. *Chem. Soc. Rev.* **2000**, *29*, 283—293.
(591) Hallik, A.; Alumaa, A.; Kurig, H.; Jänes, A.; Lust, E.; Tamm, J. On the Porosity of Polypyrrole Films. *Synth. Met.* **2007**, *157*, 1085—1090.
(592) Tamm, J.; Alumaa, A.; Hallik, A.; Sammelselg, V. Electrochemical Properties of Cation Sensitive Polypyrrole Films. *J. Electroanal. Chem.* **1998**, *448*, 25—31.
(593) Glidle, A.; Hillman, A. R.; Ryder, K. S.; Smith, E. L.; Cooper, J. M.; Dalgliesh, R.; Cubitt, R.; Geue, T. Metal Chelation and Spatial Profiling of Components in Crown Ether Functionalised Conducting Copolymer Films. *Electrochim. Acta* **2009**, *55*, 439—450.
(594) Han, J.; Fang, P.; Dai, J.; Guo, R. One-pot Surfactantless Route to Polyaniline Hollow Nanospheres with Incontinuous Multicavities and Application for the Removal of Lead Ions from Water. *Langmuir* **2012**, *28*, 6468—6475.
(595) Hosseini, S.; Ekramul Mahmud, N. H. M.; Binti Yahya, R.; Ibrahim, F.; Djordjevic, I. Polypyrrole Conducting Polymer and its Application in Removal of Copper Ions from Aqueous Solution. *Mater. Lett.* **2015**, *149*, 77—80.
(596) Olatunji, M. A.; Khandaker, M. U.; Amin, Y. M.; Ekramul-Mahmud, H. N. M. Development and Characterization of Polypyrrole-Based Nanocomposite Adsorbent and its Applications in Removal of Radioactive Materials. Presented at the International Conference for Innovation in Biomedical Engineering and Life Sciences, Dec 6—8, Putrajaya, Malaysia. 2015.
(597) Mohammad, A.; Inamuddin; Hussain, S. Poly (3,4-ethylenedioxythiophene): Polystyrene Sulfonate (PEDOT: PSS) Zr(IV) Phosphate Composite Cation Exchanger: Sol-Gel Synthesis and Physicochemical Characterization. *Ionics* **2015**, *21*, 1063—1071.
(598) Zoleikani, L.; Issazadeh, H.; ZareNezhad, B. Preparation of New Conductive Polymer Nanocomposites for Cadmium Removal from Industrial Wastewaters. *J. Chem. Technol. Metall.* **2015**, *50*, 71—80.
(599) Zhang, Y.; Mu, S.; Deng, B.; Zheng, J. Electrochemical Removal and Release of Perchlorate Using Poly(aniline-*co*-*o*-aminophenol). *J. Electroanal. Chem.* **2010**, *641*, 1—6.
(600) Hepel, M. Polypyrrole Supported Catalysts with Pt Nanoparticles. Presented at the 189th Meeting of the Electrochemical Society, Los Angeles, CA, May 5—10, 1996.
(601) Huang, Y.; Ma, H.; Wang, S.; Shen, M.; Guo, R.; Cao, X.; Zhu, M.; Shi, X. Efficient Catalytic Reduction of Hexavalent Chromium Using Palladium Nanoparticle-Immobilized Electrospun Polymer Nanofibers. *ACS Appl. Mater. Interfaces* **2012**, *4*, 3054—3061.
(602) Venkatachalam, K.; Arzuaga, X.; Chopra, N.; Gavalas, V. G.; Xu, J.; Bhattacharyya, D.; Hennig, B.; Bachas, L. G. Reductive Dechlorination of 3,3′,4,4′-Tetrachlorobiphenyl (PCB77) Using Palladium or Palladium/Iron Nanoparticles and Assessment of the Reduction in Toxic Potency in Vascular Endothelial Cells. *J. Hazard. Mater.* **2008**, *159*, 483—491.
(603) Agrisuelas, J.; Gabrielli, C.; García-Jareño, J. J.; Perrot, H.; Sanchis-Gual, R.; Sel, O.; Vicente, F. Evaluation of the Electrochemical Anion Recognition of NO_3^--Imprinted Poly(Azure A) in NO_3^-/Cl^- Mixed Solutions by AC-Electrogravimetry. *Electrochim. Acta* **2016**, *194*, 292—303.
(604) Karthikeyan, M.; Satheesh Kumar, K. K.; Elango, K. P. Studies on the Defluoridation of Water Using Conducting Polymer/Montmorillonite Composites. *Environ. Technol.* **2012**, *33*, 733—739.
(605) Karthikeyan, M.; Kumar, K. K. S.; Elango, K. P. Batch Sorption Studies on the Removal of Fluoride Ions from Water Using Eco-friendly Conducting Polymer/bio-polymer Composites. *Desalination* **2011**, *267*, 49—56.
(606) Hwang, B. J.; Lee, K. L. Electrocatalytic Oxidation of 2-Chlorophenol on a Composite PbO2/Polypyrrole Electrode in Aqueous Solution. *J. Appl. Electrochem.* **1996**, *26*, 153—159.
(607) Castagno, K.; Hasse, E. E. S.; Azambuja, D. S.; Piatnicki, C. M. S. Chromium Reduction at Polypyrrole Coated Electrodes. *Energy and Electrochemical Processing for a Cleaner Environment*; Walton, C. W.,

DOI: 10.1021/acs.chemrev.7b00482
Chem. Rev. 2018, 118, 4731—4816

Rudd, E. J., Eds.; Electrochemical Society Proceedings; The Electrochemical Society: Pennington, NJ, 1998; Vol. *97-28*, 257−265.
(608) Krishnani, K. K.; Srinives, S.; Mohapatra, B. C.; Boddu, V. M.; Hao, J.; Meng, X.; Mulchandani, A. Hexavalent Chromium Removal Mechanism Using Conducting Polymers. *J. Hazard. Mater.* **2013**, *252*−*253*, 99−106.
(609) Fernandez, L. F.; Ibanez, J. G.; Rajeshwar, K.; Basak, S. The Reduction of Cr VI with Polypyrrole on Reticulated Vitreous Carbon: Miscellaneous Effects. *Meeting Abstracts of the 189th. Electrochemical Society Meeting*; The Electrochemical Society: Pennington, NJ, 1996; Vol. *96-1*, Abstract 524.
(610) Bhaumik, M.; Setshedi, K.; Maity, A.; Onyango, M. S. Chromium (VI) Removal from Water Using Fixed Bed Column of Polypyrrole/Fe_3O_4 Nanocomposite. *Sep. Purif. Technol.* **2013**, *110*, 11−19.
(611) Bhaumik, M.; Agarwal, S.; Gupta, K. V.; Maity, A. Enhanced Removal of Cr(VI) from Aqueous Solutions Using Polypyrrole Wrapped Oxidized MWCNTs Nanocomposites Adsorbent. *J. Colloid Interface Sci.* **2016**, *470*, 257−267.
(612) Lei, Y.; Qian, X.; Shen, J.; An, X. Integrated Reductive/Adsorptive Detoxification of Cr(VI)-Contaminated Water by Polypyrrole/Cellulose Fiber Composite. *Ind. Eng. Chem. Res.* **2012**, *51*, 10408−10415.
(613) Kera, N. H.; Bhaumik, M.; Ballav, N.; Pillay, K.; Ray, S. S.; Maity, A. Selective Removal of Cr(VI) from Aqueous Solution by Polypyrrole/2,5-Diaminobenzene Sulfonic Acid Composite. *J. Colloid Interface Sci.* **2016**, *476*, 144−157.
(614) El-Naggar, I. M.; Zakaria, E. S.; Ali, I. M.; Khalil, M.; El-Shahat, M. F. Removal of Cesium on Polyaniline Titanotungstate as Composite Ion Exchanger. *Adv. Chem. Eng. Sci.* **2012**, *2*, 166−179.
(615) Tian, Y.; Yang, F. Reduction of Hexavalent Chromium by Polypyrrole-Modified Steel Mesh Electrode. *J. Cleaner Prod.* **2007**, *15*, 1415−1418.
(616) Amalraj, A.; Selvi, M. K.; Rajeswari, A.; Christy, E. J. S.; Pius, A. Efficient Removal of Toxic Hexavalent Chromium from Aqueous Solution Using Threonine Doped Polypyrrole Nanocomposite. *J. Water Proc. Eng.* **2016**, *13*, 88−99.
(617) Setshedi, K. Z.; Bhaumik, M.; Onyango, M.; Maity, A. High-Performance Towards Cr(VI) Removal Using Multi-Active Sites of Polypyrrole−Graphene Oxide Nanocomposites: Batch and Column Studies. *Chem. Eng. J.* **2015**, *262*, 921−931.
(618) Ruotolo, L. A. M.; Gubulin, J. C. A Mathematical Model to Predict the Electrode Potential Profile Inside a Polyaniline-Modified Reticulate Vitreous Carbon Electrode Operating in the Potentiostatic Reduction of Cr(VI). *Chem. Eng. J.* **2011**, *171*, 1170−1177.
(619) Rajeshwar, K.; Ibanez, J. G. *Environmental Electrochemistry: Fundamentals and Applications in Pollution Abatement*; Academic Press: San Diego, CA, 1997.
(620) Çirmi, D.; Aydın, R.; Köleli, F. The Electrochemical Reduction of Nitrate Ion on Polypyrrole Coated Copper Electrode. *J. Electroanal. Chem.* **2015**, *736*, 101−106.
(621) García-Fernández, M. J.; Sancho-Querol, S.; Pastor-Blas, M. M.; Sepúlveda-Escribano, A. Surfactant-Assisted Synthesis of Conducting Polymers. Application to the Removal of Nitrates from Water. *J. Colloid Interface Sci.* **2017**, *494*, 98−106.
(622) Ogura, K.; Endo, N.; Nakayama, M. Mechanistic Studies of CO_2 Reduction on a Mediated Electrode with Conducting Polymer and Inorganic Conductor Films. *J. Electrochem. Soc.* **1998**, *145*, 3801−3809.
(623) Zhao, X.; Lv, L.; Pan, B.; Zhang, W.; Zhang, S.; Zhang, Q. Environmental Nanotechnology. Polymer-Supported Nanocomposites for Environmental Applications: A Review. *Chem. Eng. J.* **2011**, *170*, 381−394.
(624) Ehsani, A.; Mahjani, M. G.; Jafarian, M.; Naeemy, A. Electrosynthesis of Polypyrrole Composite Film and Electrocatalytic Oxidation of Ethanol. *Electrochim. Acta* **2012**, *71*, 128−133.
(625) Bernabé, L.; Rivas, L. B.; Sánchez, J. Arsenic Removal by Functional Polymers Coupled to Ultrafiltration Membranes. In *Arsenic: Sources, Environmental Impact, Toxicity and Human Health - A Medical Geology Perspective*; Masotti, A., Ed.; Nova Science Publishers: New York, 2013; pp 267−288.
(626) Janaki, V.; Oh, B. T.; Shanthi, K.; Lee, K. J.; Ramasamy, A. K.; Kamala-Kannan, S. Polyaniline/Chitosan Composite: An Eco-Friendly Polymer for Enhanced Removal of Dyes from Aqueous Solution. *Synth. Met.* **2012**, *162*, 974−980.
(627) Zaremotlagh, S.; Hezarkhani, A. Removal of Textile Dyes from Aqueous Solution by Conducting Polymer Modified Clinoptilolite. *Environ. Earth Sci.* **2014**, *71*, 2999−3006.
(628) Din, M. I.; Ata, S.; Mohsin, I. U.; Rasool, A.; Andleeb Aziz, A. A. Evaluation of Conductive Polymers as an Adsorbent for Eradication of As(III) from Aqueous Solution Using Inductively Coupled Plasma Optical Emission Spectroscopy (ICP-OES). *Int. J. Sci. Eng.* **2014**, *6*, 154−162.
(629) Pathania, D.; Sharma, G.; Kumar, A.; Naushad, M.; Kalia, S.; Sharma, A.; ALOthman, Z. A. Combined Sorptional−Photocatalytic Remediation of Dyes by Polyaniline Zr(IV) Selenotungstophosphate Nanocomposite. *Toxicol. Environ. Chem.* **2015**, *97*, 526−537.
(630) Bhattacharya, P.; Geitner, N. K.; Sarupria, S.; Ke, P. C. Exploiting the Physicochemical Properties of Dendritic Polymers for Environmental and Biological Applications. *Phys. Chem. Chem. Phys.* **2013**, *15*, 4477−4490.
(631) Miller, L. L.; Duan, R. G.; Tully, D. C.; Tomalia, D. A. Electrically Conducting Dendrimers. *J. Am. Chem. Soc.* **1997**, *119*, 1005−1010.
(632) Seredych, M.; Pietrzak, R.; Bandosz, T. J. Role of Graphite Oxide (GO) and Polyaniline (PANi) in NO_2 Reduction on GO-PANi Composites. *Ind. Eng. Chem. Res.* **2007**, *46*, 6925−6935.
(633) Seema, H. K.; Kemp, C.; Le, N. H.; Park, S. W.; Chandra, V.; Lee, J. W.; Kim, K. S. Highly Selective CO_2 Capture by S-Doped Microporous Carbon Materials. *Carbon* **2014**, *66*, 320−326.
(634) Lakard, B.; Carquigny, S.; Segut, O.; Patois, T.; Lakard, S. Gas Sensors Based on Electrodeposited Polymers. *Metals* **2015**, *5*, 1371−1386.
(635) Yang, S.-B.; Jo, W.-K.; Cho, S.-B.; Yu, M.-S. Removal of Ammonia Gas *via* Conducting Polymer-Assisted Titania under Visible-Light or UV Exposure. *Asian J. Chem.* **2015**, *27*, 4179−4183.
(636) Páramo-Garcío, U.; Ávila-Rodríguez, M.; García-Jiménez, M. G.; Gutiérrez-Granados, S.; Ibáñez-Cornejo, J. G. Electrochemical Reduction of Hexachlorobenzene in Organic and Aquo-Organic Media with Cosalen as Catalyst. *Electroanalysis* **2006**, *18*, 904−910.
(637) Paramo-Garcia, U.; Gutierrez-Granados, S.; García-Jiménez, M. G.; Ibanez, J. G. Catalytic Behavior of Cobalt(I) Salen During the Electrochemical Reduction of Lindane and Hexachlorobenzene. *J. New Mater. Electrochem. Syst.* **2010**, *13*, 356−360.
(638) Gallardo-Rivas, N.; Guzman, J.; Gutierrez-Granados, S.; Garcia-Jimenez, M. G.; Ibanez, J. G.; Paramo-Garcia, U. Kinetics and Product Analysis of the Electrochemical Dehalogenation of Hexachlorobenzene. *J. Braz. Chem. Soc.* **2015**, *26*, 790−796.
(639) Peters, D. G.; McGuire, C. M.; Pasciak, E. M.; Peverly, A. A.; Strawsine, L. M.; Wagoner, E. R.; Barnes, J. T. Electrochemical Dehalogenation of Organic Pollutants. *J. Mex. Chem. Soc.* **2014**, *58*, 287−302.
(640) Chen, H.; Nanayakkara, C. E.; Grassian, V. H. Titanium Dioxide Photocatalysis in Atmospheric Chemistry. *Chem. Rev.* **2012**, *112*, 5919−5948.
(641) Arora, R.; Mandal, U. K.; Sharma, P.; Srivastav, A. TiO_2 and PVA Based Polyaniline Composite Materials - A Review. *Mater. Today.* **2015**, *2*, 2767−2775.
(642) Riaz, U.; Ashraf, S. M.; Ruhela, A. Catalytic Degradation of Orange G under Microwave Irradiation with a Novel Nanohybrid Catalyst. *J. Environ. Chem. Eng.* **2015**, *3*, 20−29.
(643) Singh, S.; Mahalingam, H.; Singh, P. K. Polymer-Supported Titanium Dioxide Photocatalysts for Environmental Remediation: A Review. *Appl. Catal., A* **2013**, *462*−*463*, 178−195.
(644) Yu, C.; Wu, R.; Fu, Y.; Dong, X.; Ma, H. Preparation of Polyaniline Supported TiO_2 Photocatalyst and its Photocatalytic Property. Conference Paper. 2011 International Conference on Energy, Environment and Sustainable Development, ICEESD 2011;

DOI: 10.1021/acs.chemrev.7b00482
Chem. Rev. 2018, 118, 4731−4816

Shanghai; China; 21−23 October 2011. *Adv. Mater. Res.* **2012**, *356−360*, 524−528.
(645) Liao, G.; Chen, S.; Quan, X.; Chen, H.; Zhang, Y. Photonic Crystal Coupled TiO_2/Polymer Hybrid for Efficient Photocatalysis under Visible Light Irradiation. *Environ. Sci. Technol.* **2010**, *44*, 3481−3485.
(646) Ghoreishi, K. B.; Asim, N.; Che Ramli, Z. A.; Emdadi, Z.; Yarmo, M. A. Highly Efficient Photocatalytic Degradation of Methylene Blue Using Carbonaceous WO_3/TiO_2 Composites. *J. Porous Mater.* **2016**, *23*, 629−637.
(647) Sivakumar, K.; Senthil-Kumar, V.; Shim, J. J.; Haldorai, Y. Conducting Copolymer/ZnO Nanocomposite: Synthesis, Characterization, and its Photocatalytic Activity for the Removal of Pollutants. *Synth. React. Inorg., Met.-Org., Nano-Met. Chem.* **2014**, *44*, 1414−1420.
(648) Zhang, Z.; Wang, W.; Gao, E. Polypyrrole/Bi_2WO_6 Composite with High Charge Separation Efficiency and Enhanced Photocatalytic Activity. *J. Mater. Sci.* **2014**, *49*, 7325−7332.
(649) Zhang, Q.; Xu, H.; Yan, W. Highly Ordered TiO_2 Nanotube Arrays: Recent Advances in Fabrication and Environmental Applications - A Review. *Nanosci. Nanotechnol. Lett.* **2012**, *4*, 505−519.
(650) Biallozor, S.; Zalewska, T.; Lisowska-Oleksiak, L. Reduction of Dioxygen in Neutral Solution at Polypyrrole Electrode. *J. Appl. Electrochem.* **1996**, *26*, 1053−1057.
(651) Ates, M. A Review Study of (Bio)sensor Systems Based on Conducting Polymers. *Mater. Sci. Eng., C* **2013**, *33*, 1853−1859.
(652) Park, S.; Kwon, O.; Lee, J.; Jang, J.; Yoon, H. Conducting Polymer-Based Nanohybrid Transducers: A Potential Route to High Sensitivity and Selectivity Sensors. *Sensors* **2014**, *14*, 3604−3630.
(653) Barsan, M.; Ghica, E.; Brett, C. Electrochemical Sensors and Biosensors Based on Redox Polymer/Carbon Nanotube Modified Electrodes: A Review. *Anal. Chim. Acta* **2015**, *881*, 1−23.
(654) Inzelt, G. *Conducting Polymers: A New Era in Electrochemistry*; Springer Science & Business Media, 2012.
(655) Hangarter, M.; Chartuprayoon, N.; Hernández, C.; Choa, Y.; Myung, V. Hybridized Conducting Polymer Chemiresistive Nanosensors. *Nano Today* **2013**, *8*, 39−55.
(656) Aydemir, N.; Malmström, J.; Travas-Sejdic, J. Conducting Polymer Based Electrochemical Biosensors. *Phys. Chem. Chem. Phys.* **2016**, *18*, 8264−8277.
(657) Adumitrăchioaie, A.; Tertiş, M.; Cernat, A.; Săndulescu, R.; Cristea, C. Electrochemical Methods Based on Molecularly Imprinted Polymers for Drug Detection. A Review. *Int. J. Electrochem. Sci.* **2018**, *13*, 2556−2576.
(658) Chen, L.; Wang, X.; Lu, W.; Wu, X.; Li, J. Molecular imprinting: perspectives and applications. *Chem. Soc. Rev.* **2016**, *45*, 2137−2211.
(659) Li, C.; Bai, H.; Shi, G. Conducting Polymer Nanomaterials. *Chem. Soc. Rev.* **2009**, *38*, 2397−2409.
(660) Wolfart, F.; Hryniewicz, B. M.; Góes, M. S.; Corrêa, C. M.; Torresi, R.; Minadeo, M. A. O. S.; Córdoba de Torresi, S. I.; Oliveira, R. D.; Marchesi, L. F.; Vidotti, M. Conducting Polymers Revisited: Applications in Energy, Electrochromism and Molecular Recognition. *J. Solid State Electrochem.* **2017**, *21*, 2489−2515.
(661) Walcarius, A.; Minteer, S.; Wang, J.; Lin, Y.; Merkoci, A. Nanomaterials for Bio-Functionalized Electrodes: Recent Trends. *J. Mater. Chem. B* **2013**, *1*, 4878−4908.
(662) Bandodkar, A. J.; Jeerapan, I.; Wang, J. Wearable Chemical Sensors: Present Challenges and Future Prospects. *ACS Sens.* **2016**, *1*, 464−482.
(663) Al-Ahmed, A.; Bahaidarah, H.; Mazumder, M. A. J. Biomedical Perspectives of Polyaniline Based Biosensors. *Adv. Mater. Res.* **2013**, *810*, 173−216.
(664) Ji, J.; Joh, H. I.; Chung, Y.; Kwon, Y. Glucose Oxidase and Polyacrylic Acid Based Water Swellable Enzyme−Polymer Conjugates for Promoting Glucose Detection. *Nanoscale* **2017**, *9*, 15998−16004.
(665) Shrivastava, S.; Jadon, N.; Jain, R. Next-Generation Polymer Nanocomposite-Based Electrochemical Sensors and Biosensors: A Review. *TrAC, Trends Anal. Chem.* **2016**, *82*, 55−67.
(666) Rahman, M.; Li, X.; Lopa, N.; Ahn, S.; Lee, J. Electrochemical DNA Hybridization Sensors Based on Conducting Polymers. *Sensors* **2015**, *15*, 3801−3829.
(667) Henstridge, M.; Dickinson, E.; Aslanoglu, M.; Batchelor-McAuley, C.; Compton, R. G. Voltammetric Selectivity Conferred by the Modification of Electrodes Using Conductive Porous Layers or Films: The Oxidation of Dopamine on Glassy Carbon Electrodes Modified with Multiwalled Carbon Nanotubes. *Sens. Actuators, B* **2010**, *145*, 417−427.
(668) Vasantha, V.; Chen, S. Electrocatalysis and Simultaneous Detection of Dopamine and Ascorbic Acid using Poly(3,4-ethylenedioxy)thiophene Film Modified Electrodes. *J. Electroanal. Chem.* **2006**, *592*, 77−87.
(669) Rui, Z.; Huang, W.; Chen, Y.; Zhang, K.; Cao, Y.; Tu, J. Facile Synthesis of Graphene/Polypyrrole 3D Composite for a High-Sensitivity Non-enzymatic Dopamine Detection. *J. Appl. Polym. Sci.* **2017**, *134*, 44840.
(670) Tang, H.; Lin, P.; Chan, H.; Yan, F. Highly Sensitive Dopamine Biosensors Based on Organic Electrochemical Transistors. *Biosens. Bioelectron.* **2011**, *26*, 4559−4563.
(671) Khudaish, E.; Al-Ajmi, K.; Al-Harthi, S.; Al-Hinai, A. A Solid State Sensor Based Polytyramine Film Modified Electrode for the Determination of Dopamine and Ascorbic Acid in a Moderately Acidic Solution. *J. Electroanal. Chem.* **2012**, *676*, 27−34.
(672) Ates, M.; Castillo, J.; Sezai Sarac, A.; Schuhmann, W. Carbon Fiber Microelectrodes Electrocoated with Polycarbazole and Poly-(carbazole-*co*-p-tolylsulfonyl pyrrole) Films for the Detection of Dopamine in Presence of Ascorbic Acid. *Microchim. Acta* **2008**, *160*, 247−251.
(673) Mao, H.; Liang, J.; Zhang, H.; Pei, Q.; Liu, D.; Wu, S.; et al. Poly(ionicliquids) Functionalized Polypyrrole/Graphene Oxide Nanosheets for Electrochemical Sensor to Detect Dopamine in the Presence of Ascorbic Acid. *Biosens. Bioelectron.* **2015**, *70*, 289−298.
(674) Wang, W.; Xu, G.; Cui, X.; Sheng, G.; Luo, X. Enhanced Catalytic and Dopamine Sensing Properties of Electrochemically Reduced Conducting Polymer Nanocomposite Doped with Pure Graphene Oxide. *Biosens. Bioelectron.* **2014**, *58*, 153−156.
(675) Weaver, C.; Li, H.; Luo, X.; Cui, X. A Graphene Oxide/Conducting Polymer Nanocomposite for Electrochemical Dopamine Detection: Origin of Improved Sensitivity and Specificity. *J. Mater. Chem. B* **2014**, *2*, 5209−5219.
(676) Jung, I.; Dikin, D.; Piner, R.; Ruoff, R. Tunable Electrical Conductivity of Individual Graphene Oxide Sheets Reduced at "Low" Temperatures. *Nano Lett.* **2008**, *8*, 4283−4287.
(677) Xu, G.; Li, B.; Luo, X. Carbon Nanotube Doped Poly(3,4-Ethylenedioxythiophene) for the Electrocatalytic Oxidation and Detection of Hydroquinone. *Sens. Actuators, B* **2013**, *176*, 69−74.
(678) Xu, G.; Li, B.; Cui, X.; Ling, L.; Luo, X. Electrodeposited Conducting Polymer Pedot Doped With Pure Carbon Nanotubes for the Detection of Dopamine in the Presence of Ascorbic Acid. *Sens. Actuators, B* **2013**, *188*, 405−410.
(679) Xu, G.; Li, B.; Wang, X.; Luo, X. Electrochemical Sensor for Nitrobenzene Based on Carbon Paste Electrode Modified with a Poly(3,4-Ethylenedioxythiophene) and Carbon Nanotube Nanocomposite. *Microchim. Acta* **2014**, *181*, 463−469.
(680) Deng, J.; Liu, M.; Lin, F.; Zhang, Y.; Liu, Y.; Yao, S. Self-Assembled Oligo(Phenylene Ethynylene)S/Graphene Nanocomposite with Improved Electrochemical Performances for Dopamine Determination. *Anal. Chim. Acta* **2013**, *767*, 59−65.
(681) Ghica, M.; Wintersteller, Y.; Brett, C. Poly(Brilliant Green)/Carbon Nanotube− Modified Carbon Film Electrodes and Application as Sensors. *J. Solid State Electrochem.* **2013**, *17*, 1571−1580.
(682) Feng, X.; Mao, C.; Yang, G.; Hou, W.; Zhu, J. Polyaniline/Au Composite Hollow Spheres: Synthesis, Characterization, and Application to the Detection of Dopamine. *Langmuir* **2006**, *22*, 4384−4389.
(683) Fabregat, G.; Osorio, J.; Castedo, A.; Armelin, E.; Buendía, J.; Llorca, J.; Alemán, C. Plasma Functionalized Surface of Commodity

DOI: 10.1021/acs.chemrev.7b00482
Chem. Rev. 2018, 118, 4731−4816

Polymers for Dopamine Detection. *Appl. Surf. Sci.* **2017**, *399*, 638−647.
(684) Qian, T.; Zhou, X.; Wu, S.; Shen, J.; Yu, C. Au Nanoparticles Decorated Polypyrrole/Reduced Graphene Oxide Hybrid Sheets for Ultrasensitive Dopamine Detection. *Sens. Actuators, B* **2014**, *193*, 759−763.
(685) Li, J.; Lin, X. Simultaneous Determination of Dopamine And Serotonin on Gold Nanocluster/Overoxidized Polypyrrole Composite Modified Glassy Carbon Electrode. *Sens. Actuators, B* **2007**, *124*, 486−493.
(686) Raj, M.; Gupta, P.; Goyal, R.; Shim, Y. Graphene/Conducting Polymer Nano-Composite Loaded Screen Printed Carbon Sensor for Simultaneous Determination of Dopamine and 5-Hydroxytryptamine. *Sens. Actuators, B* **2017**, *239*, 993−1002.
(687) Xue, C.; Wang, X.; Zhu, W.; Han, Q.; Zhu, C.; Hong, J.; Zhou, X.; Jiang, H. Electrochemical Serotonin Sensing Interface Based on Double-Layered Membrane of Reduced Graphene Oxide/Polyaniline Nanocomposites and Molecularly Imprinted Polymers Embedded with Gold Nanoparticles. *Sens. Actuators, B* **2014**, *196*, 57−63.
(688) Sadanandhan, N.; Cheriyathuchenaaramvalli, M.; Devaki, S.; Ravindranatha Menon, A. R. PEDOT-reduced Graphene Oxide-Silver Hybrid Nanocomposite Modified Transducer for the Detection of Serotonin. *J. Electroanal. Chem.* **2017**, *794*, 244−253.
(689) Özcan, A.; İlkbaş, S. Poly(pyrrole-3-carboxylic acid)-modified Pencil Graphite Electrode for the Determination of Serotonin in Biological Samples by Adsorptive Stripping Voltammetry. *Sens. Actuators, B* **2015**, *215*, 518−524.
(690) Babaei, A.; Taheri, A. Nafion/Ni(OH)$_2$ Nanoparticles-Carbon Nanotube Composite Modified Glassy Carbon Electrode as a Sensor for Simultaneous Determination of Dopamine and Serotonin in the Presence of Ascorbic Acid. *Sens. Actuators, B* **2013**, *176*, 543−551.
(691) Lu, X.; Li, Y.; Du, J.; Zhou, X.; Xue, Z.; Liu, X.; Wang, Z. Novel Nanocomposites Sensor for Epinephrine Detection in the Presence of Uric Acids and Ascorbic Acids. *Electrochim. Acta* **2011**, *56*, 7261−7266.
(692) Yi, H.; Zheng, D.; Hu, C.; Hu, S. Functionalized Multiwalled Carbon Nanotubes Through In Situ Electropolymerization of Brilliant Cresyl Blue for Determination of Epinephrine. *Electroanalysis* **2008**, *20*, 1143−1146.
(693) Rui, Z.; Huang, W.; Chen, Y.; Zhang, K.; Cao, Y.; Tu, J. Facile Synthesis of Graphene/Polypyrrole 3D Composite for a High-Sensitivity Non-Enzymatic Dopamine Detection. *J. Appl. Polym. Sci.* **2017**, *134*, 44840.
(694) Tsele, T.; Adekunle, A.; Fayemi, O.; Ebenso, E. Electrochemical Detection of Epinephrine using Polyaniline Nanocomposite Films Doped with TiO_2 and RuO_2 Nanoparticles on Multi-walled Carbon Nanotube. *Electrochim. Acta* **2017**, *243*, 331−348.
(695) Raoof, J.; Ojani, R.; Baghayeri, M. Fabrication of Layer-By-Layer Deposited Films Containing CNT and Poly(Malachite Green) as a Sensor for Simultaneous Determination of Ascorbic Acid, Epinephrine, and Uric Acid. *Turk. J. Chem.* **2013**, *37*, 36−50.
(696) Malinauskas, A.; Garjonyte, R.; Mažeikiene, R.; Jureviciute, I. Electrochemical Response of AA at Conducting and Electrogenerated Polymer Modified Electrodes for Electroanalytical Applications: A Review. *Talanta* **2004**, *64*, 121−129.
(697) Atta, N.; El-Kady, M.; Galal, A. Palladium Nanoclusters-Coated Polyfuran as a Novel Sensor for Catecholamine Neurotransmitters and Paracetamol. *Sens. Actuators, B* **2009**, *141*, 566−574.
(698) Li, F.; Yang, L.; Zhao, C.; Du, Z. Electroactive Gold Nanoparticles/Polyaniline/Polydopamine Hybrid Composite in Neutral Solution as High-Performance Sensing Platform. *Anal. Methods* **2011**, *3*, 1601−1606.
(699) Yoon, H. Current Trends in Sensors Based on Conducting Polymer Nanomaterials. *Nanomaterials* **2013**, *3*, 524−549.
(700) Zou, L.; Li, Y.; Cao, S.; Ye, B. Gold Nanoparticles/Polyaniline Langmuir−Blodgett Film Modified Glassy Carbon Electrode as Voltammetric Sensor for Detection of Epinephrine and Uric Acid. *Talanta* **2013**, *117*, 333−337.
(701) Peng, H.; Zhang, L.; Soeller, C.; Travas-Sejdic, J. Conducting Polymers for Electrochemical DNA Sensing. *Biomaterials* **2009**, *30*, 2132−2148.
(702) Freund, M.; Bodalbhai, L.; Brajter-Toth, A. Anion-excluding Polypyrrole Films. *Talanta* **1991**, *38*, 95−99.
(703) Pihel, K.; Walker, D.; Wightman, M. Overoxidized Polypyrrole-Coated Carbon Fiber Microelectrodes for Dopamine Measurements with Fast-Scan Cyclic Voltammetry. *Anal. Chem.* **1996**, *68*, 2084−2089.
(704) Gao, Y.; Xu, J.; Lu, L.; Wu, L.; Zhang, K.; Nie, T.; Zhu, X.; Wu, Y. Overoxidized Polypyrrole/Graphene Nanocomposite with Good Electrochemical Performance as Novel Electrode Material for the Detection of Adenine and Guanine. *Biosens. Bioelectron.* **2014**, *62*, 261−267.
(705) Liu, H.; Wang, G.; Chen, D.; Zhang, W.; Li, C.; Fang, B. Fabrication of Polythionine/NPAu/MWNTs Modified Electrode for Simultaneous Determination of Adenine and Guanine in DNA. *Sens. Actuators, B* **2008**, *128*, 414−421.
(706) Wu, H.; Jin, Y.; Wei, J.; Jin, H.; Sha, D.; Wu, J. Mode of Action of Taurine as a Neuroprotector. *Brain Res.* **2005**, *1038*, 123−131.
(707) Kupis-Rozmysłowicz, R.; Wagner, M.; Bobacka, J.; Lewenstam, A.; Migdalski, J. Biomimetic Membranes Based on Molecularly Imprinted Conducting Polymers as a Sensing Element for Determination of Taurine. *Electrochim. Acta* **2016**, *188*, 537−544.
(708) Park, S.; Boo, H.; Chung, T. Electrochemical Non-enzymatic Glucose Sensors. *Anal. Chim. Acta* **2006**, *556*, 46−57.
(709) Hui, N.; Wang, S.; Xie, H.; Xu, S.; Niu, S.; Luo, X. Nickel Nanoparticles Modified Conducting Polymer Composite of RGO Doped Poly(3,4-Ethylenedioxythiophene). *Sens. Actuators, B* **2015**, *221*, 606−613.
(710) Poletti Papi, M.; Caetano, F.; Bergamini, M.; Marcolino-Junior, L. Facile Synthesis of a Silver Nanoparticles/Polypyrrole Nanocomposite for Non-Enzymatic Glucose Determination. *Mater. Sci. Eng., C* **2017**, *75*, 88−94.
(711) Ramanavicius, A.; Ramanaviciene, A.; Malinauskas, A. Electrochemical Sensors Based on Conducting Polymer—Polypyrrole. *Electrochim. Acta* **2006**, *51*, 6025−6037.
(712) Westbroek, P.; Temmerman, E.; Kiekens, P. Electrochemical sensors for the control of the concentration of bleaching agent optimize the quality of bleached and dyed textile products. In *Surface Characteristics of Fibers and Textiles*; Pastore, C., Kiekens, P., Eds.; Surfactant Science Series; Marcel Dekker, Inc., 2001; Vol. *94*, p 123−137.
(713) Jin, D.; Sakthivel, K.; Gandhi, S.; Huy, B.; Lee, Y. An Improved Non-Enzymatic Hydrogen Peroxide Sensor Based on Europium Functionalized Inorganic Hybrid Material-Evaluation of Optical and Electrochemical Properties. *Sens. Actuators, B* **2016**, *237*, 81−89.
(714) Toledano, M.; Delaunay, A.; Monceau, L.; Tacnet, F. Microbial H_2O_2 Sensors as Archetypical Redox Signaling Modules. *Trends Biochem. Sci.* **2004**, *29*, 351−357.
(715) Chen, W.; Cai, S.; Ren, Q.; Wen, W.; Zhao, Y. Recent Advances in Electrochemical Sensing for Hydrogen Peroxide: A Review. *Analyst* **2012**, *137*, 49−58.
(716) Mahmoudian, M.; Alias, Y.; Basirun, W.; Ebadi, M. Preparation of Ultra-Thin Polypyrrole Nanosheets Decorated With Ag Nanoparticles and their Application in Hydrogen Peroxide Detection. *Electrochim. Acta* **2012**, *72*, 46−52.
(717) Xing, L.; Rong, Q.; Ma, Z. Non-enzymatic Electrochemical Sensing of Hydrogen Peroxide Based on Polypyrrole/Platinum Nanocomposites. *Sens. Actuators, B* **2015**, *221*, 242−247.
(718) Peña, R.; Bertotti, M.; Brett, C. Methylene Blue/Multiwall Carbon Nanotube Modified Electrode for the Amperometric Determination of Hydrogen Peroxide. *Electroanalysis* **2011**, *23*, 2290−2296.
(719) Pernites, R.; Ponnapati, R.; Felipe, M.; Advincula, R. Electropolymerization Molecularly Imprinted Polymer (E-MIP) SPR Sensing of Drug Molecules: Pre-polymerization Complexed Terthiophene and Carbazole Electroactive Monomers. *Biosens. Bioelectron.* **2011**, *26*, 2766−2771.

DOI: 10.1021/acs.chemrev.7b00482
Chem. Rev. 2018, 118, 4731−4816

(720) Jain, R.; Tiwari, D.; Shrivastava, S. A Sensitive Voltammetric Sensor Based on Synergistic Effect of Polyaniline and Zirconia Nanocomposite Film for Quantification of Proton Pump Inhibitor Esomeprazole. *J. Electrochem. Soc.* **2014**, *161*, B39−B44.
(721) Jain, R.; Tiwari, D.; Shrivastava, S. Polyaniline−bismuth Oxide Nanocomposite Sensor for Quantification of Anti-Parkinson Drug Pramipexole in Solubilized System. *Mater. Sci. Eng., B* **2014**, *185*, 53−59.
(722) Jain, R.; Tiwari, D.; Karolia, P. Highly Sensitive and Selective Polyaniline−Zinc Oxide Nanocomposite Sensor for Betahistine Hydrochloride in Solubilized System. *J. Mol. Liq.* **2014**, *196*, 308−313.
(723) Rezaei, B.; Boroujeni, M.; Ensafi, A. A Novel Electrochemical Nanocomposite Imprinted Sensor for the Determination of Lorazepam Based on Modified Polypyrrole@sol-gel@gold Nanoparticles/ Pencil Graphite Electrode. *Electrochim. Acta* **2014**, *123*, 332−339.
(724) Rezaei, B.; Khalili Boroujeni, M.; Ensafi, A. A. Caffeine Electrochemical Sensor Using Imprinted Film as Recognition Element Based on Polypyrrole, Sol-Gel, and Gold Nanoparticles Hybrid Nanocomposite Modified Pencil Graphite Electrode. *Biosens. Bioelectron.* **2014**, *60*, 77−83.
(725) Jain, R.; Shrivastava, S. A Graphene-polyaniline-Bi_2O_3 Hybrid Film Sensor for Voltammetric Quantification of Anti-inflammatory Drug Etodolac. *J. Electrochem. Soc.* **2014**, *161*, H189−H194.
(726) Karadas, N.; Ozkan, S. Electrochemical Preparation of Sodium Dodecylsulfate Doped Over-Oxidized Polypyrrole/Multi-Walled Carbon Nanotube Composite on Glassy Carbon Electrode and its Application on Sensitive and Selective Determination of Anticancer Drug: Pemetrexed. *Talanta* **2014**, *119*, 248−254.
(727) Shahrokhian, S.; Azimzadeh, M.; Amini, M. Modification of Glassy Carbon Electrode with a Bilayer of Multiwalled Carbon Nanotube/tiron-doped 222/polypyrrole: Application to Sensitive Voltammetric Determination of Acyclovir. *Mater. Sci. Eng., C* **2015**, *53*, 134−141.
(728) Karolia, P.; Tiwari, D.; Jain, R. Electrocatalytic Sensing of Oomeprazole. *Ionics* **2015**, *21*, 2355−2362.
(729) Noh, H.; Revin, S.; Shim, Y. Voltammetric Analysis of Anti-Arthritis Drug, Ascorbic Acid, Tyrosine, and Uric Acid Using a Graphene Decorated-Functionalized Conductive Polymer Electrode. *Electrochim. Acta* **2014**, *139*, 315−322.
(730) Ghadimi, H.; Tehrani, R. M. A.; Ali, A.; Mohamed, N.; Ab Ghani, S. Sensitive Voltammetric Determination of Paracetamol by Poly (4- Vinylpyridine)/Multiwalled Carbon Nanotubes Modified Glassy Carbon Electrode. *Anal. Chim. Acta* **2013**, *765*, 70−76.
(731) Karadas, N.; Sanli, S.; Akmese, B.; Dogan-Topal, B.; Can, A.; Ozkan, S. Analytical Application of Poly Methylene Blue−Multiwalled Carbon Nanotube Modified Glassy Carbon Electrode on Anticancer Drug Irinotecan and Determination of its Ionization Constant Value. *Talanta* **2013**, *115*, 911−919.
(732) Porfireva, A.; Evtugyn, G.; Ivanov, A.; Hianik, T. Impedimetric Aptasensors Based on Carbon Nanotubes − Poly(Methylene Blue) Composite. *Electroanalysis* **2010**, *22*, 2187−2195.
(733) Eslami, M.; Alizadeh, N. A Dual Usage Smart Sorbent/ Recognition Element Based on Nanostructured Conducting Molecularly Imprinted Polypyrrole for Simultaneous Potential-Induced Nanoextraction/Determination of Ibuprofen in Biomedical Samples by Quartz Crystal Microbalance Sensor. *Sens. Actuators, B* **2015**, *220*, 880−887.
(734) Luo, J.; Ma, Q.; Wei, W.; Zhu, Y.; Liu, R.; Liu, X. Synthesis of Water-dispersible Molecular Imprinted Electroactive Nanoparticles for the Sensitive and Selective Paracetamol Detection. *ACS Appl. Mater. Interfaces* **2016**, *8*, 21028−21038.
(735) Mahugo Santana, C.; Sosa Ferrera, Z.; Torres Padrón, M. E.; Santana Rodríguez, J. J. Methodologies for the Extraction of Phenolic Compounds from Environmental Samples: New Approaches. *Molecules* **2009**, *14*, 298−320.
(736) Fan, Y.; Liu, J.; Yang, C.; Yu, M.; Liu, P. Graphene-polyaniline Composite Film Modified Electrode for Voltammetric Determination of 4-Aminophenol. *Sens. Actuators, B* **2011**, *157*, 669−674.
(737) Wan, Q.; Yu, F.; Yang, P.; Li, L. The Electrochemical Behavior and Determination of *p*-Nitrophenol Based on Poly-Malachite Green/ Multi-Walled Carbon Nanotube Composite Film Modified Electrode. *Conference on Environmental Pollution and Public Health* **2010**, *1−2*, 900−903.
(738) Umasankar, Y.; Periasamy, A.; Chen, S. Electrocatalysis and Simultaneous Determination of Catechol and Quinol by Poly-(Malachite Green) Coated Multiwalled Carbon Nanotube Film. *Anal. Biochem.* **2011**, *411*, 71−79.
(739) Liang, Y.; Gu, L.; Liu, X.; Yang, Q.; Kajiura, H.; Li, Y.; Zhou, T.; Shi, G. Composites of Polyaniline Nanofibers and Molecularly Imprinted Polymers for Recognition of Nitroaromatic Compounds. *Chem. - Eur. J.* **2011**, *17*, 5989−5997.
(740) Wang, F.; Wang, W.; Liu, B.; Wang, Z.; Zhang, Z. Copolypeptide-doped Polyaniline Nanofibers for Electrochemical Detection of Ultratrace Trinitrotoluene. *Talanta* **2009**, *79*, 376−382.
(741) Palma-Cando, A.; Scherf, U. Electrogenerated Thin Films of Microporous Polymer Networks with Remarkably Increased Electrochemical Response to Nitroaromatic Analytes. *ACS Appl. Mater. Interfaces* **2015**, *7*, 11127−11133.
(742) Guo, Z.; Florea, A.; Cristea, C.; Bessueille, F.; Vocanson, F.; Goutaland, F.; Zhang, A.; Sandulescu, R.; Lagarde, F.; Jaffrezic-Renault, N. 1,3,5-Trinitrotoluene Detection by a Molecularly Imprinted Polymer Sensor Based on Electropolymerization of a Microporous-Metal-Organic Framework. *Sens. Actuators, B* **2015**, *207*, 960−966.
(743) Xu, G.; Li, B.; Wang, X.; Luo, X. Electrochemical Sensor for Nitrobenzene Based on Carbon Paste Electrode Modified with a Poly(3,4-Ethylenedioxythiophene) and Carbon Nanotube Nanocomposite. *Microchim. Acta* **2014**, *181*, 463−469.
(744) Zhang, D.; Fang, Y.; Miao, Z.; Ma, M.; Du, X.; Takahashi, S.; Anzai, J.; Chen, Q. Direct Electrodeposition of Reduced Graphene Oxide and Dendritic Copper Nanoclusters on Glassy Carbon Electrode for Electrochemical Detection of Nitrite. *Electrochim. Acta* **2013**, *107*, 656−663.
(745) Deng, C.; Chen, J.; Nie, Z.; Yang, M.; Si, S. Electrochemical Detection of Nitrite Based on the Polythionine/Carbon Nanotube Modified Electrode. *Thin Solid Films* **2012**, *520*, 7026−7029.
(746) Gligor, D.; Walcarius, A. Glassy Carbon Electrode Modified With a Film of Poly(Toluidine Blue O) and Carbon Nanotubes for Nitrite Detection. *J. Solid State Electrochem.* **2014**, *18*, 1519−1528.
(747) Wang, J.; Hui, N. A Nanocomposite Consisting of Flower-Like Cobalt Nanostructures, Graphene Oxide and PPy for Amperometric Sensing of Nitrite. *Microchim. Acta* **2017**, *184*, 2411.
(748) Liu, L.; Cui, H.; An, H.; Zhai, J.; Pan, Y. Electrochemical Detection of Aqueous Nitrite Based on Poly(aniline-*co*-*o*-aminophenol)-Modified Glassy Carbon Electrode. *Ionics* **2017**, *23*, 1517−1523.
(749) Hui, N.; Chai, F.; Lin, P.; Song, Z.; Sun, X.; Li, Y.; Niu, S.; Luo, X. Electrodeposited Conducting Polyaniline Nanowire Arrays Aligned on Carbon Nanotubes Network for High Performance Supercapacitors and Sensors. *Electrochim. Acta* **2016**, *199*, 234−241.
(750) Bobacka, J.; Ivaska, A.; Lewenstam, A. Potentiometric Ion Sensors. *Chem. Rev.* **2008**, *108*, 329−351.
(751) Abramova, N.; Moral-Vico, J.; Soley, J.; Ocana, C.; Bratov, A. Solid Contact Ion Sensor with Conducting Polymer Layer Copolymerized with the Ion-Selective Membrane for Determination of Calcium in Blood Serum. *Anal. Chim. Acta* **2016**, *943*, 50−57.
(752) Migdalski, J.; Błaz, T.; Lewenstam, A. Conducting Polymers - Mechanisms of Cationic Sensitivity and the Methods of Inducing Thereof. *Electrochim. Acta* **2014**, *133*, 316−324.
(753) Wu, S.; Han, T.; Guo, J.; Cheng, Y. Poly(3-aminophenylboronic acid)-reduced Graphene Oxide Nanocomposite Modified Electrode for Ultrasensitive Electrochemical Detection of Fluoride with a Wide Response Range. *Sens. Actuators, B* **2015**, *220*, 1305−1310.
(754) Aydogan, A.; Koca, A.; Şener, M. K.; Sessler, J. L. EDOT-Functionalized Calix[4]pyrrole for the Electrochemical Sensing of Fluoride in Water. *Org. Lett.* **2014**, *16*, 3764−3767.

DOI: 10.1021/acs.chemrev.7b00482
Chem. Rev. 2018, 118, 4731−4816

(755) Ndamanisha, J.; Bai, J.; Qi, B.; Guo, L. Application of Electrochemical Properties of Ordered Mesoporous Carbon to the Determination of Glutathione and Cysteine. *Anal. Biochem.* **2009**, *386*, 79−84.
(756) Rangel Argote, M.; Sánchez Guillén, E.; Gutiérrez Porras, A. G.; Serrano Torres, O.; Richard, C.; Zagal, J. H.; Bedioui, F.; Gutierrez Granados, G.; Griveau, S. Preparation and Characterization of Electrodes Modified with Pyrrole Surfactant, Multiwalled Carbon Nanotubes and Metallophthalocyanines for the Electrochemical Detection of Thiols. *Electroanalysis* **2014**, *26*, 507−512.
(757) Abdul Aziz, M.; Kawde, A. Gold Nanoparticle-modified Graphite Pencil Electrode for the High-sensitivity Detection of Hydrazine. *Talanta* **2013**, *115*, 214−221.
(758) Rębiś, T.; Sobkowiak, M.; Milczarek, G. Electrocatalytic Oxidation and Detection of Hydrazine at Conducting Polymer/lignosulfonate Composite Modified Electrodes. *J. Electroanal. Chem.* **2016**, *780*, 257−263.
(759) Xu, F.; Liu, Y.; Xie, S.; Wang, L. Electrochemical Preparation of a Three Dimensional PEDOT−Cu_xO Hybrid for Enhanced Oxidation and Sensitive Detection of Hydrazine. *Anal. Methods* **2016**, *8*, 316−325.
(760) Wang, J. Electrochemical Sensing of Explosives. *Electroanalysis* **2007**, *19*, 415−423.
(761) Park, C.; Fergus, J.; Miura, N.; Park, J.; Choi, A. Solid-state Electrochemical Gas Sensors. *Ionics* **2009**, *15*, 261−284.
(762) Broza, Y.; Haick, H. Nanomaterial-based Sensors for Detection of Disease by Volatile Organic Compounds. *Nanomedicine* **2013**, *8*, 785−806.
(763) Kukla, A.; Pavluchenko, A.; Shirshov, Y.; Konoshchuk, N.; Posudievsky, O. Application of Sensor Arrays Based on Thin Films of Conducting Polymers for Chemical Recognition of Volatile Organic Solvents. *Sens. Actuators, B* **2009**, *135*, 541−551.
(764) Athawale, A.; Bhagwat, S.; Katre, P. Nanocomposite of Pd-polyaniline as a Selective Methanol Sensor. *Sens. Actuators, B* **2006**, *114*, 263−267.
(765) Choudhury, A. Polyaniline/silver Nanocomposites: Dielectric Properties and Ethanol Vapour Sensitivity. *Sens. Actuators, B* **2009**, *138*, 318−325.
(766) Wang, Y.; Coti, K.; Wang, J.; Alam, M.; Shyue, J.; Lu, W.; Padture, N.; Tseng, H. R. Individually Addressable Crystalline Conducting Polymer Nanowires in a Microelectrode Sensor Array. *Nanotechnology* **2007**, *18*, 424021−424028.
(767) Dan, Y.; Cao, Y.; Mallouk, T.; Johnson, A.; Evoy, S. Dielectrophoretically Assembled Polymer Nanowires for Gas Sensing. *Sens. Actuators, B* **2007**, *125*, 55−59.
(768) Aldalbahi, A.; Feng, P.; Alhokbany, N.; Al-Farraj, E.; Alshehri, S.; Ahamad, T. Synthesis and Characterization of Hybrid Nanocomposites as Highly-Efficient Conducting CH_4 Gas Sensor. *Spectrochim. Acta, Part A* **2017**, *173*, 502−509.
(769) Yang, H.; Cheng, X. L.; Zhang, X. F.; Zheng, Z.; Tang, X.; Xu, Y. M.; Gao, S.; Zhao, H.; Huo, L. H. A Novel Sensor for Fast Detection of Triethylamine Based on Rutile TiO_2 Nanorod Arrays. *Sens. Actuators, B* **2014**, *205*, 322−328.
(770) Bai, S.; Zhao, Y.; Sun, J.; Tong, Z.; Luo, R.; Li, D.; Chen, A. Preparation of Conducting Films Based on α-MoO_3/PANI Hybrids and their Sensing Properties to Triethylamine at Room Temperature. *Sens. Actuators, B* **2017**, *239*, 131−138.
(771) Song, M.; Xu, J. Preparation of Polyethylenimine-Functionalized Graphene Oxide Composite and its Application in Electrochemical Ammonia Sensors. *Electroanalysis* **2013**, *25*, 523−530.
(772) Bangar, M.; Chen, W.; Myung, V.; Mulchandani, A. Conducting Polymer 1-Dimensional Nanostructures for FET Sensors. *Thin Solid Films* **2010**, *519*, 964−973.
(773) Scandurra, G.; Arena, A.; Ciofi, C.; Gambadoro, A.; Barreca, F.; Saitta, G.; Neri, G. Low Temperature Gas Sensing Applications using Copier Grade Transparency Sheets As Substrates. *Sens. Actuators, B* **2011**, *157*, 473−481.
(774) Dong, B.; Lu, N.; Zelsmann, M.; Kehagias, N.; Fuchs, H.; Sotomayor Torres, C. M.; Chi, L. F. Fabrication of High-Density, Large-Area Conducting-Polymer Nanostructures. *Adv. Funct. Mater.* **2006**, *16*, 1937.
(775) Kemp, N.; McGrouther, D.; Cochrane, J.; Newbury, R. Bridging the Gap: Polymer Nanowire Devices. *Adv. Mater.* **2007**, *19*, 2634.
(776) Hernandez, S.; Chaudhuri, D.; Chen, W.; Myung, N.; Mulchandani, A. Single Polypyrrole Nanowire Ammonia Gas Sensor. *Electroanalysis* **2007**, *19*, 2125.
(777) Hangarter, C.; Bangar, M.; Hernandez, S.; Chen, W.; Deshusses, M.; Mulchandani, A.; Myung, N. Maskless Electrodeposited Contact for Conducting Polymer Nanowires. *Appl. Phys. Lett.* **2008**, *92*, 073104.
(778) Zhang, T.; Nix, M.; Yoo, B.; Deshusses, M.; Myung, N. Electrochemically Functionalized Single-Walled Carbon Nanotube Gas Sensor. *Electroanalysis* **2006**, *18*, 1153−1158.
(779) Hong, L.; Li, Y.; Yang, M. Fabrication and Ammonia Gas Sensing Of Palladium/Polypyrrole Nanocomposite. *Sens. Actuators, B* **2010**, *145*, 25−31.
(780) Park, E.; Kwon, O.; Park, S.; Lee, J.; You, S.; Jang, J. One-pot synthesis of Silver Nanoparticles Decorated Poly(3,4-Ethylenedioxythiophene) Nanotubes For Chemical Sensor Application. *J. Mater. Chem.* **2012**, *22*, 1521−1526.
(781) Gong, J.; Li, Y.; Hu, Z.; Zhou, Z.; Deng, Y. Ultrasensitive NH3 Gas Sensor From Polyaniline Nanograin Enchased TiO_2 fibers. *J. Phys. Chem. C* **2010**, *114*, 9970−9974.
(782) Sharma, S.; Hussain, S.; Singh, S.; Islam, S. MWCNT-conducting Polymer Composite Based Ammonia Gas Sensors: A New Approach For Complete Recovery Process. *Sens. Actuators, B* **2014**, *194*, 213−219.
(783) Bedioui, F.; Griveau, S. Electrochemical Detection of Nitric Oxide: Assessment of Twenty Years of Strategies. *Electroanalysis* **2013**, *25*, 587−600.
(784) Gusain, A.; Joshi, N.; Varde, P.; Aswal, D. Flexible NO Gas Sensor Based On Conducting Polymer Poly[N-9′-heptadecanyl-2,7-carbazole-alt-5,5-(4′,7′-di-2-thienyl-2′,1′,3′-benzothiadiazole)] (PCDTBT). *Sens. Actuators, B* **2017**, *239*, 734−745.
(785) Geng, L.; Huang, X.; Zhao, Y.; Li, P.; Wang, S.; Zhang, S.; Wu, S. H_2S Sensitivity Study Of Polypyrrole/WO_3 Materials. *Solid-State Electron.* **2006**, *50*, 723−726.
(786) Geng, L.; Wang, S.; Zhao, Y.; Li, P.; Zhang, S.; Huang, W.; Wu, S. Study of the Primary Sensitivity of Polypyrrole/r-Fe_2O_3 to Toxic Gases. *Mater. Chem. Phys.* **2006**, *99*, 15−19.
(787) Kong, F.; Wang, Y.; Zhang, J.; Xia, H.; Zhu, B.; Wang, Y.; Wang, S.; Wu, S. The Preparation and Gas Sensitivity Study of Polythiophene/SnO_2 Composites. *Mater. Sci. Eng., B* **2008**, *150*, 6−11.
(788) Sadek, A.; Wlodarski, W.; Shin, K.; Kaner, R.; Kalantar-zadeh, K. A Layered Surface Acoustic Wave Gas Sensor Based on a Polyaniline/In_2O_3 Nanofibre Composite. *Nanotechnology* **2006**, *17*, 4488−4492.
(789) Tiwari, A.; Gong, S. Electrochemical Synthesis of Chitosan-*co*-polyaniline/WO_3. nH_2O Composite Electrode for Amperometric Detection of NO_2 Gas. *Electroanalysis* **2008**, *20*, 1775−1781.
(790) Goto, T.; Hyodo, T.; Ueda, T.; Kamada, K.; Kaneyasu, K.; Shimizu, Y. CO-sensing Properties of Potentiometric Gas Sensors Using an Anion-conducting Polymer Electrolyte and Au-loaded Metal Oxide Electrodes. *Electrochim. Acta* **2015**, *166*, 232−243.
(791) Chiang, C.; Tsai, K.; Lee, Y.; Lin, H.; Yang, Y.; Shih, C.; Lin, C.; Jeng, H.; Weng, Y.; Cheng, Y.; Ho, K.; Dai, C. In Situ Fabrication of Conducting Polymer Composite Film as a Chemical Resistive CO_2 Gas Sensor. *Microelectron. Eng.* **2013**, *111*, 409−415.
(792) Wang, Y.; Zhou, Z.; Yang, Z.; Chen, X.; Xu, D.; Zhang, Y. Gas Sensors Based on Deposited Single-Walled Carbon Nanotube Networks for DMMP Detection. *Nanotechnology* **2009**, *20*, 345502−345510.
(793) Tiwari, D.; Sharma, R.; Vyas, K.; Boopathi, M.; Singh, V.; Pandey, P. Electrochemical Incorporation of Copper Phthalocyanine in Conducting Polypyrrole for the Sensing of DMMP. *Sens. Actuators, B* **2010**, *151*, 256−264.

DOI: 10.1021/acs.chemrev.7b00482
Chem. Rev. 2018, 118, 4731−4816

(794) Pandey, S.; Kim, K.; Tang, K. A Review of Sensor-Based Methods for Monitoring Hydrogen Sulfide. *TrAC, Trends Anal. Chem.* **2012**, *32*, 87−99.
(795) Virji, S.; Fowler, J.; Baker, C.; Huang, J.; Kaner, R.; Weiller, B. Polyaniline Nanofiber Composites with Metal Salts: Chemical Sensors for Hydrogen Sulfide. *Small* **2005**, *1*, 624−627.
(796) Rañola, R.; Santiago, S.; Sevilla, B. F., III Use of Array of Conducting Polymers for Differentiation of Coconut Oil Products. *Talanta* **2016**, *146*, 75−82.
(797) Kane-Maguire, L. A. P.; Wallace, G. G. Chiral Conducting Polymers. *Chem. Soc. Rev.* **2010**, *39*, 2545−2576.
(798) Salmón, M.; Saloma, M.; Bidan, G.; Genies, E. M. Route to Chemically Modified Chiral Electrodes: Synthesis and Properties of Optically Active Pyrrole Monomers. *Electrochim. Acta* **1989**, *34*, 117−120.
(799) Goto, H.; Akagi, K. Preparation of Poly(3,4-ethylenedioxythiophene) in a Chiral Nematic Liquid-Crystal Field. *Macromol. Rapid Commun.* **2004**, *25*, 1482−1486.
(800) Matsushita, S.; Jeong, Y. S.; Akagi, K. Electrochromism-driven Linearly and Circularly Polarised Dichroism of Poly(3,4-Ethylenedioxythiophene) Derivatives with Chirality and Liquid Crystallinity. *Chem. Commun.* **2013**, *49*, 1883−1890.
(801) Patra, A.; Bendikov, M.; Chand, S. Poly(3,4-ethylenedioxyselenophene) and Its Derivatives: Novel Organic Electronic Materials. *Acc. Chem. Res.* **2014**, *47*, 1465−1474.
(802) Macco, A. A.; De Brouwer, R. J.; Buck, H. M. Asymmetric Induction in the Synthesis of Thiophene-Containing Steroidlike Molecules *via* Olefinic Cyclization. Precoiling as Model Description for the Stereochemical Course of the Reaction. *J. Org. Chem.* **1977**, *42*, 3196−3199.
(803) Macco, A. A.; Buck, H. M. Preparation of 6.Alpha.-Substituted Optically Pure Steroid with Thiophene as the A Ring *via* Asymmetric Induction. A Circular Dichroism Study. *J. Org. Chem.* **1981**, *46*, 2655−2660.
(804) Lemaire, M.; Delabouglise, D.; Garreau, R.; Guy, A.; Roncali, J. Enantioselective Chiral Poly(thiophenes). *J. Chem. Soc., Chem. Commun.* **1988**, 658−661.
(805) McTiernan, C. D.; Chahma, M. Synthesis and Characterization of Alanine Functionalized Oligo/Polythiophenes. *New J. Chem.* **2010**, *34*, 1417−1423.
(806) McTiernan, C. D.; Omri, K.; Chahma, M. Chiral Conducting Surfaces *via* Electrochemical Oxidation of L-Leucine-Oligothiophenes. *J. Org. Chem.* **2010**, *75*, 6096−6103.
(807) McTiernan, C. D.; Chahma, M. Chiral Conducting Surfaces Based on the Electropolymerization of 3,4-Ethylenedioxythiophene. *Synth. Met.* **2011**, *161*, 1532−1536.
(808) Groenendaal, F. B. L.; Zotti, G.; Aubert, P. H.; Waybright, S. M.; Reynolds, J. R. Electrochemistry of Poly(3,4-alkylenedioxythiophene) Derivatives. *Adv. Mater.* **2003**, *15*, 855−879.
(809) Demeter, D.; Blanchard, P.; Allain, M.; Grosu, I.; Roncali, J. Synthesis and Metal Cation Complexing Properties of Crown-Annelated Terthiophenes Containing 3,4-Ethylenedioxythiophene. *J. Org. Chem.* **2007**, *72*, 5285−5290.
(810) Hicks, R. G.; Nodwell, M. B. Synthesis and Electronic Structure Investigations of α,ω-Bis(arylthio)oligothiophenes: Toward Understanding Wire-Linker Interactions in Molecular-Scale Electronic Materials. *J. Am. Chem. Soc.* **2000**, *122*, 6746−6753.
(811) Collis, G. E.; Burrell, A. K.; Scott, S. M.; Officer, D. L. Toward Functionalized Conducting Polymers: Synthesis and Characterization of Novel β-(Styryl)terthiophenes. *J. Org. Chem.* **2003**, *68*, 8974−8983.
(812) Chahma, M.; McTiernan, C. D.; Abbas, S. A. Characterization of Phenomena Occurring at the Interface of Chiral Conducting Surfaces. *New J. Chem.* **2014**, *38*, 3379−3385.
(813) Bäuerle, P.; Emge, A. Specific Recognition of Nucleobase-Functionalized Polythiophenes. *Adv. Mater.* **1998**, *10*, 324−330.
(814) Emge, A.; Bäuerle, P. Molecular Recognition Properties of Nucleobase-Functionalized Polythiophenes. *Synth. Met.* **1999**, *102*, 1370−1373.
(815) Caras-Quintero, D.; Bäuerle, P. Synthesis of the First Enantiomerically Pure and Chiral, Disubstituted 3,4-Ethylenedioxythiophenes (EDOTs) and Corresponding Stereo- and Regioregular PEDOTs. *Chem. Commun.* **2004**, 926−927.
(816) Lu, B.; Lu, Y.; Wen, Y.; Duan, X.; Xu, J.; Chen, S.; Zhang, L. Synthesis, Characterization, and Vitamin C Detection of a Novel L-Alanine-Modified PEDOT with Enhanced Chirality. *Int. J. Electrochem. Sci.* **2013**, *8*, 2826−2841.
(817) Hu, D.; Lu, B.; Zhang, K.; Sun, X.; Xu, J.; Duan, X.; Dong, L.; Sun, H.; Zhu, X.; Zhen, S. Synthesis of Novel Chiral L-Phenylalanine Grafted PEDOT Derivatives with Electrochemical Chiral Sensor for 3,4-Dihydroxyphenylalanine Discrimination. *Int. J. Electrochem. Sci.* **2015**, *10*, 3065−3081.
(818) Percec, V.; Peterca, M.; Rudick, J. G.; Aqad, E.; Imam, M. R.; Heiney, P. A. Self-Assembling Phenylpropyl Ether Dendronized Helical Polyphenylacetylenes. *Chem. - Eur. J.* **2007**, *13*, 9572−9581.
(819) Shinohara, K.-I.; Yasuda, S.; Kato, G.; Fujita, M.; Shigekawa, H. Direct Measurement of the Chiral Quaternary Structure in a π-Conjugated Polymer at Room Temperature. *J. Am. Chem. Soc.* **2001**, *123*, 3619−3620.
(820) Jeong, Y. S.; Akagi, K. Control of Chirality and Electrochromism in Copolymer-Type Chiral PEDOT Derivatives by Means of Electrochemical Oxidation and Reduction. *Macromolecules* **2011**, *44*, 2418−2426.
(821) Stille, J. K. The Palladium-Catalyzed Cross-Coupling Reactions of Organotin Reagents with Organic Electrophiles [New Synthetic Methods (58)]. *Angew. Chem., Int. Ed. Engl.* **1986**, *25*, 508−524.
(822) Stille, J. K. Palladium Catalyzed Coupling of Organotin Reagents with Organic Electrophiles. *Pure Appl. Chem.* **1985**, *57*, 1771−1780.
(823) Perepichka, I. F.; Levillain, E.; Roncali, J. Effect of Substitution of 3,4-Ethylenedioxythiophene (EDOT) on the Electronic Properties of the Derived Electrogenerated Low Band Gap Conjugated Polymers. *J. Mater. Chem.* **2004**, *14*, 1679−1681.
(824) Marsella, M. J.; Yoon, K.; Almutairi, A.; Butt, S. K.; Tham, F. S. Helical Sexithiophenes: An Experimental and Theoretical Study Implicating the Alternating 2,2′:3,3′ Regioisomer as a Reliable Helical Motif. *J. Am. Chem. Soc.* **2003**, *125*, 13928−13929.
(825) Piao, G.; Kawamura, N.; Akagi, K.; Shirakawa, H.; Kyotani, M. Advanced Conjugated polymer-Helical Polyacetylene. *Polym. Adv. Technol.* **2000**, *11*, 826−829.
(826) Goto, H.; Akagi, K. Asymmetric Electrochemical Polymerization: Preparation of Polybithiophene in a Chiral Nematic Liquid Crystal Field and Optically Active Electrochromism. *Macromolecules* **2005**, *38*, 1091−1098.
(827) Yan, B.; Matsushita, S.; Akagi, K. An Advanced Method for Preparation of Helical Carbon and Graphitic Films Using a Carbonization Substrate. *Chem. Mater.* **2016**, *28*, 8781−8791.
(828) Langeveld-Voss, B. M. W.; Christiaans, M. P. T.; Janssen, R. A. J.; Meijer, E. W. Inversion of Optical Activity of Chiral Polythiophene Aggregates by a Change of Solvent. *Macromolecules* **1998**, *31*, 6702−6704.
(829) Goto, H.; Akagi, K. Optically Active Conjugated Polymers Prepared from Achiral Monomers by Polycondensation in a Chiral Nematic Solvent. *Angew. Chem., Int. Ed.* **2005**, *44*, 4322−4328.
(830) Matsushita, S.; Yan, B.; Yamamoto, S.; Jeong, Y. S.; Akagi, K. Helical Carbon and Graphite Films Prepared from Helical Poly(3,4-ethylenedioxythiophene) Films Synthesized by Electrochemical Polymerization in Chiral Nematic Liquid Crystals. *Angew. Chem., Int. Ed.* **2014**, *53*, 1659−1663.
(831) Goto, H.; Nomura, N.; Akagi, K. Electrochemical Polymerization of 3,4-Ethylenedioxythiophene in a DNA Liquid-Crystal Electrolyte. *J. Polym. Sci., Part A: Polym. Chem.* **2005**, *43*, 4298−4302.
(832) Goto, H.; Akagi, K. Optically Active Electrochromism of Poly(3,4-ethylenedioxythiophene) Synthesized by Electrochemical Polymerization in Lyotropic Liquid Crystal of Hydroxypropyl Cellulose/Water: Active Control of Optical Activity. *Chem. Mater.* **2006**, *18*, 255−262.

DOI: 10.1021/acs.chemrev.7b00482
Chem. Rev. 2018, 118, 4731−4816

(833) Sulaiman, Y.; Kataky, R. Chiral Acid Selectivity Displayed by PEDOT Electropolymerised in the Presence of Chiral Molecules. *Analyst* **2012**, *137*, 2386−2393.
(834) Yoneyama, H.; Tsujimoto, A.; Goto, H. Preparation of Optically Active Pyridine-Based Conducting Polymer Films Using a Liquid Crystal Electrolyte Containing a Cholesterol Derivative. *Macromolecules* **2007**, *40*, 5279−5283.
(835) Goto, H. Vortex Fibril Structure and Chiroptical Electrochromic Effect of Optically Active Poly(3,4-ethylenedioxythiophene) (PEDOT*) Prepared by Chiral Transcription Electrochemical Polymerisation in Cholesteric Liquid Crystal. *J. Mater. Chem.* **2009**, *19*, 4914−4921.
(836) Iseki, T.; Kawabata, K.; Nimori, S.; Goto, H. Synthesis of Chiral Inducers Having Double Stereogenic Centers for Electrochemical Polymerization in Cholesteric Liquid Crystal Medium. *Synth. Met.* **2014**, *187*, 217−223.
(837) Chen, S. A.; Tsai, C. C. Structure/properties of Conjugated Conductive Polymers. 2. 3-Ether-Substituted Polythiophenes and Poly(4-methylthiophenes). *Macromolecules* **1993**, *26*, 2234−2239.
(838) Chahma, M. Synthesis and Characterization of Poly(thiophene sulfides) Prepared *via* Chemically Initiated Oxidative Molymerization methods. *Synth. Met.* **2005**, *155*, 474−479.
(839) Goktas, H.; Wang, X.; Boscher, N. D.; Torosian, S.; Gleason, K. K. Functionalizable and Electrically Conductive thin Films Formed by Oxidative Chemical Vapor Deposition (oCVD) from Mixtures of 3-Thiopheneethanol (3TE) and 3,4-Ethylene dioxythiophene (EDOT). *J. Mater. Chem. C* **2016**, *4*, 3403−3414.
(840) Nilsson, K. P. R.; Olsson, J. D. M.; Stabo-Eeg, F.; Lindgren, M.; Konradsson, P.; Inganäs, O. Chiral Recognition of a Synthetic Peptide Using Enantiomeric Conjugated Polyelectrolytes and Optical Spectroscopy. *Macromolecules* **2005**, *38*, 6813−6821.
(841) Nilsson, K. P. R.; Andersson, M. R.; Inganäs, O. Conformational Transitions in a Free Amino Acid Functionalized Polythiophene. *Synth. Met.* **2003**, *135*−*136*, 291−292.
(842) Nilsson, K. P. R.; Olsson, J. D. M; Konradsson, P.; Inganäs, O. Enantiomeric Substituents Determine the Chirality of Luminescent Conjugated Polythiophenes. *Macromolecules* **2004**, *37*, 6316−6321.
(843) Ramos, J. C.; Souto-Maior, R. M.; Navarro, M. Synthesis and Characterization of Chiral Polythiophenes: Poly [(R)-(−) and (S)-(+)-2-(3′-Thienyl)ethyl N-(3″,5″-dinitrobenzoyl)-α-phenylglycinate]. *Polymer* **2006**, *47*, 8095−8100.
(844) Grenier, C. R. G.; George, S. J.; Joncheray, T. J.; Meijer, E. W.; Reynolds, J. R. Chiral Ethylhexyl Substituents for Optically Active Aggregates of π-Conjugated Polymers. *J. Am. Chem. Soc.* **2007**, *129*, 10694−10699.
(845) Loewe, R. S.; Khersonsky, S. M.; McCullough, R. D. A Simple Method to Prepare Head-to-Tail Coupled, Regioregular Poly(3-alkylthiophenes) Using Grignard Metathesis. *Adv. Mater.* **1999**, *11*, 250−253.
(846) Porter, T. L.; Minore, D.; Zhang, D. Semiempirical Calculations and Scanning Probe Microscopy Studies of Polythiophene Thin Films. *J. Phys. Chem.* **1995**, *99*, 13213−13216.
(847) Langeveld-Voss, B. M. W.; Janssen, R. A. J.; Christiaans, M. P. T.; Meskers, S. C. J.; Dekkers, H. P. J. M.; Meijer, E. W. Circular Dichroism and Circular Polarization of Photoluminescence of Highly Ordered Poly{3,4-di[(S)-2-methylbutoxy]thiophene}. *J. Am. Chem. Soc.* **1996**, *118*, 4908−4909.
(848) Zhang, H.-H.; Ma, C.; Bonnesen, P. V.; Zhu, J.; Sumpter, B. G.; Carrillo, J.- M. Y.; Yin, P.; Wang, Y.; Li, A.-P.; Hong, K. Helical Poly(5-alkyl-2,3-thiophene)s: Controlled Synthesis and Structure Characterization. *Macromolecules* **2016**, *49*, 4691−4698.
(849) Fronk, S. L.; Shi, Y.; Siefrid, M.; Mai, C.-K.; McDowell, C.; Bazan, G. C. Chiroptical Properties of a Benzotriazole−Thiophene Copolymer Bearing Chiral Ethylhexyl Side Chains. *Macromolecules* **2016**, *49*, 9301−9308.
(850) Carsten, B.; He, F.; Son, H. J.; Xu, T.; Yu, L. Stille Polycondensation for Synthesis of Functional Materials. *Chem. Rev.* **2011**, *111*, 1493−1528.
(851) Fronk, S. L.; Wang, M.; Ford, M.; Coughlin, J.; Mai, C.-K.; Bazan, G. C. Effect of Chiral 2-Ethylhexyl Side Chains on Chiroptical Properties of the Narrow Bandgap Conjugated Polymers PCPDTBT and PCDTPT. *Chem. Sci.* **2016**, *7*, 5313−5321.
(852) Baptista, F. R.; Belhout, S. A.; Giordani, S.; Quinn, S. J. Recent Developments in Carbon Nanomaterial Sensors. *Chem. Soc. Rev.* **2015**, *44*, 4433−4453.
(853) Paleček, E.; Tkáč, J.; Bartošík, M.; Bertók, T.; Ostatná, V.; Paleček, J. Electrochemistry of Nonconjugated Proteins and Glycoproteins. Toward Sensors for Biomedicine and Glycomics. *Chem. Rev.* **2015**, *115*, 2045−2108.
(854) Labib, M.; Sargent, E. H.; Kelley, S. O. Electrochemical Methods for the Analysis of Clinically Relevant Biomolecules. *Chem. Rev.* **2016**, *116*, 9001−9090.
(855) Åslund, A.; Herland, A.; Hammarström, P.; Nilsson, K. P. R.; Jonsson, B.-H.; Inganäs, O.; Konradsson, P. Studies of Luminescent Conjugated Polythiophene Derivatives: Enhanced Spectral Discrimination of Protein Conformational States. *Bioconjugate Chem.* **2007**, *18*, 1860−1868.
(856) Sharma, S. S.; Wojnarowicz, A.; Sosnowska, M.; Benincori, T.; Noworyta, K.; D'Souza, F.; Kutner, W. Potentiometric Chemosensor for Neopterin, a Cancer Biomarker, Using an Electrochemically Synthesized Molecularly Imprinted Polymer as the Recognition Unit. *Biosens. Bioelectron.* **2016**, *77*, 565−572.
(857) Huynh, T.-P.; Wojnarowicz, A.; Kelm, A.; Woznicki, P.; Borowicz, P.; Majka, A.; D'Souza, F.; Kutner, W. Chemosensor for Selective Determination of 2,4,6-Trinitrophenol Using a Custom Designed Imprinted Polymer Recognition Unit Cross-Linked to a Fluorophore Transducer. *ACS Sens.* **2016**, *1*, 636−639.
(858) Rizzo, S.; Arnaboldi, S.; Mihali, V.; Cirilli, R.; Forni, A.; Gennaro; Isse, A. A.; Pierini, M.; Mussini, P. R.; Sannicolò, F. Inherently Chiral" Ionic-Liquid Media: Effective Chiral Electroanalysis on Achiral Electrodes. *Angew. Chem., Int. Ed.* **2017**, *56*, 2079−2082.
(859) Iskierko, Z.; Checinska, A.; Sharma, P. S.; Golebiewska, K.; Noworyta, K.; Borowicz, P.; Fronc, K.; Bandi, V.; D'Souza, F.; Kutner, W. Molecularly Imprinted Polymer Based Extended-Gate Field-Effect Transistor Chemosensors for Phenylalanine Enantioselective Sensing. *J. Mater. Chem. C* **2017**, *5*, 969−977.
(860) Dong, L.; Zhang, Y.; Duan, X.; Mo, D.; Xu, J.; Zhu, X. Synthesis and Characterization of Chiral PEDOT Enantiomers Bearing Chiral Moieties in Side Chains: Chiral Recognition and its Mechanism Using Electrochemical Sensing Technology. *RSC Adv.* **2016**, *6*, 11536−11545.
(861) Dong, L.; Zhang, Y.; Duan, X.; Zhu, X.; Sun, H.; Xu, J. Chiral PEDOT-Based Enantioselective Electrode Modification Material for Chiral Electrochemical Sensing: Mechanism and Model of Chiral Recognition. *Anal. Chem.* **2017**, *89*, 9695−9702.
(862) Saksena, K.; Shrivastava, A.; Kant, R. Chiral Analysis of Ascorbic Acid in Bovine Serum Using Ultrathin Molecular Imprinted Polyaniline/Graphite Electrode. *J. Electroanal. Chem.* **2017**, *795*, 103−109.
(863) Mondal, P. C.; Kantor-Uriel, N.; Mathew, S. P.; Tassinari, F.; Fontanesi, C.; Naaman, R. Chiral Conductive Polymers as Spin Filters. *Adv. Mater.* **2015**, *27*, 1924−1927.
(864) Xie, A.; Wu, F.; Jiang, W.; Zhang, K.; Sun, M.; Wang, M. Chiral Induced Synthesis of Helical Polypyrrole (PPy) Nano-structures: a Lightweight and High-Performance Material against Electromagnetic Pollution. *J. Mater. Chem. C* **2017**, *5*, 2175−2181.
(865) Xie, A.; Wu, F.; Jiang, W.; Zhang, K.; Sun, M.; Wang, M. Chiral Induced Synthesis of Helical Polypyrrole (PPy) Nano-structures: a Lightweight and High-Performance Material against Electromagnetic Pollution. *J. Mater. Chem. C* **2017**, *5*, 2175−2181.
(866) Otero, T. F.; Martinez, J. G. Physical and Chemical Awareness from Sensing Polymeric Artificial Muscles. Experiments and Modeling. *Prog. Polym. Sci.* **2015**, *44*, 62−78.
(867) Tricoli, A.; Nasiri, N.; De, S. Wearable and Miniaturized Sensor Technologies for Personalized and Preventive Medicine. *Adv. Funct. Mater.* **2017**, *27*, 1605271.

DOI: 10.1021/acs.chemrev.7b00482
Chem. Rev. 2018, 118, 4731−4816

(868) Sekretaryova, A. N.; Eriksson, M.; Turner, A. P. F. Bioelectrocatalytic Systems for Health Applications. *Biotechnol. Adv.* **2016**, *34*, 177−197.
(869) Naveen, M. H.; Gurudatt, N. G.; Shim, Y. B. Applications of Conducting Polymer Composites to Electrochemical Sensors: A review. *Appl. Mater. Today* **2017**, *9*, 419−433.
(870) Hallett, J. P.; Welton, T. Room-Temperature Ionic Liquids: Solvents for Synthesis and *Catal. Chem. Rev.* **2011**, *111*, 3508−3576.
(871) Smith, E. L.; Abbott, A. P.; Ryder, K. S. Deep Eutectic Solvents (DESs) and Their Applications. *Chem. Rev.* **2014**, *114*, 11060−11082.

DOI: 10.1021/acs.chemrev.7b00482
Chem. Rev. 2018, 118, 4731−4816